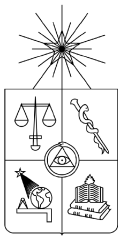

UNIVERSIDAD DE CHILE
FACULTAD DE CIENCIAS FÍSICAS Y MATEMÁTICAS
DEPARTAMENTO DE ASTRONOMÍA

PROPIEDADES FÍSICAS Y CINEMÁTICAS DE ESTRELLAS DE LA VECINDAD SOLAR PERTENECIENTES AL HEMISFERIO SUR

TESIS PARA OPTAR AL GRADO DE MAGÍSTER EN CIENCIAS, MENCIÓN ASTRONOMÍA

FELIPE ANDRÉS MURGAS ALCAÍNO

PROFESOR GUÍA:
PATRICIO ROJO RÜBKE

MIEMBROS DE LA COMISIÓN:
JAMES JENKINS
HUGH JONES
RENÉ MENDEZ BUSSARD

SANTIAGO DE CHILE
MAYO 2010

Resumen

El objetivo de este trabajo es obtener parámetros físicos y cinemáticos de un conjunto de estrellas de campo de la vecindad solar pertenecientes al hemisferio sur. Éstos parámetros ayudarán en la confección de un catálogo de estrellas para búsqueda de planetas, complementar el catálogo de Hipparcos[1] aportando velocidades radiales para estrellas en el hemisferio sur, aumentar el número de estrellas con cinemática completa y en un futuro estudiar la distribución de abundancias en la galaxia. Los datos fueron tomados a lo largo de los años 2006, 2008 y 2009 con el espectrógrafo de ESO FEROS instalado en La Silla, Chile.

Para esta muestra compuesta de 923 estrellas de tipo espectral F, G y K, se indica el número de binarias astrométricas encontradas por Hipparcos (48 en total). También se encontraron 32 binarias espectrales a través de una inspección visual de los espectros tomados con FEROS.

Ocupando datos fotométricos de Hipparcos se utilizó el método de flujo infrarrojo (IRFM) para determinar temperaturas efectivas para las estrellas de la muestra (excluyendo las binarias espectrales).

Además utilizando los espectros, se logró (1) determinar velocidades radiales a través del efecto Doppler, (2) determinar la proyección en la esfera celeste de las velocidades de rotación y (3) obtener la abundancia de hierro [Fe/H]. Para esto último se utilizó temperaturas efectivas y minimización sobre una grilla de modelos.

Utilizando las abundancias calculadas en este trabajo junto a las distancias y fotometría obtenidas de Hipparcos fue posible crear un diagrama HR para 890 estrellas de la muestra. Para cada estrella individual se empleó un ajuste de isocronas para obtener la edad, se discute los errores de tal ajuste para las estrellas de secuencia principal y gracias a un ajuste polinomial de la secuencia principal fue posible establecer que estrellas se encuentran saliendo de ésta por lo que debieran tener un mejor ajuste de la edad. También se presentan valores de indicadores de edad como la velocidad de rotación estelar, el índice de actividad cromosférica R'_{HK} y el ancho equivalente de la línea de absorción de Litio LiI 6708 Å para las estrellas que presenten esta absorción.

Empleando posiciones, distancias y movimientos propios tomadas de Hipparcos y sumando las velocidades radiales de este trabajo, se pudo calcular las componentes de velocidades heliocéntricas U, V, W. Se estudió la distribución de velocidades y se comprobó que la mayoría de las estrellas de la muestra pertenecen al disco galáctico. Se estudió la cinemática de tres estrellas de alta velocidad y se determinó gracias a las abundancias calculadas en este trabajo y al cálculo de órbitas que dichas estrellas pertenecen al halo de la Vía Láctea.

Se estudió la presencia de las estructuras cinemáticas presentes en la vecindad solar conocidas como *moving groups* a través de un método de estimación de densidad en el espacio de velocidades (U, V). También se estableció la membresía de algunas estrellas pertenecientes a estos grupos y se investigó la distribución de las estrellas en el espacio $(U, V, \log R'_{HK})$ para ver si zonas con estrellas activas concuerdan con los centros de *moving groups* conocidos.

Los resultados finales para las estrellas de la muestra se presentan en la Tabla A.1 en el Apéndice de este trabajo.

[1] **Hipparcos**: **Hi**gh **P**recision **Par**allax **Co**llecting **S**atellite.

Agradecimientos

Al Dr. James Jenkins y Dr. Patricio Rojo por sus consejos y guía durante todo este trabajo; sus críticas constructivas e ideas fueron una excelente fuente para mi aprendizaje y crecimiento como científico.

A los docentes de Cerro Calán por su tiempo para atender diversas consultas y valioso apoyo en mi proceso de formación como estudiante de pregrado y magíster, en especial al Dr. René Mendez y Dr. José Gallardo por ayudarme con algunas dudas y aspectos en la realización de esta tesis.

También quiero agradecer a mis compañeros de postgrado por su apoyo y ayuda a lo largo de toda mi estadía en Cerro Calán, compartir con ellos estos años fue verdaderamente una experiencia gratificante. A mis compañeros de la Escuela de Injeniería de la Universidad de Chile que a pesar de los años y de haber seguido rumbos distintos siempre he podido contar con ellos.

Finalmente quiero agradecer a mi familia a quienes les debo todo y me han apoyado sin cuestionar el camino que he elegido, ellos son mi fuerza para seguir.

Contents

List of Tables

List of Figures

Chapter 1

Introduction

In 1842 the French philosopher Auguste Comte (1798-1847) wrote in *Cours de philosophie positive* the following: "To attain a true idea of the nature and composition of this science [astronomy], it is indispensable...to mark the boundaries of the positive knowledge that we are able to gain of the stars....We can never by any means investigate their chemical composition". Fortunately for us and thanks to the work of pioneers like Joseph von Fraunhofer (1787-1826), Robert Bunsen (1811-1899) and Gustav Kirchoff (1824-1887), the prediction made by Auguste Comte was not true. Since its first application to astronomy made by the Italian astronomer Angelo Secchi (1818-1878), the spectroscopic study of celestial objects has opened the door for scientists to learn about the physical processes that govern the Universe: we can learn about the elements present in stars, nebulae and galaxies. Also thanks to the Doppler Effect, we can establish the kinematic properties of these objects. Discoveries like the expansion of the Universe by Edwin Hubble (1889-1953) and the spectral classification of stars would not have been possible without spectroscopy.

High resolution spectroscopic studies are important because they offer more insights and details about the object under study than the regular low resolution spectroscopy, for example we can gain more information about weak absorption lines and the physical conditions in which they are formed, allowing us to make more accurate abundance studies. One new field in astronomy that has had great benefits from high resolution spectra is the study of extrasolar planets. Since the first discovery of an extrasolar planet around a pulsar star made by Wolszczan and Frail [1992] and the first planet detected orbiting the main sequence star 51 Pegasi by Mayor and Queloz [1995], it became clear that the there is a great diversity of planetary systems in the Universe. As the number of discoveries grew, the characterization of these new planets revealed the importance of knowing the physical properties of the host stars: Gonzalez [1997] noticed that the planets discovered at that time all were orbiting stars with a higher metal abundance than the Sun (this was confirmed by Fischer and Valenti [2005]). The most successful technique to find extrasolar planets, the radial velocity method, is sensitive to changes in the chromosphere of the star and accurate spectrographs with a proper follow up and characterization of the host star can lower the limits of detection in mass range leading to the discovery of super-earths (Mayor et al. [2009]). In the same line, detection by direct imaging is more effective at infrared wavelengths for young objects. The latter because they emit more energy due to their ongoing contraction and differentiation. Thanks to this we are the first generation of human beings that can actually see an image of other planetary systems (Lafrenière et al. [2008], Marois et al. [2008], Kalas et al. [2008]).

Also by measuring the radial velocity of the stars and with additional information like distances and proper motions, spectroscopy is a key tool in kinematic studies. Kinematic studies are useful not only because they reveal the shape of the gravitational potential of the galaxy and its relationship with the presence of different structures like streams, bars, spiral arms, etc., but also because by combining this information with abundances is possible to learn about the process of formation and evolution of the Milky Way itself (Edvardsson et al. [1993]). In this effort, surveys have a key role to try to answer these questions. Space missions like Hipparcos, with the help of groundbased telescopes, have made possible new insights in the structure and dynamics of the Milky Way. Using data from Hipparcos, Dehnen [1998] confirmed the existence of the kinematical structures known as moving groups and many other studies have been made in this subject using different methods for their detection (Asiain et al. [1999], Skuljan et al. [1999], Antoja et al.

[2008], Bovy et al. [2009]). The origin of these kinematical groups is still debated (Antoja et al. [2008]): they could have a dynamical origin or they could be star forming regions that are being disrupted by disk heating processes. To help to answer these questions a great number of stars with known kinematics is needed.

Due to the large distances between stars, accurate, high signal to noise studies can only be made in the solar neighborhood. Consequently, surveys that search for planets and the stellar kinematical studies are mostly focused on nearby stars.

The main goal of this work is to measure the physical properties and kinematics of a sample of southern F, G and K stars belonging to the Hipparcos catalog. The aims are (1) building a list of possible targets for planets and low mass companion search (2) to contribute to the kinematical study of the solar neighborhood (3) a starting point into a precision abundance analysis to study the abundance distribution of the galaxy in order to help to constrain chemical evolution models.

Chapter 2 describes the observations and reduction of the data used in this work and also the origin of the ancillary data, Chapter 3 presents the astrometric and spectrum binary systems found, Chapter 4 describes the method used to calculate the effective temperatures and presents the results, Chapter 5 describes the method for obtaining the radial velocities and presents the results, in Chapter 6 describes the method used to get the [Fe/H] abundance and presents the results, Chapter 7 presents isochrone fits in order to get ages and also presents the results for indicators of age like stellar activity, stellar rotation and the presence of Lithium absorption lines.

Chapter 8 presents the distances and the kinematics for the stars and an analysis of the orbits and composition of stars that probably belong to the galactic Halo, Chapter 9 analyzes the kinematical structures that are present in the solar neighborhood known as Moving Groups, presents the star candidates that belong to such systems and analyzes the distribution of stellar activities in UV space.

Chapter 10 presents the main conclusions of this work and finally the Appendix presents the results for the stars of the sample (Table A.1).

Chapter 2

Data

2.1 Observations and Reduction

The data set is part of the work of Jenkins et al. [2008], which is a high resolution spectroscopy study in order to obtain accurate metallicities and activities for stars in the southern hemisphere (see Figure 2.1) with the goal of creating a sample of possible targets for planet search and, also, study the chemical distribution of the solar neighborhood.

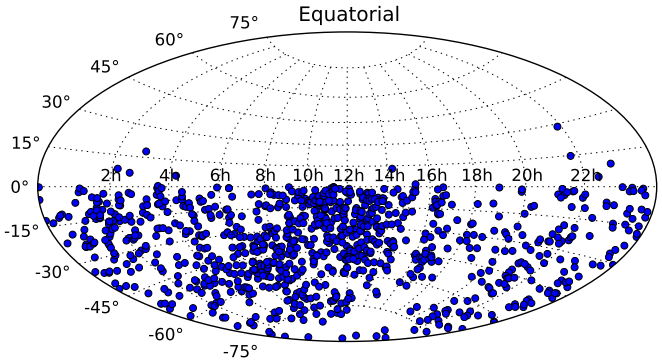

Figure 2.1: Distribution of observed stars in the sky.

The stars in the sample were observed using the Fiber-fed Extended Range Optical Spectrograph (FEROS, Kaufer et al. [1999]) mounted on the MPG/ESO 2.2 m telescope on Las Silla, Chile. FEROS is an echelle spectrograph with a resolution of $R \sim 48000$ and a wide spectral coverage ranging from ~ 3500 Å to ~ 9200 Å. The data was taken in different runs during the years 2006, 2008 and 2009 creating a sample of 949 stellar spectra of 923 stars selected by a color criteria so they have F, G and K spectral type. The stars in the sample have apparent magnitudes in the visual band ranging from 9.5 to 3.5, $(B - V)$ ranging from 0.42 to 1.08 and most stars have distances between 40-100 pc. Using the astrometric Hipparcos data, variable stars and known binary systems were excluded from selection.

The data reduction of all the spectra used in this work was done by the ESO pipeline which consisted

of bias correction, flat-fielding, extraction, wavelength calibration, correction of the barycentric velocity and merging of the orders into a one-dimensional spectrum.

2.2 Ancillary Data

Besides the observed data described above, many times data from other surveys was used in order to complement the information that can be obtained from the spectrum or as comparisons to test the results.

2.2.1 The Hipparcos Catalog

The Hipparcos Space Astrometry Mission was a project of the European Space Agency (ESA) to get unprecedented high accurate positions to more than one hundred thousand stars. The satellite was launched in 1989 and operated until 1993. The catalog containing the photometry, positions, parallaxes and proper motions was released in 1997 (Perryman et al. [1997]) and the data recently underwent a new reduction in the work of van Leeuwen [2007]. The incredible success and valuable data of the Hipparcos mission has opened the door for the future ESA astrometric mission GAIA.

All the stars in the sample were included in the Hipparcos Catalog so valuable and accurate data was available such as V magnitudes, $(B-V)$ color, positions, parallaxes and proper motions.

2.2.2 The Geneva-Copenhagen Survey

The Geneva-Copenhagen Survey (Nordström et al. [2004]) or GCS is a survey of the solar neighborhood that focused on nearly 14000 F and G stars, obtaining *uvby* photometry, metallicities, rotational velocities, effective temperatures, ages, radial velocities and galactic orbits. The GCS provides an unbiased sample (kinematically and in metallicity) for the entire sky and it should be volume complete for the F and G dwarfs to a distance ~ 40 pc.

So far the GCS has underwent two revisions, first the *uvby* photometry was re-calibrated in Holmberg et al. [2007] and more recently an astrometric update using the distances from the new reduction of the Hipparcos data (van Leeuwen [2007]) in Holmberg et al. [2009].

Of the complete sample 235 stars were in common with the GCS.

2.2.3 SPOCS

The Spectroscopic Properties of Cool Stars or SPOCS (Valenti and Fischer [2005]) is a catalog of 1040 nearby F, G and K stars that were observed in the planet search programs of Keck, Lick and AAT. Using high resolution spectra taken with the High Resolution Echelle Spectrometer (HIRES) at Keck Observatory, this catalog provides effective temperatures, surface gravities, metallicities, projected rotational velocities, abundances of elements (like Na, Si, Ti, Fe and Ni), luminosities, stellar radius, masses and ages.

Since work of Valenti and Fischer [2005] is a high resolution spectral analysis, it is a good catalog to compare results with. Of the 1040 stars that were in Valenti and Fischer [2005] 35 stars were included in this sample.

Chapter 3

Binary Stars

This chapter presents the astrometric binaries flagged in the Hipparcos Catalog and the candidates for spectrum binaries stars that were found. The spectrum binaries will not be considered in the photometric estimated effective temperatures, metal abundances, age estimation and stellar activities.

3.1 Hipparcos Astrometric Binaries

A large fraction of the stars present in the sky are found in multiple systems orbiting around a common center of mass, in fact at least 50% of the stars near 5 pc from the Sun are actually in a double or multiple systems (Binney and Merrifield [1998]). Sometimes in a binary system the light from the brightest star or *primary star* swamps its companion, making it impossible to detect both stars. However as they are orbiting a common center of mass we can detect the oscillation of the primary in the plane of the sky and infer the presence of the unseen companion. This is known as an *astrometric binary*.

The motion induced by an unseen companion and the unknown inclination of the orbit of the system affects the determination of the radial velocity of the star because we are adding a velocity component in the line of sight associated with the orbital motion of the star that we actually observe.

The selection process of the sample left out the stars flagged as astrometric binaries by Hipparcos but this was not done for the old sample used in Jenkins et al. [2008], so some previously unidentified astrometric binaries were expected to appear. In order to identify these binary systems, that could lead to incorrect results in the determination of radial velocities, a search in the new Hipparcos Catalog for stars flagged as astrometric binaries was carried out for the entire sample and 48 stars turned out to be flagged (see Table 3.1).

3.2 Spectrum Binary Candidates

In some cases the stars in binary systems are so closed that they are not resolved individually and the wiggling in the plane of the sky caused by the secondary can not be detected, but if the secondary star is bright enough the spectra of the unresolved system present the characteristic absorption lines of both stars shifted with respect to the rest frame due to the Doppler Effect (see Chapter 5) producing what is called a *spectrum binary*.

In order to discard bad spectra that showed discontinuities or excess of cosmic rays and to identify possible spectrum binary systems I proceeded to visually examine the spectra of the stars in the sample in two regions near the Lithium lines at 6104 Å and 6708 Å. For the first region we marked the FeI lines at 6102.16 Å, 6103.26 Å and the CaI line at 6102.72 Å; for the second region the FeI lines at 6703.57 Å, 6705.10 Å and the

Table 3.1: Astrometric Binaries.

Hipparcos Number	Hipparcos Number
HIP 2941	HIP 53534
HIP 5697	HIP 54104
HIP 6712	HIP 54580
HIP 8653	HIP 55875
HIP 9692	HIP 56641
HIP 9774	HIP 61687
HIP 10990	HIP 62371
HIP 11324	HIP 63742
HIP 11502	HIP 64238
HIP 13702	HIP 64573
HIP 17269	HIP 67412
HIP 20552	HIP 70741
HIP 21778	HIP 81478
HIP 29550	HIP 81592
HIP 30733	HIP 92250
HIP 31692	HIP 92304
HIP 33427	HIP 93584
HIP 36160	HIP 97676
HIP 36832	HIP 97704
HIP 37923	HIP 98274
HIP 42408	HIP 101399
HIP 48133	HIP 110785
HIP 50020	HIP 113010
HIP 53424	HIP 117081

CaI line at 6717.70 Å. Figure 3.1 shows an example of the two regions around the LiI lines after normalizing the flux and shifting the spectra to the rest frame with the radial velocities obtained in this work.

The stars that notoriously showed more than one absorption line were classified as spectrum binary candidates. Figure 3.2 presents an example of one of the binary system candidates that I found in this work. Compared with Figure 3.1 we can see clearly that the spectrum presents absorption features corresponding to two stars. Table 3.2 presents the Hipparcos number of the 32 candidates to binary systems that found in this work. Of the 32 candidates only HIP 14050, HIP 51884 and HIP 55304 appear in the catalog of spectroscopic binaries of Pourbaix et al. [2004].

The importance of identifying spectrum binaries is that as the spectra of the system is unresolved this leads to incorrect measurements in the apparent magnitudes and and hence incorrect values in quantities derived with photometry. On the other hand, binaries can be used as calibrators for some physical properties such as metal abundance. Since both stars in the system were born at the same time and place they should have the same metallicity, so in order to test if the [Fe/H] is correct we could compute the metal abundance for each star in the system and see if both values are similar.

From a planet search perspective, binary systems can be interesting targets for one main reason: they provide an excellent opportunity to study planet formation in a different environment and with different dynamics than a single star system. Planets in a binary stellar system can be formed and survive if the two components are orbiting really close or really far away, because the gravitational perturbation caused by one of the stars may lead to an orbital decay or the ejection of the planet.

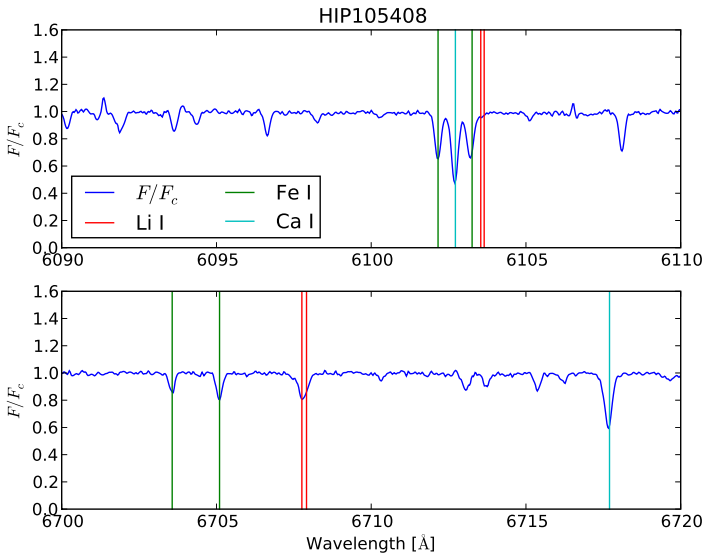

Figure 3.1: The region around the LiI lines.

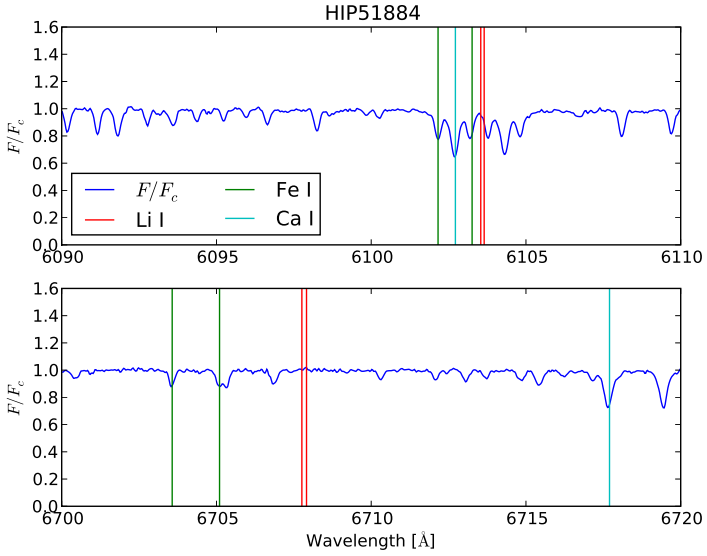

Figure 3.2: Example of a spectrum binary found in the sample.

Table 3.2: Spectrum binaries candidates.

Hipparcos Number
HIP 2368
HIP 4062
HIP 6155
HIP 7109
HIP 10365
HIP 14050
HIP 15301
HIP 21329
HIP 22064
HIP 29772
HIP 31623
HIP 33427
HIP 39007
HIP 45621
HIP 51884
HIP 53499
HIP 54926
HIP 55304
HIP 58132
HIP 60391
HIP 65403
HIP 65548
HIP 66118
HIP 67112
HIP 81179
HIP 98373
HIP 103883
HIP 103941
HIP 106336
HIP 115342
HIP 115659
HIP 117713

Chapter 4

Temperatures

This chapter describes the method used to obtain effective temperatures for the stars in the sample. Section 4.1 presents an introduction to the concept of effective temperature and name some methods to obtain this physical parameter. Section 4.2 introduces the Infrared Flux Method and presents the effective temperatures for the stars in the sample. The results of this chapter will be used to get the metallicities in chapter 6.

4.1 Effective Temperature

In the year 1792 the English pioneer in photography Thomas Wedgwood (1771-1805) noticed the relation between the color of an object and its temperature. He observed that no matter the size or composition of an object (for example an oven or a metal bar) all have the same color at a given temperature. Latter physicists discovered that any object with a temperature above absolute zero should emit radiation.

A *black body* is an idealized object that absorbs all light that it receives and re-radiates with a characteristic spectrum. This spectrum was first described by the German physicist Max Planck (1858-1947) in the year 1900; the Planck's law of black body radiation states that the specific intensity of the radiation depends on the temperature of the object as follows

$$I(\lambda, T)d\lambda = \frac{2hc^2}{\lambda^5}\frac{1}{e^{hc/\lambda kT} - 1}d\lambda \tag{4.1}$$

or written as a function of frequency

$$I(\nu, T)d\nu = \frac{2h\nu^3}{c^2}\frac{1}{e^{h\nu/kT} - 1}d\nu \tag{4.2}$$

where λ and ν are the wavelength and frequency respectively, h is the Plank constant, k the Boltzmann constant, c the speed of light and T the temperature.

The specific intensity I_λ has units of $ergs\ sec^{-1}\ cm^{-1}\ ster^{-1}\ cm^{-2}$, so the flux or total power emitted per unit area will be

$$F = \int I(\lambda, T)d\Omega d\lambda = \int_0^\infty \int_0^{2\pi} \int_0^{\pi/2} I(\lambda, T)d\theta d\phi d\lambda \tag{4.3}$$

F is called the bolometric flux because it is the flux integrated over the entire electromagnetic spectrum. Replacing Planck's function in the previous integral yields the Stephan-Boltzmann law

$$F = \sigma T^4 \tag{4.4}$$

So the bolometric flux emitted by a black body depends only on its temperature and for that reason black body radiation usually is called *thermal radiation*. The spectrum of stars follows closely the shape of a black body, so it is natural to define the effective temperature of a star as the temperature of a black body with the same flux at the surface of the star F_{sur}, i.e

$$T_{eff} = \left(\frac{F_{sur}}{\sigma}\right)^{1/4} \tag{4.5}$$

But the flux at the surface of the star is different from the flux observed on Earth because, for example, if we have an isotropic source and put two imaginary spherical surfaces at r_1 and r_2 from the source, by conservation of energy we have

$$F(r_1)4\pi r_1^2 = F(r_2)4\pi r_2^2 \tag{4.6}$$

So at a distance r_2 we receive a flux equal to

$$F(r_2) = \frac{F(r_1)r_1^2}{r_2^2} \tag{4.7}$$

The conservation of energy implies that the flux must follow an *inverse square law*. Then if a star radiates as an isotropic source we detect a flux at a distance d of

$$F(d) = F(R_\star)\left(\frac{R_\star^2}{d^2}\right) \tag{4.8}$$

where $F(R_\star) = F_{sur}$ and $R_\star$ is the radii of the star. If the radius and/or distance to the star is not known we can use the angular diameter θ, which is measurable.

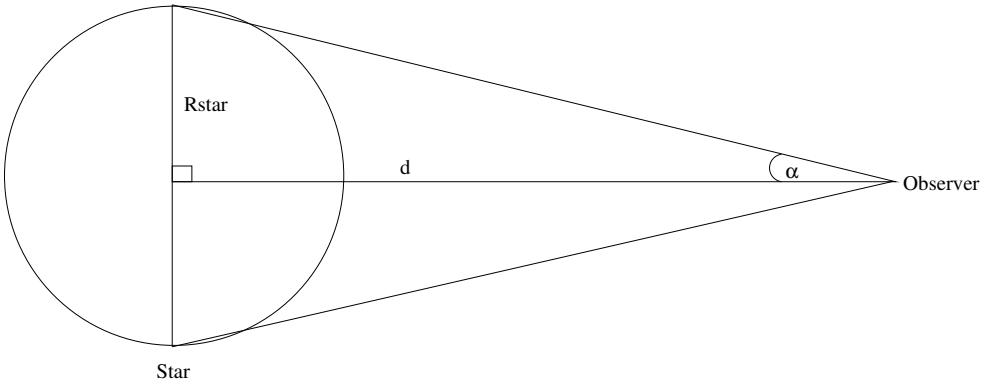

Figure 4.1: Angular diameter θ.

Using a right triangle in which the sides are the radii and distance to the star (see Figure 4.1), one can calculate the angle between the center and the edge of the star α as follows

$$\tan\alpha = \frac{R_\star}{d} \tag{4.9}$$

but usually d is big compare to the radii of the star, so α is small and we can do the approximation

$$\tan\alpha \approx \alpha \tag{4.10}$$

and the angular diameter is

$$\theta = 2\alpha = \frac{2R_\star}{d} \tag{4.11}$$

Finally assuming that our stars behave like a black body

$$F(d) = \frac{\sigma T_{eff}^4 \theta^2}{4} \tag{4.12}$$

So the effective temperature is

$$T_{eff} = \left(\frac{4}{\sigma}\right)^{1/4} \theta^{-1/2} F(d)^{-1/4} \tag{4.13}$$

We can see in equation (4.13) that the effective temperature of a star depends on its angular diameter and the total flux observed. Due to the great distances between stars the first quantity is extremely difficult to measure even for the closest stars, but some positive results can be obtained using several methods such as interferometry, lunar occultations, eclipsing binaries and photometric radii to name a few. The second quantity involved is the bolometric flux, but due to our atmosphere we can only observe some parts of the electromagnetic spectrum, or bands, making it almost impossible to obtain an entire spectrum.

For this reason we obtain T_{eff} mainly from indirect methods such as measuring the slope of the Paschen continuum (Hydrogen transition from $n = 3$ to the continuum level) and compare it with a model, using the Balmer jump or using equivalent widths of metal lines for example.

4.2 The Infrared Flux Method

One useful indirect method to determine effective temperatures in F, G and K stars is the Infrared Flux Method (IRFM) proposed by Blackwell and Shallis [1977]. As showed in the previous section the observed bolometric flux depends on the angular diameter and strongly on the effective temperature of the star. The IRFM relies on the fact that the observed infrared monochromatic flux on Earth ($F_{IR}(\oplus)$) depends on the angular diameter but weakly (to the first power) on temperature, i.e

$$F_{IR}(\oplus) = \left(\frac{\theta}{2}\right)^2 \phi(T_{eff}, g, \lambda_{IR}) \tag{4.14}$$

where $\phi(T_{eff}, g, \lambda_{IR})$ is the monochromatic surface flux of the star and $F_{IR}(\oplus)$ is the flux at infrared wavelengths received on Earth. The ratio between the bolometric and monochromatic infrared flux

$$\mathcal{R} = \frac{F_{bol}(\oplus)}{F_{IR}(\oplus)} \tag{4.15}$$

is independent of the angular diameter of the star. Using spectral models and the inverse square law for fluxes, we can calculate $\mathcal{R}$ at the surface of the star, which if our selected model is correct it should be equal to the observed ratio

$$\mathcal{R} = \frac{F_{bol}(\oplus)}{F_{IR}(\oplus)} = \frac{\sigma T_{eff}^4}{F_{IR}(model)} \tag{4.16}$$

The bolometric flux $F_{bol}(\oplus)$ can be calculated using model atmospheres that account for the flux taken outside the observed filters (bolometric correction). For example if we have observations in the Johnson filter

V and the infrared 2MASS system filter K_s, the flux encompassed by those filters (from models) will be $F_{V-K_s}(model)$ and the fraction of flux $\mathcal{C}$ of the total flux will be

$$\mathcal{C} = \frac{F_{V-K_s}(model)}{F_{bol}(model)} \tag{4.17}$$

and by dividing our observed flux in a given filter by this fraction we can obtain the bolometric flux

$$F_{bol}(\oplus) = \left(\frac{1}{\mathcal{C}}\right) F_V^{std}(\oplus) 10^{-0.4(m_V - m_V^{std})} \tag{4.18}$$

where m_V is the V magnitude of the target and $F_V^{std}(\oplus)$, m_V^{std} are the flux and magnitude of a standard star in the same filter.

The monochromatic infrared flux $F_{IR}(\oplus)$ can be obtained by applying a conversion factor $q(\lambda_{IR})$ to the observed flux in a given band

$$F_{IR}(\oplus) = q(\lambda_{IR}) F_{IR}^{std}(\oplus) 10^{-0.4(m_{IR} - m_{IR}^{std})} \tag{4.19}$$

where m_{IR} is the infrared magnitude of the target star in a given band and $F_{IR}^{std}(\oplus)$, m_{IR}^{std} are the infrared flux and magnitude of the calibrator star in the same infrared filter.

Using a combination of stellar models and observational data you can calculate a relation between the color and metallicity of a star and its effective temperature.

In this work we use the calibrations of González Hernández and Bonifacio [2009] and compare it with the calibration of Casagrande et al. [2006] for the color $V - K_s$. The first study presents an implementation of the IRFM for FGK stars (dwarfs and giants) and the second is a calibration for G an K dwarfs. Both works present the same polynomial fitting function:

$$\theta_{eff} = \frac{5040}{T_{eff}} = a_0 + a_1 X + a_2 X^2 + a_3 X[Fe/H] + a_4[Fe/H] + a_5[Fe/H]^2 \tag{4.20}$$

where a_i are the coefficients of the polynomial, X is the color and $[Fe/H]$ the iron content of the star.

The color and metallicity ranges of applicability of the calibration for each work are found in Table 4.1 and the value for the coefficients of the polynomial are found in Table 4.2, a comparison between the fitted relations for different metallicities is shown in Figure 4.2.

Table 4.1: Ranges of applicability of the T_{eff}: color-[Fe/H] calibrations.

	Color	Color range	[Fe/H] range
Casagrande et al.	$V - K_s$	[1.124, 3.010]	[-1.87, 0.34]
González Hernández et al.	$V - K_s$	[0.7, 3.0]	[-3.5, 0.5]

Table 4.2: Coefficients of the T_{eff}: color-[Fe/H] calibrations.

	a_0	a_1	a_2	a_3	a_4	a_5
Casagrande et al.	0.4609	0.3069	-0.0263	-0.0145	0.0275	0.0006
González Hernández et al.	0.5201	0.2511	-0.0118	-0.0186	0.0408	0.0033

From Figure 4.2 we can see that both calibrations are fairly insensitive to the metallicity of the star. Using this fact the effective temperatures for the stars were computed making the assumption that all stars have the iron content of the Sun, which is reasonable for such a selected sample of solar type dwarfs.

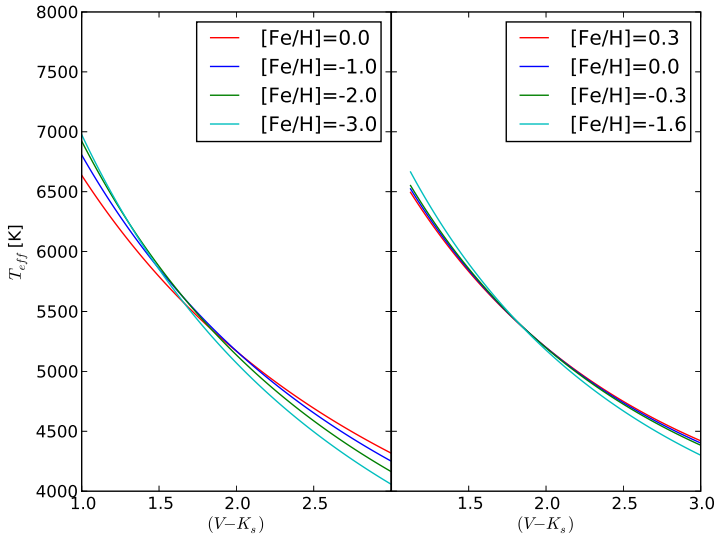

Figure 4.2: Color-Temperature relation found by Hernández et al. (left) and Casagrande et al. (right).

The color range of the sample was $0.76 \leq (V - K_s) \leq 2.69$, so some stars were out of the color range for the calibration of Casagrande et al. [2006]. Figure 4.3 shows a comparison between the values calculated with the different calibrations in the color range of overlap for G and K stars. The errors in this plot and the ones that are used in this work were calculated by propagation of errors in equation 4.20. We can see that the temperatures found with the calibration of Casagrande et al. are slightly hotter than the ones found by Hernández et al., an effect already pointed out in González Hernández and Bonifacio [2009].

Due to the range of applicability of the calibration in terms of color range and metallicity and considering the type of stars in the sample, the values calculated using the work of González Hernández and Bonifacio [2009] were chosen and used in the rest of the results presented here. Figure 4.4 presents the distribution of effective temperatures for the entire sample (excluding spectrum binaries and stars that were included for the calibration of activity), we can see that the peak of the distribution agrees with the effective temperature of the Sun as expected for solar type stars and our selection technique. Also, according to the distribution, most of the stars in the sample correspond to G stars (5200 K $< T_{eff} <$ 6000 K), the second big population is made of K stars (3700 K $< T_{eff} <$ 5200 K) and finally we have a few F stars (6000 K $< T_{eff} <$ 7500 K).

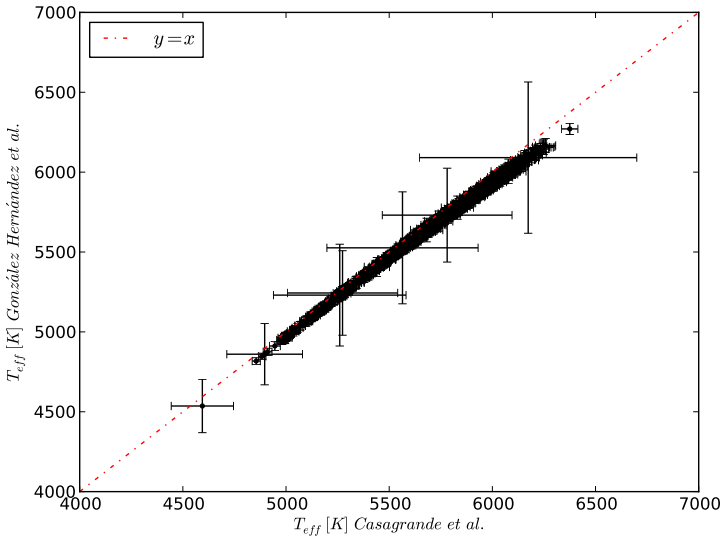

Figure 4.3: Comparison between the temperatures for our G and K stars found with the calibrations of González Hernández and Bonifacio and Casagrande et al.

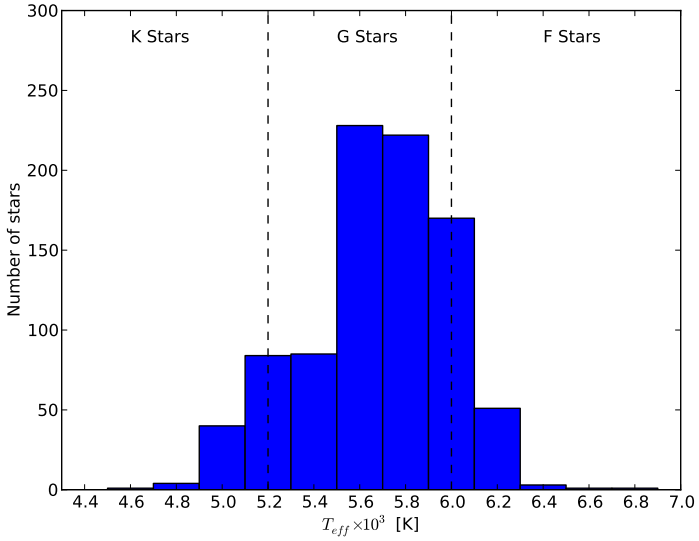

Figure 4.4: Distribution of temperatures calculated using the work of González Hernández and Bonifacio [2009] for the sample.

Chapter 5

Radial Velocities

This chapter describes the method used to calculate radial velocities for the stars in the sample. Section 5.1 describes the Doppler Effect, section 5.2 introduces the method used for obtaining the radial velocities and presents the distribution of velocities for the stars. The results in this chapter will be used to obtain the complete kinematics in Chapter 8.

5.1 The Doppler Effect

The Doppler Effect was proposed in 1842 by the Austrian physicist Christian Doppler (1803-1853) and established that an observer in relative motion from a front of waves will detect a change in wavelength in the received signal. Due to the behavior of waves the light is also affected by this phenomenon and in the case of non relativistic velocities the change in wavelength can be expressed as follows

$$\frac{\Delta\lambda}{\lambda} = \frac{\lambda_{obs} - \lambda_{rest}}{\lambda_{rest}} = \frac{V_r}{c} \tag{5.1}$$

where λ_{obs} and λ_{rest} are the observed and rest frame wavelength, c the speed of light and V_r the radial velocity of the source. So if we are able to determine the observed wavelength and we know exactly at what wavelength that wave was emitted we can calculate the radial velocity of the source. In stellar astronomy this is usually done by observing several absorption lines in the spectrum of a star and measuring the shift of each line.

Thanks to the Doppler effect and the advances in spectroscopy, we nowadays can calculate radial velocities with great accuracy to a plethora of objects such as stars, galaxies, quasars and molecular clouds.

5.2 Correlation Analysis

One powerful tool to determine radial velocities is the analysis of the observed spectrum using cross correlation with a template that could be a synthetic spectra or other reference star. This technique is described in detail in the work of Tonry and Davis [1979], and what it does in general terms is to take the cross correlation function (CCF) in Fourier space between the object of study and its template and assumes that the template spectrum broadened and shifted in wavelength is approximately the observed spectrum. By doing a χ^2 minimization between the observe CCF and an analytical function that describes the expected CCF of a broadened and shifted spectrum, it is possible to obtain the shift of the observed spectrum and hence the radial velocity of the star.

To calculate radial velocities the IRAF[1] package noao.rv was used. That package provides the task fxcor that correlates the spectrum after applying a continuum fitting and a Fourier filtering in order to eliminate the high and low frequency noise. The continuum fit was made using a third order spline and an inspection by eye for some spectrum using the interactive mode of fxcor showed that the fitting worked fine. The Fourier filtering was a key factor to reduce the errors in the measurements, tests for a sample of stars with and without the filtering process (using a Hanning filter) showed that the dispersion and errors between the radial velocities computed using different templates were notoriously reduced once the Fourier filtering was used to avoid low and high frequency noise.

Other parameter that helped to reduce the errors in the measurements was the length of the spectrum considered in fxcor to get the radial velocity. Due to its high resolution, FEROS spectrum is composed of $\sim$ 190000 pixels and the Fourier transform was very time consuming. Better results were obtained in the CCF using a small part of the spectra and also the procedure became considerable faster. Taken this into account the fxcor task was applied in two regions with abundant absorption lines of 500 Å each: from 4000 Å to 4500 Å and from 5000 Å to 5500 Å.

Instead of using spectral models, 17 stars from the sample were used. These stars have known radial velocities from the GCS and did not present large radial velocity variations (see Table 5.1).

Table 5.1: Radial velocity template stars.

Hipparcos Number	Radial Velocity (GCS) [km/s]
HIP 6125	31.8 ± 2.7
HIP 7693	26.0 ± 0.3
HIP 11514	18.3 ± 0.2
HIP 13889	11.5 ± 0.2
HIP 13908	7.6 ± 0.1
HIP 14774	21.4 ± 0.4
HIP 79149	-52.6 ± 0.2
HIP 81229	-17.8 ± 0.1
HIP 88650	14.6 ± 0.5
HIP 90896	11.6 ± 0.1
HIP 96881	-10.8 ± 0.2
HIP 98599	-15.1 ± 0.1
HIP 100359	12.4 ± 0.3
HIP 100474	-1.5 ± 0.1
HIP 100649	10.4 ± 0.1
HIP 114590	4.3 ± 0.3
HIP 114967	7.8 ± 0.2

Because the observations were taken during three years, the spectrum from the calibration lamps passed the same treatment as the stars, in order to take into account possible relative velocity shifts due to the instrument. The shifts between the lamps did not exceed 300 m/s for the entire sample in the three years of data, proving the great stability of FEROS. This shift was corrected to the final calculation of the radial velocity.

For every template we obtained one radial velocity that was calculated as follows

$$V_r = V_{r\ relative\ \ stars} - V_{r\ relative\ \ lamps} + V_{r\ \ GCS} \tag{5.2}$$

Then the final radial velocity was computed as the mean radial velocity obtained from the templates

[1]IRAF is written and supported by the IRAF programming group at the National Optical Astronomy Observatories (NOAO) in Tucson, Arizona. NOAO is operated by the Association of Universities for Research in Astronomy (AURA), Inc. under cooperative agreement with the National Science Foundation

$$V_{r\ final} = \frac{1}{N_{templates}} \sum_{i=1}^{N_{templates}} V_{r,i} \tag{5.3}$$

The errors of the radial velocities for every star were obtained from the width of the CCF and the final error of the measurement was calculated using propagation of errors.

Including the template stars, an overlap of 235 stars with the GCS was found. In order to test the accuracy of the radial velocities found here, a comparison between the radial velocities for the stars in common was made. Figure 5.1 shows the comparison between the radial velocities obtained in this work and the GCS; we can see that the agreement was good except for a few stars (∼5 % of the stars in common were outliers).

This disagreement is probably caused by bad observing conditions, saturation and cosmic rays. Some of these outliers correspond to the brightest stars (in apparent magnitude) in the sample and some had two spectra with different exposure times, the ones with the shortest exposition time gave a value in agreement with the GCS. The saturation and/or excess of cosmic rays alters the shape of the spectrum and hence the cross correlation analysis delivers a wrong velocity. Inspection of the spectra does not indicate any binary companions.

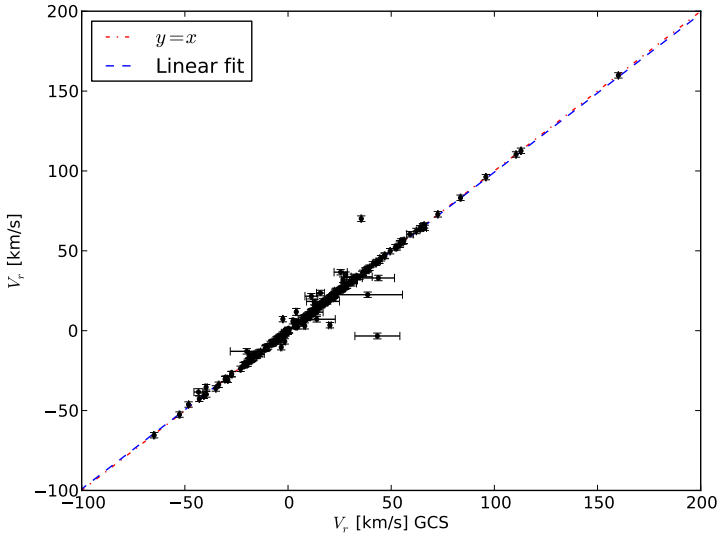

Figure 5.1: Comparison between the radial velocities obtained in this work and the Geneva-Copenhagen Survey.

When the radial velocities were computed, the spectra that were overexposed or had too many cosmic rays gave extremely high velocities (of the order of thousands km/s) and high dispersion between the values measured from the different templates. To take out these cases the spectra that had $V_r \leq 500$ km/s and dispersions between measurement of the templates $\sigma_{templates} \leq 500$ km/s were left out. Then the cases were I had two spectra of the same star that had different radial velocities were checked and the ones that were in agreement with the literature (in case we found a measurement) were kept.

By putting the spectrum of the stars in the rest frame using the computed radial velocities, it was found that the velocity computed for the stars that are spectrum binary candidates (see Chapter 3) were not entirely incorrect and most of the times it fitted one of the components seen in the spectrum (see Figure 3.2 for an example). For this reason, these stars were kept for the kinematical analysis (see Chapter 8).

Figure 5.2 shows the distribution of radial velocities obtained in this work. We can see that the distribution is very symmetric and centered near the velocity of the Sun. A gaussian fit gave a mean $\mu = 10$ km/s and a width $\sigma = 29.8$ km/s.

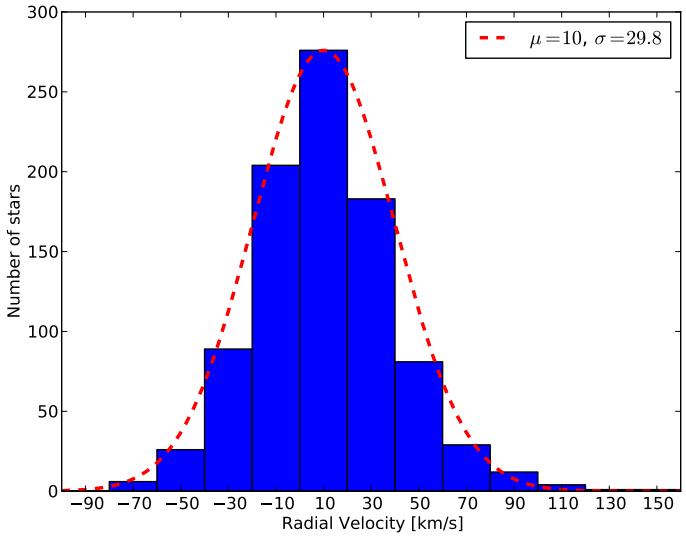

Figure 5.2: Distribution of radial velocities and a gaussian fit for the distribution.

Figure 5.3 presents the radial velocities mean errors for the sample. The peak of the distribution is near 1.7 km/s and no stars with errors higher than 2.8 km/s were present.

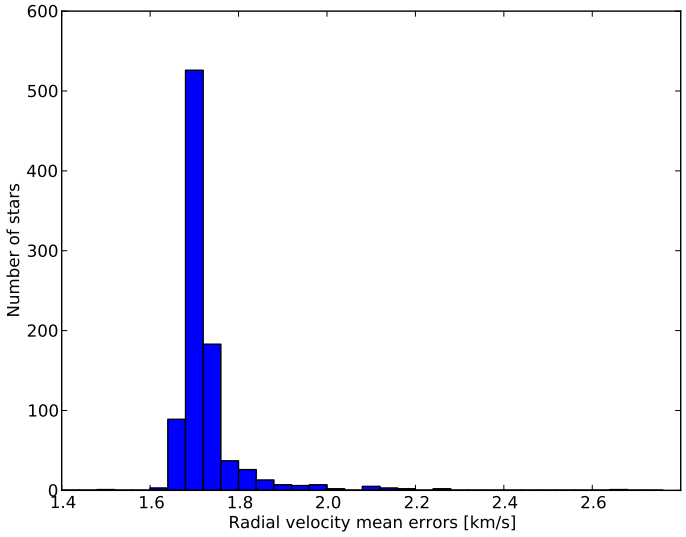

Figure 5.3: Distribution of the mean radial velocities errors.

Chapter 6

Metallicities

This chapter describes the method for obtaining metal abundances for the stars in the sample. Section 6.1 describes the stellar parameters that are important to obtain the metallicities, section 6.2 describes the method to obtain the rotational velocities for the stars, section 6.3 presents the lines used to estimate the metal abundances and the continuum normalization used in this work, section 6.4 presents the distribution of metallicities and compare the values with other works and finally section 6.5 analyzes the relationship between metal content of a star and extrasolar planets. The results of this chapter will be used to establish the age of the stars in Chapter 7.

6.1 Stellar Parameters

Obtaining metal abundances is important to understand the chemical evolution of the galaxy and because it is a key parameter in the determination of stellar ages.

In this work the metal abundances for the stars in the sample were obtained by doing a χ^2 minimization, comparing the observed spectra with a grid of models written using the WITA6 program (Pavlenko [2000]), following the same procedure as Jenkins et al. [2008].

χ^2 minimization is of vital importance to carefully select the correct model to do the comparison with the observed spectrum. For that reason a detailed knowledge of the physical processes that help to form and change the shape of the spectrum is crucial. The shape of the stellar spectra and absorption lines are mainly dependant on four parameters: the effective temperature, the surface gravity, the chemical composition of the star and the stellar rotation.

The effective temperature affects the peak of the black body emission and the degree of ionization of the different elements in the stellar atmosphere. The effective temperatures for our stars were computed using the Infrared Flux Method and, as explained in Chapter 4, this method is fairly independent of the metal abundance of the star.

The surface gravity ($\log g$) affects the gradient pressure (through hydrostatic equilibrium) and determines the densities at which the absorption lines are formed. As discussed in Chapter 4, there are some spectral indices used to compute the surface gravity, but $\log g$ was left as a free parameter in the grid of models. The surface gravities used in the grid of models covered a wide range of values from 3.5 to 5.0 dex in steps of 0.5. Jenkins et al. [2008] found that the metalicities computed leaving $\log g$ as a free parameter were only weakly dependant on this physical quantity.

The chemical composition has the effect of changing the opacity and the relative strength of spectral lines of different elements. A good tracer of the overall metallicity of a solar type star is made by measuring the abundance of a heavy element like Fe, because stars rich in Fe tend to be rich in other heavier elements. The grid of models used in this work uses a range in [Fe/H] from -1.5 to 0.5 dex.

Other physical parameters that can alter the shape of the lines are caused by motions of the stellar atmosphere: microturbulence, macroturbulence and stellar rotation. Microturbulences are small scale mass motions compared to the unit optical depth and macroturbulence are mass motions with sizes larger than the unit optical depth, both are due to granulations in convective zones and non-radial oscillations. These motions introduce a Doppler shift in the spectral lines, changing their shapes and leading to potentially incorrect determinations of metal abundances. Jenkins et al. [2008] found that the effects of micro and macroturbulence are small compared to stellar rotation for the stars in his sample using weak lines which are formed deeper in the star and are less affected by microturbulence.

6.2 Rotational Velocities

As pointed out in the previous section the most dominant stellar atmosphere motion that can affect the metallicity estimation is the stellar rotation. Due to the Doppler Effect the rotational velocity has the effect of broadening the absorption lines of the star, affecting the line profile and hence the estimation of the abundance.

One method to find the projected rotational velocity of the star ($v \sin i$) for slow rotators (velocities up to $\sim$ 25 km/s) was proposed by Smith and Gray [1976] and consists of taking the Fourier spectrum of an absorption line. The observed line is modeled as the convolution between the instrumental profile of the spectrograph and a rotational profile, that has an analytic expression in a solid rigid approximation. If we divide the Fourier transform of the line and the Fourier transform of the instrumental profile we can obtain the rotational profile of our star. The shape of the rotational profile is the same for every $v \sin i$ but increasing the rotational velocity has the effect of producing a translation of the Fourier transform of the rotational profile to lower frequencies. By comparing the observed profile with a set of modeled profiles it is possible to estimate the rotational velocity of a star. This technique is fully described in Gray [2008].

Another method makes use of the cross correlation function (CCF) in order to estimate $v \sin i$ (Benz and Mayor [1984], Santos et al. [2002]). The CCF acts as an absorption line in the sense that is sensitive to any change in the spectral lines caused by physical processes and also instrumental effects. The width of the CCF σ is affected by the temperature, surface gravity, metallicity, the magnetic field and the rotation of the star which is independent of the stellar atmosphere properties.

The metallicity content of a star changes the width of the CCF by increasing the number of saturated lines as the metallicity increases. To avoid this the CCF must be dominated by weak lines that are less sensitive to saturation. Benz and Mayor [1984] showed that the broadening caused by magnetic fields is important for K and M stars. The sample is made of mostly F and G stars with a few K stars and no M stars.

Considering that each star in the sample has essentially the same instrumental profile, it is expectable that at a given temperature and gravity the stars with no rotation will have a minimum width of the CCF (σ_0) and the excess of width is caused mainly by the rotational velocity of the star. Benz and Mayor [1984] have shown that the width of the CORAVEL CCF can be related with the rotational velocity as follows

$$v \sin i = A\sqrt{\sigma^2 - \sigma_0^2} \tag{6.1}$$

Following the procedure of Santos et al. [2002] to find σ_0, the width σ of each star versus the color $(V - K_s)$ was plotted (Figure 6.1) and the lower envelope of the distribution of points was adjusted. This lower envelope represent the minimum width σ_0, i.e, the stars with no rotation. For the stars in the sample a third degree polynomial was fitted (equation 6.2). The top panel of Figure 6.1 shows the distribution of σ for the entire sample and we can see that, with some exceptions, no stars can be found below the fitted envelope (that represent the stars with no rotation). The bottom panel is a zoomed area of the top panel and it shows the fitted envelope and with dashed lines an uncertainty of ± 0.025 km/s in the adjusted line.

$$\sigma_0 = 8.337 - 3.632(V - K_s) + 1.540(V - K_s)^2 - 0.214(V - K_s)^3 \tag{6.2}$$

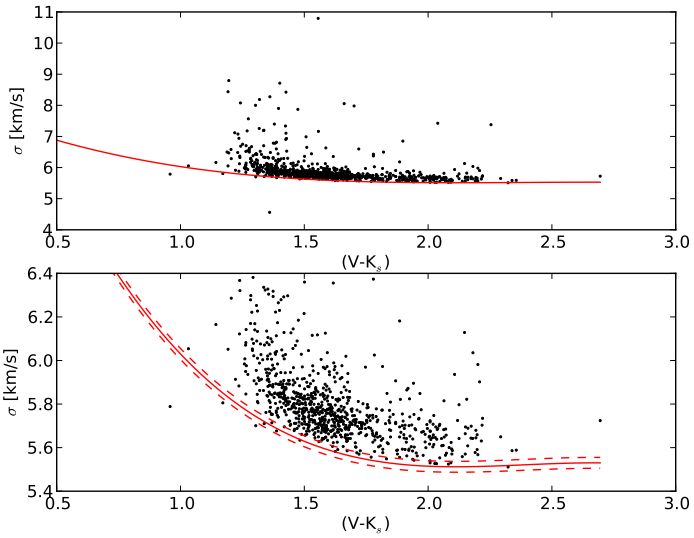

Figure 6.1: σ vs $(V - K_s)$ for the entire sample (top) and a zoomed area (bottom) showing the adjusted lower envelope representing σ_0 (red line). The dashed lines in the bottom graph represent an uncertainty of ± 0.025 km/s.

The determination of A is done by selecting stars that are suspected to be non rotators, convolve their CCF with different rotational profiles and measure the change in σ. Using different instruments Queloz et al. [1998] and Santos et al. [2002] found a value of $A = 1.9 \pm 0.1$, which was adopted in this work.

Using equation 6.1 and a value of $A = 1.9$, the $v \sin i$ for the stars in the sample were computed. Then the projected rotational velocity values were compared against the values of the GCS and Valenti and Fischer [2005] for the stars that were in common.

Figure 6.2 shows a comparison between the values found in this work, the GCS and Valenti and Fischer [2005] values and also a comparison between the last two. The same is shown in Figure 6.3 for the residuals. From both figures we can see that there is a spread in the $v \sin i$ values between every work and this spread is bigger if we increase the rotational velocity. The standard deviation of the residuals is 0.99, 1.56 and 2.11 km/s for this work versus Valenti and Fischer [2005], this work versus GCS and GCS versus Valenti and Fischer [2005] respectively. The higher standard deviation of the residual GCS versus Valenti and Fischer [2005] is due to the presence of an outlier and if we take out this value the standard deviaion drops to 1.43 km/s.

6.3 Line Selection and Normalization

The lines selected in this work were the same iron lines used in Jenkins et al. [2008]. The lines were selected because they appear unblended in the FEROS spectra and also they are weak. Weak lines are more sensitive to changes in the model parameters because they are not saturated and hence they are in the linear part of the curve of growth. Also they formed deeper in the stellar atmosphere and are less affected by microturbulence. A list of the lines with their rest frame wavelength, oscillator strength (gf) and excitation energies are shown in Table 6.1.

The FEROS data did not have a flux calibration so the spectra presented a gradient across the entire wavelength. To find the continuum in the data, the `IRAF` task `continuum` from the `noao.onedspec` package was used in three wavelength ranges where the lines used in the determination of abundances were present.

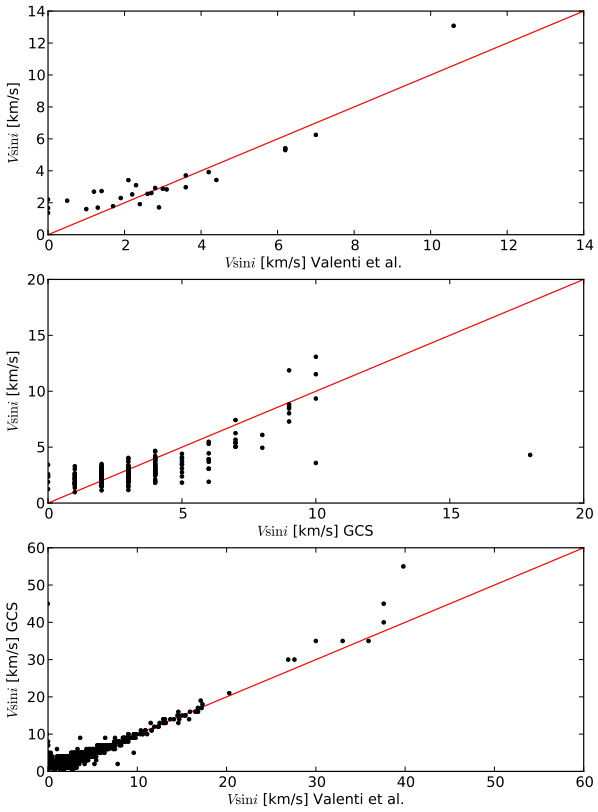

Figure 6.2: Comparison between the $v \sin i$ values of this work vs Valenti and Fischer [2005] (top), this work vs the GCS (middle) and the GCS vs Valenti and Fischer [2005] (bottom).

6.4 Metal Abundances

Before computing the metal abundances, the radial velocities computed in Chapter 5 were used to put the observed spectrum in the rest frame, then the continuum normalization was performed in the regions were the lines described in Table 6.1 were present.

The `IDL` code of Jenkins et al. [2008] was used to compute the [Fe/H]. The first step in the program was to take the effective temperature from Chapter 4 and find the models with the nearest upper and lower temperatures. Then the models were broadened to account for the broadening caused by stellar rotation using the velocities found in this work and the rotational profile of Gray [2008]. Also the broadening caused by the instrumental profile of FEROS was taken into account using an instrumental profile with a gaussian shape and a width calculated from the resolution of FEROS of $R = 48000$, which at the wavelengths of the absorption lines correspond to ~ 0.15 Å.

After the synthetic spectra were broadened, each line in Table 6.1 was compared with the lines from the models using a χ^2 approach. The χ^2 is a function that compares one observation with a model and considers the errors in the measurements (see equation 6.3).

$$\chi^2 = \frac{(O - M)^2}{\sigma^2} \tag{6.3}$$

O is the observed line, M is the model, σ is the error in both and the sum is over wavelength channels.

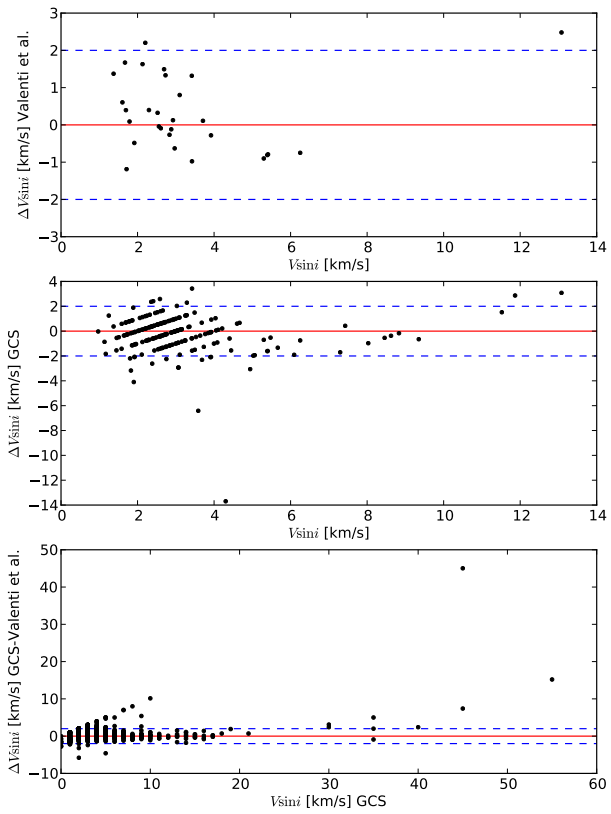

Figure 6.3: Residuals ($\Delta v \sin i$) between the $v \sin i$ values of this work vs Valenti and Fischer [2005] (top), this work vs the GCS (middle) and the GCS vs Valenti and Fischer [2005] (bottom). The dashed blue lines represent an uncertainty of ± 2 km/s.

By minimizing this function it is possible to find the model with the best parameters that fit our observation.

The typical width of the lines was ~ 0.2 Å, so the χ^2 was applied to each line in a region of 0.4 Å of width around the center in order to include the wings of absorption feature. As the program works with a fixed window it will include more continuum in some lines than others, so the median value of the χ^2 was used to eliminate any outliers. For every model with different surface gravity a χ^2 value for the metallicity was obtained and a second order polynomial fit was applied for the different values of $\log g$ and [Fe/H]. The minimum of this polynomial fit represents the metal abundance of the target star and the fitted χ^2 was used to determine the 1, 2 and 3σ error values (see Figure 6.4).

Due to the range in metallicities of the models (-1.5 to 0.5 dex) some stars that have a metal abundance lower than [Fe/H]$=-1.5$ are out of the grid limits and the abundance for these stars was set to the minimum value of the grid.

Figure 6.5 presents a comparison between the values computed in this work and the photometrically determined values using Strömgren bands (*uvby*) of the Geneva-Copenhagen Survey and the high resolution spectroscopic values in Valenti and Fischer [2005]. The standard deviation for the rest between the metallicities for the metal abundances computed this work and Valenti and Fischer [2005] and this work and the GCS was 0.29 and 0.28 respectively and the comparison between GCS and Valenti and Fischer [2005] had a lower standard deviation equal to 0.09. Despite the use of different methods between the works we can see a good general agreement between the values for the stars in common, except for some metal rich stars in which we see an underestimation in [Fe/H] compared to the values of the GCS and Valenti and Fischer [2005].

Table 6.1: Fe lines used in the abundance measurements.

Element	λ (Å)	gf	E(keV)
FeI	5806.723	1.096E-01	4.610
FeI	5852.215	5.623E-02	4.550
FeI	5855.082	2.239E-02	4.610
FeI	5856.086	2.291E-02	4.290
FeI	6027.051	5.888E-02	4.070
FeI	6151.621	4.266E-04	2.180
FeI	6159.379	1.148E-02	4.610
FeI	6165.359	2.754E-02	4.140
FeI	6173.340	1.259E-03	2.220
FeI	6229.227	9.120E-04	2.840
FeI	6608.027	9.120E-05	2.280
FeI	6627.547	2.570E-02	4.550
FeI	6703.566	8.318E-04	2.760
FeI	6725.359	5.370E-03	4.100
FeI	6750.152	2.344E-03	2.420
FeI	6810.266	8.710E-02	4.610
FeI	7158.477	1.148E-03	3.650
FeI	7189.152	1.585E-03	3.070
FeI	7445.758	6.761E-01	4.260
FeI	7491.656	8.710E-02	4.300
FeI	7568.906	1.288E-01	4.280
FeI	7586.023	7.079E-01	4.310
FeI	7751.109	1.514E-01	4.990
FeI	7780.562	1.148E+00	4.470
FeI	7807.914	2.754E-01	4.990
FeI	7832.207	1.259E+00	4.430
FeI	8047.625	2.239E-05	0.860
FeI	8239.137	3.715E-04	2.420

This underestimation of the metallicity should not be caused by the determination of the stellar velocity of rotation $v \sin i$, because as we saw in the previous section there is a lot of scatter between the values when we compared with different works, so a bad estimation of the stellar rotation profile should induced a random error and not a systematic effect as the one we observed for some metal rich stars. A revision of the normalized and rest frame spectra used to compute the metallicities for those stars led to the conclusion that due to the bad S/N the normalization of the spectrum was not the optimal, thus affecting the χ^2 fitting in the sense that the absorption lines appeared weaker than they really are, leading to lower metal abundances. Also in other cases, and for the same cause, the radial velocity was not accurate enough to shift the centroid of the line in the correct restframe wavelength so the observed spectrum presented a small shift at the time of comparison with the synthetic model. These two effects acted as a bias toward lower metallicity values and for future work a careful inspection of the normalization (and probably a re-normalization) is advised.

Also, Figure 6.5 presents a comparison between the metallicities for the stars in common between the GCS and Valenti and Fischer [2005]. Even if both works have good general agreement, we can see that there is a spread between their values and a systematic whereby the values from Valenti and Fischer [2005] tend to be higher in iron content than the ones derived from the GCS.

Figure 6.6 shows the total distribution of metallicities computed in this work (excluding the spectrum binaries) and as a comparison the distributions found in Valenti and Fischer [2005] and the GCS. As mentioned before, stars with metal abundances lower than -1.5 dex are left out of the grid of models and the program assigned the lower metallicity value in the grid to these stars. Of a total sample of 890 stars, 16 had metallicities lower than -1.5 dex and this is reflected in the lower part of the [Fe/H] distribution.

The peak of the distribution found in this work is at ~ 0.1 dex, which is close to the peak that is seen in

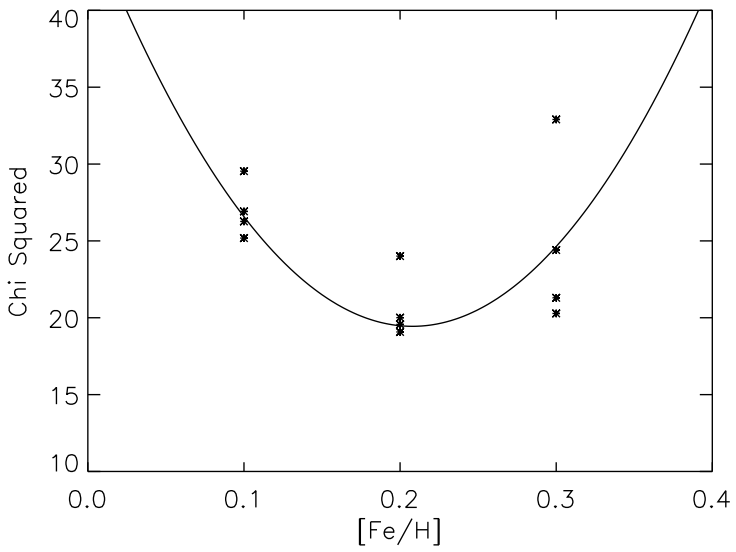

Figure 6.4: Image taken from Jenkins et al. [2008] showing the χ^2 fit for HIP 1803. The points represent the means of four different surface gravities at each metallicity value. Also it is shown the second order polynomial fit.

the distribution of Valenti and Fischer [2005]. Both samples are biased to metal rich stars due to selection effects so they do not reflect the metal abundance distribution of the solar neighborhood. The distribution of the GCS is an unbiased sample because their stars were selected with a volume limited criteria; we can see that the GCS distribution has a different peak than our sample at ~ -0.2 dex and is more symmetric than the distribution of this work and Valenti and Fischer [2005].

Figure 6.7 presents the distribution of $1-\sigma$ errors for the metalicities found in this work. We can see that the distribution has a peak at $\sim \pm 0.07$ dex, then drops until $\sim \pm 0.15$ dex and goes up to a bump at $\sim \pm 0.20$. This second bump and the extension to higher uncertainties are mostly stars with bad S/N due to poor weather conditions at the time of taking the spectrum.

6.5 Planets and Metallicities

As the sample of discovered extrasolar planets grew, an important relation between the stars that host at least one planet and their metallicity became clear: one has a higher probability of finding planets in a metal rich star than in a metal poor one. Figure 6.8 presents the distribution of metallicities of the stars that host planets and we can see that more planets have been found in metal rich stars than in metal poor ones, this trend steadily increases until the distribution reaches its peak at [Fe/H] ~ 0.2 and then drops. The drop in the distribution is caused by the lack of metal richer stars in the solar neighborhood which is were most of all the planet search are focus.

This interesting link between the host star and the planet can be explained by two main hypothesis (Cassen et al. [2006], Udry and Santos [2007]): either the metallicity of the star plays a role in the formation of planets or the stellar atmosphere that host the planet has been contaminated with metal rich material from another source like a planet that has migrated all the way into the star. The discussion of this subject has not yet settled, but apparently the metallicity plays a key role by increasing the probability of forming planetary systems at the time of stellar formation in the sense that they possess a disk with more metals that favours

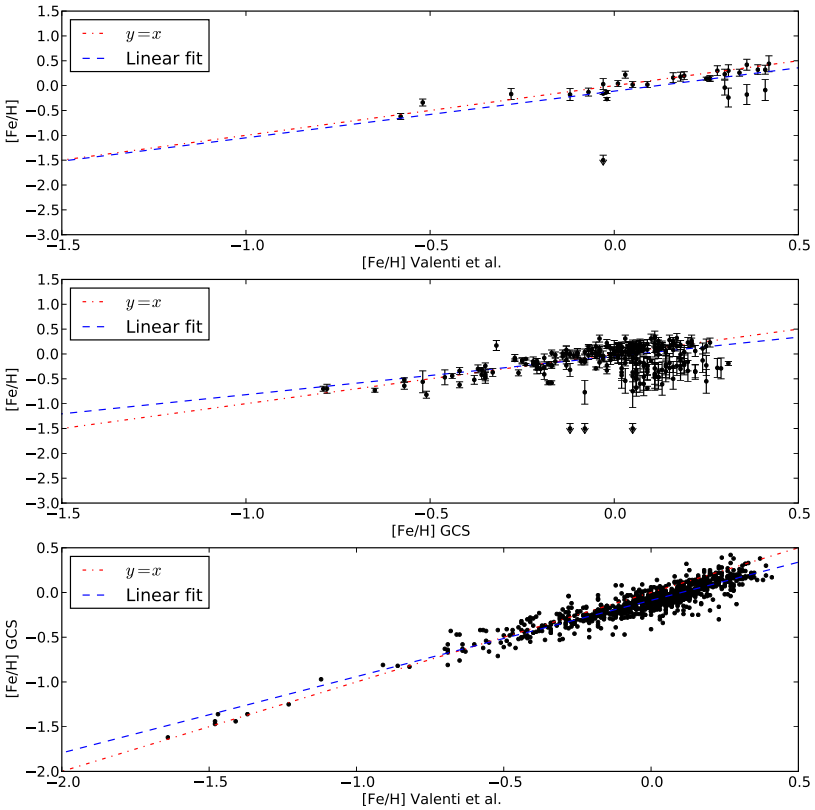

Figure 6.5: Comparison between the metallicities for the stars in common with Valenti and Fischer [2005] (top) and the Geneva-Copenhagen Survey (middle). The stars that had metallicities lower than −1.5 dex are marked with arrows. In the bottom panel we present a comparison between the values of the GCS and Valenti and Fischer [2005].

the process known as core accretion in which the planets are formed by the merging of smaller structures (planetesimals).

Fischer and Valenti [2005] calculated the probability of forming a gas giant planet with an orbital period shorter than 4 yr that induced velocity amplitudes greater than 30 m/s in the host star. They found that this probability increases with metallicity, following a power law described by

$$P(planet) = 0.03 \times 10^{2.0[Fe/H]} \tag{6.4}$$

Using equation 6.4 is possibly to calculate the number of planets that could be detected in our sample of 890 stars. For the stars in our sample we found that ~ 28 gas giant planets should be present in our sample that follows the characteristics described in the previous paragraph. This result considers the underestimation of the metallicities discussed in the previous section, so this number will probably increase.

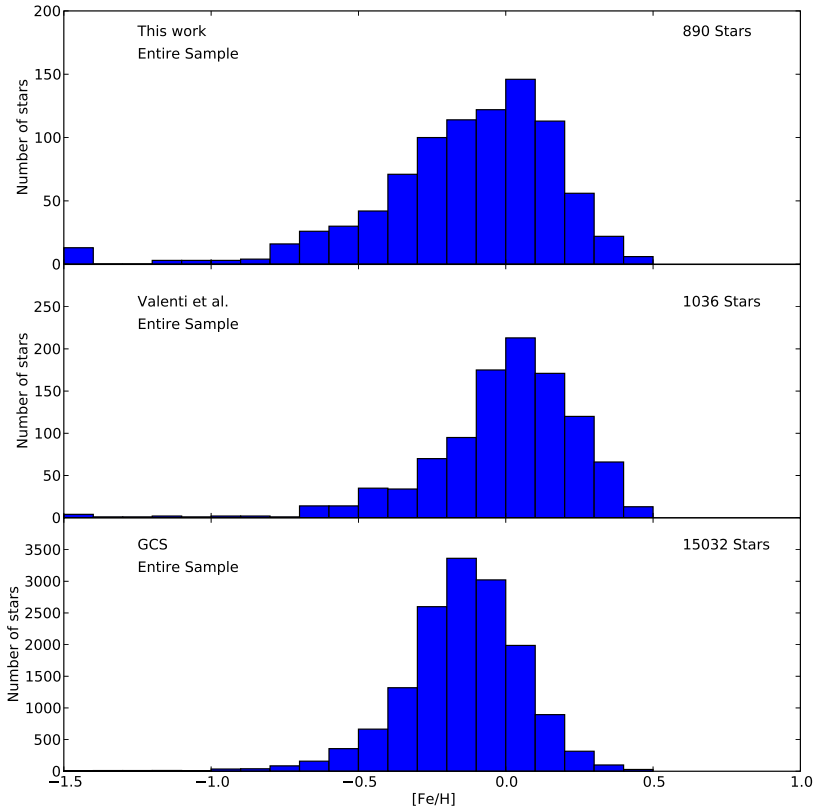

Figure 6.6: Distribution of metallicities for this work (top), Valenti and Fischer [2005] (middle) and the Geneva-Copenhagen Survey (bottom).

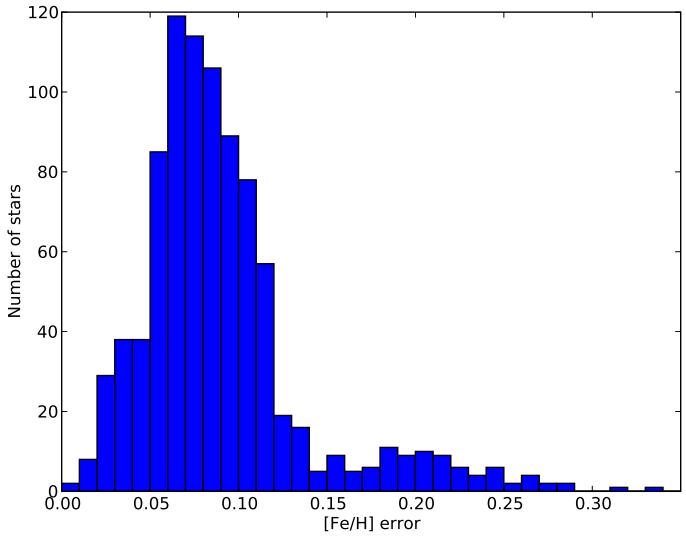

Figure 6.7: Distribution of $1-\sigma$ errors in the determination of [Fe/H].

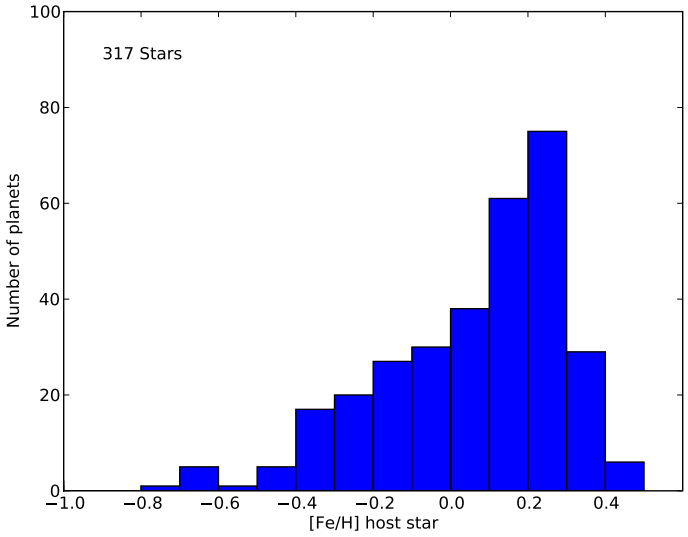

Figure 6.8: Distribution of metallicities for stars that host extrasolar planets, the data was taken from `http://exoplanet.eu/` in September of 2009. We can see that the number of planets discovered increases as the metallicity increases. The drop at ~ 0.3 dex is due to the lack of metal rich objects in the solar neighborhood.

Chapter 7

Stellar Ages

This chapter describes the method used to compute ages for the stars in the sample. Section 7.1 analyses the importance of the HR diagram for astronomy, section 7.2 presents the isochrone set used in the age estimation, section 7.3 describes the method used to calculate the ages, section 7.4 analyses and presents the results for age indicators such as the rotational velocity, the stellar activity and the presence of Lithium absorption lines.

7.1 The Hertzsprung-Russell Diagram

At the beginning of the twentieth century astronomers had spectral classifications and absolute magnitudes for a considerable number of stars. In 1905 the Danish engineer and astronomer Ejnar Hertzsprung (1873-1967) realized that there exists a correlation between the spectral type of a star and its absolute magnitude. At the same time the American astronomer Henry Norris Russell (1877-1957) came to the same conclusion as Hertzsprung. Later the Danish astronomer Bengt Strömgren (1908-1987) named this diagram as *Hertzsprung-Russell diagram* (HR diagram) in honor of its two inventors.

The HR diagram is one of the most important correlations found to date among stellar properties because it can relate the absolute magnitude of a star with its spectral type. The absolute magnitude of a star is nothing other than a measurement of its luminosity and the spectral type of a star can be related to its effective temperature and its color.

Also the position of a star in the HR diagram can tell us a lot information about many physical properties and its evolutionary state. In the HR diagram the vast majority of the stars lie in a band that is called **main sequence** (MS), which is the stage of stellar evolution where the stars live most of their lives burning hydrogen into helium inside their cores through nuclear reactions. The main sequence is not a thin band, it has width produced by the different metallicities of the stars: a star with lower metal abundance than the Sun will have a minor opacity producing a smaller stellar radius (increasing the gravity) and hence a less luminous star. Once all the hydrogen is transformed into helium, in the core the temperature is not enough to start a helium burning nuclear reaction and the star is supported by a hydrogen-helium burning shell outside the core that produces an increase in the output of energy that increases the stellar radius thus decreasing the effective temperature. In the HR diagram the stars moves to the right and up to the stage known as the **subgiant branch**. The boundary between the subgiant branch and the main sequence is known as the **turnoff point**.

The time spent in the main sequence and also in other stages of the stellar evolution that we do not mention in the previous paragraph depend strongly on the mass of the star: stars with $M > 8M_{\odot}$ evolve faster and their lives end differently (with a supernova explosion) than stars with $M < 8M_{\odot}$.

The absolute magnitude in the V Johnson band can be calculated once we know the distance to our star

(see Chapter 8) as follows:

$$M_V = m_V - 5\log(d) + 5 \tag{7.1}$$

where M_V and m_V are the absolute and apparent magnitude respectively and d is the distance to the star in pc units. In Figure 7.1 we show a HR diagram made with data from Hipparcos using 7125 stars that are near 60 pc or less with errors in their parallaxes less than 10%. We can clearly see from the figure the main sequence, the subgiant branch and the horizontal branch.

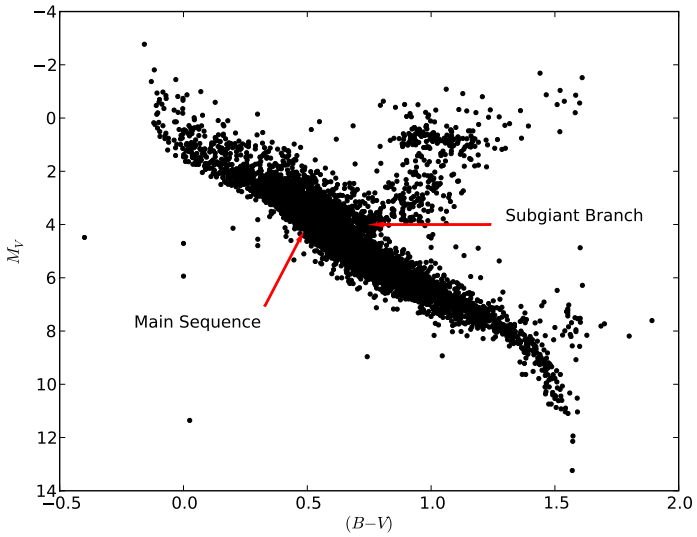

Figure 7.1: Observed HR diagram using 7125 stars from Hipparcos that are near 60 pc or less with errors in their parallaxes less than 10%.

The HR diagram is a fundamental tool in astronomy because it can relate the observations (absolute magnitude, color) with the theoretical work and it allow one to test stellar evolution models. Along with the expansion of the Universe, the HR diagram surely is one of the most important astronomical discoveries of the past century.

Figure 7.2 shows the HR diagram for the stars in the sample using the apparent magnitudes m_V and the color $(B-V)$ from Hipparcos. Because the system is unresolved the spectrum binaries that were found in this work were excluded. We can see that most of our stars are in the main sequence, the spread in the MS due to the metallicity is more evident than the Figure 7.1 and also there are some evolved star that are leaving the main sequence.

7.2 Isochrones

An *isochrone* is the set of points of equal age for stars of different masses in the HR diagram. The use of isochrones started in the 1960s. Thanks to its application in the study of open and globular clusters it has been a fundamental tool in understanding the formation and evolution of the Milky Way.

The set of isochrones chosen for the estimation of ages was the set of the Yale-Yonsei (Y^2) isochrones (Yi et al. [2001]) with the latest version of their stellar evolution code (Demarque et al. [2004]). The Y^2 isochrones cover a wide range in metallicty ($0.00001 < Z < 0.08$) and age (0.1 Gyr $< Age <$ 20 Gyr) and also provides an interpolator[1] written in `FORTRAN` that calculates an isochrone with a given metallicity, α-enhancement and

[1]The interpolator and the set of isochrones can be found in http://www.astro.yale.edu/demarque/yyiso.html .

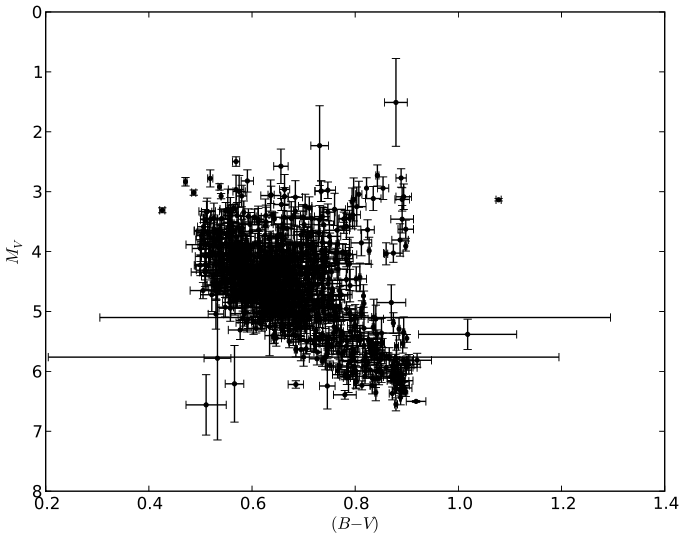

Figure 7.2: HR diagram for the stars in our sample. The absolute magnitudes and $(B - V)$ color were calculated using data from Hipparcos.

a given set of ages based on the original set of Y^2 isochrones.

Figure 7.3 shows an example of a set of Y^2 isochrones for ages in the range 1.25 Gyr to 15.5 Gyr for stars with solar abundance and $[\alpha/Fe] = 0$. It is important to notice that older isochrones have a fainter and redder main-sequence turnoff and also that in the color range $1.0 < (B - V) < 1.8$ all the isochrones are pretty much indiscernible between each other. We will discuss the consequences of this in the next section.

7.3 Age Estimation

Once the metallicities were obtanined, I proceeded to the estimation of the ages of the stars in the sample by performing the technique known as *isochrone fitting*. In simple terms isochrone fitting consist of creating an HR diagram and finding the isochrone that passes through the position of a given star, thus getting an estimate of the age. The errors are computed by doing the same procedure described before but for the position of the errors in M_V and $(B - V)$.

However, as simple the procedure may sound, there is an important catch. The isochrone fitting is best suited for star clusters because we know that all the stars in the cluster are at essentially the same distance and are coeval, so the HR diagram of a cluster closely resembles an isochrone making the fitting of the age more simple. For field stars in the main sequence the things are more complicated mainly because, as we mentioned before, in the MS there is a degeneracy between the isochrones (see Figure 7.3). For that reason age determination for field stars is full of large uncertainties.

Due to errors, ages for field stars are difficult to obtain but if the star has evolved ff the main sequence discrimination is easier. As previously mentioned older isochrones have a fainter and redder main-sequence turnoff and if the star is near that point it is possibly to obtain a more accurate estimation of the age. To established which stars were evolved and which not, we used a polynomial fit of the main sequence taken from Wright [2004] (see equation 7.2). Wright [2004] fitted the main sequence using a ninth-order polynomial using stars taken from the Hipparcos Catalogue that are within 60 pc and with 4σ precision in the parallaxes. The coefficients a_i are 1.11255, 5.79062, -16.76829, 76.47777, -140.08488, 127.38044, -49.71805, -8.24265, 14.07945, -3.43155.

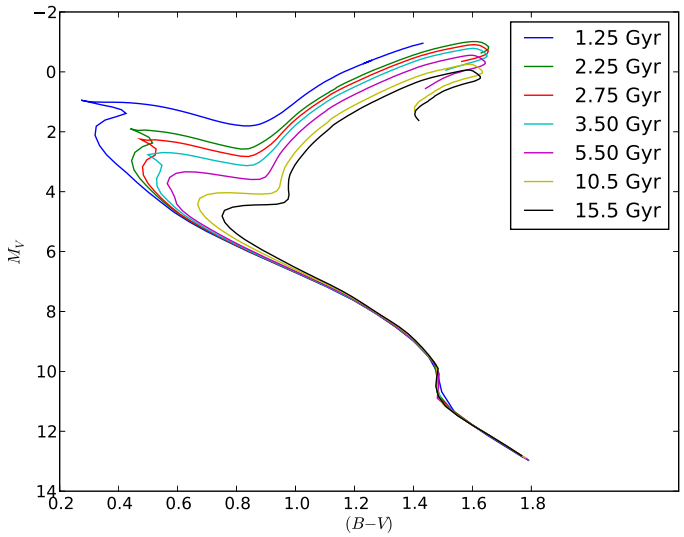

Figure 7.3: An example of a set of Y^2 isochrones for stars with [Fe/H]=0.0.

$$M_{V,MS} = \sum a_i (B-V)^i \tag{7.2}$$

Wright [2004] estimated that a star with [Fe/H]=0.3 and a star with [Fe/H]=-0.3 will lie above and below the fitted main sequence ~ 0.45 mag. Taking into account this spread due to the metallicity, we defined as an evolved star (i.e a star that is leaving the main sequence) all the stars that were above the fitted main sequence 1 mag (see Figure 7.4). In the sample we found a total of 138 stars that are over 1 mag above the fit of the main sequence (see Table 7.1).

Once the stars that should have lower uncertainty in the age determination than field stars were identified, we proceeded to calculate the ages for the entire sample of stars knowing that the MS stars will have a poorly accurate age estimation. For each star, using the interpolator provided with the Y^2 isochrones, a grid was created using the metallicty of the star calculated in this work and with ages ranging from 0.1 Gyr to 14.6 Gyr in steps of 0.5 Gyr. Then the minimum distance in the HR diagram between the position of the observed star and the different isochrones was calculated. Once a minimum distance to the corresponding isochrone was found, a new grid was created starting with an age ranging from the minimum distance isochrone minus 1.5 Gyr to the age of the minimum distance isochrone plus 1.5 Gyr in steps of 0.1 Gyr. Using this new and thinner grid the minimum distance isochrone-star was recalculated and did the same procedure with the position of the errors. All the grids were created using a α-enhancement of zero.

That way an age estimation for the central position of the star in the HR diagram was obtained and using this computed age with errors, a lower and upper limit for the age estimation was computed. Of the entire sample, 133 stars had ages greater than the age of Universe (13.7 ± 0.12 Gyr according to Hinshaw et al. [2009]); this is an example of the errors that are present in isochrone fitting for field main sequence stars.

Figure 7.5 shows an example of isochrone fitting for one of our evolved stars, in this case the fitted age was 4.9 Gyr with a lower limit of 4.0 Gyr and an upper limit of 6.3 Gyr.

7.4 Age Indicators

Because of the great uncertainties in the age determination for main sequence stars astronomers often work with indicators of the age, which most of them are suited to find relatively young objects. Some indicators

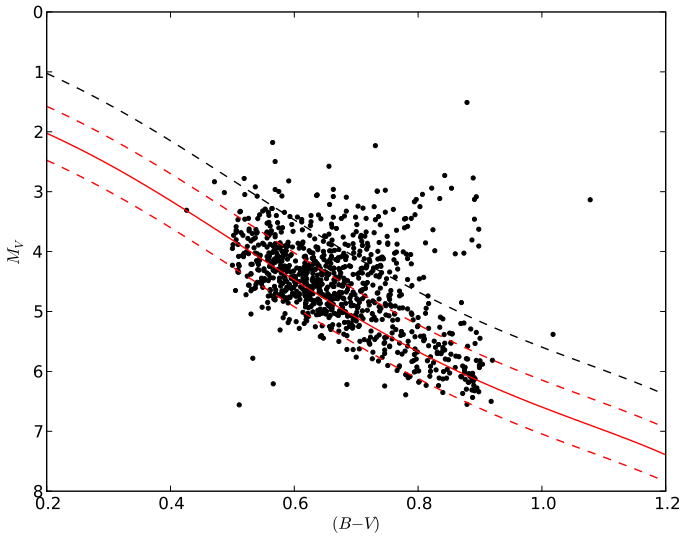

Figure 7.4: HR diagram for the stars in the sample with the fitted main sequence (red line). The dashed red line represent stars with metallicities of $[Fe/H] = 0.3$ and $[Fe/H] = -0.3$, the dashed black line represent the limit between main sequence - evolved stars.

of age are the rotational velocity of the star, the stellar activity and the presence of Lithium absorption lines in the stellar spectrum. We examine these in following subsections.

7.4.1 Rotational Velocity

The rotational velocity $v \sin i$ (see Chapter 6) is an indicator of age because of the process of stellar formation: stars form from a gravitational collapsing molecular cloud that is subject to external torques (interactions with other clouds, galactic rotation) and in the process of contraction the angular momentum of the cloud is conserved, hence the cloud (and the central proto-star) has to increase its rotational velocity. As a result of the contraction process of the molecular cloud, a star is born with a high velocity of rotation and during its lifetime the star looses this rapid rotation due to the interaction of magnetic fields and stellar winds (magnetic braking). The time scales of the magnetic braking depends on the mass of the star; low mass stars take a longer time to slow down their rotation rates. For a typical G dwarf it decreases from 50 m/s at an age of ~ 625 Myr to $\lesssim 5$ m/s at the age of the Sun (Cassen et al. [2006]).

7.4.2 Stellar Activity

One physical phenomenon that is closely related with the rotational velocity is the activity of the chromosphere of the stars. The stellar chromospheric activity is closely related to the magnetic fields and rotational velocity through the dynamo effect, so a young star with high rotational velocity will be more magnetically active than an older star. Stronger magnetic activity has as a consequence the presence of spots, X-ray emission and chromospheric emission lines.

For cold stars a good indicator of activity are the CaII H and K lines at 3968.5 Å and 3933.7 Å. For active stars the H and K lines consist of a narrow emission component superimposed on a broad absorption line. The ratio between the chromospheric emission lines and the total bolometric emission of the star gives the activity index R'_{HK} (Noyes et al. [1984]). The R'_{HK} index is correlated with the radial velocity jitter that can mimic the presence of a planet, for that reason measuring the activity index is of great importance to select stars for a survey that expects to find planets using the radial velocity method.

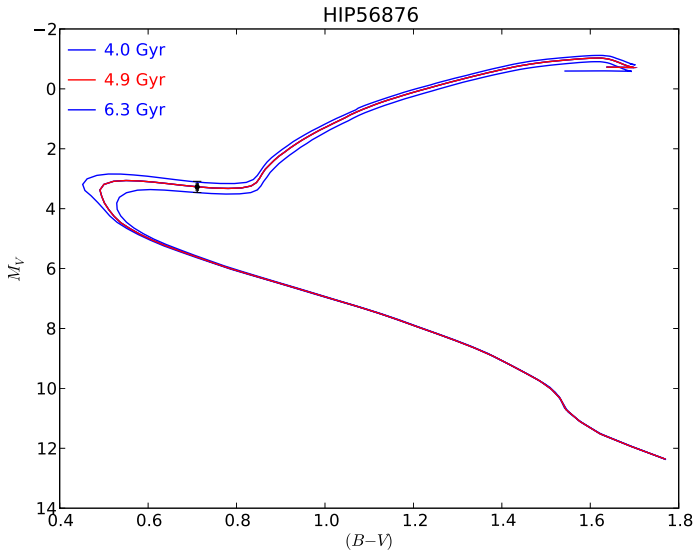

Figure 7.5: Example of a fitted isochrone for an evolved star. The blue lines represent the lower and upper limit in age.

The activities presented in this work were computed by James Jenkins using the same procedure described in his paper Jenkins et al. [2008]. In Figure 7.6 we present the distribution of activities found for the stars in the sample; the distribution shows a bimodal feature with peaks representing active stars at ~ -4.5 dex and inactive stars at ~ -5.0 dex as already been found (Duncan et al. [1991], Henry et al. [1996], Gray et al. [2006a], Jenkins et al. [2008]).

As mentioned before there is a relation between the rotational velocity and the activity of the star. Figure 7.9 presents a plot of these two quantities (top panel). We can see that despite the spread in velocities there exist a general tendency of increase in activity as the rotational velocity increases, as one would expect. Also there is a big accumulation of stars with low velocity values in the position of the peak of inactive stars.

Figure 7.7 shows the distribution of activities across the metallicity space. As mentioned before the activity introduces radial velocity noise (jitter) and also in Chapter 6 we saw that a metal rich star has a higher probability of hosting a planet than a metal poor one. In this plot are marked with red points the stars with low activity ($\log R'_{HK} \leq -4.5$) and that are metal rich ($[Fe/H] \geq 0.1$ dex). A total of 195 stars with these characteristics were found and they can be used as program objects in a search of planets using the radial velocity technique.

7.4.3 Lithium Lines

Another indicator of age is the presence of Lithium absorption lines in the spectrum of the star. Lithium as ^{7}Li is one of the elements produced in the big bang and the study of its abundance in stars and in the interstellar medium is of great importance to constrain the baryonic distribution of mass of the Universe (Boesgaard and Steigman [1985]).

Lithium is burned in the nuclear reactions that convert Hydrogen into Helium known as proton-proton chain reactions. Even more, the Lithium depletion starts in the Pre-Main Sequence, where the core proto-star reaches temperatures hot enough ($T_{eff} \sim 5 \times 10^5$ K) to star burning light elements like Deuterium. So the presence of absorption lines of Li is an indicator of the youth of the star, assuming that the presence of Lithium is not due to external contamination.

To establish the presence of Li absorption lines in the sample spectra, a program to measure the equivalent width of the LiI line at 6708 Å (see Figure 3.1) was developed. The equivalent width is a measure of the area

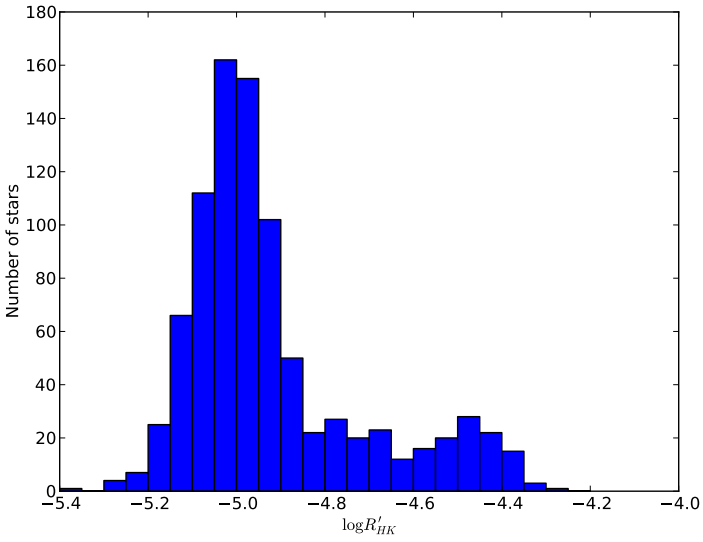

Figure 7.6: Distribution of the activity index $\log R'_{HK}$ for the star in the sample.

under the absorption line in a normalized spectrum:

$$W(\lambda) = \int \frac{F_c - F_\lambda}{F_c} d\lambda = \int \left(1 - \frac{F_\lambda}{F_c}\right) d\lambda \tag{7.3}$$

where F_λ and F_c are the flux of the spectrum and continuum respectively. The equivalent width is a positive quantity, it has units of wavelength and has the good quality of being independent of line broadening such as the resolution of the spectrograph or the stellar rotation velocity.

Using the restframe and normalized spectra I proceeded to integrate the absorption line at 6708 Å for lines that had a minimum value $F_\lambda/F_c < 0.9$ to ensure detection. I was careful to select the width use in the integration (0.8 Å) to avoid an absorption FeI line at 6707.4 Å. Using this criteria I managed to measure the equivalent width of LiI 6708 Å for 307 of 890 stars (no spectrum binaries).

Figure 7.8 presents the distribution of the equivalent widths measured in this work; the peak of the distribution is near ~ 45 mÅ and then it decreases with higher equivalent width values. Figure 7.9 shows a comparison between the rotational velocities versus the equivalent width (middle panel), as the top panel in the same figure, we can see a spread in the values of $v \sin i$ for every equivalent width but there is a tendency towards an increase in the rotational velocity as the equivalent width increases. A linear correlation analysis found a correlation coefficient $\rho = 0.45$, so there is no linear relation between $v \sin i$ and the equivalent width of LiI 6708 Å.

Finally the bottom panel of Figure 7.9 presents a plot of the activities versus the equivalent width for the stars in the sample. We can see that the stars with lower activity present a wide range in equivalent widths and that the more active stars tend to have a larger equivalent width, particularly beyond a $\log R'_{HK}$ of -4.5. A linear correlation analysis found a correlation coefficient $\rho = 0.40$ for all the values, $\rho = 0.48$ for the stars that presented an activity index $\log R'_{HK}$ higher than -4.5 and $\rho = 0.03$ for the stars that presented an activity index $\log R'_{HK}$ less than -4.5. These values reveal that apparently a relationship between the active stars and the presence of Lithium exist as one would expect because both are indicators of youngness, however a further statistical analysis with an increased dataset and a more accurate determination of the equvalenth width of Li is needed.

The rotational velocity, stellar activity and the presence of Lithium lines can be used to select young and old stars without knowing the exact age of the star. Young stars are important for planet search because the

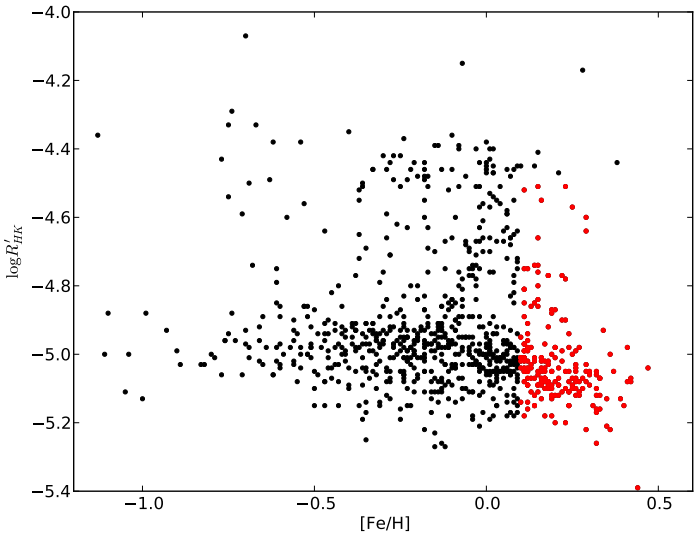

Figure 7.7: Metallicities versus activities. The red points mark the stars with $\log R'_{HK} \leq -4.5$ and $[Fe/H] \geq 0.1$ dex.

planets can be detected using direct image in the near infrared because young planets are still in gravitational contraction and they release energy in this process in the form of heat. Selecting old stars is important for the radial velocity method because they have less radial velocity jitter as we commented above.

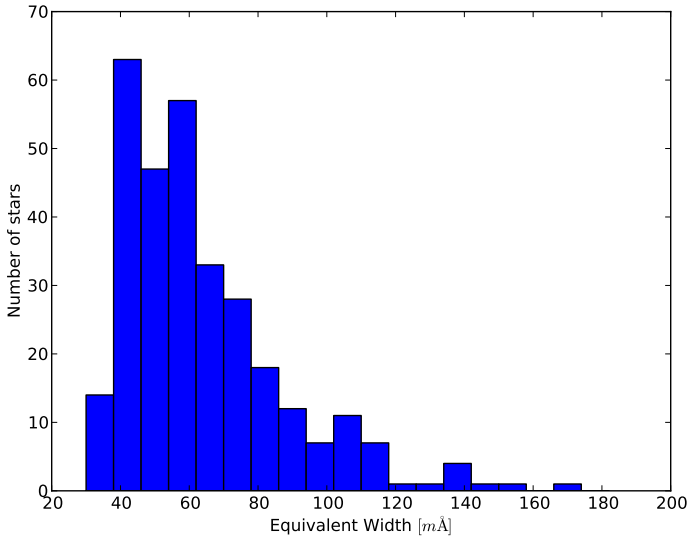

Figure 7.8: Distribution of LiI 6708 Å equivalent widths.

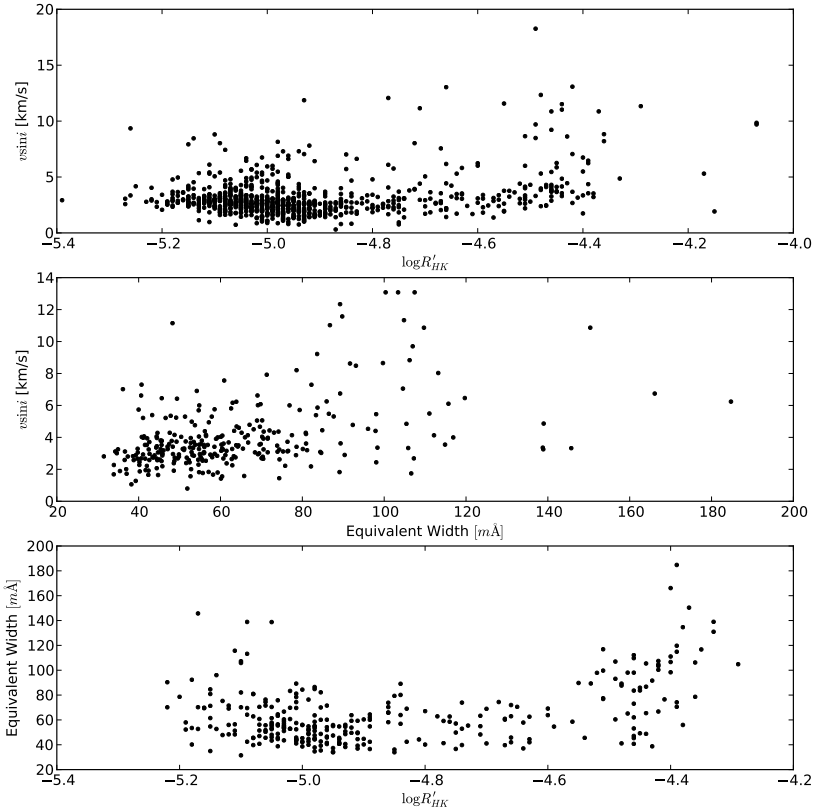

Figure 7.9: Activities versus rotational velocity (top panel), equivalent width of LiI 6708 Å versus rotational velocity (middle panel) and activities versus equivalent width of LiI 6708 Å (bottom panel).

Table 7.1: Evolved stars.

Hipparcos Number	Hipparcos Number	Hipparcos Number
HIP 1970	HIP 27720	HIP 65548
HIP 2574	HIP 28181	HIP 66990
HIP 2902	HIP 29094	HIP 67035
HIP 3185	HIP 29193	HIP 67117
HIP 3605	HIP 31179	HIP 67534
HIP 4242	HIP 31895	HIP 69536
HIP 6044	HIP 32742	HIP 71296
HIP 6100	HIP 34747	HIP 72562
HIP 6125	HIP 35058	HIP 73061
HIP 6158	HIP 35279	HIP 74464
HIP 6497	HIP 35881	HIP 74904
HIP 6712	HIP 37520	HIP 78408
HIP 6987	HIP 38574	HIP 78998
HIP 6993	HIP 39007	HIP 79296
HIP 7276	HIP 39327	HIP 79749
HIP 7693	HIP 42581	HIP 80064
HIP 9036	HIP 42581	HIP 80129
HIP 9346	HIP 43287	HIP 80486
HIP 9837	HIP 47856	HIP 81129
HIP 10061	HIP 48323	HIP 81347
HIP 10090	HIP 48583	HIP 81845
HIP 10212	HIP 50020	HIP 81952
HIP 10325	HIP 50121	HIP 83983
HIP 10426	HIP 50458	HIP 85454
HIP 10990	HIP 50839	HIP 88650
HIP 12094	HIP 51078	HIP 90896
HIP 12479	HIP 51500	HIP 93281
HIP 12839	HIP 52023	HIP 97125
HIP 13724	HIP 52500	HIP 98373
HIP 13889	HIP 54195	HIP 99115
HIP 14050	HIP 54580	HIP 99661
HIP 14180	HIP 54926	HIP 100649
HIP 16084	HIP 55300	HIP 103898
HIP 16579	HIP 56876	HIP 104768
HIP 17269	HIP 57366	HIP 107453
HIP 19126	HIP 57744	HIP 109491
HIP 19191	HIP 57927	HIP 110785
HIP 19921	HIP 59341	HIP 112826
HIP 20611	HIP 59968	HIP 113807
HIP 20627	HIP 60096	HIP 114016
HIP 21141	HIP 60457	HIP 114244
HIP 21872	HIP 62371	HIP 115572
HIP 22587	HIP 62583	HIP 116517
HIP 23290	HIP 63851	HIP 116559
HIP 24692	HIP 64259	HIP 116951
HIP 27158	HIP 64656	HIP 117144

Chapter 8

Distances and Kinematics

This chapter presents the distances and heliocentric space velocities for the sample. Section 8.1 presents the distribution of parallaxes and distances, section 8.2 shows the method used to compute the heliocentric space velocities, section 8.3 presents the heliocentric velocities and study the distribution for the stars in the sample and in section 8.4 we analyzed the presence of nearby halo stars. The results of this chapter will be use in Chapter 9.

8.1 Stellar Parallax and Distances

One of the oldest and most fundamental problems in astronomy is to find the distance to the object of study. The stellar parallax was one of the first methods suggested to measure the distance to the stars and consists of detecting the displacement of a star between two different epochs against a fixed background (see Figure 8.1).

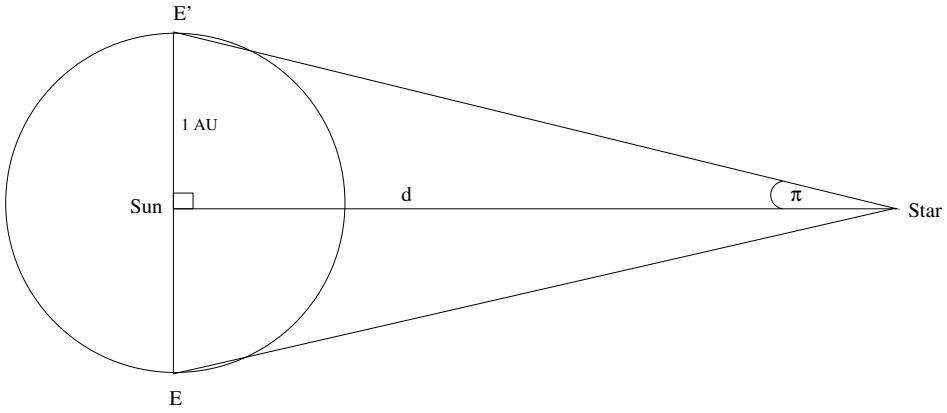

Figure 8.1: Stellar parallax.

If we have one observation taken at a time when the position of the earth was E and a second observation taken six month later (E') we will see that our target star will move an angle 2π (see Figure 8.1, the angle measured in radians) in the sky. We know the sun-earth distance (1 AU) and we have the angle of displacement compared to fixed position background stars, using trigonometry we can calculate the distance d to the star

$$d = \frac{1AU}{\tan \pi} \tag{8.1}$$

in practice π is a very small angle so we can make the approximation $\tan \pi \approx \pi$. Now if we transform π

from radians to arcseconds, we have

$$d = \frac{206265}{\pi''} AU \tag{8.2}$$

and defining 1 pc = 206265 AU

$$d = \frac{1}{\pi''} pc \tag{8.3}$$

Because of the great distances between stars the angles of displacement are small and hence difficult to measure. In fact the angles involved are so small that the first succesfull measurement of a stellar parallax was done almost 230 years after the invention of the telescope by the German mathematician and astronomer Friedrich Bessel who in 1838 observed 61 Cygni and determined a parallax of 0.314 arcseconds.

As mentioned in Chapter 2 all the stars in the sample are in the Hipparcos Catalogue, so we have parallaxes with reliable errors. Figure 8.2 presents the distribution of parallaxes and also shows the relative parallax error σ_π/π. We can see that most of our sample has errors less than 10% in parallaxes.

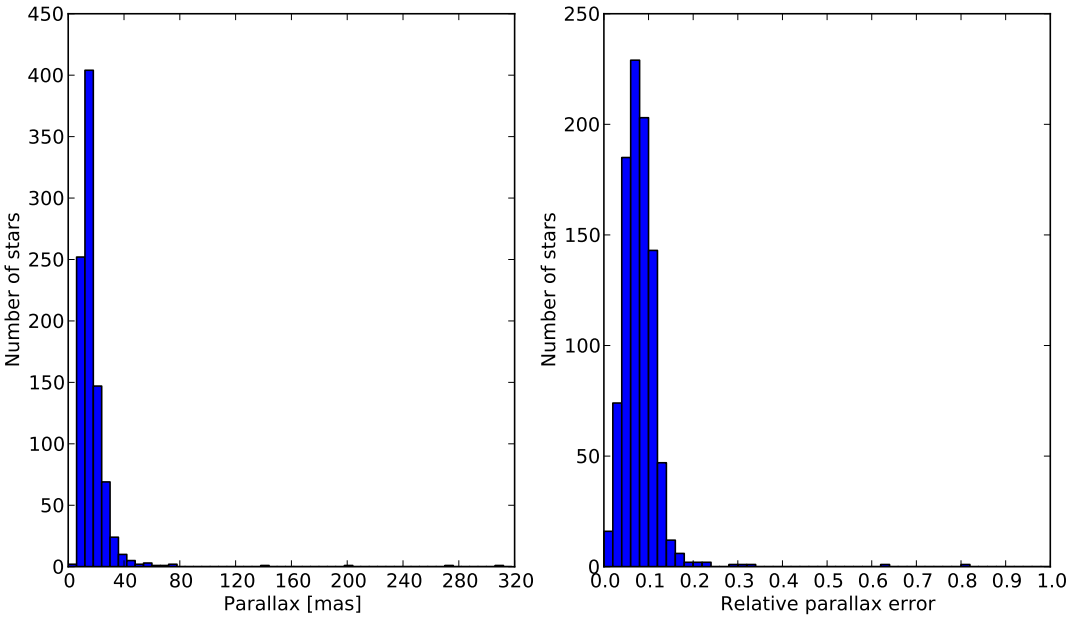

Figure 8.2: Distribution of parallaxes (left) and relative parallax error σ_π/π (right).

Using the equation 8.3 the distances were computed and Figure 8.3 shows the distribution of distances of the sample. We can see that most of the stars are near 100 pc from the sun and the most distant star is at about 240 pc. Also Figure 8.3 shows the relative distance error σ_d/d and for the sample most of the star present distance errors less than 15%.

8.2 Space Velocities

Using the coordinates, parallaxes, radial velocities and proper motions it is possible to obtain the three components of the galactic velocity reference system: U, V and W. In this work a right-handed coordinate system it is used. The velocity component U is defined as positive in the direction of the galactic center, V

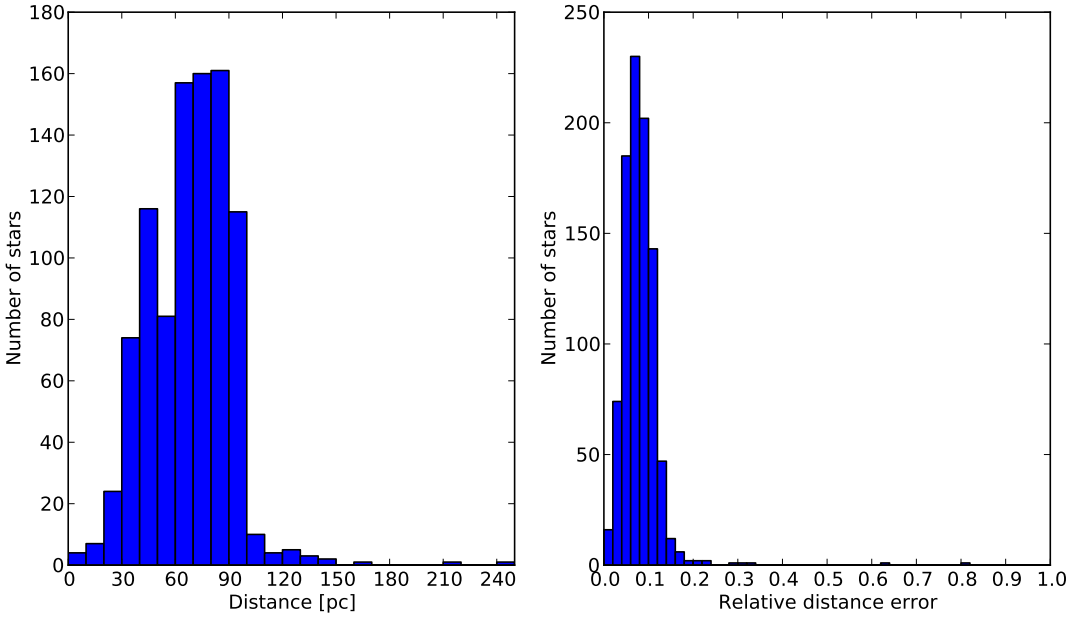

Figure 8.3: Distribution of distances (left) and relative distance error σ_d/d (right)

is positive in the direction of the galactic rotation and W is positive towards the north galactic pole (NGP) (see Figure 8.4).

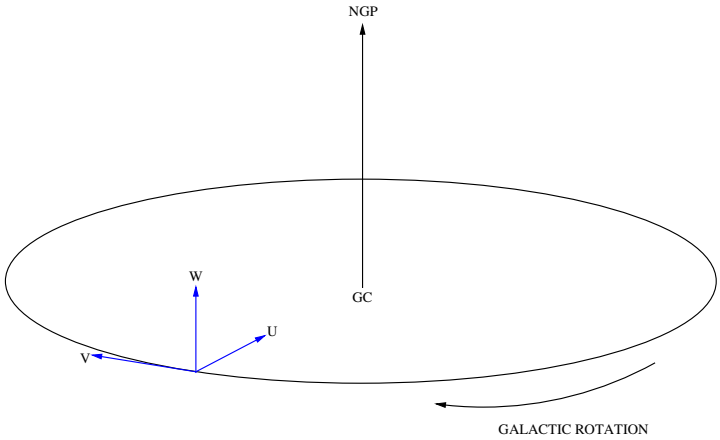

Figure 8.4: Galactic velocity system.

The galactic reference system was defined in the equinox B1950.0, so the accurate way of obtaining U,V and W is to precess the equatorial coordinates, proper motions and radial velocities to that equinox and then precess the result to the J2000.0 system. As an approximation we computed the galactic velocities using the values in the J2000.0 equinox and due to the observational errors we are confident that our values are precise to less than 5 km/s despite this approximation.

Following the work of Johnson and Soderblom [1987] we defined the following quantities:

- $\alpha_{NGP} = 192.85948°$ the right ascension of the NGP in J2000.0.
- $\delta_{NGP} = 27.12825°$ the declination of the NGP in J2000.0.

- $\theta = 122.93192^\circ$ the position angle of the NGP in J2000.0.
- α, δ the right ascension and declination of the star respectively (both assumed with no errors).
- $\pi \pm \sigma_\pi$ the parallax in arcsec.
- $V_r \pm \sigma_{V_r}$ the radial velocity in km/s.
- $\mu_\alpha \pm \sigma_{\mu_\alpha}$ the proper motion in right ascension corrected for declination in arcsec/yr.
- $\mu_\delta \pm \sigma_{\mu_\delta}$ the proper motion in declination in arcsec/yr.

One can obtain the galactic coordinates (l, b) by resolving the system

$$\begin{pmatrix} \cos b \cos l \\ \cos b \sin l \\ \sin b \end{pmatrix} = \mathbf{T} \begin{pmatrix} \cos\delta \cos\alpha \\ \cos\delta \sin\alpha \\ \sin\delta \end{pmatrix} \tag{8.4}$$

where $\mathbf{T}$ is the transformation matrix

$$\mathbf{T} = \begin{bmatrix} +\cos\theta & +\sin\theta & 0 \\ +\sin\theta & -\cos\theta & 0 \\ 0 & 0 & +1 \end{bmatrix} \begin{bmatrix} -\sin\delta_{NGP} & 0 & +\cos\delta_{NGP} \\ 0 & -1 & 0 \\ +\cos\delta_{NGP} & 0 & +\sin\delta_{NGP} \end{bmatrix} \begin{bmatrix} +\cos\alpha_{NGP} & +\sin\alpha_{NGP} & 0 \\ +\sin\alpha_{NGP} & -\cos\alpha_{NGP} & 0 \\ 0 & 0 & +1 \end{bmatrix} \tag{8.5}$$

We will define the coordinate matrix $\mathbf{A}$ as

$$\mathbf{A} \equiv \begin{bmatrix} +\cos\alpha\cos\delta & -\sin\alpha & -\cos\alpha\cos\delta \\ +\sin\alpha\cos\delta & +\cos\alpha & -\sin\alpha\cos\delta \\ +\sin\delta & 0 & +\cos\delta \end{bmatrix} \tag{8.6}$$

The galactic velocities are then

$$\begin{pmatrix} U \\ V \\ W \end{pmatrix} = \mathbf{B} \begin{pmatrix} V_r \\ k\mu_\alpha/\pi \\ k\mu_\delta/\pi \end{pmatrix} \tag{8.7}$$

where $\mathbf{B} = \mathbf{T} \cdot \mathbf{A}$ and $k = 4.74057$ km/s which is the velocity of an object that travels 1 AU in one tropical year.

The errors of the velocity components are calculated by the propagation of errors formula for a function of several variables

$$\sigma^2_{F(x,y,z)} = \left(\frac{\partial F}{\partial x}\right)^2 \sigma_x^2 + \left(\frac{\partial F}{\partial y}\right)^2 \sigma_y^2 + \left(\frac{\partial F}{\partial z}\right)^2 \sigma_z^2 \tag{8.8}$$

Applying the previous formula to equation (8.7) we obtain

$$\begin{pmatrix} \sigma_U^2 \\ \sigma_V^2 \\ \sigma_W^2 \end{pmatrix} = \mathbf{C} \begin{pmatrix} \sigma_{V_r}^2 \\ (k/\pi)^2 \left[\sigma_{\mu_\alpha}^2 + (\mu_\alpha^2 + (\mu_\alpha \sigma_\pi/\pi)^2)\right] \\ (k/\pi)^2 \left[\sigma_{\mu_\delta}^2 + (\mu_\delta^2 + (\mu_\delta \sigma_\pi/\pi)^2)\right] \end{pmatrix} + 2\mu_\alpha \mu_\delta k^2 \sigma_\pi^2/\pi^4 \begin{pmatrix} b_{12} \cdot b_{13} \\ b_{22} \cdot b_{23} \\ b_{32} \cdot b_{33} \end{pmatrix} \tag{8.9}$$

where $\mathbf{C}$ is the matrix with components equal to the components of $\mathbf{B}^2$, i.e, $c_{ij} = b_{ij}^2$.

The velocities given above are in a heliocentric reference system. To change these velocities to a galactic reference system you need to know the peculiar velocity of the Sun with respect to the current velocity of a fictional particle that moves in a circular orbit that passes through the present location of the Sun or local standard of rest (LSR) and add this to the V velocity of the LSR to the heliocentric velocities. Mihalas and Routly [1968] found a peculiar solar motion with respect to the LSR of $(U_\odot, V_\odot, W_\odot)_{LSR} = (10.4, 15.0, 7.5)$ and more recently Dehnen and Binney [1998] using the Hipparcos data found $(U_\odot, V_\odot, W_\odot)_{LSR} = (10, 5.25, 7.17)$.

Figure 8.5 shows a comparison between the space velocities U, V and W obtained in this work and the values found by the GCS for 231 stars in common. We can see that despite the approximation of taken the J2000.0 values for the position of the north galactic pole, the velocities are in fair agreement with the ones of the GCS although the presence of some outlayers can not be neglect. The standard deviation of the residuals is 3.0, 4.6 and 2.6 km/s for U, V and W respectively. From equation (8.7) we can see that only U is affected by the radial velocity and V and W depend on the proper motions and distances. As mentioned in Chapter 5 the radial velocities are in good agreement with the GCS values which is reflected in the low dispersion for the U component, the higher dispersion in V can not be explained by errors in the distances because we also would have seen a higher dispersion in W, which is not the case, so the problem may come from the use of coordinates in the J2000.0 system.

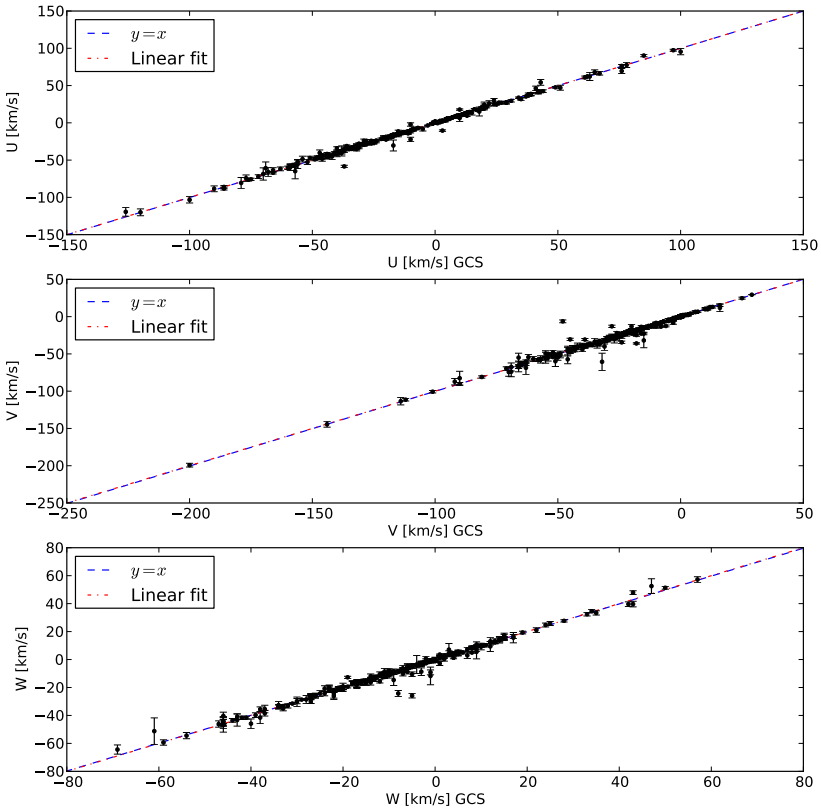

Figure 8.5: Comparison between the space velocities of this work and the GCS.

8.3 Kinematics

Figures 8.6, 8.7 and 8.8 present the heliocentric space velocities for the stars in the sample. Figure 8.6 shows the stars that belong to the old disk (stars inside the red ellipse) and the ones that belong to the young disk

(stars inside the rectangle) according to the kinematical classification proposed by Eggen [1969]. With this criteria we can see that the majority of our stars belong to the disk as one would expect for stars in the solar neighborhood and a few stars probably belong to the Halo of the galaxy. I will study in more depth the distribution of the stars in the UV plane in section 9.

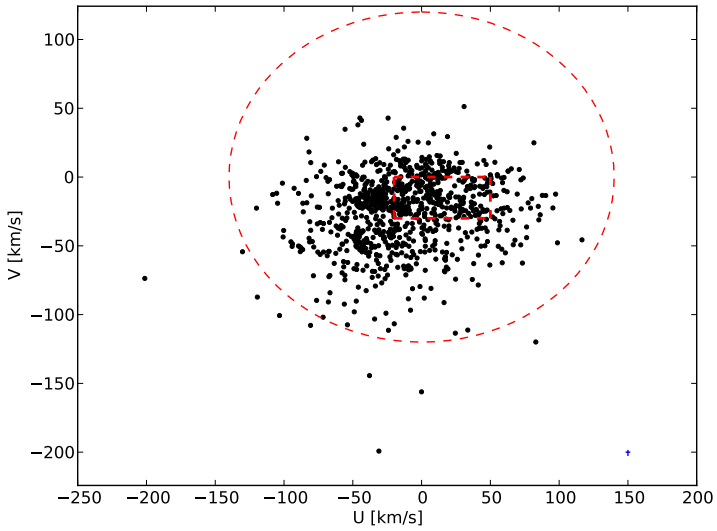

Figure 8.6: UV plane of heliocentric space velocities, the blue cross represent the mean error bar in the sample ($\sigma_U = 2.4$ km/s, $\sigma_V = 2.3$ km/s).

From Figure 8.7 we can see that there is a bigger dispersion in U than in the vertical velocity W. A low W velocity means that the stars do not go to far above and below the plane of the galaxy as one would expect for a star that belongs to the disk. In Figure 8.8 we see that the stars in our sample show a small dispersion in W and in the velocity component that follows the rotation of the galaxy V, indicating that most of our stars are near the plane of the disk and they rotate almost in the same manner.

The Figure 8.9 shows a Toomre diagram in which the dash lines are the lines of constant kinetic energy for velocities of 50 km/s up to 300 km/s. The Toomre diagram helps to constrain the escape velocity of the Milky Way, thus providing an estimation of the galactic mass if you know the potential. The escape velocity in the solar neighborhood is in the range of 498 km/s $< V_{esc} <$ 608 km/s (Smith et al. [2007]), so we can confirm that all the stars in our sample are bound to the galaxy.

The Figure 8.10 shows the distribution of the total heliocentric velocity $V_{total} = \sqrt{U^2 + V^2 + W^2}$ km/s. We can see that we have three stars with high velocities ($V_{total} > 170$ km/s) that probably belong to the halo of the galaxy (see Table 8.1).

Table 8.1: High velocity stars.

Hipparcos Number	Radial Velocity [km/s]	Proper Motion RA [mas/yr]	Proper Motion DEC [mas/yr]	Parallax [mas]
HIP 30514	133.3 ± 1.7	150.56 ± 0.91	413.46 ± 0.93	11.55 ± 1.08
HIP 58401	159.8 ± 1.6	-769.46 ± 0.82	-265.58 ± 0.67	31.35 ± 1.05
HIP 117702	-28.1 ± 1.6	178.75 ± 1.06	-815.82 ± 1.08	20.70 ± 1.20

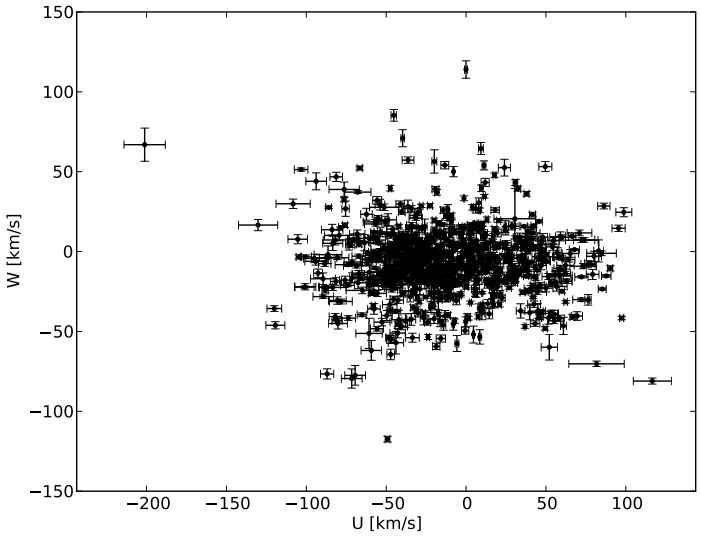

Figure 8.7: UW plane of heliocentric space velocities.

8.4 Halo Stars

The Halo of the galaxy is a spheroidal structure of the Milky Way and the stars that belong here do not rotate in the same direction and in the same plane as the stars from the galactic disk do. The halo stars follow a thermal velocity distribution with orbits with different orientations and eccentricities. Also the stars from the Halo are different in chemical composition than the stars from the disk: they possess less metals than the Sun. These characteristics are due to the formation of the Halo which was the first formed structure in the Milky Way (explaining the lower metallicities) and the stars formed in clouds dominated by chaotic motions that were infalling in the potential well of the proto-galaxy (explaining their orbits).

Due to their eccentric and chaotic orbits, sometimes a halo star can pass through the disk, so it is possible to have a star from the halo that is passing near the position of the Sun like the very well known star Arcturus. According to Cox [2000] the local stellar density of halo star in the disk is $0.002 \times disk$, so if the sample were complete we would expect to find $0.002 \times 923 \approx 2$ halo stars.

To test if the stars described in Table 8.1 belong to the Halo of the Milky Way we decided to plot their orbits using a code written in `FORTRAN` (Scholz et al. [1996]) that uses the galactic potential composed by three components: the bulge, the disk and the halo of Allen and Santillan [1991]. The code uses the peculiar solar motion compared to the LSR of Mihalas and Routly [1968] $(U_\odot, V_\odot, W_\odot) = (10, 15, 8)$ km/s, an orbital V velocity of the LSR of 220 km/s and a distance to the galactic center of 8.5 kpc.

Figure 8.11 presents the computed orbit of the Sun with a position of $X_\odot = -8.5$ kpc, $Y_\odot = 0.000$ kpc, $Z_\odot = 0.005$ kpc and a galactic velocity of $U = 10$ km/s, $V = 235$ km/s and $W = 8$ km/s. The green and red dots represent the starting and final position of the star respectively, the black cross marks the center of the galaxy and the radius of the orbit is calculated as follows $r = \sqrt{X^2 + Y^2 + Z^2}$ kpc. We can see that the Sun follows a fairly circular orbit in the plane of the galaxy, its orbit oscillates above and below the plane of the galaxy reaching a maximum distance to the plane of ~ 100 pc and has an orbital period around the galaxy of ~ 200 Myr.

Figures 8.12, 8.13 and 8.14 show the orbits for the stars that probably belong to the Halo. We can see that the three stars follow an eccentric orbit in the plane of the galaxy: HIP 30514 has an eccentricity of $e = 0.58$, HIP 58401 has the highest eccentricity with $e = 0.86$ and HIP 117702 has an eccentricity of $e = 0.35$. The stars HIP 30514 and HIP 117702 reach distances over the plane of the galaxy of about 2.5 kpc and 3.2 kpc respectively. The case of HIP 58401 is interesting because according to our simulation of the orbit, this star

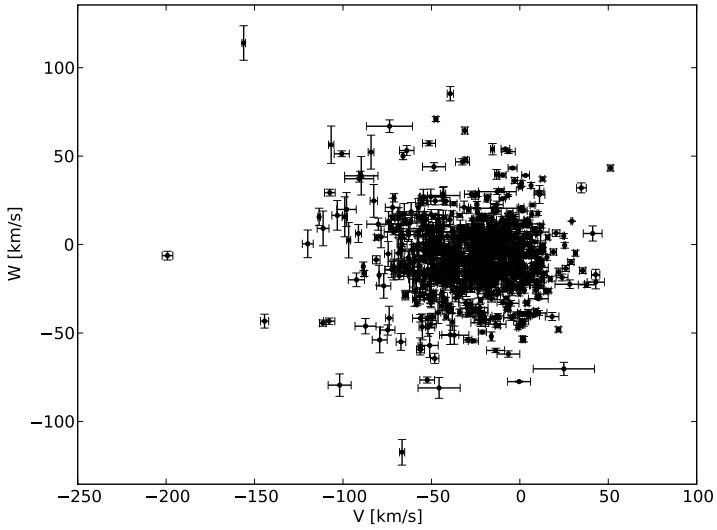

Figure 8.8: VW plane of heliocentric space velocities.

does not go too far above the plane of the galaxy, in fact this star stays closer than the Sun to the galactic plane.

Table 8.2: High velocity stars heliocentric space velocities and [Fe/H].

Hipparcos Number	U [km/s]	V [km/s]	W [km/s]	[Fe/H]
HIP 30514	-201.2 ± 12.9	-73.6 ± 3.5	66.9 ± 10.3	-0.99 ± 0.1
HIP 58401	-31.0 ± 3.0	-199.2 ± 2.4	-6.2 ± 2.1	-0.7 ± 0.09
HIP 117702	0.0 ± 0.9	156.1 ± 9.7	113.9 ± 5.4	-0.71 ± 0.11

Table 8.2 presents the heliocentric space velocities and their abundances found in this work. We can see that the three stars have a lower metallicity than the Sun, as one would expect for stars that belong to the Halo. With this evidence I believe that the stars HIP30514, HIP58401 and HIP117702 are indeed part of the Galactic Halo and because our sample is composed of bright and nearby stars, these provide a great opportunity to do a detailed spectroscopic study of objects from the halo with lower metallicty than the Sun.

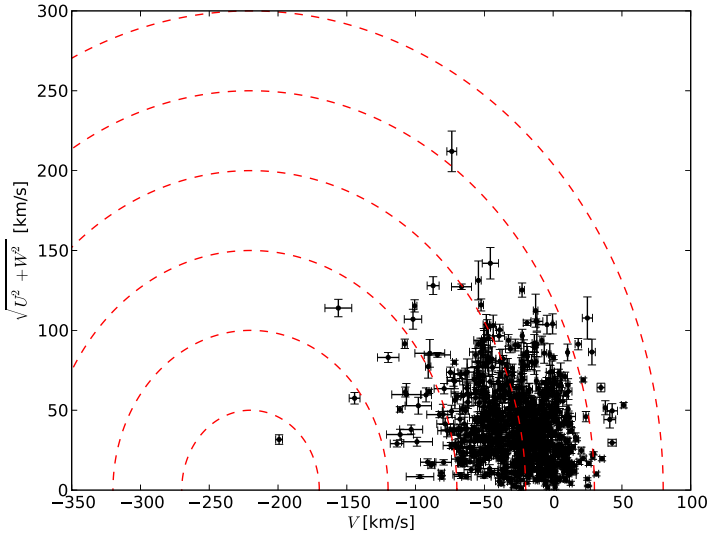

Figure 8.9: Toomre diagram.

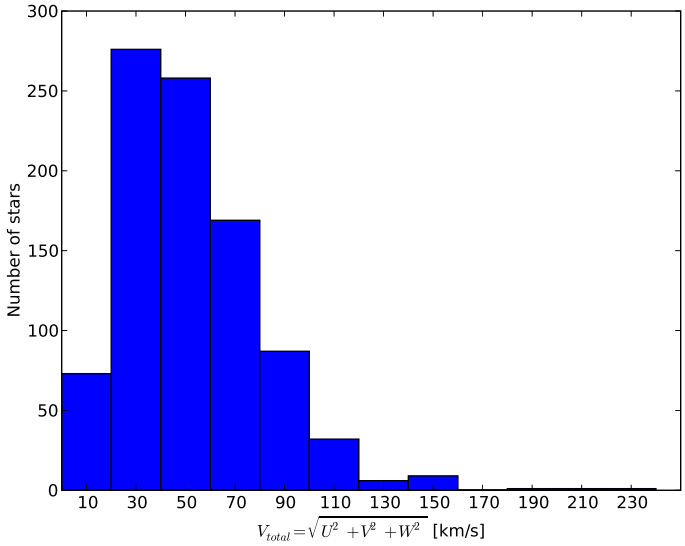

Figure 8.10: Total velocity distribution.

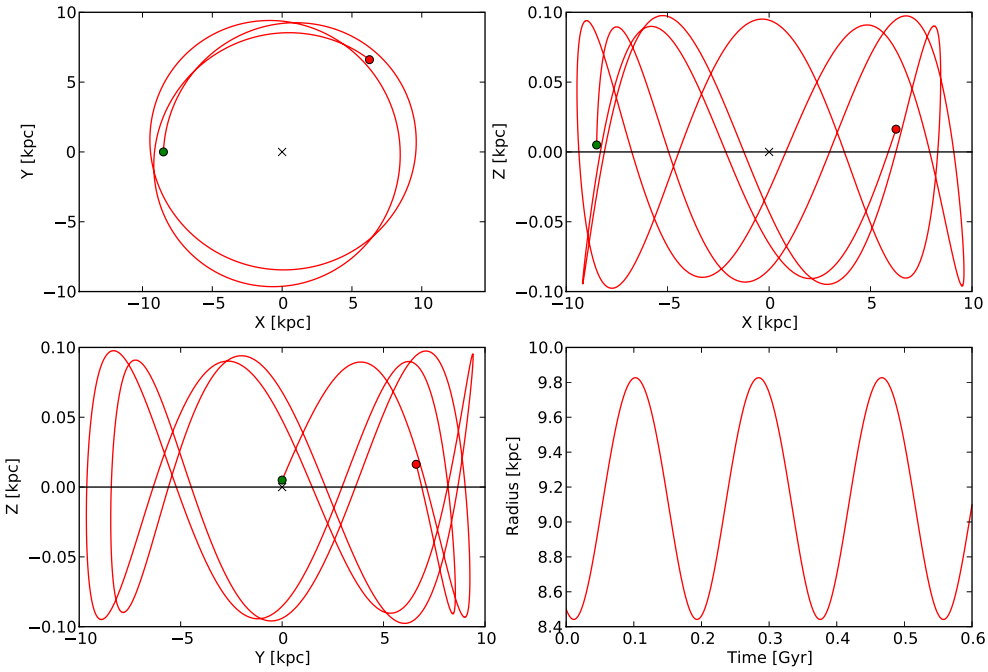

Figure 8.11: Sun's orbit computed with the code.

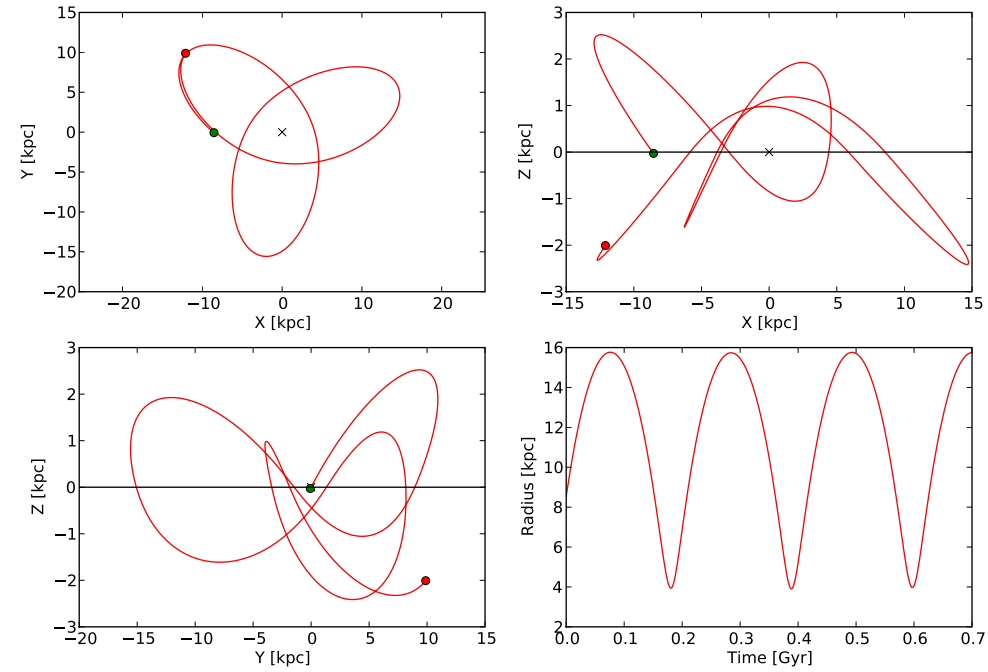

Figure 8.12: HIP30514 orbit computed with the code.

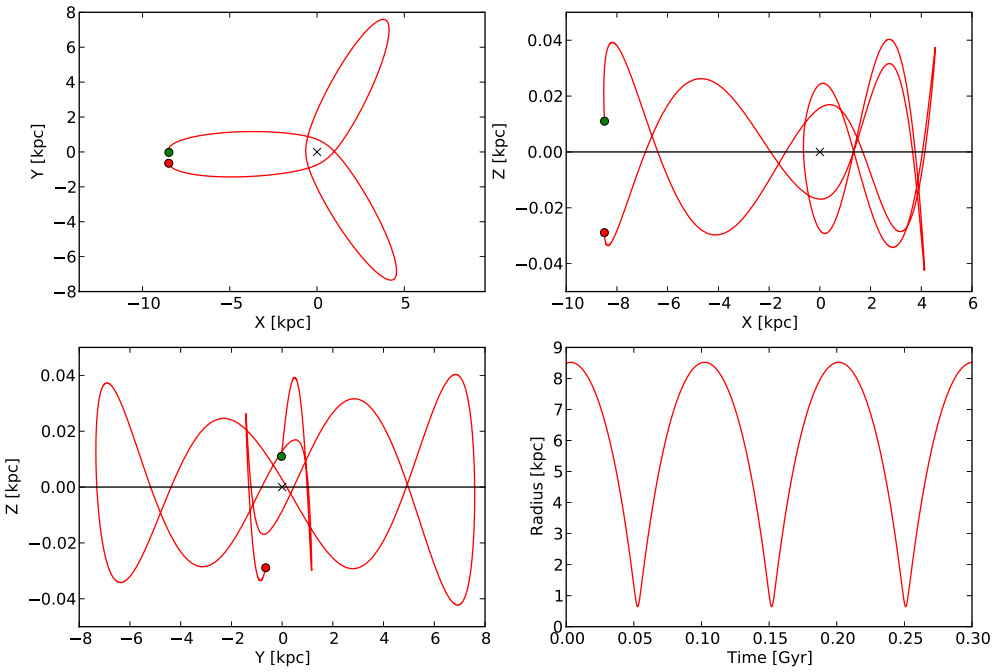

Figure 8.13: HIP58401 orbit computed with the code.

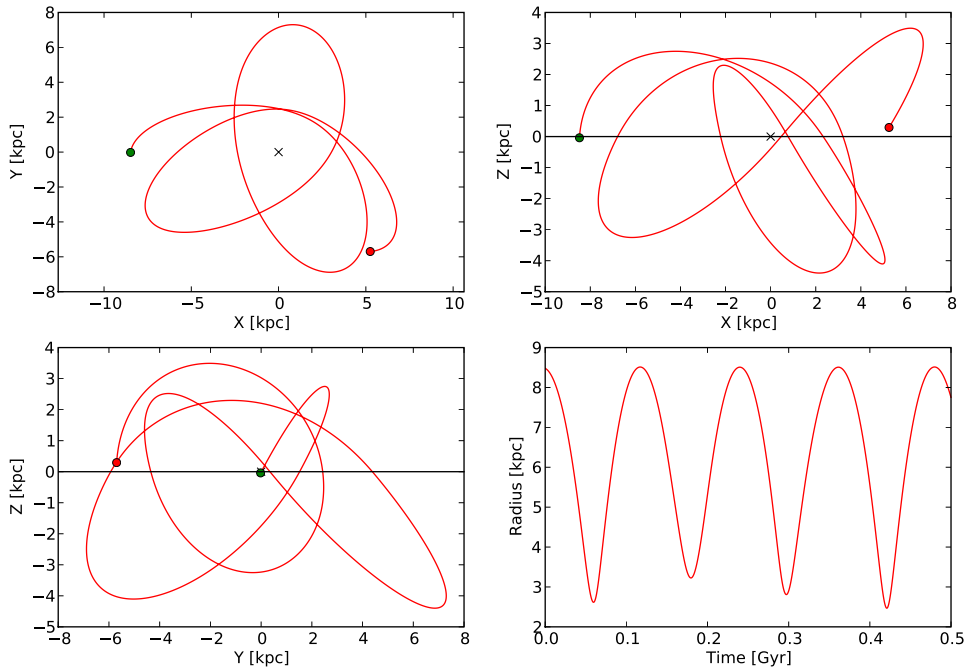

Figure 8.14: HIP117702 orbit computed with the code.

Chapter 9

Moving Groups

If you look a plot of the UV heliocentric space velocities for the stars in the solar neighborhood like Figure 8.6, one can see that the distribution of stars in this velocity space is not homogeneous, i.e, certain velocity components are more populated than others. Olin Eggen (1919-1998) established the existence of several streams of stars (or moving groups: MG) in velocity space (Eggen [1958]) and proposed the idea that these streams are clusters that are being disrupted by disk heating processes. With the help of the Hipparcos data Dehnen [1998] (and more recently Antoja et al. [2008]) confirmed the existence of these structures in the solar neighborhood.

The origin of these structures is still debated, but the two main hypothesis are: the moving groups have a dynamical origin (Dehnen [1998], Skuljan et al. [1999], Antoja et al. [2008]) in the sense that they are formed by resonance interactions between stars and structures like the spiral arms or the galactic bar. The evidence in favor of this idea is the fact that some moving groups like the Pleiades moving group shows a wide spread in the age of member stars, which contradicts the image of a cluster where all the stars have essentially the same age, also some theoretical models have managed to reproduced some of the kinematic features seen in the solar neighborhood (Dehnen [2000]).

The other hypothesis is that moving groups are indeed clusters that are being disrupted, i.e, the moving groups are the intermediate step between bound clusters and field stars. Evidence that support this idea is the homogeneity in the chemical composition and ages of some moving groups (De Silva et al. [2006], De Silva et al. [2007]). If this idea is correct then the moving groups should be composed of young stars, because the survival time of a MG is ~ 1 Gyr before being dispersed by disk heating mechanisms (De Simone et al. [2004]).

If the second hypothesis is correct the detection of moving groups is of great importance if you want to study young objects and the heating processes that occur in the galactic disk. The consequence for planet detection (and the detection of low mass companions like brown dwarfs) is that if the star is young, the planets are also young and they could still be in a process of gravitational contraction . The energy release in this stage is in mainly in the form of heat, making them more easy to directly image using adaptive optics in near the infrared for example (Lafrenière et al. [2008], Marois et al. [2008]) and even in visual bands (Kalas et al. [2008]).

9.1 Detection

Several methods of detecting these structures had been proposed over the years: wavelet analysis (Antoja et al. [2008]) and statistical methods based on density estimation (Asiain et al. [1999], Skuljan et al. [1999], Bovy et al. [2009]).

One widely used statistical method is the technique known as Kernel Density Estimation (KDE, Silverman

[1986]) which consists of determining the distribution of probability of a given vector $\hat{f}(\mathbf{x})$ by a summatory of functions. If we have a dataset $\mathbf{x}$ of n components, KDE approximates the distribution of probability as follows

$$\hat{f}(\mathbf{x}) = \frac{1}{nh} \sum_{i=1}^{n} K\left(\frac{\mathbf{x} - \mathbf{x_i}}{h}\right) \tag{9.1}$$

where $K(\mathbf{x})$ is the kernel function that could be for example a biweight function as used in Skuljan et al. [1999] or a normal distribution. The parameter h is the bandwidth of the distribution and plays the role of the bin size in a histogram.

In the case of a vector $\mathbf{x} \in \Re^d$ with n components and a normal kernel function, the probability distribution is

$$\hat{f}(\mathbf{x}) = \frac{det(\Sigma)^{-1/2}}{nh^d(2\pi)^{d/2}} \sum_{i=1}^{n} \exp\left[-\frac{1}{2h^2}(\mathbf{x} - \mathbf{x_i})^T \Sigma^{-1} (\mathbf{x} - \mathbf{x_i})\right] \tag{9.2}$$

were Σ is the covariance matrix of the vector and $\mathbf{x}_i$ is the sample set.

For a normal kernel and a true normal probability distribution, the optimal bandwidth h is (Silverman [1986]):

$$h = \left(\frac{4}{d+2}\right)^{1/(d+4)} n^{-1/(d+4)} \tag{9.3}$$

In order to detect moving groups in the sample, a procedure like the one used in Asiain et al. [1999] was followed, but with some differences. Asiain et al. [1999] uses a KDE technique applied to the vector $\mathbf{x} = (U, V, W, \log\tau)$ were τ is the age of the stars in yr. First, the W velocities were left out because the distribution of stars in this component is very symmetrical as I checked by computing the KDE of the (U, V, W) velocities using the package `npudens` from the programming language `R`[1] (see Figure 9.1). Second, age estimation for stars that are in the main sequence leads to great uncertainties as we saw in Chapter 7, so I decided to just explored the presence of MG in velocity space.

Asiain et al. [1999] postulated that the total distribution of densities of stars was composed of two components: the density of the field stars and the overdensities known as moving groups (see equation 9.4).

$$\rho_{tot}(\mathbf{x}) = \rho_{field}(\mathbf{x}) + \rho_{MG}(\mathbf{x}) \tag{9.4}$$

$\rho_{tot}(\mathbf{x})$ was modeled using a normal kernel probability distribution, i.e

$$\rho_{tot}(\mathbf{x}) = \frac{det(\Sigma)^{-1/2}}{nh_{tot}^d(2\pi)^{d/2}} \times \sum_{i=1}^{n} \exp\left[-\frac{1}{2h_{tot}^2}(\mathbf{x} - \mathbf{x_i})^T \Sigma^{-1} (\mathbf{x} - \mathbf{x_i})\right] \tag{9.5}$$

The field distribution $\rho_{field}(\mathbf{x})$ was assumed to be composed by

$$\rho_{field}(\mathbf{x}) = \rho_v(\mathbf{v}) \tag{9.6}$$

were $\mathbf{v} = (U, V)$ and $\rho_v(\mathbf{v})$ was assumed to follow an ellipsoidal distribution, i.e the field stars have a normal distribution described by

[1] http://www.r-project.org/

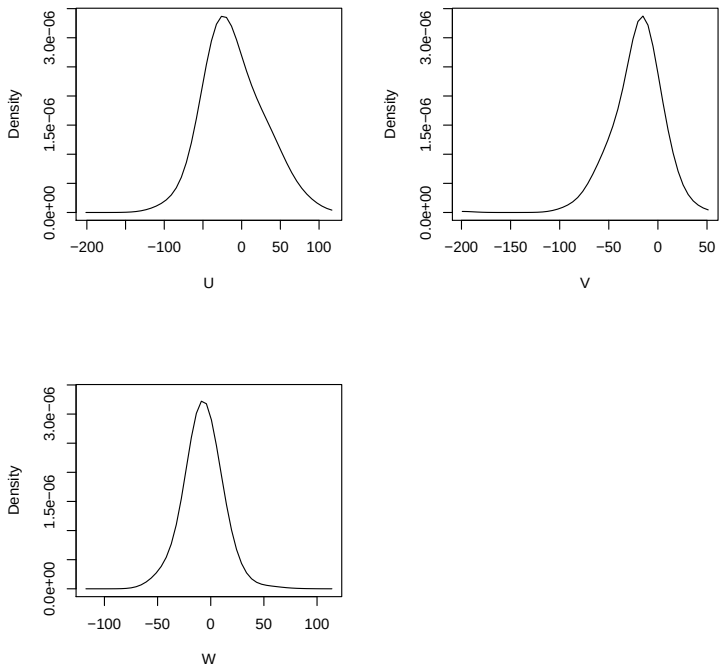

Figure 9.1: Density distribution of heliocentric velocities computed with the KDE from `R` (in units of [km/s]). We can see that the distribution in W is very symmetrical.

$$\rho_v(\mathbf{v}) = \frac{det(\Sigma)^{-1/2}}{(2\pi)^{d/2}} \times \exp\left[-\frac{1}{2}(\mathbf{v}-\mu)^T\Sigma^{-1}(\mathbf{v}-\mu)\right] \tag{9.7}$$

were μ was the mean velocity components vector.

As mentioned before the bandwidth h plays the role of the bin size in a histogram and is a key parameter for the structures that the KDE is sensitive to detect. Asiain et al. [1999] showed that their four dimensional distribution had several bumps and was far from being gaussian, so they adopted $h_{tot} = 0.5h_{gau}$ and $h_{field} = 1.5h_{gau}$ were h_{gau} is the bandwidth for a gaussian distribution (see equation 9.3). According to Asiain et al. [1999] the effects of the chosen value for the bandwidth parameter h was not significant for the velocity and age of the members of the moving groups.

Once the distribution is computed you can find the distribution of moving groups by simply doing the subtraction

$$\rho_{MG}(\mathbf{x}) = \rho_{tot}(\mathbf{x}) - \rho_{field}(\mathbf{x}) \tag{9.8}$$

To avoid noisy structures Asiain et al. [1999] put the condition that $\rho_{MG}(\mathbf{x})$ has to be higher than a threshold function $C(\mathbf{x})$

$$\rho_{MG}(\mathbf{x}) = \rho_{tot}(\mathbf{x}) - \rho_{field}(\mathbf{x}) > C(\mathbf{x}) \tag{9.9}$$

$C(\mathbf{x})$ was computed by shifting the values of (U, V) with a normal distribution around the errors in the measurements $m = 100$ times and taking the rest between $\rho_{tot}(\mathbf{x})$ and its mean, i.e

$$C(\mathbf{x}) = \left[\sum_{i=1}^{m} \left(\rho_{tot,i}(\mathbf{x}) - < \rho_{tot}(\mathbf{x}) > \right)^2 / m \right]^{1/2} \tag{9.10}$$

Figure 9.2 shows the densities $\rho_{MG}(\mathbf{x})$ obtained using the procedure described above and the positions of known moving groups were marked using data taken from Antoja et al. [2008] (Table 3) and Montes et al. [2001] for the Castor MG. The blue crosses show the positions of moving groups that have no name.

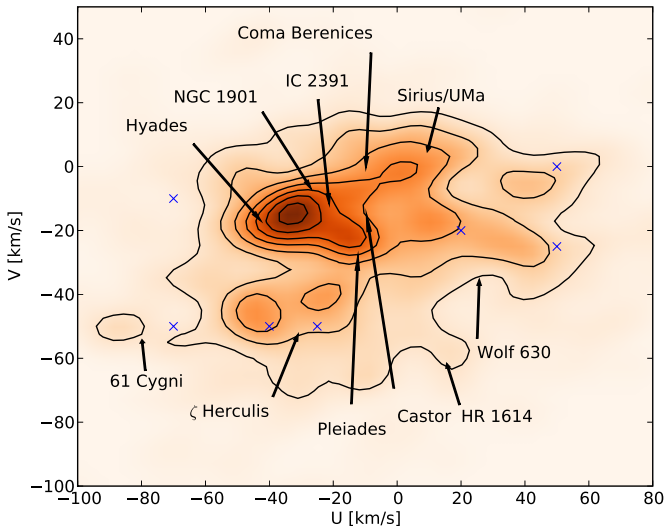

Figure 9.2: Moving groups found in this sample. The data was taken from Table 3 of Antoja et al. [2008] and in the case of the Castor group, from Table 1 of Montes et al. [2001]. The blue crosses correspond to MG with no name in Table 3 from Antoja et al. [2008].

In Figure 9.2 we can see that the method detects the expected asymmetry in the distribution of heliocentric velocities and shows a bigger concentration of stars in the position of the Hyades, Pleiades, IC 2391, NGC 1901, Coma Berenices and Castor groups. The method used in this work was not able to isolate the center of the MGs; this is probably due to the adoption of the bandwidth and also in the elimination of $\log \tau$ as a discriminant, despite this we managed to detect the known kinematical structure in the solar neighborhood for the stars in our sample.

9.2 Membership

Once the moving group it is detected it is desirable to know exactly which stars belong to this structure. If you use a density estimation is possible to establish the probability that a certain star belongs to the MG (Asiain et al. [1999]), but it is not enough to really decide if the star belongs to the group.

In this work the candidates for stars that belong to a moving group were chosen based in a kinematic criteria. Using the data from Montes et al. [2001] (see Table 9.1) the stars that are closer than 5 km/s from the center of the MG in velocity space were selected as members.

To test if these stars belong to the MG I transformed their proper motions into a new reference system. Objects that share the same space motion (like stars in a bound cluster) all move towards the same point named *convergence point* (CP), then by using proper motions toward the convergence point (μ_{tcp}) and in the direction perpendicular to this (μ_{pcp}), it is possible to establish if the star belongs to the system.

To calculate the proper motions in this new system I followed the equations of Reid [1992]. First we

Table 9.1: Properties of moving groups taken from Montes et al. [2001].

Name	Age [Myr]	U [km/s]	V [km/s]	W [km/s]	Convergence Point (RA,DEC)=(^{h}, $^\circ$)
Pleiades	20-150	−11.6	−21.0	−11.4	(5.98,-35.15)
IC 2391	35-55	−20.6	−15.7	−9.1	(5.82,-12.44)
Castor	200	−10.7	−8.0	−9.7	(20.55,-38.10)
Ursa Major	300	14.9	1.0	−10.7	(20.55,-38.10)
Hyades	600	−39.7	−17.7	−2.4	(6.40,6.50)

calculate the angular distance λ_i between a star with position (α_i, δ_i) and the convergence point (α_p, δ_p) (see Table 9.1)

$$\cos\lambda_i = \sin\delta_i \sin\delta_p + \cos\delta_i \cos\delta_p \cos(\alpha_p - \alpha_i) \tag{9.11}$$

the position angle θ_H between the position of the star and the CP is

$$\cos\theta_H = \frac{\sin\delta_p - \sin\delta_i \cos\lambda_i}{\cos\delta_i \sin\lambda_i} \tag{9.12}$$

and the proper motions toward the CP μ_{tcp} and perpendicular to this direction μ_{pcp} are given by

$$\mu_{tcp} = \mu_\alpha \sin\theta_H + \mu_\delta \cos\theta_H \tag{9.13}$$

$$\mu_{pcp} = -\mu_\alpha \cos\theta_H + \mu_\delta \sin\theta_H \tag{9.14}$$

where μ_α and μ_δ are the proper motions of the star in right ascension and declination respectively.

The expected values for μ_{pcp} for stars that belong to the group are

$$\mu_{pcp} = 0.0 \tag{9.15}$$

but due to disk heating processes and uncertainties in the measurements, a spread around zero is expected.

Table 9.2 presents the $v \sin i$, [Fe/H], LiI 6708 Å equivalent width and activity index $\log R'_{HK}$ for the stars in the sample that are less than 5 km/s away from the (U, V, W) center of the moving group and Figure 9.3 presents the (μ_{tcp},μ_{pcp}) diagrams where the red dots marked the positions of the stars that are candidate members of the corresponding MG. From Figure 9.3 we can see that the stars that are marked as candidate members to belong to the Hyades MG have a $\mu_{pcp} \sim 0$ which is a good indicator that they belong to the kinematical structure. The other moving groups present some candidate stars that are near the zero line in μ_{pcp} but others stars are far from this region. The stars that are far from $\mu_{pcp} \sim 0$ could be explained by disk heating processes but in order to be clear on this you need to know the distance to the MG to transform the spread in proper motion into a spread in velocity. I tried to determine a mean distance using the candidate stars, but all the distances were almost the same $\sim 70 \pm 20$ pc (which is near the peak of the distribution of distances), so I believe that this is a bias and not the real distance to the MG. Also from Figure 9.3 we see that a lot of stars are near the zero μ_{pcp} line and their membership to a moving group is not completely discarded.

Another thing that is worth notice is the metal abundances. For the Pleiades Boesgaard and Friel [1990] found an iron content of [Fe/H] $= -0.034 \pm 0.024$ and only one star HIP 117043 is in this range. For the Hyades Paulson et al. [2003] found [Fe/H] $= 0.13 \pm 0.01$ and only HIP 64497 is close to this range. Boesgaard and Friel [1990] found for the Sirius moving group [Fe/H] $= -0.09 \pm 0.04$ and only HIP 6011 is in this range.

For IC 2391 Randich et al. [2001] found [Fe/H] $= -0.03 \pm 0.07$ and none of our candidates is in this range; and finally for the Castor MG Paulson and Yelda [2006] found [Fe/H] $= 0.00 \pm 0.04$ and only HIP 42581 is in this range. Due to the continuum fitting problem mentioned in Chapter 6 we have a bias to lower metal abundances, so the inclusion of new stars that are in the range of metallicities of the MG is not discarded.

Finally a lot of the stars that are candidates to belong to MG are active, specially in the Pleiades and Hyades which possess a considerable fraction of stars with $\log R'_{HK} \sim -4.5$ indicating that they are young. This is in agreement with the fact that the moving groups studied by Montes et al. [2001] are young kinematic groups (see the ages in Table 9.1). The stars with low activities ($\log R'_{HK} \sim -5.0$), i.e old stars, could be field stars with no relation with the moving group or in fact they could be part of MG as some of these structures seem to be composed of stars with a wide range in age.

Table 9.2: Candidate moving group members.

Hipparcos Number	$v \sin i$ [km/s]	$[Fe/H]$	LiI EW [Å]	$\log R'_{HK}$	Moving Group
HIP 5189	5.3	0.14	0.08	-5.02	Pleiades
HIP 7576	1.7	0.01	0.10	-4.40	Pleiades
HIP 11514	1.8	0.14	—	-4.85	Pleiades
HIP 19658	4.2	0.02	0.06	-4.47	Pleiades
HIP 37183	9.7	-0.27	0.10	-4.49	Pleiades
HIP 44657	2.6	-0.37	—	-4.55	Pleiades
HIP 51950	7.9	-0.31	0.07	-5.15	Pleiades
HIP 69971	7.8	-0.28	—	-4.92	Pleiades
HIP 107350	13.0	-0.27	0.10	-4.42	Pleiades
HIP 117043	2.9	-0.03	0.05	-4.71	Pleiades
HIP 26973	4.1	0.21	—	-4.47	Hyades
HIP 64497	5.8	0.10	0.08	-4.45	Hyades
HIP 70608	2.8	-0.36	—	-4.5	Hyades
HIP 108708	3.2	0.38	0.06	-4.44	Hyades
HIP 111697	3.4	-0.05	0.05	-4.98	Hyades
HIP 6011	4.0	-0.13	0.06	-4.86	Sirius
HIP 19859	2.4	0.02	0.09	-4.47	Sirius
HIP 58132	4.0	-0.81	—	—	Sirius
HIP 72020	6.6	-0.76	0.04	-4.96	Sirius
HIP 67412	3.1	-0.47	—	-4.64	IC 2391
HIP 104024	3.3	-0.29	—	-4.59	IC 2391
HIP 42581	3.9	0.03	—	-4.94	Castor
HIP 42581	4.1	-0.31	—	-4.94	Castor
HIP 49736	3.7	0.09	0.05	-4.73	Castor
HIP 58387	5.4	0.08	0.09	-4.46	Castor
HIP 70741	6.1	-1.05	0.11	-5.11	Castor

9.3 Stellar Activity and Moving Groups

At the end of the last section it was pointed out that the stars that are candidates to belong to MG have a high level of stellar activity. In order to explore this I did a contour plot of the position of our stars in the UV velocity space and used the stellar activity index $\log R'_{HK}$ as a third dimension in order to see if the regions with more active stars are near the center of known moving groups. Figure 9.4 shows a contour plot for 869 stars of our sample with known kinematics and activities, we can see that there is an abundance of active stars near the centers of NGC 1901, IC 2391 and Coma Berenices and also clumps of active stars with $\log R'_{HK} \sim -4.5$ in the zone were we have the biggest density of stars in our sample (see Figure 9.2).

In order to see if this was not a selection effect, I decided to plot the stars in the sample of Gray et al.

[2006b]. The work of Gray et al. [2006b] was a project dedicated to do spectroscopic observations of 3600 main sequence stars that are near than 40 pc from the Sun and are included in the Hipparcos Catalog. In Figure 9.5 we can see the same contour plot as Figure 9.4 for 951 stars from Gray et al. [2006b] with known UVW velocities taken from the GCS. Even if the stellar activity axis has changed due to the presence of more active stars than our sample, we still can observed the clumps of active stars with $\log R'_{HK} \sim -4.5$ near the Hyades, NGC 1901, IC 2391, Coma Berenices, Sirius and Pleiades moving groups.

As a final exercise we proceeded to merge and plot the 951 stars from Gray et al. [2006b] and the 869 stars from our sample. The main results are the same as shown in Figure 9.6. In this figure it is worth notice that more clumpy and complex structures appear thanks to the increase in the number of stars used in the plot.

This clumpy structures of active stars appear to be close to the position of known MG and they could support the idea that these structures have a common origin if contamination by field stars is not common. Future statistical analysis can quantify this apparent correlation.

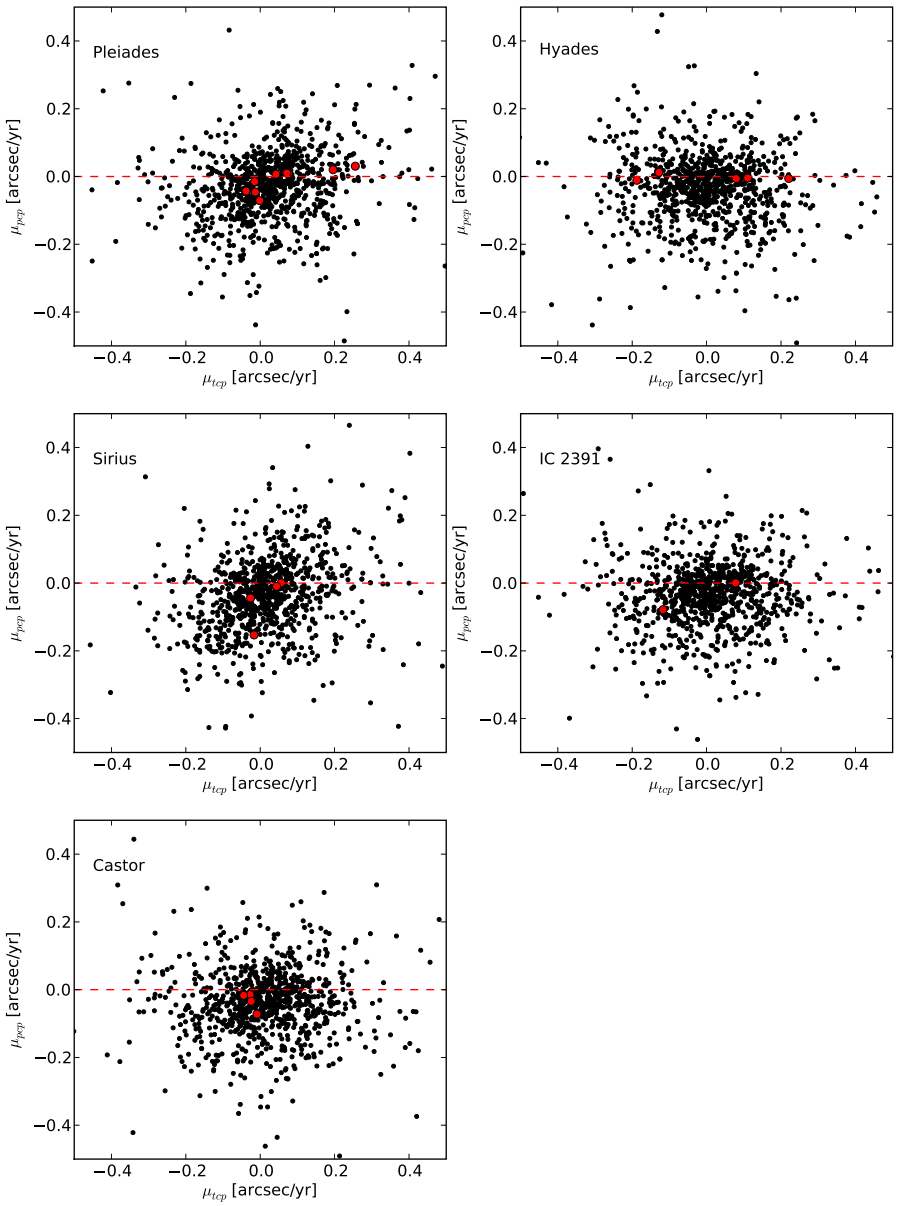

Figure 9.3: (μ_{tcp},μ_{pcp}) diagram for the MG of Montes et al. [2001]. The red dots show the stars that are less than 5 km/s away from the (U, V, W) center of the moving group.

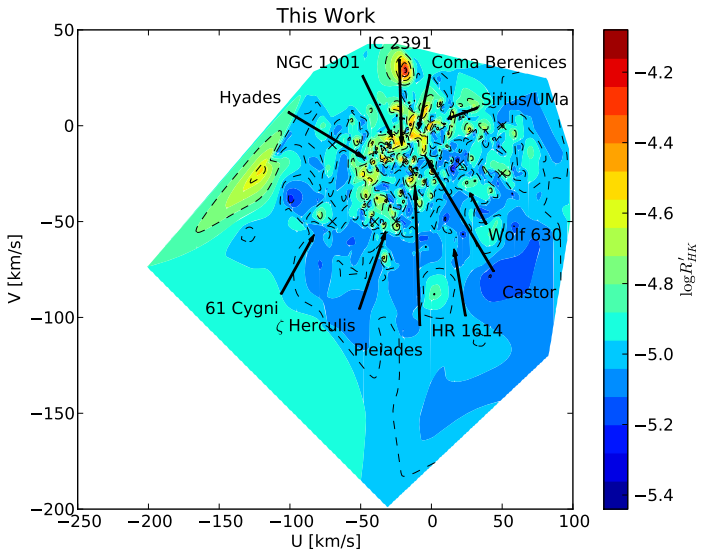

Figure 9.4: The center of moving groups and stellar activities for the star in our sample.

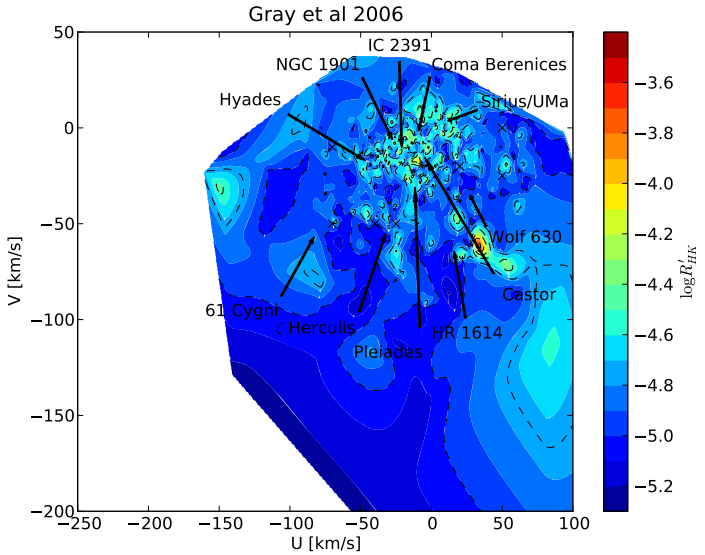

Figure 9.5: The center of moving groups and stellar activities for the star in Gray et al. [2006b].

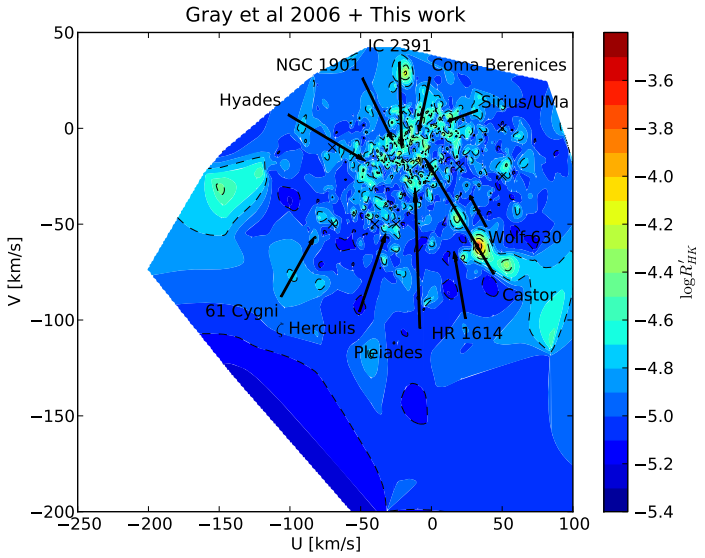

Figure 9.6: The center of moving groups and stellar activities for the star in Gray et al. [2006b] plus our sample.

Chapter 10

Conclusions

The main conclusions of this work are:

- **Binary Systems :** I identify 32 spectrum binaries, 29 of them could be new systems. I was interested in such systems because they lead to wrong values derived from photometry as we can not resolve the individual components and also because they have to be discarded in a radial velocity planet search due to the difficulty of detecting the motion induced by the planet in one of the components. However spectrum binaries are interesting to study because it is possible to establish the mass of the components through Kepler's Laws and follow up of these systems to establish orbital periods is a nice future project.

- **Effective Temperatures :** I present effective temperatures computed using the Infrared Flux Method for 890 southern stars. The IRFM is fairly insensitive to the metallicity but as it is one of the parameters needed in the computation of metallicities a higher accuracy in T_{eff} may be needed. This could be achievable by using some spectral index or refining the method used to compute the abundances by creating a loop: use the temperatures assuming [Fe/H] = 0.0 to compute the metallicity as in this work and once obtained recompute the T_{eff} again and so on until convergence in abundances and temperatures is reached.

- **Radial Velocities :** I present radial velocity measurements for 911 stars in the sample. The determination of radial velocities was done by using the spectra that belong to stars in the sample with known radial velocity. This has the advantage of being a relatively quick process to get physical parameters that need radial velocity values like the metallicities, but if one wants to achieve a greater accuracy synthetic models may be the answer. Some radial velocity values may be wrong for $\sim 8\%$ of the stars based on our comparison with the GCS. This is probably due to bad signal to noise in some spectra caused by bad weather at the time of observation. The radial velocity measurements for the spectrum binaries almost always corresponded to one of the components of the system and for that reason they were not left out of the kinematical analysis.

- **Metal Abundances :** Using the temperatures, radial velocities and rotational velocities found in this work, the metal abundances for 890 stars were computed. Our values compared to other works have a slight bias to lower metal abundances probably caused by a bad continuum normalization. Leaving this aside, our values are accurate compared with other works and using the probability law of finding planets of Fischer and Valenti [2005], we can estimate that in our sample of 890 stars 28 planets could be detected through the radial velocity technique. The distribution of metallicities was not representative for the distribution in the solar neighborhood because of the bias in the selection of the sample.

- **Stellar Ages :** I present ages computed using isochrone fitting for 890 stars. I have selected the evolved stars that should have a better age constraint using a fitted main sequence from Wright [2004]. Also I present the values of age indicators from the stellar velocity of rotation ($v \sin i$), the stellar activity index ($\log R'_{HK}$) and the equivalent width of Lithium absorption lines, if they were present, and I did a comparison between these quantities.

- **Kinematics :** Using our radial velocities and data from Hipparcos we were able to compute the heliocentric space velocities (U, V, W) for 911 stars in the sample. A comparison with the values of the GCS for the stars in common showed that our space velocities are in fair agreement with their values. We studied the U, V, W distribution of stars and concluded that all the stars in our sample are bound to the galaxy. Also we focused on three high velocity stars and thanks to the abundances and an orbit determination we were able to conclude that these stars belong to the Halo of the galaxy, offering a great opportunity to study nearby metal poor objects and old.

- **Moving Groups :** Using a Kernel Density Estimation we were able to detect the presence of known moving groups in our sample and we tried to select possible members of this kinematical structures. The detection and selection techniques should be refined in the future to establish in a more secure way the presence and members of moving groups for the stars in our sample. The relationship between the moving groups and stars with high stellar acitivity was investigated and we found several clumps of active stars near the center of known moving groups. The detection and selection of members was not the main goal of this work, but we thought that as we were working with local stars these structures are of great importance.

For future work we expect to expand the sample of stars in order to complete the Hipparcos catalog in the southern hemisphere. Following that objective an ESO proposal to observed 500 new stars was recently submitted. In the case of the stars that we suspect that belong to Moving Groups an ESO proposal was also recently submitted in order try to detect planets or low mass companions the using adaptive optics instrument NaCo at Paranal, Chile. Finally the kinematics and the abundances of different elements will be used to do a complete abundance study to constrain chemical evolution models.

Acknowledgments: This research has made use of the SIMBAD database, operated at CDS, Strasbourg, France.

Appendices

Appendix A

Table of Results

Symbols used in Table A.1 :

- HIP : Hipparcos number.
- α : Right ascension (ICRS) in format hh mm ss.ss.
- δ : Declination (ICRS) in format dd mm ss.ss.
- V_r : Radial velocity in km/s.
- U : Heliocentric velocity component U in km/s.
- V : Heliocentric velocity component V in km/s.
- W : Heliocentric velocity component W in km/s.
- $V \sin i$: Rotational velocity in km/s.
- $\log R'_{HK}$: Activity index.
- $[Fe/H]$: Metal abundance.
- EW : Li 6708 Å equivalent width in Å.
- T_{eff} : Effective temperature in K.
- Age : Age determined by isochrone fitting in Gyr.
- σ_{age}^{low} : Low limit in age in Gyr.
- σ_{age}^{high} : Upper limit in age in Gyr.

Table A.1: Table of Results.

HIP	α	δ	V_r	U	V	W	$V \sin i$	$\log R'_{HK}$	$[Fe/H]$	EW	T_{eff}	Age	σ_{age}^{low}	σ_{age}^{high}
72	00 00 52.78	-12 49 44.25	-52.1 ± 1.6	-48.9 ± 5.4	-97.9 ± 9.6	19.8 ± 3.8	2.1	-5.09	0.02	—	5708	9.4	8.4	9.9
81	00 00 58.41	-04 55 57.12	-0.2 ± 1.6	49.6 ± 2.7	-10.8 ± 0.9	-5.7 ± 1.5	2.0	-4.94	-0.46	—	5633	12.0	11.1	12.6
135	00 01 42.43	-00 13 03.99	-7.8 ± 1.6	9.2 ± 0.6	-26.1 ± 1.6	-6.3 ± 1.6	2.2	-4.80	-0.22	0.040	5833	3.9	3.9	6.0
599	00 07 15.37	-41 53 22.43	10.1 ± 1.6	15.8 ± 0.9	11.1 ± 0.8	-7.9 ± 1.6	1.2	-4.99	-0.34	—	5777	13.4	12.6	13.7
772	00 09 30.68	-34 06 39.10	-26.1 ± 1.6	3.9 ± 0.6	-6.7 ± 0.4	27.6 ± 1.6	2.1	-5.05	0.08	—	5605	10.4	9.1	10.4
846	00 10 23.07	-13 59 02.23	-12.9 ± 1.6	-67.8 ± 6.4	-12.1 ± 0.9	8.1 ± 1.6	1.0	-4.93	-0.23	0.038	5910	7.4	7.4	7.6
1000	00 12 30.27	-22 04 02.33	34.5 ± 1.8	-40.5 ± 3.8	-51.9 ± 5.0	-46.8 ± 2.1	7.0	-4.93	-0.33	—	5495	14.7	14.7	16.1
1173	00 14 39.08	-39 47 39.39	18.8 ± 1.6	-1.8 ± 0.7	-24.1 ± 2.2	-16.8 ± 1.6	1.7	-4.92	0.18	—	5841	2.3	1.9	4.1
1567	00 19 29.46	-54 00 41.78	21.2 ± 1.7	11.3 ± 0.7	-19.0 ± 1.1	-12.6 ± 1.6	4.1	-5.03	-0.04	0.066	6018	5.7	4.7	6.4
1683	00 21 02.97	-58 45 38.29	43.4 ± 1.7	16.4 ± 0.7	-35.7 ± 2.2	-27.5 ± 1.8	2.4	-5.04	0.12	—	5804	7.5	6.3	7.7
1712	00 21 33.13	-35 21 37.84	-40.4 ± 1.7	-18.2 ± 1.3	12.8 ± 1.1	37.0 ± 1.7	4.0	-5.07	-0.08	0.040	6084	5.1	4.0	5.1
1803	00 22 51.78	-12 12 33.97	-2.7 ± 1.8	-35.7 ± 0.6	-14.6 ± 0.5	-0.0 ± 1.7	6.2	-4.45	0.14	0.085	5750	2.6	1.5	3.8
1914	00 24 13.36	-75 40 45.89	8.9 ± 1.7	8.9 ± 0.8	-23.4 ± 1.4	14.1 ± 1.5	3.3	-4.81	0.11	0.044	5880	5.8	5.8	6.9
1937	00 24 26.62	-78 15 01.38	3.7 ± 1.6	0.6 ± 0.7	-3.9 ± 1.1	-1.5 ± 1.0	2.0	-5.20	0.2	—	5676	9.6	8.6	9.7
1970	00 24 56.37	-41 53 09.70	1.2 ± 1.7	-34.5 ± 2.8	-18.0 ± 1.5	-5.6 ± 1.6	3.2	-4.79	0.08	—	5231	2.4	2.0	2.9
1977	00 25 03.97	-51 28 45.93	2.1 ± 1.7	-45.0 ± 3.9	-40.4 ± 3.4	-2.8 ± 1.5	3.0	-5.00	0.25	0.084	6166	0.9	0.2	1.9
2066	00 26 08.67	-11 22 37.08	-23.9 ± 1.7	-9.1 ± 0.7	-24.0 ± 1.2	18.4 ± 1.6	2.6	-4.93	-0.44	0.054	5751	13.4	12.8	15.1
2311	00 29 28.58	-11 01 01.76	-33.0 ± 1.6	-29.9 ± 2.1	-41.7 ± 2.1	24.4 ± 1.6	0.8	-5.00	-0.54	—	5071	14.6	14.6	14.8
2318	00 29 33.40	-35 49 25.21	-11.5 ± 1.6	17.7 ± 1.5	3.9 ± 0.3	14.0 ± 1.6	1.4	-4.89	-0.07	0.060	5875	4.4	4.3	6.9
2368	00 30 12.93	-19 11 39.91	72.5 ± 1.6	116.5 ± 11.9	-45.6 ± 5.8	-81.0 ± 1.9	0.9	—	-0.82	—	5651	14.1	12.6	15.6
2542	00 32 21.07	-51 59 25.72	-0.4 ± 1.7	-19.8 ± 2.1	-16.4 ± 1.8	0.3 ± 1.5	3.1	-5.06	0.09	0.076	6087	2.9	2.5	3.3
2574	00 32 40.97	-35 25 30.15	-25.4 ± 1.6	-31.5 ± 3.5	-12.9 ± 1.9	22.6 ± 1.7	2.4	-5.08	0.24	—	5674	8.8	7.1	10.1
2766	00 35 15.97	-29 12 35.55	-1.9 ± 1.7	10.8 ± 1.1	-31.3 ± 2.9	2.6 ± 1.7	2.5	-5.03	0.01	0.055	5986	6.0	5.3	7.6
2864	00 36 18.26	-43 14 24.55	51.9 ± 1.7	55.1 ± 4.2	0.7 ± 1.1	-43.3 ± 1.7	2.1	-4.95	-0.2	—	5998	5.7	5.1	5.8
2902	00 36 46.81	-24 30 03.37	5.9 ± 1.6	14.0 ± 1.1	-16.0 ± 1.3	-6.7 ± 1.6	2.8	-5.18	0.17	0.053	5343	5.9	4.8	7.5
2941	00 37 19.78	-24 46 02.01	18.5 ± 1.6	-88.1 ± 1.9	-54.2 ± 1.2	-24.2 ± 1.6	1.2	-4.96	0.01	—	5730	12.8	12.1	13.3
3028	00 38 33.23	-12 10 20.70	33.1 ± 1.6	-30.3 ± 1.4	10.3 ± 0.4	-28.7 ± 1.6	2.0	-4.92	-0.27	—	5143	13.7	12.8	14.6
3148	00 40 01.88	-46 54 44.82	5.1 ± 1.7	-27.4 ± 2.5	9.1 ± 1.0	-14.2 ± 1.8	3.0	-4.52	-0.11	—	5854	5.7	5.0	5.8
3185	00 40 32.80	-23 48 17.55	-46.2 ± 1.6	-47.4 ± 1.0	-90.1 ± 1.8	39.5 ± 1.6	1.7	-5.06	-0.62	—	5388	12.9	12.8	13.6
3238	00 41 12.04	-68 27 28.36	35.0 ± 1.6	62.8 ± 3.4	4.3 ± 1.8	-18.5 ± 1.3	2.7	-4.87	-0.5	—	5605	14.4	14.1	14.7
3292	00 42 00.93	-53 11 56.28	-2.7 ± 1.7	-42.0 ± 3.3	23.8 ± 1.9	-18.5 ± 2.2	1.6	-4.90	-0.46	0.044	6001	8.0	7.3	8.3
3443	00 43 58.93	-24 52 20.98	7.3 ± 1.7	6.7 ± 0.7	-5.4 ± 0.6	-7.6 ± 1.7	3.7	-4.99	0.26	0.076	6113	2.0	0.5	2.1
3605	00 46 10.82	-20 39 49.94	68.9 ± 1.6	81.6 ± 17.3	24.8 ± 3.6	-70.2 ± 1.7	2.1	-5.03	-0.32	—	5665	7.9	6.6	9.2
3643	00 46 38.73	-36 02 01.03	0.0 ± 1.7	20.2 ± 1.1	-14.4 ± 0.8	3.6 ± 1.7	2.6	-4.93	-0.34	0.040	5900	9.0	8.2	9.6
4062	00 52 01.50	-74 52 12.27	55.5 ± 1.7	18.3 ± 0.7	-48.1 ± 1.3	-27.1 ± 1.3	3.1	—	-0.74	—	5867	16.1	16.1	16.1
4194	00 53 34.97	-22 12 12.87	-1.1 ± 1.6	-27.6 ± 1.8	-44.7 ± 2.9	-0.3 ± 1.6	1.4	-4.66	-0.1	—	5509	2.4	1.9	4.5
4195	00 53 35.44	-24 01 48.54	14.1 ± 1.6	-1.1 ± 0.3	-79.6 ± 5.6	-17.3 ± 1.6	1.3	-4.95	-0.24	—	5660	13.2	12.6	13.7
4242	00 54 09.16	-18 01 55.75	-1.3 ± 1.6	-18.4 ± 1.6	-51.1 ± 4.4	-3.4 ± 1.7	2.7	-5.15	0.4	—	5454	9.8	9.4	10.2
4403	00 56 28.12	-06 43 15.69	9.9 ± 1.7	-35.3 ± 2.7	-13.5 ± 1.4	-6.8 ± 1.6	2.2	-5.04	0.11	0.075	6227	3.1	1.7	3.5
4420	00 56 37.76	-23 39 22.98	-4.4 ± 1.7	-23.9 ± 2.1	20.5 ± 1.8	6.4 ± 1.7	2.5	-4.94	-0.36	0.044	6004	10.3	10.3	10.4
4864	01 02 32.75	-57 20 28.95	60.3 ± 1.7	-55.7 ± 4.1	-74.6 ± 2.8	-48.2 ± 1.4	2.3	-4.99	0.11	—	5872	5.9	5.6	5.9
4951	01 03 29.65	-14 30 27.24	-4.1 ± 1.7	28.5 ± 3.8	-23.7 ± 3.1	-4.2 ± 2.0	2.5	-5.07	0.14	—	5892	6.8	6.8	8.0
4981	01 03 50.35	-31 47 10.97	-6.6 ± 1.6	2.9 ± 0.3	9.2 ± 0.7	5.8 ± 1.6	1.6	-4.93	-0.3	—	5823	1.9	1.9	2.7
5031	01 04 26.47	-02 21 59.74	-14.5 ± 1.6	48.3 ± 2.0	-2.2 ± 0.5	0.6 ± 1.5	0.7	-4.94	-0.55	—	5132	12.6	11.8	13.8
5189	01 06 25.71	-00 44 58.02	8.5 ± 1.7	-15.5 ± 1.1	-20.1 ± 1.8	-11.9 ± 1.6	5.3	-5.02	0.14	0.083	6039	3.9	3.9	4.5
5311	01 07 57.61	-37 53 53.36	-23.9 ± 1.7	-12.6 ± 1.4	7.1 ± 0.5	22.3 ± 1.6	2.7	-4.86	-0.07	0.070	6012	1.4	0.2	1.4
5462	01 09 56.60	-64 21 33.15	0.5 ± 1.7	-0.3 ± 0.5	1.5 ± 0.9	-1.8 ± 1.3	3.5	-4.39	-0.14	0.114	5587	1.1	0.4	1.1
5549	01 11 11.22	-82 32 55.73	-40.7 ± 1.6	-45.2 ± 1.7	-39.3 ± 4.0	85.2 ± 3.6	2.3	-4.88	-0.74	—	5600	14.4	14.4	16.1
5697	01 13 18.82	-01 51 43.61	-6.4 ± 1.6	45.2 ± 2.5	12.0 ± 0.9	-4.4 ± 1.6	2.1	-4.96	-0.32	—	5537	4.8	3.5	5.1
5740	01 13 44.53	-30 18 37.50	-13.7 ± 1.7	6.3 ± 0.7	-15.6 ± 1.7	15.0 ± 1.6	2.2	-5.00	-0.05	—	5852	1.9	1.4	1.9
5769	01 14 03.82	-11 49 55.66	7.3 ± 1.8	-0.4 ± 0.6	-10.3 ± 1.3	-9.3 ± 1.7	6.4	-4.91	-0.35	0.049	5895	9.4	8.9	11.1
5817	01 14 40.45	-64 45 51.10	55.8 ± 1.6	24.5 ± 0.7	-113.4 ± 4.9	15.6 ± 3.6	1.9	-5.03	-0.1	—	5424	14.7	13.7	15.9
5831	01 14 47.15	-29 23 25.37	-38.2 ± 1.6	-19.1 ± 2.1	3.2 ± 0.3	39.1 ± 1.6	2.0	-5.01	-0.2	—	5659	14.8	13.9	15.3
6011	01 17 17.86	-34 39 49.84	9.7 ± 1.7	15.0 ± 0.9	-0.8 ± 0.3	-9.8 ± 1.7	4.0	-4.86	-0.13	0.065	6060	4.5	3.6	6.0
6024	01 17 23.68	-61 34 45.59	37.4 ± 1.6	17.3 ± 0.7	-60.4 ± 2.8	-2.8 ± 2.2	2.5	-5.01	-0.36	—	5585	14.0	13.3	14.0
6044	01 17 37.04	-27 00 44.57	-3.2 ± 1.7	-29.4 ± 5.6	-10.1 ± 2.0	6.3 ± 1.7	2.9	-5.15	0.24	—	5634	8.2	6.6	9.3
6074	01 17 58.43	-49 20 28.13	21.5 ± 1.7	-25.9 ± 4.3	-21.4 ± 2.2	-19.0 ± 1.6	3.6	-5.07	0.33	0.060	5791	4.7	3.6	4.7
6100	01 18 19.00	-23 29 59.44	-3.3 ± 1.7	8.0 ± 0.8	-50.1 ± 5.0	2.7 ± 1.6	3.2	-5.11	-0.05	—	5284	3.4	2.8	4.0
6125	01 18 37.97	-25 53 56.32	31.5 ± 1.6	-64.8 ± 10.2	-22.6 ± 3.5	-24.3 ± 2.0	3.0	-5.09	0.12	—	5426	3.6	2.8	5.0
6155	01 18 57.71	-71 06 55.82	27.2 ± 1.8	-52.6 ± 5.0	-22.6 ± 1.2	-44.1 ± 2.3	5.9	—	-0.71	—	6121	6.1	5.2	7.1
6158	01 18 58.09	-10 58 27.40	13.6 ± 1.7	40.4 ± 4.1	9.5 ± 0.8	-23.1 ± 1.9	4.0	-5.01	0.02	0.044	5609	5.7	4.5	7.1
6197	01 19 29.06	-24 57 04.35	9.3 ± 1.6	21.5 ± 1.4	-21.8 ± 1.3	-11.1 ± 1.6	1.6	-4.77	0.18	—	5637	7.3	7.3	7.9
6305	01 21 00.55	-12 44 34.50	4.6 ± 1.7	-28.9 ± 2.9	-16.3 ± 1.8	-0.0 ± 1.7	2.8	-5.00	-0.02	0.038	5915	2.3	0.3	3.0
6422	01 22 26.84	-47 42 35.02	30.6 ± 1.7	51.5 ± 4.0	-28.9 ± 1.6	-15.6 ± 1.9	2.0	-4.98	-0.24	0.044	5950	7.2	6.9	7.5
6456	01 23 02.63	-12 57 57.84	34.2 ± 1.6	-59.1 ± 1.5	-37.7 ± 1.2	-25.7 ± 1.6	1.9	-5.08	0.41	—	5243	12.8	11.1	12.8
6497	01 23 25.98	-14 12 24.91	19.4 ± 1.7	-32.2 ± 2.1	-12.1 ± 1.1	-13.7 ± 1.6	3.3	-5.10	0.26	0.105	5819	5.6	4.7	6.9
6712	01 26 19.20	-04 40 26.79	-23.8 ± 1.6	54.2 ± 3.8	-13.4 ± 0.8	2.9 ± 2.1	2.6	-4.87	0.2	—	5617	7.2	6.3	8.4
6772	01 27 05.77	-51 57 56.78	49.3 ± 1.6	-73.7 ± 4.4	-56.2 ± 2.1	-41.6 ± 1.5	1.9	-4.94	-0.15	0.041	5898	6.2	5.2	6.2
6987	01 29 55.85	-10 33 54.15	115.7 ± 1.7	-49.1 ± 1.4	-66.6 ± 7.2	-117.4 ± 1.7	3.2	-5.06	-0.77	—	5683	8.2	6.7	9.6
6990	01 29 59.89	-22 31 27.22	30.4 ± 1.6	-22.4 ± 1.0	-32.1 ± 1.8	-26.3 ± 1.6	2.7	-5.07	0.12	—	5783	7.2	7.2	8.6
6993	01 30 01.00	-19 36 16.20	22.8 ± 1.7	22.2 ± 2.2	-56.5 ± 4.5	-29.0 ± 1.7	3.0	-5.22	0.36	—	5577	8.6	8.0	8.6
7023	01 30 30.53	-14 04 23.99	37.2 ± 1.6	-20.8 ± 0.9	3.6 ± 0.3	-32.7 ± 1.6	2.4	-4.62	-0.26	—	5249	14.0	13.6	14.3

Continued on next page

Table A.1 – continued from previous page

HIP	α	δ	V_r	U	V	W	$V \sin i$	$\log R'_{HK}$	$[Fe/H]$	EW	T_{eff}	Age	σ_{age}^{low}	σ_{age}^{high}
7076	01 31 11.05	-09 18 44.05	26.5 ± 1.6	-10.0 ± 0.5	-15.5 ± 0.9	-27.6 ± 1.5	1.1	-4.93	-0.13	—	5786	7.5	6.5	8.6
7107	01 31 33.87	-69 59 33.27	12.2 ± 1.8	-17.3 ± 1.7	-21.6 ± 1.5	-6.5 ± 1.3	6.6	-5.04	0.16	—	6118	3.4	3.2	3.8
7109	01 31 34.99	-13 41 24.36	-23.2 ± 1.6	37.8 ± 3.0	-62.9 ± 5.6	7.3 ± 2.1	2.3	—	-0.87	—	5640	15.6	15.6	16.1
7167	01 32 24.58	-37 17 04.44	20.3 ± 1.6	-8.7 ± 0.6	-8.1 ± 0.5	-18.8 ± 1.6	1.8	-4.75	-0.05	0.057	5806	0.5	0.4	1.2
7233	01 33 15.39	-12 42 28.70	52.8 ± 1.6	-80.5 ± 5.5	10.4 ± 0.5	-30.6 ± 2.3	2.2	-5.03	0.29	—	5548	0.6	0.5	0.7
7276	01 33 42.83	-07 01 31.22	-15.3 ± 1.7	-8.1 ± 0.6	-26.7 ± 0.6	14.3 ± 1.6	3.9	-5.12	0.14	0.071	5803	5.3	5.2	5.5
7396	01 35 20.97	-21 12 03.94	5.1 ± 1.6	-11.5 ± 0.5	-23.8 ± 0.9	-2.4 ± 1.6	1.4	-4.91	-0.39	—	5024	14.7	13.3	16.0
7427	01 35 40.96	-05 04 38.57	27.5 ± 1.7	-35.7 ± 1.6	-3.4 ± 0.6	-16.8 ± 1.6	2.9	-5.01	0.1	0.057	6053	3.6	3.0	3.8
7576	01 37 35.46	-06 45 37.52	11.2 ± 1.6	-12.9 ± 0.6	-18.1 ± 0.5	-10.7 ± 1.5	1.7	-4.40	0.01	0.106	5271	3.7	2.9	3.7
7693	01 39 01.95	-33 28 05.27	26.0 ± 1.7	26.0 ± 3.6	-59.8 ± 7.1	-16.9 ± 2.0	3.3	-5.05	0.23	0.138	5714	5.6	4.7	6.4
7799	01 40 22.45	-10 26 40.05	12.8 ± 1.6	-38.8 ± 3.0	-37.6 ± 3.3	-5.0 ± 1.6	1.9	-4.55	0.08	—	5712	0.3	0.3	1.5
7814	01 40 32.24	-69 59 13.07	53.6 ± 1.7	-56.1 ± 4.6	-92.3 ± 3.8	-19.9 ± 1.7	3.2	-5.09	0.01	0.042	5879	5.9	5.9	6.6
7823	01 40 36.51	-31 42 58.26	23.5 ± 1.6	-17.6 ± 1.2	-56.5 ± 4.0	-12.1 ± 1.8	-	-4.98	0.0	0.037	5958	5.0	4.4	5.7
7934	01 41 59.52	-17 10 44.49	-14.8 ± 1.6	36.1 ± 3.4	-18.1 ± 1.9	5.0 ± 1.9	2.6	-5.02	-0.18	—	5618	12.6	11.1	12.7
8060	01 43 32.34	-19 24 12.66	12.3 ± 2.1	-24.4 ± 1.7	-9.4 ± 0.7	-6.4 ± 2.0	11.0	-4.44	-0.21	0.086	6092	8.5	8.2	8.8
8102	01 44 05.12	-15 56 22.40	-16.9 ± 1.6	18.8 ± 0.4	29.3 ± 0.1	13.2 ± 1.6	1.6	-4.97	-0.34	—	5526	14.0	13.9	14.1
8188	01 45 16.36	-15 53 44.42	-9.2 ± 1.7	-34.1 ± 3.0	-103.2 ± 8.3	16.4 ± 1.7	2.9	-4.97	-0.11	—	5800	8.1	7.6	8.4
8349	01 47 40.11	-03 14 14.89	22.2 ± 1.7	-83.8 ± 6.7	-2.4 ± 0.8	13.6 ± 3.3	4.4	-4.98	-0.54	—	6020	9.1	8.1	9.4
8507	01 49 42.92	-18 56 09.84	-9.7 ± 1.6	-6.8 ± 0.8	-3.0 ± 0.3	12.1 ± 1.6	1.3	-4.95	-0.12	—	5629	10.0	9.6	10.5
8653	01 51 31.19	-07 44 23.65	44.2 ± 1.7	-31.1 ± 1.0	-7.0 ± 0.8	-36.2 ± 1.5	3.3	-4.49	-0.18	0.060	5678	1.7	1.6	3.3
8799	01 53 07.68	-59 24 45.23	14.6 ± 1.6	-35.5 ± 2.0	-10.7 ± 0.9	-18.5 ± 1.4	1.8	-5.09	0.15	—	5655	11.2	9.9	11.2
8881	01 54 22.18	-15 43 26.32	-1.2 ± 1.6	-24.1 ± 1.2	-51.5 ± 2.3	8.8 ± 1.6	2.8	-4.46	-0.29	0.053	4946	14.3	13.1	15.4
8923	01 54 54.04	-11 30 40.78	-23.3 ± 1.7	13.0 ± 0.7	1.1 ± 0.3	20.0 ± 1.6	3.0	-5.00	0.36	0.055	5906	3.3	3.3	3.6
9029	01 56 17.86	-25 16 50.87	45.0 ± 1.7	-42.5 ± 3.3	-50.5 ± 4.5	-30.4 ± 2.1	4.2	-5.04	-0.1	0.044	6012	5.7	5.0	6.0
9036	01 56 22.89	-60 11 33.77	73.3 ± 1.6	58.2 ± 3.1	-52.4 ± 1.3	-41.7 ± 1.9	2.3	-5.21	-0.02	—	5131	10.0	8.6	11.6
9346	01 59 59.86	-31 44 59.91	5.1 ± 1.7	1.2 ± 0.5	2.4 ± 0.6	-6.0 ± 1.7	4.5	-5.14	0.06	0.096	5833	6.1	5.1	6.8
9404	02 00 48.75	-12 52 29.93	15.8 ± 1.6	-51.1 ± 2.3	-8.9 ± 0.5	2.7 ± 1.7	0.7	—	-0.2	—	5433	9.6	8.7	10.5
9692	02 04 40.49	-16 17 15.26	-2.3 ± 1.7	-3.2 ± 1.7	0.7 ± 1.0	3.7 ± 1.7	4.4	-4.71	-0.28	0.063	5844	0.9	0.1	0.9
9769	02 05 37.47	-24 22 46.14	40.6 ± 1.6	-67.3 ± 3.8	-72.4 ± 4.4	-14.0 ± 2.3	1.4	-5.01	-0.24	—	5307	14.0	13.6	14.5
9774	02 05 41.51	-24 22 33.73	40.6 ± 1.7	-66.6 ± 4.7	-71.5 ± 5.6	-14.3 ± 2.6	4.5	-4.98	-0.42	—	4962	15.1	15.1	15.1
9837	02 06 34.49	-14 27 50.49	2.8 ± 1.7	49.9 ± 4.4	1.6 ± 0.3	-22.8 ± 2.3	3.1	-5.13	-0.28	0.075	5729	7.1	6.0	8.4
9883	02 07 10.18	-47 47 54.59	-30.0 ± 1.6	9.5 ± 1.1	-13.1 ± 2.7	39.6 ± 1.9	2.5	-5.13	0.02	—	5502	12.3	10.6	12.6
10061	02 09 30.24	-41 23 14.22	6.4 ± 1.7	-32.2 ± 2.2	-12.3 ± 0.9	0.1 ± 1.6	3.2	-5.15	0.14	—	5728	7.9	7.3	9.1
10090	02 09 44.46	-30 44 46.48	8.7 ± 1.6	73.2 ± 8.2	-62.5 ± 6.6	-9.1 ± 1.6	2.7	-5.15	0.24	—	5515	8.1	6.6	9.6
10190	02 10 59.59	-25 27 28.17	37.6 ± 1.7	-9.2 ± 0.6	-50.2 ± 4.6	-28.4 ± 1.8	3.5	-5.05	-0.18	0.055	5803	8.5	7.1	9.1
10212	02 11 21.07	+08 34 11.29	-15.4 ± 1.7	38.3 ± 1.4	-2.5 ± 0.5	-10.1 ± 1.5	3.5	-5.16	0.32	0.069	6045	2.8	2.8	3.3
10325	02 13 00.13	-40 00 20.50	19.7 ± 1.6	41.2 ± 3.6	-78.4 ± 6.1	4.2 ± 2.4	2.7	-5.21	0.35	—	5171	8.9	7.1	10.1
10346	02 13 15.99	-59 34 01.08	16.1 ± 1.6	-21.4 ± 1.3	-34.1 ± 1.6	-0.3 ± 1.5	3.2	-4.38	0.0	—	5143	14.5	14.5	16.1
10365	02 13 35.08	-08 48 58.81	-4.2 ± 1.6	-9.7 ± 1.1	12.2 ± 0.9	10.2 ± 1.5	2.5	—	-0.82	—	5278	15.6	14.8	15.6
10426	02 14 20.58	-37 06 27.75	15.7 ± 1.7	-79.4 ± 9.1	-46.8 ± 4.9	10.1 ± 3.3	3.4	-4.64	0.29	—	5645	8.8	7.7	9.2
10460	02 14 52.14	-06 06 21.40	24.3 ± 1.7	-37.2 ± 2.3	-23.3 ± 2.2	-9.8 ± 1.8	2.4	-5.01	0.04	0.052	6065	2.5	2.4	3.9
10532	02 15 41.72	-09 00 47.23	46.2 ± 1.6	-26.3 ± 0.8	-0.4 ± 0.3	-38.6 ± 1.5	0.7	-4.75	-0.12	—	5139	15.3	14.7	15.7
10543	02 15 47.42	-24 46 20.45	-8.0 ± 1.7	-19.7 ± 1.6	3.9 ± 0.4	13.6 ± 1.7	4.1	-5.03	0.26	0.060	6004	3.2	3.0	3.2
10545	02 15 49.38	-15 53 34.73	-17.7 ± 1.6	42.1 ± 2.7	-12.3 ± 1.0	2.5 ± 1.8	0.7	-4.96	0.06	0.051	5987	1.6	0.6	2.2
10561	02 15 57.50	-04 05 42.44	18.0 ± 1.7	-44.8 ± 3.0	-52.9 ± 4.3	-1.6 ± 1.8	2.3	-5.09	-0.1	—	5800	7.7	7.0	9.1
10725	02 18 02.33	-50 49 07.50	-0.7 ± 1.7	-41.9 ± 1.8	-9.5 ± 0.9	4.4 ± 1.5	2.9	-4.51	-0.17	—	5754	10.6	9.4	11.7
10758	02 18 26.04	-06 36 20.97	-3.1 ± 1.7	-76.3 ± 9.4	-89.6 ± 10.8	38.8 ± 4.6	2.4	-5.05	-0.38	—	5863	8.9	7.6	10.6
10870	02 19 53.52	-23 38 04.77	-10.9 ± 1.7	20.6 ± 2.1	3.6 ± 0.5	4.3 ± 1.7	1.7	-5.06	-0.24	0.055	6076	6.6	6.0	7.9
10973	02 21 21.11	-30 32 52.14	12.0 ± 1.6	33.5 ± 3.3	-111.2 ± 9.8	9.1 ± 2.4	2.2	-4.98	-0.12	—	5679	6.8	5.7	6.8
10990	02 21 38.63	-15 46 04.72	0.4 ± 1.7	2.0 ± 0.8	-26.8 ± 3.4	0.4 ± 1.5	4.0	-5.11	-0.01	0.056	5674	4.0	3.4	5.5
11263	02 24 58.77	-54 13 51.99	13.1 ± 1.6	-11.3 ± 0.6	10.5 ± 1.2	-22.9 ± 1.5	1.5	-4.90	-0.09	0.060	5984	6.7	5.4	6.7
11324	02 25 44.95	-21 18 47.84	29.8 ± 1.5	-17.3 ± 5.3	-3.9 ± 2.3	-25.1 ± 13.2	-	-4.77	1.5	—	6001	0.3	0.1	0.3
11359	02 26 15.36	-23 53 17.20	-12.2 ± 1.6	43.0 ± 2.1	-21.1 ± 1.3	2.4 ± 1.6	2.1	-4.81	-0.07	—	5584	8.1	7.1	8.7
11363	02 26 20.63	-29 08 33.72	80.2 ± 1.7	-47.1 ± 2.7	-67.2 ± 4.7	-55.0 ± 2.5	2.5	-4.96	-0.76	—	5788	15.5	14.0	16.1
11398	02 26 51.18	-17 09 42.60	14.9 ± 1.6	17.0 ± 2.3	-0.7 ± 0.4	-23.7 ± 1.8	2.1	-4.88	-0.26	—	5742	3.4	1.1	3.7
11501	02 28 18.09	-14 12 26.68	17.5 ± 1.6	-3.5 ± 0.9	-29.5 ± 3.2	-15.8 ± 1.5	2.2	-5.13	-0.07	—	5591	10.9	9.6	12.6
11502	02 28 18.27	-52 21 02.97	21.6 ± 1.7	29.7 ± 2.9	-24.6 ± 1.6	-9.1 ± 1.7	3.2	—	-0.23	0.060	5750	10.2	8.6	11.2
11514	02 28 28.86	-45 01 22.59	18.5 ± 1.6	-15.3 ± 0.8	-20.2 ± 1.0	-9.7 ± 1.5	1.8	-4.85	0.14	—	5766	6.0	5.7	6.5
11693	02 30 49.41	-59 53 50.32	14.6 ± 1.6	-47.0 ± 2.5	-49.0 ± 2.3	10.1 ± 1.7	1.5	-4.99	0.03	0.052	5990	5.1	4.4	6.2
11819	02 32 25.53	-69 36 18.91	38.6 ± 1.7	-13.3 ± 1.3	-47.9 ± 1.6	-14.6 ± 1.4	3.0	-4.99	0.22	—	5938	3.6	3.1	4.6
11973	02 34 26.50	-33 50 50.48	-8.4 ± 1.6	-2.0 ± 0.5	-7.5 ± 0.9	12.3 ± 1.5	-	-4.95	-0.32	0.055	6036	8.5	7.3	8.5
12094	02 35 53.06	-03 00 28.66	47.0 ± 1.7	-86.4 ± 8.6	-52.7 ± 8.0	-1.9 ± 5.4	2.8	-5.09	0.15	—	5700	8.1	6.6	9.4
12114	02 36 03.83	+06 53 00.11	25.4 ± 1.6	-76.3 ± 1.1	0.3 ± 0.3	32.4 ± 1.2	1.7	-4.83	-0.18	—	4860	4.6	4.6	5.6
12479	02 40 37.34	-03 42 31.10	-0.5 ± 1.7	-16.3 ± 5.8	-1.9 ± 1.5	11.9 ± 4.2	4.1	-5.25	-0.35	—	4955	2.5	1.6	3.8
12839	02 45 02.90	-17 34 49.75	37.6 ± 1.6	-15.9 ± 0.9	-43.8 ± 5.7	-27.0 ± 1.7	2.9	-5.18	0.02	—	5346	3.8	3.0	5.5
12997	02 47 07.61	-57 26 14.73	12.5 ± 1.7	-36.6 ± 1.5	-15.6 ± 1.0	-7.3 ± 1.3	3.0	-4.74	0.14	0.039	6012	1.3	0.8	2.4
13508	02 53 59.37	-49 21 41.28	18.2 ± 1.8	-31.1 ± 1.2	-11.2 ± 1.0	-12.6 ± 1.5	7.0	-4.42	-0.3	0.104	5670	12.5	11.2	13.8
13514	02 54 02.65	-48 43 38.25	13.1 ± 1.7	64.1 ± 4.0	-24.2 ± 1.4	-4.9 ± 1.5	3.7	-5.06	-0	0.045	6156	3.1	2.6	3.1
13702	02 56 26.15	+18 01 23.22	$- \pm -$	$- \pm -$	$- \pm -$	$- \pm -$	-	-4.86	1.5	—	6351	7.6	7.0	8.1
13724	02 56 46.77	-13 14 19.13	56.8 ± 1.6	-47.7 ± 1.6	-6.9 ± 0.3	-36.8 ± 1.6	2.6	-5.11	-0.04	—	5465	8.9	7.7	10.6
13754	02 57 02.95	-56 11 31.50	-0.2 ± 1.7	-3.4 ± 0.1	8.4 ± 1.0	-6.2 ± 1.4	4.3	-4.39	-0.15	0.070	5056	14.7	13.1	14.8
13889	02 58 51.14	-52 05 45.53	11.4 ± 1.6	-27.4 ± 2.0	-39.6 ± 2.6	14.0 ± 2.2	3.0	-5.15	0.14	0.084	5531	5.3	4.7	6.4
13908	02 59 08.14	-40 43 24.55	7.6 ± 1.7	7.6 ± 0.6	-18.0 ± 1.1	-0.8 ± 1.5	3.0	-5.09	0.12	—	5838	7.7	6.4	8.3
14050	03 00 54.25	-10 02 07.36	-32.6 ± 1.9	30.5 ± 13.1	-14.6 ± 2.6	20.5 ± 18.9	8.1	—	1.5	—	5719	16.1	16.0	16.1
14122	03 02 06.88	-25 27 12.60	53.2 ± 1.7	-89.5 ± 7.8	-11.8 ± 0.7	-17.0 ± 3.6	2.8	-5.01	-0.22	0.045	5981	5.9	5.9	7.3

Continued on next page

Table A.1 – continued from previous page

HIP	α	δ	V_r	U	V	W	$V \sin i$	$\log R'_{HK}$	$[Fe/H]$	EW	T_{eff}	Age	σ_{age}^{low}	σ_{age}^{high}
14180	03 02 51.05	-72 27 26.08	41.8 ± 1.6	-44.0 ± 3.1	-40.7 ± 1.3	-37.3 ± 1.2	2.4	-5.10	0.17	—	5743	7.0	6.5	7.7
14250	03 03 47.96	-14 33 19.42	0.5 ± 1.6	-1.5 ± 1.0	-32.7 ± 4.5	6.6 ± 1.7	1.4	-4.87	0.19	—	5681	4.7	3.2	5.3
14307	03 04 33.14	-51 19 19.56	19.9 ± 1.8	-28.5 ± 1.0	-17.4 ± 1.0	-10.8 ± 1.5	6.0	-4.77	0.18	—	6144	2.8	2.2	3.1
14648	03 09 18.54	-16 01 08.75	-3.5 ± 1.6	39.1 ± 3.3	-23.8 ± 2.1	-14.5 ± 2.0	1.7	-4.64	0.09	0.037	5743	6.7	6.6	8.4
14684	03 09 42.28	-09 34 46.58	14.2 ± 1.8	-5.1 ± 1.1	-28.9 ± 1.4	-9.7 ± 1.4	6.2	-4.39	-0.08	0.184	5422	13.0	12.8	14.5
14684	03 09 42.28	-09 34 46.58	$- \pm -$	$- \pm -$	$- \pm -$	$- \pm -$	6.4	-4.39	1.5	0.119	5422	13.7	13.7	15.0
14774	03 10 43.33	-06 31 33.61	21.4 ± 1.7	-25.6 ± 1.5	-15.3 ± 1.2	-5.3 ± 1.6	1.8	-4.84	0.15	0.089	6156	2.4	1.7	3.3
14836	03 11 36.08	-52 53 22.41	36.8 ± 1.7	56.1 ± 3.8	-38.4 ± 1.5	-19.3 ± 1.5	2.8	-5.00	-0.13	—	5686	8.7	8.1	9.3
14973	03 13 01.77	-36 57 57.50	-14.5 ± 1.7	47.3 ± 2.4	-6.9 ± 1.0	6.3 ± 1.5	3.7	-5.05	0.04	0.048	6014	5.1	4.2	6.2
15012	03 13 31.15	-21 57 51.19	38.8 ± 1.6	-53.4 ± 3.1	-41.6 ± 2.6	-3.0 ± 2.9	1.3	-4.93	-0.13	—	5689	4.4	4.3	5.8
15301	03 17 23.00	-40 28 11.76	-68.5 ± 1.7	30.8 ± 1.4	51.2 ± 1.6	43.2 ± 1.8	3.1	—	-0.98	—	5825	16.1	14.3	16.1
15376	03 18 17.85	-21 55 30.03	-8.6 ± 1.6	-41.1 ± 2.7	10.8 ± 0.7	29.7 ± 1.8	1.0	-4.93	-0.93	—	5231	15.3	14.2	15.8
15815	03 23 44.27	-29 07 37.90	-26.5 ± 1.7	65.2 ± 5.0	5.9 ± 0.8	-1.2 ± 2.5	2.4	-5.06	0.03	—	5861	6.2	6.2	7.6
15989	03 25 57.65	-22 03 48.99	58.1 ± 1.6	-75.7 ± 3.4	-21.8 ± 0.6	-17.8 ± 2.4	2.7	-5.07	0.28	—	5622	9.5	8.1	9.5
16084	03 27 12.24	-48 51 45.23	30.5 ± 1.6	9.5 ± 0.9	-48.7 ± 2.4	-3.4 ± 2.0	3.0	-5.27	-0.12	—	5044	5.6	5.6	5.7
16087	03 27 14.01	-50 27 45.17	48.8 ± 1.7	16.3 ± 1.7	-91.2 ± 5.1	6.2 ± 3.8	2.5	-5.02	-0.41	—	5820	10.7	10.3	12.1
16115	03 27 37.18	-73 26 22.43	9.3 ± 1.6	-41.3 ± 2.0	-15.3 ± 1.3	-13.8 ± 1.1	2.8	-5.08	0.26	—	5786	7.1	5.6	7.1
16460	03 32 01.84	-52 28 25.88	52.1 ± 1.6	-9.4 ± 0.3	-64.5 ± 1.5	-14.2 ± 1.5	1.9	-5.04	0.17	—	5591	9.8	9.2	10.6
16537	03 32 55.84	-09 27 29.74	15.9 ± 1.6	-3.2 ± 1.0	7.1 ± 0.3	-20.3 ± 1.2	1.9	-4.55	0.03	—	5230	0.6	0.6	0.6
16579	03 33 25.14	-04 23 04.22	26.6 ± 1.6	-7.8 ± 1.6	-58.5 ± 5.5	-20.0 ± 1.2	2.4	-5.18	-0.04	0.040	5277	8.4	7.1	10.1
16727	03 35 12.90	-00 44 20.03	-5.4 ± 1.6	6.1 ± 1.2	-37.4 ± 2.1	5.6 ± 1.1	1.3	-5.02	0.16	—	5416	13.8	12.6	15.1
16770	03 35 48.83	-09 03 38.71	-37.0 ± 1.6	79.2 ± 3.9	-22.5 ± 2.0	-14.2 ± 3.1	1.9	-5.01	0.0	—	5671	10.7	9.9	11.2
16783	03 35 59.24	-23 31 05.30	-2.9 ± 1.6	20.1 ± 1.4	10.5 ± 0.8	-13.3 ± 1.6	2.0	-4.74	-0.03	—	5383	11.1	10.5	11.7
16852	03 36 52.38	+00 24 05.98	27.5 ± 1.7	1.5 ± 1.3	-15.2 ± 0.1	-41.6 ± 1.1	3.4	-5.07	-0.13	0.047	5857	6.5	6.4	6.7
16971	03 38 17.31	-02 33 30.23	42.0 ± 1.7	-41.7 ± 1.5	-0.0 ± 0.5	-17.4 ± 1.5	4.6	-4.84	-0.03	0.063	6116	3.2	1.5	3.9
17047	03 39 16.76	-42 45 45.18	16.5 ± 1.7	30.4 ± 1.7	-15.2 ± 1.0	-18.2 ± 1.4	3.9	-4.91	-0.13	0.059	6115	3.6	2.2	4.3
17205	03 41 09.64	-05 17 16.31	6.6 ± 1.7	-12.0 ± 1.3	13.0 ± 1.2	-0.2 ± 1.2	1.4	-5.01	-0.18	0.074	6025	4.6	3.5	5.9
17265	03 41 51.97	-10 41 52.27	1.7 ± 1.6	2.3 ± 1.0	-54.5 ± 1.9	12.2 ± 1.3	1.6	-5.00	-0.59	—	5310	13.9	13.9	15.5
17269	03 41 54.66	-57 59 56.51	69.0 ± 1.6	-9.5 ± 0.6	-88.5 ± 2.5	-12.3 ± 2.4	2.5	-5.13	0.39	—	5592	8.6	7.7	8.7
17492	03 44 49.93	-00 45 26.59	-47.7 ± 1.7	59.0 ± 3.0	-26.5 ± 3.7	9.5 ± 2.8	3.4	-5.05	0.11	—	5726	8.9	8.6	9.1
17663	03 46 57.91	-50 29 36.30	15.9 ± 1.6	-47.7 ± 3.8	1.6 ± 1.5	-15.4 ± 1.3	2.3	-5.15	-0.43	0.061	5689	13.8	12.1	15.1
17683	03 47 17.42	-64 19 46.32	98.6 ± 1.6	-80.7 ± 3.2	-107.8 ± 1.7	-43.3 ± 1.4	2.6	-4.88	-1.1	—	5523	14.0	14.0	15.6
17795	03 48 34.32	-45 10 23.55	25.6 ± 1.7	-17.9 ± 1.2	-35.9 ± 2.0	-0.5 ± 2.1	3.9	-5.06	0.01	0.071	5967	5.0	5.0	6.7
17903	03 49 43.86	-13 53 10.92	11.2 ± 1.8	-14.2 ± 1.2	-5.0 ± 0.6	-1.2 ± 1.3	6.7	-4.40	-0.08	0.166	5373	14.6	13.6	15.6
17917	03 49 53.10	-08 04 14.34	$- \pm -$	$- \pm -$	$- \pm -$	$- \pm -$	-	-4.43	1.5	—	6270	16.1	13.8	16.1
18427	03 56 25.29	-52 55 51.11	46.9 ± 1.6	-88.5 ± 3.8	-50.7 ± 1.4	-7.5 ± 1.7	2.2	-4.75	0.09	—	5264	12.3	12.2	13.6
18527	03 57 43.91	-20 16 04.05	28.1 ± 1.6	-38.7 ± 1.5	-11.9 ± 0.6	-2.3 ± 1.5	3.6	-4.45	0.09	—	5100	10.3	9.2	11.3
18857	04 02 33.55	-38 23 25.94	-17.4 ± 1.6	32.8 ± 1.6	4.3 ± 1.0	6.0 ± 1.3	1.6	-4.99	-0.05	—	5849	9.1	8.1	9.1
19126	04 06 01.24	-38 59 49.28	-2.4 ± 1.6	59.9 ± 4.8	-22.5 ± 2.2	-4.0 ± 1.3	3.3	-5.04	-0.4	—	5549	13.9	12.6	15.6
19191	04 06 45.23	-21 40 19.34	15.9 ± 1.6	-19.8 ± 1.5	-106.6 ± 10.6	56.4 ± 7.2	1.9	-5.13	-1.0	—	5078	13.1	13.1	14.6
19344	04 08 39.63	-54 38 16.98	4.2 ± 1.7	-8.5 ± 0.7	6.9 ± 1.4	-12.1 ± 1.4	1.8	-4.89	-0.02	0.054	6079	3.1	1.7	3.1
19479	04 10 20.14	-71 20 38.54	12.2 ± 1.7	45.9 ± 3.0	-0.7 ± 1.4	-3.8 ± 1.1	2.7	-5.02	0.18	—	5667	3.4	1.1	3.6
19494	04 10 34.65	-26 36 30.23	-36.8 ± 1.7	11.2 ± 1.1	-15.4 ± 3.2	53.9 ± 2.8	2.6	-5.12	-0.02	—	5780	8.3	7.9	8.4
19658	04 12 43.74	-47 33 56.56	28.1 ± 1.7	-14.4 ± 0.5	-23.0 ± 1.1	-13.9 ± 1.3	4.2	-4.47	0.02	0.065	5696	8.6	7.7	8.7
19807	04 14 51.35	-25 00 40.37	36.9 ± 1.6	-10.4 ± 1.4	-33.6 ± 2.1	-21.8 ± 1.3	1.4	-4.97	0.17	—	5833	6.6	5.1	7.4
19849	04 15 17.63	-07 38 40.41	-42.6 ± 1.6	97.4 ± 1.2	-12.4 ± 0.4	-41.5 ± 1.0	2.1	-4.97	-0.17	—	5243	11.1	11.0	11.3
19859	04 15 28.80	+06 11 12.68	-7.6 ± 1.7	14.5 ± 1.4	-0.5 ± 0.2	-9.2 ± 0.9	2.4	-4.47	0.02	0.098	5913	1.4	1.4	2.0
19921	04 16 29.02	-59 18 07.76	28.7 ± 1.6	15.1 ± 0.1	-21.7 ± 1.2	-18.7 ± 1.1	2.9	-5.39	0.44	—	4536	7.2	6.9	7.6
20168	04 19 21.79	-41 57 43.16	2.0 ± 1.6	30.1 ± 1.8	-19.1 ± 1.5	2.3 ± 1.2	1.9	-4.90	-0.09	—	5621	3.3	2.5	5.1
20316	04 21 08.01	-31 11 46.48	-1.1 ± 1.6	38.3 ± 3.5	-19.3 ± 2.0	-7.5 ± 1.4	1.2	-4.97	-0.16	0.039	5848	9.1	9.0	9.2
20478	04 23 20.16	-25 23 42.00	11.8 ± 1.7	31.8 ± 1.6	-40.4 ± 1.4	-12.4 ± 1.1	2.0	-4.95	-0.08	—	5790	7.0	6.0	8.5
20524	04 23 53.34	-34 45 24.28	-14.5 ± 1.6	77.4 ± 3.2	-18.7 ± 1.5	-7.3 ± 1.4	1.7	-5.00	0.02	—	5614	8.1	7.2	9.0
20552	04 24 12.20	-57 04 16.81	-4.9 ± 1.6	13.2 ± 0.3	9.9 ± 1.2	-4.3 ± 1.1	-	-4.94	0.02	0.044	6721	9.5	9.1	10.0
20611	04 24 53.97	-44 43 46.33	-20.9 ± 1.7	7.4 ± 0.5	10.1 ± 1.1	17.5 ± 1.2	2.8	-5.12	0.32	—	5634	8.8	7.1	9.5
20627	04 25 12.71	-61 37 19.52	13.7 ± 1.7	-48.0 ± 2.9	-16.2 ± 1.3	-4.8 ± 1.1	2.2	-5.01	0.2	—	6004	3.7	3.7	5.3
20882	04 28 31.32	-07 33 08.56	80.3 ± 1.7	-92.6 ± 2.7	-8.1 ± 1.4	-13.5 ± 2.6	2.8	-5.01	-0.51	0.043	6000	8.2	7.9	8.3
20913	04 28 54.77	-11 03 28.82	35.9 ± 1.7	-16.2 ± 1.5	-37.8 ± 2.1	-18.0 ± 1.1	4.6	-5.08	0.01	—	6256	4.5	3.2	4.2
20932	04 29 19.17	-05 40 51.35	-18.7 ± 1.7	58.6 ± 7.8	-62.3 ± 11.8	-15.0 ± 4.5	3.1	-5.05	0.01	0.046	5932	5.4	5.2	5.5
20984	04 30 02.21	-03 03 47.01	38.1 ± 1.6	-25.8 ± 1.5	-98.9 ± 11.2	15.6 ± 4.7	1.9	-5.03	-0.22	—	5721	12.3	12.1	13.4
21141	04 31 55.95	-75 40 52.42	50.7 ± 1.6	33.2 ± 1.5	-43.5 ± 1.3	-14.0 ± 1.4	2.5	-5.19	-0.04	0.052	5575	5.8	5.0	6.7
21327	04 34 38.49	-35 39 28.99	-10.2 ± 1.7	33.7 ± 0.9	0.5 ± 1.0	-5.1 ± 1.1	2.8	-4.76	0.15	—	5400	3.6	3.2	5.1
21329	04 34 39.65	-11 38 09.04	22.4 ± 1.6	-13.5 ± 1.1	-12.5 ± 0.7	-13.4 ± 0.9	-	—	-0.87	—	5337	13.7	13.7	15.1
21622	04 38 32.47	-40 11 04.75	33.9 ± 1.6	-93.8 ± 6.4	-48.5 ± 2.3	43.9 ± 5.3	1.0	-5.01	-0.28	—	5708	13.4	13.1	13.8
21731	04 39 57.99	-71 30 20.20	-21.4 ± 1.6	4.9 ± 0.4	24.8 ± 1.3	4.9 ± 1.0	2.6	-5.08	0.2	—	5524	9.5	8.9	10.0
21757	04 40 18.38	-46 17 35.77	2.5 ± 1.7	8.8 ± 0.8	-5.1 ± 1.2	-1.3 ± 1.1	4.1	-5.08	0.03	—	5683	9.9	8.6	10.3
21778	04 40 42.43	-28 12 04.45	5.9 ± 1.7	42.5 ± 1.7	-30.9 ± 1.3	-15.6 ± 1.1	3.1	-4.95	-0.05	—	5749	4.9	4.7	5.1
21850	04 41 54.37	-58 01 14.72	62.1 ± 1.6	-3.2 ± 0.2	-58.8 ± 1.3	-26.3 ± 1.2	2.8	-5.17	0.32	—	5527	10.2	8.9	10.2
21872	04 42 08.89	-35 28 34.29	22.0 ± 1.7	13.6 ± 3.1	-9.7 ± 1.3	-32.6 ± 2.6	3.3	-5.17	-0.01	0.145	5659	2.9	2.3	3.6
21889	04 42 19.97	-61 37 14.49	46.1 ± 1.6	-65.1 ± 2.9	-29.5 ± 1.3	-39.5 ± 1.1	1.6	-5.09	0.3	—	5376	11.3	9.9	12.6
21960	04 43 13.68	-54 35 36.33	63.9 ± 1.6	17.2 ± 0.4	-58.1 ± 1.2	-33.2 ± 1.0	2.2	-5.03	-0.12	—	5389	12.0	11.6	12.5
21963	04 43 16.40	-09 37 05.19	31.8 ± 1.7	-33.9 ± 1.4	-12.7 ± 0.7	-2.7 ± 1.3	4.1	-4.51	0.15	0.077	5926	6.0	5.8	7.1
22002	04 43 47.74	-12 17 40.06	-5.0 ± 1.6	5.2 ± 1.2	1.6 ± 0.7	1.0 ± 1.0	2.6	-4.60	0.29	—	5475	5.5	4.7	7.1
22052	04 44 33.83	-16 03 54.13	22.0 ± 1.7	-21.6 ± 1.2	-11.1 ± 0.8	-3.9 ± 1.0	3.5	-4.67	-0.12	0.060	6103	4.5	3.7	5.7
22064	04 44 46.35	-20 00 50.46	70.1 ± 1.7	-58.4 ± 1.5	-35.9 ± 0.9	-25.8 ± 1.6	3.9	—	-0.6	0.037	5620	13.4	13.1	14.6
22122	04 45 38.58	-50 04 27.22	24.9 ± 1.6	36.8 ± 0.6	-1.1 ± 1.2	-46.8 ± 1.1	2.0	-4.67	0.03	—	5110	6.8	5.6	6.9

Continued on next page

Table A.1 – continued from previous page

HIP	α	δ	V_r	U	V	W	$V \sin i$	$\log R'_{HK}$	$[Fe/H]$	EW	T_{eff}	Age	σ_{age}^{low}	σ_{age}^{high}
22142	04 45 53.80	-48 02 08.19	14.1 ± 1.6	21.0 ± 1.1	4.1 ± 1.3	-33.1 ± 1.5	1.5	-4.98	-0.11	—	5067	13.2	11.9	14.4
22162	04 46 05.88	-29 03 43.41	65.8 ± 1.6	-63.5 ± 3.3	-62.7 ± 2.7	5.5 ± 5.0	2.2	-5.12	0.08	—	5733	9.6	8.1	10.0
22263	04 47 36.29	-16 56 04.04	21.4 ± 1.7	-23.7 ± 1.1	-8.3 ± 0.8	-2.7 ± 0.9	2.9	-4.56	0.04	0.058	5804	3.7	2.6	3.7
22278	04 47 48.76	-58 21 40.93	23.0 ± 1.7	-19.9 ± 1.1	-15.2 ± 1.3	-16.6 ± 1.0	2.8	-5.06	0.15	—	5675	8.1	6.8	8.1
22320	04 48 28.48	-28 25 09.47	65.3 ± 1.6	-57.8 ± 1.9	-69.6 ± 2.3	9.4 ± 3.6	2.3	-5.03	0.09	—	5407	8.6	8.2	9.0
22360	04 48 50.03	-23 16 44.97	-14.6 ± 1.8	41.6 ± 2.1	-27.2 ± 2.2	8.3 ± 1.1	5.7	-4.99	-0.21	0.039	6212	5.6	4.2	6.5
22373	04 48 57.94	-28 43 26.17	11.4 ± 1.6	-13.3 ± 0.9	13.0 ± 1.4	-20.0 ± 1.2	1.7	-4.91	-0.24	—	5284	12.7	11.8	13.5
22430	04 49 36.50	-42 36 29.75	19.3 ± 1.8	-1.6 ± 0.7	-31.3 ± 1.8	5.1 ± 1.7	5.6	-5.03	-0.07	0.054	6084	5.0	5.0	5.6
22587	04 51 38.98	-59 00 37.15	18.8 ± 1.6	44.2 ± 3.3	-7.2 ± 1.4	-22.9 ± 1.3	2.5	-5.14	0.12	—	5610	8.8	7.6	9.4
22953	04 56 18.31	-51 02 51.05	44.0 ± 1.6	16.8 ± 0.9	-68.8 ± 1.8	9.4 ± 1.7	2.6	-5.14	-0.09	—	5589	15.1	15.1	16.1
23243	05 00 02.74	-27 49 56.86	2.1 ± 1.6	-12.5 ± 1.3	21.8 ± 2.1	-15.4 ± 1.5	1.5	-4.95	-0.14	—	5671	11.2	11.0	11.4
23290	05 00 35.18	-46 39 23.74	-14.1 ± 1.7	29.9 ± 3.2	-3.6 ± 2.1	15.8 ± 1.4	3.6	-5.18	0.11	—	6015	4.4	3.6	5.3
24037	05 10 02.07	-07 04 18.33	64.0 ± 1.6	-18.6 ± 2.2	-56.1 ± 1.8	-59.3 ± 1.9	2.4	-4.91	-0.47	—	5491	13.8	13.8	15.1
24210	05 11 54.24	-09 06 47.35	4.5 ± 1.7	46.0 ± 2.1	-49.9 ± 1.8	-40.9 ± 1.5	2.8	-4.85	-0.09	—	5271	13.3	11.7	13.3
24692	05 17 45.10	-08 39 06.54	3.1 ± 1.7	16.5 ± 2.4	-26.5 ± 2.8	-9.6 ± 1.2	3.6	-5.08	0.09	0.080	5664	7.3	5.7	8.6
24754	05 18 28.17	-51 25 37.15	0.4 ± 1.7	27.1 ± 0.8	-2.2 ± 1.3	-5.3 ± 1.0	3.2	-4.46	-0	0.047	5448	5.5	5.3	5.7
24777	05 18 42.79	-14 01 06.44	54.4 ± 1.6	-38.4 ± 1.2	-57.4 ± 1.8	7.3 ± 1.9	2.5	-4.93	-0.14	—	5181	4.8	4.4	5.9
24965	05 20 50.62	-77 55 13.13	37.5 ± 1.6	-47.9 ± 2.3	-29.4 ± 1.3	-53.8 ± 1.5	1.7	-5.00	-0.21	—	5253	13.1	13.1	14.5
25358	05 25 23.03	-47 05 39.12	6.8 ± 1.7	-2.9 ± 0.5	-5.2 ± 1.3	-3.4 ± 0.9	-	-4.86	1.5	—	6316	13.4	12.4	14.9
25449	05 26 37.12	-54 00 12.47	3.8 ± 1.8	22.1 ± 1.3	4.4 ± 1.5	-18.3 ± 1.3	6.1	-4.66	-0.01	0.062	6061	3.8	3.3	4.6
25654	05 28 48.33	-13 32 32.47	39.8 ± 1.6	-3.8 ± 2.3	-63.0 ± 3.4	-7.4 ± 1.0	2.0	-4.99	0.09	—	5355	4.4	4.4	6.9
25670	05 28 59.12	-17 25 45.26	-9.8 ± 1.6	19.9 ± 1.3	6.1 ± 0.9	-16.9 ± 1.3	1.4	-5.01	0.1	—	5736	2.3	1.9	4.4
25679	05 29 03.27	-19 08 34.65	26.3 ± 1.6	-4.1 ± 1.3	-27.3 ± 1.1	-16.1 ± 0.8	2.6	-4.96	-0.56	—	5581	13.4	13.4	14.6
26141	05 34 25.15	-42 45 55.95	52.9 ± 1.7	-47.3 ± 2.2	-39.5 ± 1.3	-13.0 ± 1.3	2.4	-5.05	0.17	—	5973	3.6	3.4	4.0
26553	05 38 46.81	-52 29 19.86	56.1 ± 1.7	-32.8 ± 1.2	-56.3 ± 1.5	-8.0 ± 1.4	2.6	-4.97	-0.16	—	5917	8.1	6.9	9.0
26641	05 39 44.25	-05 03 02.58	19.9 ± 1.7	-55.6 ± 2.7	34.7 ± 2.8	32.0 ± 2.4	2.5	-4.89	-0.52	—	5530	12.8	12.5	13.4
26973	05 43 26.45	-47 49 22.71	26.1 ± 1.7	-41.5 ± 1.0	-19.0 ± 1.4	-1.6 ± 0.9	4.1	-4.47	0.21	—	5233	5.2	3.4	5.7
27090	05 44 39.35	-29 55 00.01	-18.1 ± 1.6	62.1 ± 3.1	-10.6 ± 1.8	-13.8 ± 1.4	2.8	-5.10	-0.23	0.031	5721	11.0	9.8	11.9
27134	05 45 13.40	-59 55 25.62	52.7 ± 1.9	-29.4 ± 1.1	-41.8 ± 1.7	-31.5 ± 1.0	9.7	-4.07	-1.5	—	4911	14.1	14.1	15.6
27158	05 45 25.60	-12 26 04.86	-27.4 ± 1.7	47.6 ± 2.3	-11.0 ± 2.1	-6.1 ± 1.3	3.3	-5.26	0.32	—	5474	9.0	7.7	9.5
27491	05 49 16.48	-37 30 48.00	48.3 ± 1.6	-11.4 ± 0.8	-71.1 ± 2.3	26.4 ± 2.9	2.5	-5.08	0.42	—	5445	9.2	8.2	10.1
27720	05 52 11.43	-17 33 10.88	37.2 ± 1.6	-49.5 ± 1.8	0.1 ± 1.8	-9.1 ± 0.6	2.5	-5.07	-0.07	—	5291	5.0	4.3	6.2
27891	05 54 06.43	-41 20 38.62	9.9 ± 1.8	-2.9 ± 0.7	-16.3 ± 1.6	9.3 ± 1.4	6.9	-4.96	-0.47	0.054	6039	7.5	6.5	8.6
27923	05 54 31.04	-55 50 37.84	36.2 ± 1.6	-74.2 ± 4.3	-22.0 ± 1.5	-21.1 ± 0.8	1.8	-4.80	-0.43	—	5549	13.9	13.9	15.1
27957	05 54 53.97	-75 27 32.02	56.3 ± 1.7	-14.4 ± 1.2	-55.0 ± 1.4	-28.5 ± 0.8	2.3	-4.94	0.02	—	5801	7.5	7.5	8.6
27980	05 55 01.95	-00 30 28.69	24.3 ± 1.7	-16.5 ± 1.5	-7.6 ± 0.7	-30.1 ± 1.3	3.0	—	0.16	0.068	5790	6.9	5.7	6.9
28181	05 57 16.06	-28 26 20.81	34.5 ± 1.7	-68.1 ± 4.7	-3.0 ± 2.4	11.0 ± 2.4	2.8	-5.10	0.32	—	5758	6.4	7.1	8.0
28462	06 00 34.70	-51 28 04.95	1.1 ± 1.8	4.3 ± 0.4	-10.0 ± 1.6	14.3 ± 1.1	5.0	-4.96	-0.21	—	6196	4.7	4.3	5.4
28641	06 02 52.59	-30 24 28.79	-6.3 ± 1.7	51.6 ± 4.4	-4.7 ± 1.5	-41.3 ± 4.0	2.7	-4.99	0.06	—	5747	8.3	8.1	8.6
28648	06 02 57.61	-61 11 34.81	40.5 ± 1.7	-44.0 ± 3.6	-48.0 ± 1.8	2.3 ± 2.0	3.2	-4.84	-0.2	0.080	6163	5.8	5.7	7.0
28941	06 06 29.85	-72 30 45.58	36.2 ± 1.6	87.7 ± 2.9	-13.3 ± 1.5	-15.2 ± 0.8	2.7	-5.12	0.21	—	5126	11.5	10.1	13.0
29093	06 08 12.73	-50 59 35.72	12.6 ± 1.8	-24.8 ± 1.5	-7.9 ± 1.6	-3.0 ± 0.9	6.2	-4.60	-0.18	0.063	6133	5.4	4.7	6.5
29094	06 08 13.62	-53 16 58.01	35.4 ± 1.7	-33.7 ± 1.7	-24.6 ± 1.6	-20.1 ± 0.8	5.0	-5.10	-0.32	0.070	5939	7.0	6.2	7.7
29193	06 09 27.70	-51 23 21.98	34.7 ± 1.7	-20.1 ± 0.7	-26.9 ± 1.5	-17.1 ± 0.8	4.2	—	-0.17	—	5809	5.0	4.4	5.6
29272	06 10 14.39	-37 51 02.94	28.5 ± 1.7	-30.8 ± 1.6	-14.1 ± 1.6	-11.9 ± 0.7	2.8	-4.77	0.22	0.059	6158	2.4	1.0	2.4
29391	06 11 39.06	-22 53 47.88	35.5 ± 1.7	-31.2 ± 7.1	-17.4 ± 8.3	-11.7 ± 3.6	5.3	-4.48	0.07	0.087	5930	4.4	3.1	4.9
29442	06 12 13.96	-14 39 00.07	81.3 ± 1.6	-101.1 ± 6.0	-4.4 ± 6.7	-22.2 ± 0.6	2.3	-5.05	0.3	—	5276	12.2	10.6	13.6
29550	06 13 35.66	-29 53 50.16	72.0 ± 1.6	-35.8 ± 0.9	-72.9 ± 2.3	9.5 ± 4.2	2.9	-5.11	-0.13	—	5424	15.4	15.2	16.1
29644	06 14 48.25	-19 43 43.88	-25.9 ± 1.7	55.0 ± 2.2	1.7 ± 1.4	-39.2 ± 2.5	2.9	-5.05	0.16	—	5280	14.3	13.1	15.6
29754	06 15 56.56	-14 26 01.78	-6.8 ± 1.7	44.8 ± 4.8	-24.9 ± 3.6	-37.2 ± 4.6	2.2	-5.02	0.08	—	5844	5.9	5.9	7.3
29772	06 16 08.37	-41 38 29.33	-13.5 ± 1.7	58.1 ± 4.2	-0.7 ± 1.7	-12.0 ± 1.5	3.5	—	-0.57	—	5744	13.7	12.1	15.1
30037	06 19 14.93	-68 49 52.99	49.2 ± 1.6	-21.1 ± 1.7	-41.1 ± 1.4	-34.6 ± 1.0	2.0	-4.99	0.01	—	5686	5.1	3.7	6.0
30045	06 19 18.84	-37 27 46.44	17.3 ± 1.6	-7.1 ± 0.6	2.1 ± 1.5	-43.5 ± 1.3	1.5	-4.97	0.05	—	5221	11.8	10.3	11.9
30106	06 20 07.54	-47 12 34.45	19.1 ± 1.7	-57.1 ± 3.5	-5.2 ± 1.7	-2.8 ± 0.8	2.6	-4.98	-0.11	0.045	5941	7.6	6.8	8.3
30183	06 21 01.93	-54 56 04.65	25.0 ± 1.7	35.7 ± 2.2	-28.7 ± 1.6	-6.7 ± 0.8	4.7	-5.03	0.13	0.053	5952	5.0	5.0	5.7
30232	06 21 37.34	-18 10 00.06	20.3 ± 1.6	0.1 ± 1.2	-21.4 ± 1.2	-21.8 ± 0.8	1.9	-4.94	-0.2	—	5715	11.5	10.3	11.5
30377	06 23 14.66	-46 49 24.16	24.3 ± 1.6	10.2 ± 0.8	-38.3 ± 1.6	17.4 ± 1.4	2.7	-5.11	-0.21	—	5601	15.2	14.2	16.1
30514	06 24 51.47	-32 07 18.89	133.3 ± 1.6	-201.2 ± 12.9	-73.6 ± 3.5	66.9 ± 10.3	1.9	-4.88	-0.99	—	5687	14.6	14.3	16.1
30545	06 25 16.54	-00 56 45.17	46.8 ± 1.7	-17.3 ± 1.6	-65.6 ± 1.5	12.4 ± 0.5	5.2	-5.11	-0.16	0.051	5979	5.5	5.3	5.7
30545	06 25 16.54	-00 56 45.17	$- \pm -$	$- \pm -$	$- \pm -$	$- \pm -$	5.4	-5.11	1.5	—	5979	12.7	12.7	14.0
30733	06 27 24.10	-25 44 04.55	25.2 ± 1.6	-27.5 ± 1.7	-11.8 ± 1.5	-1.9 ± 0.8	2.1	-4.51	-0.03	—	5181	13.9	13.9	15.6
30995	06 30 19.21	-52 52 16.59	22.5 ± 1.6	-41.7 ± 1.9	-13.0 ± 1.5	-12.7 ± 0.7	3.1	-4.74	-0.68	0.073	5571	16.0	16.0	16.1
31034	06 30 44.77	-61 36 30.44	51.0 ± 1.7	10.2 ± 0.8	-38.6 ± 1.6	-36.6 ± 1.4	2.7	-5.02	-0.66	—	5660	13.0	11.6	14.6
31134	06 31 56.73	-68 42 35.51	42.4 ± 1.7	62.3 ± 1.0	-22.1 ± 1.5	-31.5 ± 0.8	2.8	-4.95	-0.41	—	5174	14.7	14.1	15.4
31179	06 32 34.31	-55 38 54.94	-15.6 ± 1.6	37.8 ± 1.5	-2.9 ± 1.6	36.1 ± 1.4	3.2	-5.15	-0.47	0.034	5379	9.1	8.7	10.6
31188	06 32 37.99	-06 29 18.50	3.0 ± 1.7	9.2 ± 1.5	-31.0 ± 1.9	64.4 ± 3.7	2.2	-4.85	-0.61	0.033	5885	13.7	12.9	14.6
31540	06 36 08.78	-27 37 20.26	3.8 ± 1.6	37.5 ± 1.5	-24.6 ± 1.5	-15.2 ± 0.6	2.2	-5.05	0.24	—	5618	6.3	5.1	6.9
31623	06 37 03.98	-32 13 30.70	3.4 ± 1.6	17.7 ± 0.9	-30.5 ± 1.5	47.8 ± 1.3	2.0	—	-1.2	—	5433	13.1	13.1	14.6
31692	06 37 50.57	-70 55 57.38	17.3 ± 1.6	-55.5 ± 5.6	-17.7 ± 1.5	-26.2 ± 1.9	2.2	-4.76	-0.3	—	5339	10.5	10.5	12.1
31831	06 39 19.29	-49 40 49.78	54.8 ± 1.7	-57.4 ± 3.5	-48.8 ± 1.5	-0.2 ± 1.6	3.0	-5.12	0.27	0.055	5830	4.5	3.8	5.1
31895	06 40 01.72	-48 32 31.03	22.9 ± 1.7	-14.2 ± 0.7	-24.0 ± 1.5	4.5 ± 1.0	4.0	-5.22	-0.18	0.070	5651	4.9	4.3	6.0
32103	06 42 23.24	-61 13 29.88	26.7 ± 1.7	-39.7 ± 1.5	-17.9 ± 1.5	-26.4 ± 0.9	3.2	-4.76	-0.17	—	5605	14.5	14.5	16.0
32127	06 42 34.91	-56 26 42.37	40.9 ± 1.6	-7.8 ± 0.3	-66.0 ± 2.0	50.0 ± 3.2	2.5	-5.03	-0.65	—	5338	13.2	13.0	14.6
32241	06 43 51.45	-41 00 00.71	-2.1 ± 1.7	46.1 ± 2.8	-6.6 ± 1.6	-20.8 ± 1.4	1.8	-4.92	-0.19	0.059	5959	3.7	3.6	5.9
32735	06 49 40.55	-74 33 26.25	-12.7 ± 1.7	-24.2 ± 1.3	5.7 ± 1.5	4.3 ± 0.7	3.2	-5.02	0.07	—	5381	12.8	11.8	13.8

Continued on next page

Table A.1 – continued from previous page

HIP	α	δ	V_r	U	V	W	$V \sin i$	$\log R'_{HK}$	$[Fe/H]$	EW	T_{eff}	Age	σ_{age}^{low}	σ_{age}^{high}
32742	06 49 43.08	-19 23 01.65	33.7 ± 1.7	-39.5 ± 2.3	-13.6 ± 1.9	10.7 ± 1.8	3.8	-5.15	-0.37	—	5712	3.9	2.9	5.4
32764	06 49 53.77	-50 08 57.95	1.7 ± 1.7	33.2 ± 1.5	-6.8 ± 1.5	-2.9 ± 0.6	2.2	-4.78	-0.07	0.062	5964	2.0	2.0	2.2
32860	06 50 55.87	-52 27 49.14	57.6 ± 1.7	2.7 ± 0.6	-50.2 ± 1.5	-31.9 ± 0.9	2.4	-4.97	0.06	—	5652	9.5	8.7	10.5
32897	06 51 14.56	-88 32 05.55	-42.6 ± 1.7	-70.7 ± 2.7	8.6 ± 1.7	7.3 ± 1.0	2.6	-4.91	-0.17	—	5820	9.5	8.3	9.5
32994	06 52 25.07	-37 51 02.17	70.9 ± 1.6	-31.4 ± 0.7	-62.8 ± 1.5	-13.0 ± 0.6	2.8	-5.07	-0.2	—	5641	13.8	12.1	14.5
33025	06 52 50.49	-38 39 08.53	-15.8 ± 1.7	27.9 ± 2.0	10.5 ± 1.5	-11.9 ± 1.5	2.5	-4.89	-0.04	0.036	5885	3.8	2.0	4.2
33033	06 52 58.02	-39 01 14.84	64.6 ± 1.7	-62.3 ± 3.6	-55.4 ± 1.5	23.3 ± 3.7	2.5	-5.06	-0.2	—	5746	10.8	9.1	11.1
33144	06 54 04.78	-41 55 56.03	12.9 ± 1.8	14.0 ± 1.6	-16.2 ± 1.7	-7.9 ± 0.7	7.0	-4.85	-0.11	0.036	5777	9.7	8.1	9.8
33228	06 54 50.59	-33 01 09.93	17.6 ± 1.7	-14.7 ± 1.0	-6.9 ± 1.6	-21.8 ± 1.5	3.9	-4.48	-0.06	0.041	5583	12.9	12.4	13.1
33366	06 56 21.14	-51 37 37.42	-3.3 ± 1.7	-31.7 ± 2.6	4.2 ± 1.5	11.0 ± 1.0	2.7	-4.93	-0.09	—	5693	12.8	12.3	13.1
33388	06 56 36.48	-64 34 34.25	28.9 ± 1.7	11.7 ± 0.5	-34.7 ± 1.6	9.2 ± 1.2	3.3	-4.93	-0.25	0.056	6009	5.3	3.9	5.9
33427	06 57 03.92	-72 02 12.33	72.3 ± 1.7	43.2 ± 2.9	-50.2 ± 2.0	-45.0 ± 1.7	3.3	—	-1.5	—	6178	16.0	14.8	16.1
33503	06 57 50.23	-64 51 11.62	19.1 ± 1.7	28.0 ± 1.9	-17.0 ± 1.5	-3.2 ± 0.8	2.6	-4.67	-0.03	0.039	5835	1.3	0.6	2.5
33736	07 00 29.59	-41 22 47.29	60.3 ± 1.6	-47.0 ± 0.8	-50.9 ± 1.5	1.3 ± 0.6	2.5	-4.86	0.15	—	5091	12.4	11.7	13.1
34147	07 04 49.76	-49 49 23.79	32.1 ± 1.7	42.5 ± 3.9	-30.6 ± 1.6	-32.9 ± 2.0	2.7	-5.07	0.17	—	5800	8.8	7.3	9.1
34293	07 06 33.87	-48 15 02.72	-6.4 ± 1.7	25.1 ± 1.7	3.8 ± 1.6	-6.1 ± 0.8	4.2	-4.98	-0.27	0.047	6097	4.7	3.7	6.1
34609	07 10 07.07	-57 46 03.24	6.5 ± 1.7	-20.1 ± 1.1	-8.6 ± 1.6	5.8 ± 0.8	4.1	-4.44	-0.02	0.048	5663	2.5	2.5	5.0
34747	07 11 38.07	-35 38 06.12	14.0 ± 1.7	39.8 ± 5.6	-23.7 ± 2.0	-38.2 ± 4.4	3.2	-5.08	-0.28	0.039	5700	13.7	12.1	14.8
34877	07 12 57.93	-61 36 47.43	20.9 ± 1.6	18.2 ± 0.9	-22.4 ± 1.5	2.0 ± 0.8	2.7	-5.02	-0.31	—	5648	16.1	15.5	16.1
35052	07 14 56.39	-68 04 16.12	18.5 ± 1.7	44.5 ± 1.7	-8.2 ± 1.6	-11.6 ± 0.7	5.2	-4.96	-0.11	0.046	5793	8.9	8.7	9.7
35058	07 14 59.75	-32 48 10.69	0.2 ± 1.6	-15.2 ± 2.0	10.0 ± 1.9	-16.2 ± 2.0	3.0	-5.09	-0.4	—	5489	5.8	4.2	7.1
35096	07 15 29.11	-48 13 48.02	14.1 ± 1.7	-39.0 ± 1.0	-3.1 ± 1.6	-15.4 ± 0.5	2.8	-4.97	-0.14	—	5820	7.7	6.2	7.7
35151	07 15 56.46	-41 01 48.05	16.2 ± 1.6	-81.8 ± 3.8	18.2 ± 2.2	-40.6 ± 1.8	1.9	-4.93	-0.28	—	5641	10.6	9.8	11.5
35279	07 17 18.02	-40 39 23.59	54.1 ± 1.7	-42.0 ± 1.1	-48.6 ± 1.5	15.8 ± 1.1	3.6	-5.17	-0.16	0.052	5674	6.9	6.0	7.8
35691	07 21 51.29	-34 34 18.93	33.1 ± 1.8	-27.9 ± 1.4	-23.6 ± 1.7	-6.1 ± 0.4	6.7	-5.01	0.14	0.089	6154	3.5	3.1	3.7
35711	07 22 02.78	-37 55 57.17	-11.0 ± 1.7	-17.2 ± 1.7	18.9 ± 1.7	-4.1 ± 0.6	3.1	-4.95	-0.35	0.034	5921	7.7	6.3	7.9
35739	07 22 18.85	-39 15 11.96	6.7 ± 1.6	-3.4 ± 0.5	-0.3 ± 1.5	-27.4 ± 0.9	1.6	-4.91	0.01	—	5090	8.1	6.9	9.4
35881	07 23 51.78	-05 16 16.92	-0.5 ± 1.6	7.0 ± 1.3	-5.3 ± 1.1	15.2 ± 1.0	2.3	-5.15	0.03	—	5406	10.0	8.6	11.5
35985	07 24 57.15	-38 21 07.07	-17.6 ± 1.6	29.5 ± 1.5	10.6 ± 1.6	-9.6 ± 0.8	2.0	-4.66	0.07	—	5103	7.1	6.5	7.7
36104	07 26 14.90	-49 25 20.19	4.7 ± 1.7	2.5 ± 0.5	-7.5 ± 1.7	7.8 ± 0.9	4.0	-5.06	0.07	0.050	6034	6.0	4.8	7.5
36160	07 26 57.62	-34 18 55.84	64.3 ± 1.6	-60.7 ± 8.2	-37.0 ± 5.1	-51.2 ± 9.4	1.9	-4.96	-0.15	—	5690	3.3	2.3	4.9
36187	07 27 09.01	-80 49 26.45	47.2 ± 1.7	36.5 ± 1.4	-39.9 ± 1.4	-2.6 ± 1.3	2.4	-4.97	-0.09	—	5842	6.5	5.6	7.1
36312	07 28 30.05	-49 08 58.89	$- \pm -$	$- \pm -$	$- \pm -$	$- \pm -$	-	-4.46	1.5	0.062	6239	15.6	15.6	16.1
36477	07 30 21.22	-57 26 47.50	94.2 ± 1.7	-53.9 ± 3.0	-107.4 ± 1.9	29.3 ± 3.3	3.0	-5.10	-0.13	—	5638	9.8	8.6	9.8
36670	07 32 38.21	-16 49 28.36	63.2 ± 1.6	-39.6 ± 1.0	-47.4 ± 1.3	70.9 ± 5.3	1.4	-4.92	-0.66	—	5711	13.7	13.6	13.9
36731	07 33 16.39	-22 18 05.46	48.9 ± 1.6	16.5 ± 2.5	-68.1 ± 2.0	-17.7 ± 0.9	2.1	-4.92	-0.17	—	5700	11.5	10.7	12.5
36832	07 34 28.03	-52 58 05.37	23.5 ± 1.7	-38.1 ± 0.6	-22.6 ± 1.6	4.9 ± 0.5	3.6	-4.42	-0.25	0.066	5251	14.6	14.0	15.2
36866	07 34 44.38	-66 38 36.62	44.3 ± 1.7	-41.6 ± 1.6	-51.6 ± 1.6	-6.2 ± 0.6	3.1	-4.57	0.25	—	5250	10.0	8.7	11.6
37063	07 36 59.00	-54 04 49.54	71.4 ± 1.7	-25.4 ± 1.1	-64.7 ± 1.6	-28.4 ± 0.7	3.2	-5.06	-0.49	0.074	5885	9.3	8.2	9.4
37183	07 38 23.42	-32 30 03.45	28.3 ± 2.0	-10.5 ± 0.8	-25.4 ± 1.8	-9.4 ± 0.5	9.7	-4.49	-0.27	0.106	6139	4.2	2.2	5.1
37358	07 40 06.40	-59 13 47.21	1.7 ± 1.7	2.8 ± 0.4	-0.3 ± 1.6	-4.7 ± 0.6	2.5	-5.05	-0.11	0.056	5998	5.6	4.4	5.6
37411	07 40 50.86	-77 16 15.64	24.7 ± 1.7	-29.4 ± 2.4	-41.2 ± 1.9	4.7 ± 1.2	2.0	-5.02	0.06	0.052	6203	2.6	2.6	4.0
37520	07 42 01.97	-11 51 09.72	106.6 ± 1.7	-78.6 ± 1.2	-71.7 ± 1.3	15.0 ± 0.3	3.3	-5.14	-0.31	—	5723	11.4	10.1	12.7
37567	07 42 37.78	-33 46 51.90	24.2 ± 1.7	14.4 ± 2.1	-28.1 ± 1.6	-38.9 ± 3.1	3.0	-5.08	0.27	—	5767	8.2	7.1	8.5
37727	07 44 16.47	-50 27 59.81	8.2 ± 1.8	-26.0 ± 0.5	-4.0 ± 1.7	-6.4 ± 0.4	6.0	-4.60	-0.58	0.069	5629	14.7	14.7	16.1
37732	07 44 19.74	-05 03 17.79	83.1 ± 1.7	-86.0 ± 1.8	-25.2 ± 2.0	27.6 ± 0.8	3.0	-4.98	0.01	—	5846	6.1	5.7	6.9
37878	07 45 50.79	-45 25 34.81	87.5 ± 1.6	1.9 ± 1.2	-87.9 ± 1.6	-16.3 ± 0.4	2.3	-4.79	-0.61	—	5597	13.7	13.3	14.2
37923	07 46 16.96	-59 48 34.23	17.2 ± 1.7	-19.3 ± 2.5	-18.0 ± 1.6	-2.3 ± 0.8	3.1	-4.41	0.15	0.076	5327	0.5	0.1	1.7
38041	07 47 49.71	-54 15 50.92	22.1 ± 1.6	47.6 ± 1.1	-23.9 ± 1.6	-4.8 ± 0.4	2.2	-4.80	-0.08	—	5416	6.9	4.3	6.9
38072	07 48 05.97	-27 31 10.67	58.2 ± 1.7	-47.6 ± 2.1	-41.0 ± 1.8	-17.7 ± 1.5	3.1	-4.51	0.04	—	5754	4.1	3.0	5.1
38131	07 48 49.74	-56 00 28.86	5.6 ± 1.7	-30.1 ± 1.9	4.8 ± 1.7	-38.4 ± 2.4	2.2	-4.95	-0.04	—	5698	7.4	6.7	8.2
38250	07 50 08.13	-39 04 50.84	38.2 ± 1.7	-48.9 ± 1.8	-25.6 ± 1.7	-2.4 ± 0.3	3.8	-4.48	-0.17	—	5204	12.2	11.2	13.5
38574	07 53 54.35	-67 27 18.57	20.2 ± 1.7	3.8 ± 0.4	-22.9 ± 1.6	5.0 ± 1.1	3.3	-5.03	-0.09	—	5633	10.4	9.3	12.0
38576	07 53 55.51	-68 53 58.56	43.0 ± 1.6	-78.3 ± 7.1	-50.8 ± 1.8	-31.2 ± 1.5	2.6	-4.98	-0.61	—	5479	14.3	14.2	14.3
38645	07 54 46.72	-66 12 43.08	32.2 ± 1.7	-61.1 ± 4.7	-42.2 ± 1.8	-4.7 ± 0.7	4.6	-5.00	-0.26	—	5417	15.1	15.0	16.1
38809	07 56 33.12	-67 46 21.70	6.8 ± 1.9	-38.3 ± 2.8	-15.2 ± 1.9	2.7 ± 0.8	8.1	-4.98	0.07	—	6232	3.5	3.2	3.5
38998	07 58 52.17	-13 18 54.81	-14.4 ± 1.6	7.5 ± 1.0	5.0 ± 1.3	-40.6 ± 1.4	1.5	-4.91	-0.14	—	5012	14.0	12.6	15.5
39007	07 58 58.56	-40 54 03.26	42.9 ± 1.7	-37.3 ± 2.0	-34.6 ± 1.7	-7.0 ± 0.3	3.2	—	-0.37	0.056	5817	9.6	8.1	11.1
39026	07 59 07.06	-41 35 11.79	44.6 ± 1.7	-81.2 ± 3.9	-32.4 ± 1.7	46.7 ± 2.8	1.8	-4.97	-0.27	0.035	5959	10.1	8.7	10.1
39088	07 59 47.59	-59 12 43.91	3.5 ± 1.6	5.2 ± 0.3	-0.1 ± 1.6	-12.1 ± 0.6	2.7	-4.89	-0.6	—	5226	13.9	13.9	15.1
39186	08 00 54.31	-27 13 35.55	17.8 ± 1.7	-3.5 ± 0.8	-17.6 ± 1.5	11.7 ± 0.7	3.0	-5.05	0.07	—	5826	9.1	7.9	9.1
39242	08 01 32.54	-70 01 25.96	14.6 ± 1.7	-17.5 ± 0.8	-23.4 ± 1.6	9.5 ± 0.7	2.6	-5.05	-0.18	0.070	5970	8.9	8.2	9.7
39298	08 02 05.36	-12 48 16.64	25.5 ± 1.7	0.7 ± 1.2	-41.6 ± 1.6	-40.9 ± 2.0	2.7	-5.05	0.19	—	5566	9.6	8.5	9.6
39327	08 02 26.56	-30 25 05.54	8.2 ± 1.7	41.9 ± 4.3	-26.0 ± 2.3	11.6 ± 1.1	2.0	-5.05	0.15	—	5803	6.2	5.9	7.4
39330	08 02 26.98	-46 20 10.69	22.7 ± 1.7	-47.7 ± 0.9	-15.7 ± 1.6	-0.7 ± 0.2	3.4	-4.80	0.15	—	5771	3.7	2.9	5.2
39338	08 02 29.58	-52 28 13.22	11.9 ± 1.9	-26.2 ± 1.6	-7.9 ± 1.9	-13.5 ± 0.8	9.2	-4.46	-0.18	0.083	5903	7.2	5.8	8.1
39364	08 02 48.09	-43 17 05.82	29.7 ± 1.7	-12.8 ± 0.7	-26.7 ± 1.7	-10.6 ± 0.6	4.2	-4.65	0.08	—	5986	1.6	0.4	1.6
39417	08 03 28.66	-01 09 45.75	43.7 ± 1.6	-13.0 ± 1.7	-64.7 ± 2.7	-28.5 ± 2.7	2.2	-5.07	-0.24	—	5665	14.3	14.3	15.6
39457	08 03 53.79	-31 32 39.32	25.8 ± 1.7	-66.9 ± 5.8	-1.8 ± 2.7	6.1 ± 0.7	3.1	-5.12	0.14	—	5676	9.6	9.1	9.6
39589	08 05 23.69	-74 24 37.48	10.6 ± 1.7	-37.5 ± 2.6	-16.3 ± 1.6	-17.3 ± 1.1	3.0	-4.93	0.34	—	5920	0.8	0.5	1.1
39989	08 09 59.42	-34 30 20.87	18.1 ± 1.7	-41.0 ± 3.9	-5.6 ± 2.0	-6.4 ± 0.7	3.2	-4.94	-0.12	0.054	6003	3.8	2.7	5.4
40051	08 10 52.59	-42 48 41.08	27.6 ± 1.6	41.9 ± 1.3	-33.7 ± 1.6	-28.6 ± 0.7	2.3	-4.70	-0.01	—	4983	6.0	4.7	7.4
40138	08 11 50.23	-30 19 21.39	19.7 ± 1.7	-49.5 ± 3.3	-3.3 ± 1.9	-40.0 ± 3.1	2.7	-5.00	-0.09	—	5936	7.5	7.0	8.1
40174	08 12 15.96	-40 30 10.01	-3.6 ± 1.7	-35.3 ± 1.2	12.3 ± 1.6	-10.3 ± 0.3	1.9	-4.83	-0.24	0.042	5773	6.7	5.9	8.0
40227	08 12 56.87	-40 32 22.18	45.3 ± 1.6	41.3 ± 2.6	-56.7 ± 1.7	15.0 ± 0.9	2.6	-4.86	-0.3	—	5160	14.4	13.4	15.2

Continued on next page

Table A.1 – continued from previous page

HIP	α	δ	V_r	U	V	W	$V \sin i$	$\log R'_{HK}$	$[Fe/H]$	EW	T_{eff}	Age	σ_{age}^{low}	σ_{age}^{high}
40229	08 12 58.88	-14 57 09.35	7.4 ± 1.7	40.3 ± 3.8	-38.0 ± 3.0	-6.5 ± 0.7	2.6	-4.94	-0.16	—	5641	3.3	2.6	4.6
40498	08 16 06.57	-05 14 32.02	-7.4 ± 1.7	-44.8 ± 4.8	42.9 ± 3.7	-21.2 ± 1.9	1.8	-4.90	-0.56	0.040	5822	13.1	12.6	13.8
40613	08 17 29.34	-03 59 22.61	112.6 ± 1.7	-37.8 ± 2.3	-144.3 ± 3.9	-43.2 ± 4.3	2.6	-4.98	-0.64	—	5753	13.3	13.3	14.6
40663	08 18 01.66	-04 01 08.54	79.7 ± 1.6	-71.2 ± 1.7	-54.5 ± 1.2	-16.2 ± 2.9	2.3	-5.02	0.09	—	5296	14.4	13.9	15.0
40695	08 18 25.54	-40 21 30.76	2.7 ± 1.6	-7.9 ± 0.8	0.9 ± 1.6	-45.3 ± 3.8	2.5	-5.07	-0.45	—	5733	14.0	12.6	15.6
40840	08 20 02.26	-50 53 00.59	8.3 ± 1.7	-49.2 ± 2.6	-2.8 ± 1.7	-19.3 ± 1.0	2.5	-4.94	-0.33	0.045	5851	10.2	10.2	11.5
40914	08 21 00.16	-28 37 30.81	18.9 ± 1.7	47.6 ± 6.3	-39.5 ± 3.0	-3.2 ± 0.6	2.9	-5.12	0.2	0.048	5691	3.3	3.3	3.3
41010	08 22 09.05	-65 28 35.64	30.3 ± 1.7	-49.5 ± 4.3	-43.3 ± 1.9	10.7 ± 1.6	2.8	-4.98	0.07	—	5712	8.2	7.8	8.6
41217	08 24 37.82	-70 09 32.29	71.2 ± 1.7	72.0 ± 5.3	-49.3 ± 2.2	-30.1 ± 1.0	2.3	-5.04	0.13	—	5825	8.1	6.8	8.3
41351	08 26 11.97	-05 45 05.40	-32.8 ± 1.6	50.3 ± 2.4	-0.2 ± 2.1	-6.1 ± 0.6	2.4	-4.58	0.06	—	5162	0.8	0.6	2.1
41353	08 26 12.57	-57 54 14.86	6.6 ± 1.7	-0.9 ± 0.2	-3.3 ± 1.6	-17.5 ± 0.9	1.9	-4.93	-0.38	0.048	5996	6.8	4.4	6.8
41659	08 29 37.81	-54 16 33.04	62.9 ± 1.6	-87.0 ± 4.1	-52.3 ± 1.7	-76.5 ± 3.1	1.0	-5.00	-0.52	—	5236	12.8	12.8	14.6
41690	08 29 55.67	-45 11 05.22	29.8 ± 1.7	-20.0 ± 1.1	-28.8 ± 1.7	19.4 ± 1.4	3.3	-5.03	0.08	0.053	5885	4.7	4.5	5.4
42098	08 34 52.59	-14 27 24.09	-39.0 ± 1.7	72.2 ± 4.1	-2.0 ± 2.9	-15.8 ± 0.6	2.5	-5.03	0.18	—	5633	6.6	5.1	7.9
42408	08 38 49.53	-05 56 55.37	-5.5 ± 1.6	67.8 ± 3.2	-45.8 ± 2.6	1.2 ± 0.6	2.3	-5.02	-0.03	—	5546	10.4	9.3	11.5
42581	08 40 43.76	-11 55 37.93	12.2 ± 1.7	-11.8 ± 1.0	-10.4 ± 1.3	-7.1 ± 1.0	4.1	-4.94	-0.31	—	5624	3.5	2.9	4.4
42581	08 40 43.76	-11 55 37.93	12.1 ± 1.7	-11.7 ± 1.0	-10.3 ± 1.3	-7.2 ± 1.0	3.9	-4.94	0.03	—	5624	3.5	3.1	4.1
42655	08 41 35.37	-42 35 33.24	46.9 ± 1.7	-5.9 ± 0.4	-46.4 ± 1.7	-20.2 ± 1.6	2.6	-5.02	0.11	0.060	5952	4.0	3.1	4.6
42751	08 42 46.05	-34 41 51.27	16.7 ± 1.7	13.3 ± 1.8	-20.1 ± 1.7	5.5 ± 0.5	2.8	-4.95	-0.23	0.037	5864	12.1	10.6	12.2
42796	08 43 12.46	-63 14 00.07	8.4 ± 1.8	-34.8 ± 2.9	-14.5 ± 1.8	1.6 ± 0.5	5.7	-4.85	0.11	0.079	6092	1.8	0.5	2.5
42847	08 43 52.59	-46 29 57.68	24.6 ± 1.7	-28.8 ± 1.4	-22.0 ± 1.7	-9.9 ± 0.5	2.2	-4.92	-0.1	—	5842	7.6	6.7	8.5
43190	08 47 58.09	-35 43 39.16	11.7 ± 1.6	20.4 ± 1.2	-14.9 ± 1.6	19.3 ± 0.9	2.4	-5.04	-0.54	—	5674	14.7	14.6	16.1
43267	08 48 49.54	-32 28 15.43	28.9 ± 1.7	19.8 ± 2.6	-38.2 ± 1.9	-21.9 ± 2.4	2.7	-5.07	0.25	—	5670	0.9	0.9	3.4
43287	08 49 03.75	-30 13 11.28	12.0 ± 1.7	13.0 ± 1.5	-18.2 ± 1.7	-10.0 ± 1.1	4.7	-5.07	0.13	—	5746	7.0	5.9	7.2
43290	08 49 05.68	-39 57 15.79	21.9 ± 1.9	-33.3 ± 0.8	-17.0 ± 1.9	-1.1 ± 0.1	8.8	-4.36	-0.1	0.106	5711	5.9	4.1	5.9
43371	08 50 02.47	-45 41 41.64	6.5 ± 1.6	-3.5 ± 0.6	-6.2 ± 4.9	-4.8 ± 0.5	2.4	-4.47	0.0	—	5480	10.1	9.9	10.3
43374	08 50 07.07	-56 09 57.29	-8.6 ± 1.6	4.8 ± 0.4	6.7 ± 1.6	17.2 ± 1.0	1.4	-4.91	0.12	—	5778	6.2	4.6	7.4
43449	08 50 59.81	-74 05 03.49	10.5 ± 1.8	-18.8 ± 1.2	-16.5 ± 1.6	-4.1 ± 0.6	5.7	-4.76	0.01	0.058	6053	4.7	3.8	4.9
43470	08 51 17.33	-06 15 46.19	23.6 ± 1.6	-58.1 ± 5.7	2.6 ± 2.8	-15.8 ± 3.2	2.4	-5.01	0.11	—	5428	7.6	6.7	8.8
44059	08 58 22.48	-14 22 26.68	40.8 ± 1.6	18.0 ± 2.4	-65.4 ± 2.4	-15.6 ± 1.9	2.6	-5.05	0.07	—	5223	13.7	13.0	14.5
44152	08 59 30.73	-55 00 55.57	-3.3 ± 1.9	15.2 ± 1.0	4.8 ± 1.9	-4.7 ± 0.4	8.6	-4.51	-0.25	0.099	6037	8.7	8.1	9.5
44171	08 59 47.03	-20 48 37.93	-23.1 ± 1.7	-9.8 ± 1.9	25.9 ± 1.6	-13.5 ± 0.9	4.2	-5.03	-0.6	—	6079	8.9	7.5	8.9
44212	09 00 21.66	-09 07 24.70	8.0 ± 1.7	26.8 ± 1.7	-28.4 ± 1.7	-1.9 ± 0.7	3.4	-4.89	-0.31	0.064	5973	3.6	3.2	4.7
44255	09 00 45.60	-69 46 12.06	4.6 ± 1.7	-16.9 ± 1.4	-9.5 ± 1.6	-0.5 ± 0.5	2.7	-5.05	0.02	0.043	5907	7.4	6.2	7.4
44279	09 01 05.47	-37 46 17.79	43.6 ± 1.6	-57.0 ± 3.3	-36.2 ± 1.7	-10.2 ± 0.9	2.6	-4.90	0.23	—	5481	10.3	9.5	11.3
44291	09 01 12.49	-25 31 37.42	7.5 ± 1.7	39.1 ± 2.0	-27.7 ± 1.8	-24.8 ± 1.3	2.8	-5.05	0.29	—	5315	4.1	4.1	5.1
44291	09 01 12.49	-25 31 37.42	7.5 ± 1.6	39.1 ± 2.0	-27.7 ± 1.8	-24.8 ± 1.3	2.8	-5.05	0.19	—	5315	8.2	7.6	9.1
44483	09 03 47.50	-19 49 31.62	$- \pm -$	$- \pm -$	$- \pm -$	$- \pm -$	-	-4.43	1.5	0.038	5875	15.1	13.6	15.1
44657	09 05 57.53	-21 31 57.34	16.1 ± 1.7	-12.3 ± 0.7	-16.6 ± 1.5	-10.0 ± 1.1	2.6	-4.55	-0.37	—	5744	12.8	12.3	13.4
44668	09 06 09.99	-37 09 09.82	0.1 ± 1.7	6.2 ± 0.5	-2.2 ± 1.6	-8.8 ± 0.6	2.6	-5.08	-0.24	—	5794	13.9	12.6	14.5
44698	09 06 31.02	-42 00 19.01	38.3 ± 1.7	-17.0 ± 1.1	-38.2 ± 1.7	-20.0 ± 1.9	3.1	-5.05	0.11	0.061	6015	3.4	2.5	3.9
44799	09 07 46.71	-29 57 15.14	43.1 ± 1.7	-22.7 ± 1.3	-37.9 ± 1.6	8.2 ± 0.4	2.0	-4.95	-0.25	—	5825	5.8	4.3	6.6
44811	09 07 56.57	-50 28 56.80	-1.5 ± 1.7	10.1 ± 0.3	2.6 ± 1.7	-25.7 ± 0.7	2.6	-4.96	-0.73	—	5733	13.4	13.4	15.1
44953	09 09 30.16	-00 23 54.35	5.3 ± 1.6	13.5 ± 1.1	-28.1 ± 1.5	-12.2 ± 1.0	1.4	-4.92	-0.42	—	5190	14.0	14.0	15.4
45621	09 17 55.38	-03 23 14.10	-34.4 ± 1.7	25.1 ± 0.9	17.2 ± 1.2	-19.4 ± 0.8	3.8	—	-0.86	—	5102	13.6	13.6	15.1
45685	09 18 48.64	-24 27 27.71	23.3 ± 1.7	-12.6 ± 0.7	-22.3 ± 1.6	-1.9 ± 0.9	4.9	-5.02	-0.03	0.052	5964	2.9	2.9	4.1
45957	09 22 20.50	-32 08 54.49	35.0 ± 1.6	-120.0 ± 4.5	-22.5 ± 1.6	-35.6 ± 1.7	2.6	-4.52	-0.37	—	5158	13.8	13.8	15.1
46203	09 25 15.12	-09 51 00.56	-26.0 ± 1.6	58.8 ± 3.8	-4.0 ± 2.3	-10.5 ± 0.8	2.6	-4.68	-0.06	—	5484	11.1	10.8	11.4
46384	09 27 29.47	-62 35 38.88	6.5 ± 1.7	-29.5 ± 2.6	-12.2 ± 1.7	-4.4 ± 0.5	3.9	-4.72	0.09	—	5910	5.4	4.7	6.1
46603	09 30 11.50	-26 00 51.22	36.3 ± 1.7	-54.0 ± 5.3	-25.9 ± 1.8	0.4 ± 1.4	2.8	-4.92	-0.14	—	5858	1.8	1.2	1.8
46649	09 30 41.39	-36 38 36.42	7.5 ± 1.7	-25.9 ± 2.2	-7.4 ± 1.6	-13.1 ± 1.3	3.8	-4.46	0.06	0.045	5618	9.4	9.1	9.8
47002	09 34 46.24	-24 11 33.09	16.7 ± 1.7	36.3 ± 2.0	-21.7 ± 1.5	15.7 ± 0.7	3.0	-4.63	-0.02	—	5342	2.9	2.6	5.1
47059	09 35 25.76	-06 28 27.05	19.8 ± 1.7	-22.2 ± 1.7	-24.5 ± 1.6	-14.3 ± 2.9	2.7	-4.98	-0.14	0.063	5935	6.3	4.9	6.3
47135	09 36 17.82	-78 20 41.58	$- \pm -$	$- \pm -$	$- \pm -$	$- \pm -$	-	-4.33	-0.67	0.130	5894	13.0	13.0	14.4
47156	09 36 32.52	-22 25 46.75	20.9 ± 1.6	-13.3 ± 0.6	-16.1 ± 1.5	8.4 ± 0.6	2.2	-4.87	-0.18	—	5494	4.1	3.3	5.3
47171	09 36 45.27	-03 54 14.19	-6.8 ± 1.7	-43.7 ± 5.3	41.1 ± 4.2	6.2 ± 1.5	2.5	-4.92	-0.51	—	5804	14.3	13.4	15.2
47255	09 37 55.67	-36 55 33.49	36.6 ± 1.7	-28.0 ± 0.9	-34.5 ± 1.6	3.5 ± 0.3	3.1	-4.98	-0.22	—	5530	14.9	13.5	14.9
47418	09 39 44.47	-64 59 44.12	24.8 ± 1.6	9.2 ± 0.5	-23.0 ± 1.6	-3.4 ± 0.4	1.9	-4.99	-0.07	—	5642	9.5	8.8	10.3
47732	09 43 48.04	-25 57 28.38	61.8 ± 1.6	-94.1 ± 6.8	-50.4 ± 1.6	-6.0 ± 2.3	2.1	-4.94	0.0	—	5629	5.6	4.3	6.8
47734	09 43 48.94	-09 59 27.92	-6.2 ± 1.7	-59.2 ± 6.4	-6.4 ± 1.7	-61.8 ± 6.1	2.7	-4.94	-0.47	—	5807	12.4	11.9	12.9
47856	09 45 15.14	-20 40 19.47	2.2 ± 1.7	-47.7 ± 4.5	-5.0 ± 1.5	-33.2 ± 3.3	3.9	-5.14	-0.35	0.052	5649	6.9	5.2	8.1
47947	09 46 13.33	-40 38 08.27	-0.5 ± 1.7	-1.3 ± 0.1	6.3 ± 1.7	33.3 ± 1.5	3.1	-4.96	-0.2	0.060	5918	5.7	4.7	6.0
47961	09 46 25.98	-14 31 45.47	-9.0 ± 1.7	-83.4 ± 8.3	28.1 ± 2.4	-22.4 ± 1.9	2.6	-4.91	-0.33	—	5541	13.8	13.2	14.4
47990	09 46 53.93	-04 17 53.05	6.2 ± 1.7	-6.1 ± 0.8	-15.0 ± 1.5	-11.9 ± 1.6	3.5	-4.63	0.06	0.042	5777	8.2	6.6	8.6
48133	09 48 46.75	-52 36 56.55	-0.4 ± 1.6	-40.2 ± 0.9	-4.5 ± 1.6	4.1 ± 0.1	2.4	-4.89	0.02	—	4970	13.5	13.5	15.1
48323	09 51 01.59	-21 04 06.68	-20.4 ± 1.8	-0.2 ± 0.6	2.2 ± 2.1	-43.9 ± 3.1	7.4	-5.08	-0.47	—	5958	3.9	3.1	4.9
48365	09 51 36.52	-02 52 43.60	18.1 ± 1.6	-22.0 ± 1.2	-44.2 ± 2.4	-34.8 ± 3.3	2.8	-5.00	-0.05	—	5120	4.6	3.4	6.1
48471	09 53 02.86	-49 30 45.40	-3.9 ± 1.6	8.5 ± 0.8	1.3 ± 1.7	-53.4 ± 4.5	2.1	-5.01	-0.27	—	5716	13.0	12.8	14.6
48476	09 53 11.26	-50 55 58.50	-12.1 ± 1.8	0.1 ± 0.4	11.7 ± 1.8	-10.5 ± 0.8	6.6	-4.83	-0.12	0.069	6191	6.4	4.9	6.8
48583	09 54 31.16	-45 43 51.52	22.0 ± 1.7	8.5 ± 0.5	-18.6 ± 1.7	25.8 ± 1.4	3.4	-5.05	-0.25	—	5668	8.6	7.6	10.0
48637	09 55 02.33	-40 45 33.35	37.8 ± 1.7	-100.6 ± 6.6	-43.5 ± 1.7	-22.0 ± 1.9	2.5	-4.97	-0.51	0.048	6041	10.2	9.0	10.2
48754	09 56 38.43	-08 50 04.40	37.3 ± 1.6	-56.0 ± 1.8	-19.5 ± 1.3	8.0 ± 1.1	1.7	-4.70	-0.15	—	5397	3.3	2.4	3.5
49161	10 01 58.58	-10 24 19.38	50.0 ± 1.7	-43.3 ± 1.8	-54.3 ± 1.6	-7.9 ± 2.4	2.8	-5.09	0.21	—	5241	5.6	4.3	6.8
49366	10 04 37.66	-11 43 46.93	-12.5 ± 1.7	-11.5 ± 0.6	5.0 ± 1.3	-20.9 ± 1.0	3.7	-4.46	-0.13	—	5006	4.9	2.5	4.9
49531	10 06 49.99	-29 57 58.54	-3.6 ± 1.6	4.6 ± 0.6	-16.1 ± 2.5	-51.9 ± 5.2	1.7	-4.97	-0.25	—	5770	11.4	11.1	11.7

Continued on next page

Table A.1 – continued from previous page

HIP	α	δ	V_r	U	V	W	$V \sin i$	$\log R'_{HK}$	$[Fe/H]$	EW	T_{eff}	Age	σ_{age}^{low}	σ_{age}^{high}
49542	10 06 55.96	-12 52 47.67	84.7 ± 1.7	-130.2 ± 12.2	-54.3 ± 2.0	16.6 ± 3.5	2.9	-5.02	-0.23	—	5750	10.9	10.3	11.4
49644	10 07 58.20	-58 28 45.78	18.1 ± 1.7	-43.6 ± 1.9	-28.2 ± 1.7	-8.5 ± 0.3	3.3	-4.51	-0.02	—	5451	0.3	0.3	2.0
49674	10 08 26.57	-11 06 54.74	28.3 ± 1.7	-37.6 ± 1.4	-23.2 ± 1.3	0.9 ± 1.2	3.7	-4.45	0.02	0.049	5571	5.4	5.0	5.7
49736	10 09 12.11	-47 36 55.91	4.6 ± 1.7	-11.2 ± 1.0	-7.6 ± 1.7	-13.7 ± 1.2	3.7	-4.73	0.09	0.055	5855	5.8	5.7	5.9
49793	10 09 49.58	-36 45 14.94	110.3 ± 1.6	-103.2 ± 4.2	-100.6 ± 1.6	51.3 ± 1.0	1.8	-4.93	-0.56	—	5729	13.5	13.5	14.9
49985	10 12 17.30	-11 08 06.27	-2.5 ± 1.7	-52.1 ± 5.6	3.9 ± 1.3	-21.3 ± 2.3	2.6	-5.04	-0.09	0.055	6087	4.4	4.4	5.6
50020	10 12 43.97	-64 23 40.30	29.6 ± 1.7	-48.6 ± 3.8	-43.4 ± 1.9	-19.9 ± 1.1	5.0	-4.96	-0.26	—	5826	4.5	3.8	5.3
50121	10 13 56.13	-72 40 44.06	-14.0 ± 1.7	-32.8 ± 1.6	9.0 ± 1.5	-25.8 ± 1.6	3.2	-4.89	-0.17	—	5344	5.6	4.8	6.4
50458	10 18 10.11	-27 11 31.41	71.6 ± 1.7	-55.7 ± 5.2	-71.4 ± 1.6	7.1 ± 2.4	2.9	-5.13	-0.11	—	5160	10.2	8.6	11.6
50490	10 18 36.65	-07 30 08.30	17.4 ± 1.6	0.3 ± 0.8	-23.1 ± 1.7	1.0 ± 1.6	1.9	-4.15	-0.07	0.542	5763	10.6	10.1	11.0
50617	10 20 21.84	-12 09 09.42	0.7 ± 1.6	-80.1 ± 5.8	-13.6 ± 1.6	-45.0 ± 3.4	2.3	-5.00	-0.41	—	5563	14.2	13.9	14.6
50701	10 21 10.66	-17 35 50.19	-7.8 ± 1.7	21.4 ± 1.6	-11.5 ± 2.0	-26.4 ± 1.9	3.6	-4.97	-0.3	—	5560	14.6	14.2	14.8
50839	10 22 51.43	-28 00 48.59	11.3 ± 1.7	-33.5 ± 2.4	-11.4 ± 1.5	-1.3 ± 0.8	3.9	-5.07	-0.28	0.070	5740	8.8	7.6	10.3
51027	10 25 28.37	-02 29 37.10	7.8 ± 1.7	55.7 ± 5.1	-50.3 ± 4.1	-14.4 ± 2.1	2.7	-5.08	-0.13	—	5721	9.8	9.1	9.9
51053	10 25 51.60	-10 01 51.96	12.0 ± 2.1	-12.0 ± 1.2	-25.2 ± 2.3	-15.1 ± 2.8	11.1	-4.71	-0.28	0.048	6193	6.4	4.9	6.4
51078	10 26 10.64	-45 33 45.15	19.4 ± 1.7	-32.2 ± 1.6	-22.6 ± 1.7	10.0 ± 0.4	4.6	-5.01	-0.24	0.069	5870	6.8	6.0	7.6
51114	10 26 35.02	-21 45 22.85	53.0 ± 1.7	-12.6 ± 0.7	-66.5 ± 2.3	-11.0 ± 3.3	2.9	-5.01	0.16	—	5445	11.5	11.3	11.7
51258	10 28 13.92	-16 17 20.97	39.6 ± 1.7	-28.0 ± 1.1	-23.9 ± 1.4	28.5 ± 1.0	3.1	-5.11	-0.18	—	5618	15.1	13.7	15.5
51293	10 28 37.07	-24 23 30.48	-41.1 ± 1.7	-46.2 ± 4.8	37.9 ± 1.5	-22.7 ± 0.9	2.5	-4.99	-0.33	0.042	5898	9.2	7.6	9.2
51297	10 28 42.88	-27 21 57.74	30.1 ± 1.6	66.4 ± 2.3	-31.3 ± 1.5	9.5 ± 0.7	2.4	-4.96	-0.3	—	5164	5.1	4.4	6.1
51494	10 31 00.97	-26 52 03.16	-10.8 ± 1.7	19.6 ± 1.9	8.2 ± 1.5	-6.4 ± 0.8	2.6	-5.06	0.07	—	5725	9.9	9.8	10.0
51500	10 31 04.03	-78 09 53.95	17.7 ± 1.7	-59.4 ± 4.5	-52.4 ± 2.9	8.7 ± 1.1	3.2	-5.05	-0.5	—	5614	12.7	11.1	14.1
51608	10 32 32.39	-72 25 41.58	-0.3 ± 1.7	-8.9 ± 0.8	1.5 ± 1.5	-20.7 ± 1.1	2.7	-5.02	0.01	—	5888	7.5	6.6	7.5
51611	10 32 35.12	-72 26 29.22	-0.3 ± 1.7	-9.0 ± 0.8	1.6 ± 1.5	-21.2 ± 1.2	2.4	-4.96	0.05	—	5704	9.0	8.2	10.0
51655	10 33 12.11	-48 07 36.62	-25.1 ± 1.6	-2.5 ± 0.4	25.3 ± 1.6	-0.4 ± 0.4	2.0	-4.93	-0.41	—	5763	14.1	14.0	14.1
51783	10 34 50.18	-07 55 32.36	53.1 ± 1.7	18.1 ± 2.6	-54.7 ± 1.9	26.0 ± 1.4	2.8	-5.05	-0.02	—	5438	1.7	1.7	4.4
51884	10 36 02.21	-11 54 47.92	-54.5 ± 1.7	49.5 ± 1.3	21.8 ± 1.4	-48.0 ± 1.1	4.5	—	-0.89	0.034	5113	14.8	14.8	16.1
51884	10 36 02.21	-11 54 47.92	-37.8 ± 1.7	46.9 ± 1.3	9.0 ± 1.4	-37.4 ± 1.1	4.3	—	-0.93	—	5113	16.0	14.9	16.1
51950	10 36 46.23	-06 53 33.31	11.4 ± 1.9	-9.7 ± 1.1	-21.7 ± 2.1	-8.4 ± 2.3	7.9	-5.15	-0.31	0.071	5897	6.2	5.6	6.8
51987	10 37 18.97	-11 30 39.96	-6.2 ± 1.7	73.8 ± 6.6	-0.6 ± 1.4	7.3 ± 1.5	2.9	-5.07	0.42	—	5648	1.3	0.6	3.5
52023	10 37 44.29	-11 02 58.99	8.1 ± 1.7	-26.9 ± 2.3	-16.2 ± 1.5	-12.9 ± 1.9	2.7	-5.12	0.06	—	5519	11.2	10.2	12.2
52089	10 38 38.05	-13 45 35.75	21.2 ± 1.6	28.5 ± 1.8	-46.2 ± 2.1	-17.8 ± 2.0	2.5	-4.92	-0.39	—	5146	14.0	13.2	14.6
52166	10 39 29.22	-20 50 59.30	6.2 ± 1.7	-28.9 ± 2.0	-2.6 ± 1.4	4.3 ± 0.9	3.5	-4.95	-0.13	0.047	5982	0.6	0.3	1.6
52461	10 43 28.12	-76 34 50.68	30.6 ± 1.7	27.6 ± 1.0	-21.3 ± 1.5	-2.2 ± 0.5	2.8	-4.98	0.41	—	5620	5.5	5.1	6.8
52500	10 44 05.03	-54 54 40.57	40.1 ± 1.7	-18.1 ± 2.7	-47.5 ± 1.8	-13.3 ± 1.5	2.6	-5.02	0.22	—	5592	10.0	8.6	10.7
52629	10 45 45.40	-45 45 31.89	23.5 ± 1.7	10.3 ± 0.6	-19.3 ± 1.6	14.8 ± 0.9	2.4	-4.97	-0.17	—	5936	7.6	7.4	7.9
52787	10 47 31.15	-22 20 52.92	23.4 ± 1.7	-15.0 ± 0.5	-27.5 ± 1.5	-0.2 ± 1.0	5.4	-4.40	-0.03	0.111	5296	13.7	12.1	15.1
52828	10 48 05.56	-26 23 54.25	20.6 ± 1.7	-27.9 ± 1.2	-28.5 ± 1.6	-7.8 ± 1.1	3.6	-4.89	-0.05	0.061	6112	0.9	0.4	0.9
52933	10 49 31.69	-06 46 10.60	0.9 ± 1.6	-48.0 ± 3.5	-6.2 ± 1.2	-15.2 ± 1.6	2.4	-5.05	0.37	—	5149	12.1	11.6	12.6
52939	10 49 35.40	-29 59 39.91	8.2 ± 1.7	-25.0 ± 1.7	-18.9 ± 1.7	-16.7 ± 1.5	3.0	-5.08	-0.16	—	6153	5.9	5.5	6.7
52986	10 50 19.89	-71 10 52.34	77.1 ± 1.7	98.7 ± 4.9	-47.8 ± 2.2	24.6 ± 2.8	4.3	-4.94	-0.75	—	5461	15.6	15.2	15.6
52990	10 50 25.51	-15 06 15.07	42.9 ± 1.7	-46.9 ± 2.0	-63.5 ± 1.9	-16.1 ± 2.2	3.0	-5.05	-0.35	—	5900	10.8	10.3	11.9
52995	10 50 27.74	-06 40 30.23	23.7 ± 1.7	4.4 ± 1.0	-39.1 ± 2.8	-3.4 ± 2.6	2.7	-4.98	-0.13	0.055	6143	4.2	2.8	4.8
53015	10 50 45.97	-04 44 18.37	-7.9 ± 1.7	2.9 ± 0.7	4.2 ± 1.2	-6.3 ± 1.3	2.9	-4.99	0.12	—	6004	3.3	2.9	4.0
53023	10 50 54.20	-68 21 44.64	-4.4 ± 1.8	-60.6 ± 3.9	-17.1 ± 2.1	-17.3 ± 1.2	5.3	-5.13	-0.16	0.047	6029	5.4	5.2	5.8
53084	10 51 36.51	-16 24 15.47	36.9 ± 1.7	-47.7 ± 3.1	-50.0 ± 1.9	-8.8 ± 2.4	2.7	-5.05	0.32	—	5566	8.4	7.3	9.1
53087	10 51 39.23	-22 04 18.58	3.9 ± 1.7	-46.2 ± 1.7	-15.4 ± 1.5	-17.1 ± 1.1	2.5	-4.94	0.09	—	5591	8.1	7.2	9.3
53101	10 51 47.41	-38 47 55.25	31.8 ± 1.7	84.8 ± 9.2	-21.3 ± 1.9	-1.0 ± 1.4	4.5	-5.01	0.05	—	5562	12.6	11.1	13.4
53172	10 52 39.28	-17 01 48.89	20.2 ± 1.7	1.7 ± 0.2	-34.8 ± 1.6	-12.1 ± 1.5	2.1	-5.00	0.0	—	5909	7.4	6.5	7.4
53186	10 52 44.43	-11 25 22.86	-5.0 ± 1.7	-43.4 ± 1.6	-1.7 ± 1.2	-16.0 ± 1.2	2.5	-4.91	-0.44	0.044	5888	10.6	9.1	10.7
53250	10 53 27.63	-15 49 13.89	27.1 ± 1.6	-62.1 ± 2.6	-35.5 ± 1.4	-6.9 ± 1.4	2.6	-4.98	0.27	—	5488	9.2	8.1	10.4
53301	10 54 06.54	-23 11 05.44	28.7 ± 1.7	62.2 ± 5.4	-38.6 ± 1.9	-8.6 ± 2.3	4.6	-5.04	-0.6	0.064	5912	10.3	8.7	11.6
53314	10 54 16.97	-34 57 49.96	4.3 ± 1.7	-19.8 ± 1.9	-16.4 ± 1.9	-22.3 ± 2.3	3.5	-4.98	0.2	0.054	6079	3.7	2.8	3.8
53321	10 54 22.58	-70 44 27.78	27.8 ± 1.6	-11.9 ± 1.6	-35.9 ± 1.6	-0.7 ± 0.4	1.6	-4.89	-0.65	0.042	5882	8.2	6.6	8.8
53416	10 55 36.22	-26 21 06.62	31.1 ± 1.7	-57.8 ± 3.9	-48.7 ± 2.0	-17.1 ± 2.3	2.6	-4.96	-0.18	0.041	5901	6.5	5.4	7.1
53424	10 55 43.37	-05 33 05.73	4.4 ± 1.7	-13.6 ± 1.0	-21.7 ± 1.8	-16.3 ± 1.9	3.3	-5.01	-0.46	—	5601	15.1	15.1	15.1
53443	10 55 58.74	-02 53 34.02	16.5 ± 1.7	2.1 ± 0.6	-28.7 ± 2.0	-1.7 ± 1.8	3.4	-4.63	-0.17	0.044	5553	13.5	12.1	14.2
53499	10 56 38.34	-36 34 49.11	87.7 ± 1.7	-67.7 ± 8.2	-90.8 ± 1.9	37.2 ± 0.9	3.9	—	-0.69	0.051	5848	13.8	12.1	15.1
53534	10 57 09.15	-69 58 50.24	26.2 ± 1.7	2.4 ± 1.1	-26.5 ± 1.5	-8.1 ± 0.6	3.0	-5.04	-0.46	—	5439	15.5	13.8	16.1
53647	10 58 33.07	-39 55 45.56	-2.3 ± 1.7	6.3 ± 0.8	-4.9 ± 1.7	-26.1 ± 2.5	3.1	-5.04	-0.29	—	5744	11.4	10.1	13.1
53657	10 58 38.71	-57 29 00.13	26.9 ± 1.7	45.6 ± 2.1	-12.6 ± 1.7	18.9 ± 1.0	2.8	-4.97	-0.21	—	5829	8.6	7.9	9.6
53719	10 59 26.30	-56 37 22.94	96.1 ± 1.6	-24.0 ± 1.8	-111.4 ± 1.7	-44.4 ± 1.6	2.4	-4.97	0.11	—	5137	13.4	13.4	15.1
54104	11 04 15.14	-27 17 11.84	9.4 ± 1.7	-34.0 ± 3.2	-20.7 ± 1.8	-11.4 ± 1.7	2.9	-5.08	-0.29	—	5454	16.0	13.6	16.1
54114	11 04 20.77	-78 52 06.74	0.1 ± 1.7	-46.2 ± 2.1	-21.1 ± 1.7	-9.4 ± 0.6	3.7	-4.55	0.16	—	5356	6.5	4.6	7.1
54195	11 05 15.06	-10 17 28.68	11.3 ± 1.7	-17.0 ± 1.8	-16.3 ± 1.5	-1.8 ± 1.6	3.6	-5.16	0.33	—	5740	5.6	4.8	6.4
54259	11 06 00.87	-05 22 52.21	27.8 ± 1.7	-24.0 ± 2.9	-40.2 ± 3.1	-1.2 ± 3.2	3.4	-4.86	-0.53	0.073	5932	13.1	11.6	14.3
54285	11 06 18.92	-29 58 01.83	18.6 ± 1.7	-71.2 ± 5.0	-33.8 ± 1.9	-6.5 ± 1.3	2.9	-4.95	-0.07	—	5820	7.2	6.6	8.0
54530	11 09 30.08	-25 59 26.68	17.8 ± 1.6	42.3 ± 1.6	-6.6 ± 1.4	16.1 ± 0.9	2.1	-4.92	-0.24	—	5376	1.4	0.7	2.9
54580	11 10 11.92	-11 21 36.55	-3.8 ± 1.7	12.2 ± 0.8	-12.8 ± 1.6	-17.9 ± 1.5	3.2	-5.05	-0.29	—	5736	7.8	6.9	9.1
54724	11 12 13.28	-37 34 38.29	47.0 ± 1.6	-39.8 ± 4.2	-64.5 ± 2.4	-11.3 ± 2.5	2.6	-5.00	-0.08	—	5189	13.8	13.7	13.8
54728	11 12 16.33	-01 11 13.89	-19.5 ± 1.7	35.3 ± 1.5	-8.3 ± 1.3	-25.5 ± 1.4	3.0	-4.98	0.01	—	5742	6.2	4.6	7.1
54804	11 13 10.53	-18 09 55.05	-4.4 ± 1.7	-47.1 ± 2.3	-48.1 ± 2.9	-64.3 ± 3.2	2.6	-4.98	-0.38	—	5719	13.3	13.2	14.6
54884	11 14 17.15	-36 15 07.20	-8.9 ± 1.7	-46.9 ± 5.0	0.7 ± 1.7	1.4 ± 0.9	2.8	-5.01	-0.15	0.078	5982	5.1	3.7	6.6
54926	11 14 51.26	-43 48 45.39	-3.3 ± 1.8	-10.4 ± 0.9	-6.3 ± 1.8	-24.2 ± 2.1	6.2	—	-0.56	—	5600	11.9	10.6	13.6
55057	11 16 16.70	-03 45 41.87	0.5 ± 1.6	-47.1 ± 3.8	-19.9 ± 1.9	-19.7 ± 2.1	1.6	-4.88	0.19	—	5558	4.0	3.9	5.9

Continued on next page

Table A.1 – continued from previous page

HIP	α	δ	V_r	U	V	W	$V \sin i$	$\log R'_{HK}$	$[Fe/H]$	EW	T_{eff}	Age	σ_{age}^{low}	σ_{age}^{high}
55235	11 18 39.70	-10 07 34.36	7.6 ± 1.7	-55.5 ± 2.9	-15.2 ± 1.2	-5.2 ± 1.3	2.8	-4.81	0.11	—	5253	10.7	9.7	11.7
55285	11 19 21.60	-05 56 17.17	1.0 ± 1.6	56.7 ± 6.5	-32.2 ± 3.7	-21.8 ± 2.9	1.9	-4.87	-0.11	—	5564	14.6	13.9	15.2
55300	11 19 29.90	-74 00 20.03	-12.9 ± 1.7	-52.2 ± 2.9	-8.3 ± 1.9	-12.4 ± 1.0	3.2	-4.54	-0.75	—	5454	16.1	16.1	16.1
55304	11 19 32.93	-00 11 17.85	6.0 ± 1.6	43.0 ± 3.3	-32.0 ± 2.3	-9.6 ± 1.7	-	—	-0.98	—	5956	13.3	11.6	14.6
55409	11 20 51.76	-23 13 02.43	3.7 ± 1.7	-17.4 ± 0.7	-34.1 ± 1.9	-38.4 ± 1.9	2.1	-4.99	-0.03	—	5678	8.1	6.9	9.1
55438	11 21 09.14	-00 37 50.62	12.6 ± 1.6	72.4 ± 10.1	-23.1 ± 2.4	7.1 ± 1.4	1.7	-4.89	-0.28	—	5712	11.6	10.8	13.1
55618	11 23 42.41	-38 47 35.39	88.5 ± 1.6	49.6 ± 4.0	-63.9 ± 2.7	53.1 ± 3.1	2.2	-5.04	-0.36	—	5563	15.1	13.1	16.1
55664	11 24 17.35	-01 31 44.67	32.6 ± 1.6	-24.7 ± 1.8	-71.2 ± 4.2	-12.4 ± 3.3	2.2	-5.06	0.3	—	5236	13.4	12.9	14.0
55875	11 27 10.77	-15 38 54.82	1.7 ± 1.9	13.9 ± 1.0	-18.3 ± 1.8	-18.6 ± 1.9	8.0	-4.72	-0.37	—	5282	15.1	14.8	15.6
56175	11 30 53.81	-22 46 59.29	8.3 ± 1.7	-30.9 ± 3.3	-12.0 ± 1.4	5.1 ± 1.0	2.4	-4.99	-0.02	—	5793	4.1	2.7	5.2
56413	11 33 56.67	-48 49 09.24	18.6 ± 1.6	-32.9 ± 1.7	-40.3 ± 1.8	-35.0 ± 1.6	2.3	-4.85	0.08	—	5567	8.6	7.7	9.7
56641	11 36 49.85	-12 21 02.30	-28.9 ± 1.7	5.6 ± 1.1	14.7 ± 1.4	-26.5 ± 1.4	3.0	-4.86	-0.42	—	5160	14.9	14.5	15.3
56738	11 37 59.10	-01 35 57.96	3.8 ± 1.7	-61.7 ± 2.5	-6.7 ± 0.9	-1.0 ± 1.4	1.5	-4.86	-0.13	0.065	5947	5.1	3.9	5.1
56791	11 38 34.91	-16 46 15.29	-27.9 ± 1.6	53.2 ± 4.6	10.7 ± 1.4	-38.6 ± 1.9	2.4	-5.07	0.16	—	5575	7.2	7.2	9.0
56798	11 38 38.18	-11 14 21.36	6.7 ± 1.7	-0.4 ± 0.3	-5.8 ± 1.1	3.8 ± 1.2	3.5	-4.94	-0.32	0.041	5756	13.8	12.1	15.1
56869	11 39 33.32	-30 29 01.82	20.3 ± 1.6	-67.6 ± 8.8	-54.1 ± 4.7	-19.4 ± 3.7	2.4	-5.11	0.22	—	5602	9.9	9.4	10.3
56876	11 39 36.58	-35 13 57.12	10.8 ± 1.7	-80.5 ± 7.2	-38.6 ± 2.9	-3.8 ± 1.0	4.2	-5.15	-0.23	0.080	5620	4.9	4.0	6.3
57177	11 43 32.53	-39 40 59.59	18.1 ± 1.7	30.2 ± 1.9	-18.1 ± 1.5	-19.3 ± 2.0	2.8	-4.86	-0.6	—	5848	13.7	13.6	13.9
57207	11 43 49.78	-35 14 52.78	$- \pm -$	$- \pm -$	$- \pm -$	$- \pm -$	-	-4.38	-0.54	0.134	5907	12.7	12.6	13.1
57285	11 44 47.36	-58 15 53.17	$- \pm -$	$- \pm -$	$- \pm -$	$- \pm -$	-	-4.46	1.5	0.040	6079	15.1	13.8	15.1
57331	11 45 17.30	-57 34 29.21	-0.5 ± 1.7	-73.6 ± 8.2	-33.0 ± 4.0	-8.1 ± 1.0	2.7	-5.07	0.17	—	5622	12.7	12.3	12.9
57366	11 45 38.46	-16 04 41.17	20.7 ± 1.8	-11.8 ± 1.6	-24.3 ± 1.6	7.3 ± 1.4	5.4	-5.09	-0.36	—	6012	4.6	3.6	6.0
57441	11 46 30.98	-28 46 12.09	3.1 ± 1.7	-17.5 ± 1.5	-9.8 ± 1.5	-1.3 ± 0.9	3.0	-4.60	-0.09	—	5535	6.0	5.2	6.1
57460	11 46 42.35	-19 28 11.15	-7.9 ± 1.9	-30.8 ± 1.5	-9.5 ± 1.6	-15.1 ± 1.3	8.6	-4.43	-0.77	0.091	6041	13.3	13.3	14.6
57468	11 46 48.95	-21 28 29.70	2.9 ± 1.8	-45.0 ± 4.2	-22.0 ± 2.3	-8.7 ± 1.5	7.2	-4.97	-0.35	0.082	5978	7.3	6.5	8.7
57552	11 47 46.23	-46 36 05.45	8.3 ± 1.7	5.7 ± 0.6	-12.9 ± 1.6	-20.6 ± 1.8	3.0	-4.74	-0.04	0.052	5900	7.4	7.0	7.9
57645	11 49 13.15	-20 20 34.66	-9.8 ± 1.6	-36.1 ± 1.5	-5.5 ± 1.3	-11.5 ± 1.1	1.8	-4.69	-0.17	—	4965	14.1	12.9	15.5
57668	11 49 39.80	-15 25 30.41	19.7 ± 1.7	-22.6 ± 2.3	-43.7 ± 3.0	-10.4 ± 2.5	3.5	-4.92	-0.13	0.053	5904	3.9	3.9	5.7
57739	11 50 26.04	-58 17 12.93	55.4 ± 1.6	-9.8 ± 4.0	-64.8 ± 2.3	14.2 ± 1.3	2.2	-5.04	0.1	—	5637	8.3	6.8	8.4
57744	11 50 29.05	-17 44 24.79	1.4 ± 1.7	-59.8 ± 4.9	-20.4 ± 2.0	-4.8 ± 1.2	3.8	-5.07	0.09	—	5998	4.4	3.3	4.4
57927	11 52 47.33	-24 28 22.95	3.2 ± 1.7	-108.2 ± 10.6	-12.7 ± 1.6	29.9 ± 2.9	2.9	-5.13	0.16	—	5517	8.2	7.2	8.7
57931	11 52 52.97	-50 17 34.15	-4.7 ± 1.6	-18.8 ± 1.4	-3.6 ± 1.6	-3.5 ± 0.4	2.6	-5.07	0.26	—	5196	4.5	3.6	4.7
57999	11 53 47.77	-73 25 37.76	0.5 ± 1.7	12.0 ± 1.3	3.4 ± 1.5	11.4 ± 1.1	2.6	-5.01	-0.69	0.044	5948	13.1	12.6	13.3
58132	11 55 23.69	-03 35 58.08	-10.4 ± 1.7	18.7 ± 1.7	1.3 ± 1.0	-13.1 ± 1.5	4.0	—	-0.81	—	5835	15.3	15.3	16.1
58152	11 55 32.09	-15 57 10.40	10.5 ± 1.6	-45.6 ± 3.7	-43.9 ± 3.0	-17.0 ± 2.2	2.5	-5.01	0.11	—	5344	12.3	11.9	12.8
58180	11 55 57.08	-77 00 30.27	8.4 ± 1.7	-4.6 ± 0.8	-11.5 ± 1.4	-4.0 ± 0.4	4.1	-4.45	-0	—	5551	4.3	3.1	4.3
58226	11 56 30.96	-50 45 34.97	30.5 ± 1.7	-26.3 ± 4.0	-47.1 ± 2.5	-5.2 ± 1.2	3.8	-4.72	0.06	—	5553	10.0	9.9	10.1
58387	11 58 19.51	-55 14 22.43	-0.0 ± 1.7	-8.4 ± 1.1	-5.1 ± 1.6	-8.5 ± 0.8	5.4	-4.46	0.08	0.098	5889	1.8	1.4	2.2
58395	11 58 26.14	-33 08 36.55	3.1 ± 1.7	-1.3 ± 0.7	-10.4 ± 1.6	-10.5 ± 1.5	2.8	-5.11	0.24	—	5555	10.8	10.6	10.8
58401	11 58 28.01	-41 55 19.22	159.8 ± 1.6	-31.0 ± 3.0	-199.2 ± 2.4	-6.2 ± 2.1	1.8	-4.97	-0.7	—	5065	14.2	12.8	14.3
58523	12 00 06.99	-55 15 17.88	30.3 ± 1.7	4.6 ± 1.1	-30.9 ± 1.6	5.4 ± 0.4	5.2	-5.01	-0.19	0.041	5947	7.0	6.8	7.0
58558	12 00 27.45	-04 32 55.71	42.5 ± 1.7	-0.8 ± 0.3	-54.2 ± 1.7	15.3 ± 1.6	2.8	-5.02	0.03	—	5404	13.4	12.1	14.9
58691	12 02 13.56	-48 43 29.67	-10.9 ± 1.6	-51.9 ± 4.7	-16.0 ± 2.9	-17.6 ± 1.5	2.8	-4.98	-0.44	—	5363	15.0	14.5	15.9
58722	12 02 39.45	-10 42 49.09	0.0 ± 1.7	8.7 ± 0.6	0.8 ± 1.0	-1.0 ± 1.3	3.5	-4.38	-0.62	0.055	5339	14.2	14.2	15.6
58840	12 04 05.40	-48 57 09.78	28.0 ± 1.6	37.4 ± 2.9	-13.9 ± 1.9	1.2 ± 0.7	1.0	-4.97	-0.31	—	5807	10.8	9.4	10.8
58949	12 05 12.52	-01 30 32.54	16.2 ± 1.6	-72.1 ± 2.4	-38.0 ± 1.3	3.9 ± 1.4	1.9	-5.01	-0.23	—	5350	13.5	13.5	15.1
59027	12 06 07.75	-50 14 38.92	53.6 ± 1.7	-45.9 ± 6.5	-80.0 ± 3.4	11.5 ± 0.4	2.1	-5.00	-0.8	—	5732	16.1	15.1	16.1
59051	12 06 29.85	-71 48 47.53	-3.4 ± 1.7	-27.9 ± 2.9	-8.6 ± 1.9	-16.8 ± 1.9	3.9	-5.00	0.19	0.042	5964	3.4	2.2	3.9
59197	12 08 21.70	-30 57 49.78	57.3 ± 1.7	47.8 ± 3.0	-46.8 ± 1.3	9.0 ± 2.2	2.7	-4.99	-0.15	—	5927	9.0	9.0	9.1
59230	12 08 54.12	-03 54 02.17	-7.2 ± 1.7	-20.8 ± 2.1	-21.4 ± 2.8	-18.9 ± 2.0	3.2	-5.03	0.07	0.051	5895	6.3	4.9	6.3
59341	12 10 22.15	-43 52 15.29	31.9 ± 1.7	-37.6 ± 6.7	-54.6 ± 3.9	0.6 ± 1.4	4.9	-5.03	-0.43	0.057	5672	8.1	6.6	9.6
59380	12 10 57.93	-46 19 19.14	13.4 ± 1.7	11.4 ± 0.7	0.9 ± 1.5	34.5 ± 1.1	2.6	-4.86	-0.52	—	5904	13.6	13.5	15.1
59417	12 11 17.86	-05 55 33.88	-7.5 ± 1.7	-45.3 ± 2.2	-43.2 ± 2.5	-29.7 ± 1.8	2.9	-4.97	-0.02	—	5786	5.7	4.8	6.0
59419	12 11 19.15	-44 51 40.77	-5.4 ± 1.6	-44.7 ± 2.4	-19.1 ± 1.9	-11.7 ± 0.7	2.1	-4.76	0.02	—	5162	9.4	8.6	10.3
59639	12 13 51.85	-69 03 37.63	72.8 ± 1.6	6.8 ± 1.1	-80.9 ± 1.5	4.0 ± 0.3	2.8	-4.91	-0.08	—	5011	12.1	11.4	13.1
59968	12 17 56.87	-35 49 54.17	39.2 ± 1.7	57.7 ± 3.1	-23.1 ± 1.5	-3.4 ± 1.7	2.8	-5.19	-0.25	—	5455	11.8	10.1	13.1
60096	12 19 27.34	-26 06 26.52	32.9 ± 1.7	47.1 ± 3.3	-30.7 ± 1.4	-8.6 ± 2.7	2.7	-5.15	-0.22	—	5581	9.7	8.1	11.1
60391	12 22 59.15	-50 00 45.17	-1.5 ± 1.7	-43.1 ± 9.4	-20.6 ± 14.6	3.0 ± 3.6	2.6	—	1.5	—	5651	16.1	15.7	16.1
60457	12 23 39.64	-20 05 17.16	53.3 ± 1.7	41.5 ± 1.8	-37.4 ± 1.1	23.1 ± 1.4	3.1	-5.18	-0.11	—	4944	9.6	9.4	10.1
60462	12 23 42.60	-30 46 33.74	55.9 ± 1.6	-36.3 ± 3.6	-51.4 ± 1.4	57.2 ± 1.9	2.3	-4.98	-0.48	—	5037	12.3	12.1	12.4
60653	12 25 54.20	-17 14 54.57	34.2 ± 1.6	-29.9 ± 2.8	-66.5 ± 3.2	0.1 ± 2.0	1.7	-5.00	-0.32	—	5696	13.6	12.9	14.0
60658	12 25 56.38	-45 25 46.37	17.8 ± 1.6	35.7 ± 3.3	-5.8 ± 1.7	-11.1 ± 2.0	2.3	-4.77	-0.05	—	5621	10.7	9.1	10.8
60788	12 27 31.38	-71 25 22.71	56.2 ± 1.6	2.6 ± 1.6	-67.7 ± 1.8	16.6 ± 1.3	2.3	-5.08	-0.55	—	5111	15.1	14.4	16.1
60808	12 27 48.47	-50 20 11.75	-27.0 ± 1.6	-57.5 ± 2.1	2.7 ± 1.7	12.0 ± 0.8	2.7	-4.67	-0.02	—	5101	14.7	13.3	16.1
60829	12 28 04.06	-15 39 07.62	20.4 ± 1.6	-32.8 ± 1.7	-60.3 ± 2.3	-10.4 ± 1.6	2.0	-5.02	0.04	—	5608	9.9	8.8	11.2
60930	12 29 19.10	-30 50 26.33	15.2 ± 1.7	69.5 ± 3.3	-12.3 ± 1.2	-40.3 ± 2.6	3.0	-4.82	-0.45	—	5209	12.8	12.2	13.8
61052	12 30 49.36	-34 32 13.14	17.1 ± 1.7	34.1 ± 2.7	-26.3 ± 1.8	-37.1 ± 4.4	2.0	-5.03	-0.02	—	5839	5.0	4.5	5.0
61123	12 31 35.50	-59 12 28.68	31.7 ± 1.7	24.0 ± 1.0	-22.4 ± 1.5	4.5 ± 0.3	2.5	-4.96	-0.3	—	5514	13.2	12.9	13.3
61391	12 34 48.70	-41 14 04.56	-4.2 ± 1.7	-34.8 ± 1.4	-11.8 ± 1.4	5.8 ± 0.6	2.8	-4.57	-0.02	—	4989	3.8	3.8	5.6
61476	12 35 49.14	-20 27 57.11	-6.3 ± 1.7	-39.4 ± 1.3	-21.7 ± 1.4	-10.1 ± 1.1	2.6	-4.78	-0.03	—	5593	5.3	3.5	5.3
61608	12 37 31.64	-03 34 25.96	-2.6 ± 1.7	-11.3 ± 0.8	-42.1 ± 3.0	-22.7 ± 2.0	2.9	-4.97	-0.1	—	5604	10.7	10.1	11.3
61687	12 38 44.26	-05 19 39.63	24.6 ± 1.6	70.9 ± 7.7	5.4 ± 2.2	11.6 ± 1.7	-	-5.04	0.47	—	5817	10.2	8.6	10.2
61698	12 38 49.09	-51 12 56.14	-7.2 ± 1.7	-19.6 ± 1.4	-3.7 ± 1.6	-2.7 ± 0.4	3.9	-4.51	-0.36	0.116	5918	13.4	12.9	13.5
61794	12 39 54.59	-23 33 40.48	25.5 ± 1.7	26.9 ± 1.4	-37.0 ± 1.8	-15.3 ± 2.5	3.3	-5.04	0.03	—	5958	5.1	4.2	5.1
61804	12 40 00.08	-17 41 03.67	-14.7 ± 2.1	-15.0 ± 0.9	0.2 ± 1.4	-13.3 ± 1.5	11.3	-4.29	-0.74	0.104	5519	13.6	13.2	14.3

Continued on next page

Table A.1 – continued from previous page

HIP	α	δ	V_r	U	V	W	$V \sin i$	$\log R'_{HK}$	$[Fe/H]$	EW	T_{eff}	Age	σ_{age}^{low}	σ_{age}^{high}
61907	12 41 12.46	-47 39 37.95	27.5 ± 1.6	8.3 ± 0.9	-39.5 ± 1.7	-35.4 ± 2.6	2.4	-4.97	-0	—	5099	11.2	10.5	11.9
61984	12 42 08.86	-31 49 10.67	-4.2 ± 2.1	-21.1 ± 1.8	-18.1 ± 2.3	-16.2 ± 1.6	12.3	-4.48	-0.2	0.089	5900	9.1	8.9	9.5
61985	12 42 10.02	-21 58 03.33	-18.6 ± 1.6	-44.0 ± 3.2	-19.4 ± 2.9	-22.5 ± 1.4	2.0	-5.01	0.1	—	5415	6.6	5.5	8.1
61999	12 42 20.75	-43 28 46.67	39.1 ± 1.7	-14.1 ± 4.4	-50.1 ± 2.7	16.9 ± 0.8	2.7	-5.05	-0.28	—	5633	12.7	11.3	12.8
62063	12 43 13.15	-27 22 21.50	-5.1 ± 1.6	-23.8 ± 2.3	-24.0 ± 3.0	-20.8 ± 2.0	2.3	-4.99	-0.38	—	5657	15.0	15.0	15.6
62093	12 43 32.05	-31 23 09.17	-8.3 ± 1.7	-65.9 ± 5.8	-39.9 ± 4.4	-16.5 ± 1.4	2.9	-5.04	-0.35	—	5566	14.6	14.6	16.1
62118	12 43 52.28	-32 03 05.01	41.5 ± 1.6	17.4 ± 0.7	-58.1 ± 2.0	-17.4 ± 2.4	1.8	-4.99	-0.41	—	5068	12.4	11.9	13.0
62174	12 44 28.91	-18 30 03.72	3.6 ± 1.8	-29.5 ± 3.2	-32.6 ± 3.3	-8.1 ± 1.7	5.5	-5.05	-0.24	—	6274	5.3	5.0	5.7
62304	12 46 01.17	-09 18 48.29	52.1 ± 1.7	95.4 ± 4.1	-22.4 ± 0.9	14.5 ± 1.9	2.5	-5.02	0.1	—	5732	4.9	4.9	7.0
62371	12 46 59.03	-07 47 59.30	18.3 ± 1.7	-6.8 ± 1.2	-33.8 ± 2.4	4.5 ± 1.7	3.4	-5.07	-0.34	—	5726	5.1	3.9	6.5
62410	12 47 23.07	-39 28 54.49	-18.3 ± 1.7	-34.3 ± 2.7	-19.5 ± 3.7	-42.4 ± 3.7	2.4	-4.95	-0.06	—	5796	9.7	9.0	9.9
62583	12 49 25.38	-25 17 47.03	17.3 ± 1.7	-21.2 ± 2.4	-49.5 ± 3.2	-11.2 ± 2.0	4.0	-5.15	-0.5	0.054	5743	7.4	6.1	8.8
62809	12 52 11.64	-56 34 27.99	2.9 ± 1.7	-119.3 ± 5.9	-87.2 ± 4.3	-46.1 ± 2.2	2.5	-4.93	-0.7	—	5674	15.2	13.9	16.1
62841	12 52 40.76	-28 42 32.86	-1.7 ± 1.7	6.8 ± 0.9	-8.4 ± 1.3	-18.9 ± 1.5	2.8	-5.04	0.09	0.063	6068	3.4	3.2	3.9
62921	12 53 41.95	-13 38 41.76	-17.5 ± 1.7	8.8 ± 1.1	31.4 ± 1.6	-4.8 ± 1.3	2.1	-4.89	-0.12	—	5689	7.6	6.9	8.3
63009	12 54 39.85	-48 03 42.58	7.2 ± 1.7	-68.6 ± 8.2	-57.2 ± 5.9	-8.9 ± 1.3	2.5	-5.08	-0.47	—	5533	16.1	13.9	16.1
63366	12 59 01.56	-09 50 02.70	2.9 ± 1.6	-75.7 ± 1.5	-34.0 ± 1.0	16.5 ± 1.3	2.3	-5.00	-0.52	—	5156	13.2	12.6	14.0
63419	12 59 45.50	-04 25 49.00	-10.3 ± 1.7	1.4 ± 0.5	2.1 ± 0.7	-11.6 ± 1.4	3.9	-4.46	-0.1	—	5263	10.5	9.3	11.6
63426	12 59 51.92	-42 33 40.71	32.1 ± 1.7	-6.7 ± 2.5	-54.1 ± 3.2	-17.5 ± 2.9	2.9	-5.00	0.06	—	5711	5.2	2.9	5.2
63742	13 03 49.65	-05 09 42.52	-13.1 ± 1.7	-10.3 ± 0.6	-22.1 ± 1.0	-22.4 ± 1.5	4.8	-4.33	-0.75	0.138	4982	13.4	13.4	15.1
63778	13 04 21.10	-26 41 12.70	12.5 ± 1.7	-17.7 ± 1.9	-37.5 ± 2.3	-5.6 ± 1.3	2.8	-4.95	-0.2	—	5756	8.3	7.8	8.7
63792	13 04 28.48	-34 08 59.61	-3.7 ± 1.9	-17.8 ± 1.5	-5.2 ± 1.5	3.6 ± 1.0	8.4	-4.49	-0.23	0.093	5900	6.5	4.8	6.7
63798	13 04 33.38	-22 49 32.72	7.1 ± 1.7	-16.8 ± 1.7	-5.6 ± 1.0	17.9 ± 1.4	1.5	-4.93	-0.21	—	5990	8.6	8.2	9.0
63851	13 05 10.40	-28 31 03.15	11.6 ± 1.6	-54.3 ± 5.3	-53.4 ± 4.1	5.1 ± 0.9	2.7	-5.11	-0.15	—	5129	3.6	3.0	4.2
63931	13 06 09.20	-08 25 24.76	22.7 ± 1.7	-56.6 ± 7.0	-65.2 ± 5.9	17.3 ± 1.4	2.8	-5.03	-0.44	—	5657	15.2	12.6	15.6
63964	13 06 29.12	-10 27 42.45	22.6 ± 1.7	-51.2 ± 9.2	-43.0 ± 5.0	27.7 ± 2.0	2.8	-4.97	-0.04	—	5736	7.9	7.0	8.8
64005	13 06 56.27	-56 44 38.96	34.3 ± 1.7	29.6 ± 1.4	-23.3 ± 1.4	-15.0 ± 1.8	2.9	-4.97	0.01	0.042	5788	8.5	8.4	8.5
64011	13 06 59.11	-37 44 40.15	$- \pm -$	$- \pm -$	$- \pm -$	$- \pm -$	-	-4.35	-0.4	0.116	5883	14.2	13.4	14.5
64058	13 07 40.48	-50 21 03.64	25.2 ± 1.6	-24.1 ± 2.4	-50.2 ± 2.2	-4.0 ± 0.6	2.5	-5.04	0.05	—	5435	2.8	2.6	5.5
64079	13 07 53.73	-19 50 52.44	1.0 ± 1.6	-54.7 ± 4.6	-46.6 ± 3.9	-1.4 ± 1.1	2.0	-4.87	-0.25	—	5601	13.4	13.4	13.4
64214	13 09 40.24	-45 50 59.52	-16.2 ± 1.8	-15.2 ± 1.1	8.0 ± 1.4	-4.9 ± 0.5	5.8	-4.63	-0.23	0.062	6087	6.1	4.7	6.5
64259	13 10 13.46	-44 35 23.49	20.6 ± 1.6	-56.7 ± 7.5	-61.4 ± 5.1	18.5 ± 1.4	2.7	-5.15	0.03	—	5275	14.8	13.1	16.1
64497	13 13 13.04	-08 55 54.21	-13.3 ± 1.8	-40.5 ± 3.0	-18.6 ± 2.2	-6.7 ± 1.5	5.8	-4.45	0.1	0.083	5790	7.5	6.2	9.1
64535	13 13 40.36	-04 22 37.77	12.9 ± 1.7	12.8 ± 1.1	-16.6 ± 1.5	2.1 ± 1.7	2.4	-5.10	-0.07	—	5683	10.5	9.1	11.5
64573	13 14 09.47	-16 33 31.42	42.7 ± 1.7	54.8 ± 3.5	-24.5 ± 0.9	6.9 ± 2.6	3.6	-4.69	-0.35	—	5293	14.9	14.9	16.1
64656	13 15 13.38	-19 12 17.77	21.7 ± 1.7	19.8 ± 1.3	-35.5 ± 2.6	-10.7 ± 2.9	3.1	-5.14	0.1	—	5771	6.3	5.3	7.2
64966	13 18 57.16	-25 15 20.92	17.2 ± 1.6	-28.9 ± 4.0	-76.9 ± 6.9	-23.3 ± 3.6	2.1	-5.10	-0.5	0.082	5708	15.1	14.2	15.1
64993	13 19 17.65	-15 34 02.75	-5.8 ± 1.7	8.1 ± 1.2	0.1 ± 0.9	-13.1 ± 1.4	2.2	-4.59	0.06	0.054	5767	3.1	2.6	4.4
65126	13 20 47.21	-52 15 20.47	-19.6 ± 1.7	-16.0 ± 1.1	11.8 ± 1.4	-4.1 ± 0.4	5.0	-4.70	-0.05	0.068	6123	7.6	6.1	7.6
65232	13 22 05.59	-09 03 35.62	33.5 ± 1.7	-31.5 ± 4.1	-71.9 ± 5.1	21.0 ± 1.4	2.1	-4.89	-0.08	—	5793	5.1	4.5	5.8
65346	13 23 33.66	-37 33 52.58	8.6 ± 1.6	6.0 ± 1.0	-17.3 ± 1.4	-16.5 ± 1.7	1.8	-4.59	0.06	—	5559	3.1	2.1	4.6
65377	13 23 54.24	-46 12 00.49	$- \pm -$	$- \pm -$	$- \pm -$	$- \pm -$	-	-5.03	-0.83	—	6291	13.4	12.6	15.1
65390	13 24 03.74	-45 14 14.28	9.1 ± 1.7	-13.5 ± 1.8	-23.6 ± 1.9	-1.0 ± 0.6	3.3	-4.40	0.02	0.098	5686	1.1	0.7	2.5
65403	13 24 18.17	-37 17 01.35	-35.8 ± 2.0	-33.3 ± 1.8	13.3 ± 1.8	-16.8 ± 0.9	10.0	—	-0.75	—	5505	16.1	16.0	16.1
65548	13 26 13.93	-14 47 34.99	-3.9 ± 1.6	-19.3 ± 2.4	-22.6 ± 3.2	-7.3 ± 1.3	-	—	-0.73	—	5474	16.1	16.1	16.1
65963	13 31 28.68	-08 00 26.42	-7.3 ± 1.7	-36.9 ± 2.0	-48.3 ± 2.9	-11.4 ± 1.4	2.4	-4.97	-0.6	—	5461	13.0	13.0	14.6
66014	13 32 02.31	-22 53 37.78	-10.3 ± 1.7	-36.3 ± 2.3	-25.5 ± 2.4	-6.9 ± 1.0	2.7	-4.84	-0.07	—	5716	0.7	0.7	1.3
66018	13 32 04.70	-11 15 22.98	-53.5 ± 1.6	-23.7 ± 0.8	2.2 ± 1.5	-53.5 ± 1.5	2.1	-4.97	-0.18	—	5460	11.2	10.7	11.8
66108	13 33 06.24	-28 14 33.95	25.3 ± 1.7	-34.3 ± 5.9	-50.3 ± 4.3	27.0 ± 1.8	2.5	-5.08	-0.21	—	5728	11.9	11.2	12.8
66118	13 33 13.66	-28 58 17.25	-10.3 ± 1.7	-26.1 ± 2.0	-12.2 ± 1.9	-4.6 ± 0.9	4.2	—	-0.67	0.053	5537	12.5	12.5	12.7
66123	13 33 18.50	-38 43 50.04	17.4 ± 1.7	52.1 ± 5.0	-13.6 ± 1.2	-59.8 ± 8.0	2.9	-5.05	0.0	—	5648	9.7	8.7	10.3
66418	13 36 58.97	-64 38 15.88	-37.6 ± 1.7	-86.3 ± 5.3	-19.0 ± 4.3	-3.8 ± 0.5	3.0	-5.05	0.12	—	5810	8.6	7.1	8.7
66676	13 40 07.64	-60 33 23.78	0.8 ± 1.7	-3.6 ± 1.1	-3.4 ± 1.3	15.6 ± 1.0	4.0	-4.77	0.08	0.041	5903	2.8	0.6	2.8
66813	13 41 42.35	-40 36 34.47	36.0 ± 1.7	2.5 ± 2.3	-44.9 ± 2.4	10.6 ± 0.7	3.0	-4.98	-0.18	0.034	5924	8.6	8.5	8.7
66885	13 42 25.12	-30 39 58.90	0.6 ± 1.6	-5.7 ± 1.1	-56.3 ± 4.8	-57.5 ± 4.9	1.9	—	-0.4	—	5672	14.3	14.2	14.4
66990	13 43 44.55	-51 37 35.68	-15.4 ± 1.7	-58.4 ± 3.5	-35.2 ± 3.4	-20.6 ± 1.2	3.3	-5.12	0.26	—	5595	8.9	8.6	10.2
67031	13 44 12.91	-08 29 17.94	-15.9 ± 1.6	-8.5 ± 0.8	3.5 ± 0.6	-13.1 ± 1.3	2.2	-5.03	-0.89	—	4948	13.3	13.3	15.1
67035	13 44 15.75	-33 12 02.79	-29.7 ± 1.7	-46.4 ± 3.5	-17.4 ± 4.4	-23.8 ± 1.4	2.8	-5.08	-0.11	—	5456	13.3	11.6	14.6
67055	13 44 29.66	-16 51 15.93	-10.6 ± 1.7	-30.6 ± 1.7	-9.2 ± 1.1	3.1 ± 1.3	3.3	-4.56	-0.53	—	5199	14.1	13.8	15.6
67112	13 45 19.82	-10 31 27.85	22.1 ± 1.7	10.3 ± 0.9	-59.6 ± 5.1	-7.5 ± 2.7	3.1	—	-0.65	0.032	5858	15.9	13.1	16.1
67117	13 45 22.59	-10 31 50.31	17.2 ± 1.7	7.5 ± 0.9	-9.2 ± 0.8	12.8 ± 1.3	3.2	-5.12	0.19	—	5555	10.8	9.1	12.1
67282	13 47 21.40	-08 30 09.47	-6.9 ± 1.7	-0.8 ± 0.8	-2.8 ± 0.6	-9.5 ± 1.3	3.0	-4.59	-0.71	—	5210	12.8	12.6	14.1
67348	13 48 13.25	-39 23 39.17	-42.7 ± 1.7	-55.4 ± 3.4	7.0 ± 2.7	-5.1 ± 1.4	3.0	-5.02	0.12	—	5691	2.9	1.6	3.3
67412	13 48 58.19	-01 35 34.64	-13.5 ± 1.7	-21.2 ± 1.1	-18.5 ± 1.2	-10.0 ± 1.4	3.1	-4.64	-0.47	—	5504	13.0	12.9	14.6
67415	13 48 59.77	-31 22 52.26	30.3 ± 1.7	16.6 ± 1.1	-59.5 ± 4.1	-30.7 ± 4.5	3.0	-5.06	-0.62	—	5409	15.6	14.4	15.6
67502	13 49 58.29	-28 11 11.77	-43.4 ± 1.6	-89.4 ± 6.3	-50.1 ± 7.5	-28.1 ± 1.0	2.1	-5.08	-0.43	—	5694	16.1	14.5	16.1
67534	13 50 16.30	-57 15 43.13	23.6 ± 1.7	-71.5 ± 6.5	-101.8 ± 6.3	-79.4 ± 6.0	2.9	-5.08	0.29	—	5588	8.7	8.2	8.7
68688	14 03 37.18	-27 00 35.92	-43.9 ± 1.6	-87.9 ± 4.5	-51.1 ± 5.5	-22.1 ± 0.9	2.7	-5.12	0.33	—	5296	9.6	9.1	10.0
68696	14 03 42.63	-13 17 19.55	10.0 ± 1.7	12.8 ± 1.5	-12.4 ± 1.5	-2.8 ± 1.9	2.7	-4.91	-0.35	0.049	5935	11.1	10.5	12.1
68914	14 06 29.76	-20 04 22.42	-14.6 ± 2.0	-31.6 ± 2.5	-11.2 ± 1.9	1.1 ± 1.7	10.8	-4.46	-0.22	0.109	5829	6.1	4.7	7.6
69129	14 09 01.27	-51 56 16.14	15.7 ± 1.7	-42.5 ± 3.4	-67.7 ± 3.6	-12.6 ± 0.9	2.8	-4.98	-0.69	—	5135	15.2	14.8	15.8
69536	14 14 05.17	+12 57 33.99	-39.8 ± 1.7	-39.0 ± 0.9	-32.5 ± 0.8	-26.0 ± 1.6	4.9	-5.17	0.09	—	6125	3.9	3.8	4.0
69660	14 15 24.69	-37 57 32.97	-4.4 ± 1.7	-40.3 ± 3.9	-54.9 ± 5.8	-20.8 ± 2.0	3.0	-5.02	-0.61	—	5813	13.3	13.2	14.6
69724	14 16 20.16	-04 17 06.71	3.4 ± 1.7	-26.7 ± 2.9	-67.1 ± 6.3	5.3 ± 1.3	2.5	-5.07	0.33	—	5600	6.2	4.8	7.0
69971	14 19 04.95	-26 50 18.53	-2.3 ± 1.9	-13.1 ± 1.9	-24.9 ± 3.3	-9.1 ± 1.4	7.8	-4.92	-0.28	—	5901	9.6	8.2	9.6

Continued on next page

Table A.1 – continued from previous page

HIP	α	δ	V_r	U	V	W	$V \sin i$	$\log R'_{HK}$	$[Fe/H]$	EW	T_{eff}	Age	σ_{age}^{low}	σ_{age}^{high}
70227	14 22 02.64	-44 52 20.12	20.2 ± 1.7	7.4 ± 1.6	-26.1 ± 2.1	-6.3 ± 1.7	1.6	-4.95	-0.06	0.033	5878	7.7	6.5	9.0
70608	14 26 34.70	-18 49 12.20	-19.9 ± 1.7	-40.5 ± 2.1	-18.5 ± 1.8	2.0 ± 1.4	2.8	-4.50	-0.36	—	5284	13.0	13.0	14.6
70627	14 26 50.11	-39 38 49.62	-5.4 ± 1.7	6.1 ± 1.8	11.1 ± 1.4	-10.7 ± 1.2	3.6	-4.53	0.01	0.089	5873	5.0	4.1	6.8
70724	14 27 49.96	-45 57 48.07	9.6 ± 1.6	-20.4 ± 2.4	-43.1 ± 3.0	-9.1 ± 1.0	1.9	-4.95	-0	—	5712	8.6	8.3	8.9
70741	14 27 59.62	-01 46 08.82	-15.1 ± 1.8	-9.5 ± 2.7	-8.3 ± 7.2	-13.5 ± 2.3	6.1	-5.11	-1.05	0.115	5996	2.2	2.2	5.1
71103	14 32 24.57	-37 49 02.47	-30.1 ± 1.7	-44.1 ± 2.2	-14.4 ± 2.7	-13.0 ± 0.7	3.2	-4.65	-0.37	0.070	6020	12.1	11.8	12.1
71262	14 34 26.46	-54 16 37.56	-24.5 ± 1.7	-44.5 ± 3.0	-12.1 ± 3.1	1.1 ± 0.5	2.6	-4.82	0.08	—	5742	3.2	2.3	5.0
71296	14 34 51.26	-38 36 15.04	8.1 ± 1.7	3.6 ± 1.3	-13.1 ± 1.2	-5.4 ± 1.0	2.7	-5.11	0.15	—	5508	13.7	12.1	14.5
71343	14 35 23.46	-67 25 50.75	5.1 ± 1.8	-45.8 ± 4.0	-46.9 ± 3.6	-15.2 ± 1.1	6.8	-4.98	-0.31	—	6178	6.3	5.6	6.3
71423	14 36 20.30	-53 30 56.23	-26.8 ± 1.6	-57.6 ± 3.9	-29.9 ± 4.8	-35.9 ± 3.2	1.9	-4.97	-0.39	—	5668	12.8	12.8	14.6
71481	14 37 04.88	-25 48 09.22	39.5 ± 1.6	30.8 ± 1.2	-28.7 ± 0.7	8.8 ± 0.9	2.4	-4.77	-0.38	—	4875	0.1	0.1	1.0
71640	14 39 12.84	-41 57 01.53	12.0 ± 1.7	-0.2 ± 1.6	-19.1 ± 1.6	4.6 ± 0.6	2.9	-4.70	0.01	0.041	5797	8.3	6.6	8.3
71720	14 40 12.86	-07 30 52.97	31.9 ± 1.6	-13.3 ± 2.4	-8.1 ± 0.4	54.0 ± 2.3	1.9	-4.99	-0.9	—	5148	13.4	13.2	13.5
71818	14 41 28.12	-41 23 52.72	-27.6 ± 1.7	-37.3 ± 2.6	-9.3 ± 3.7	-13.3 ± 1.0	4.7	-4.80	-0.03	0.067	6079	4.6	3.1	5.7
71932	14 42 43.10	-49 14 59.94	-34.5 ± 1.7	-13.0 ± 1.7	35.5 ± 1.6	-14.7 ± 0.8	2.4	-4.97	-0.36	—	5622	12.7	12.5	12.7
72020	14 43 50.95	-06 41 17.69	0.5 ± 1.8	11.8 ± 2.0	-2.3 ± 0.7	-10.6 ± 2.0	6.6	-4.96	-0.76	0.040	5959	13.5	12.1	13.5
72042	14 44 10.54	-55 48 20.40	34.6 ± 1.7	24.2 ± 1.3	-24.7 ± 1.2	2.3 ± 0.4	3.3	-5.05	0.03	0.053	6026	6.1	5.7	6.3
72053	14 44 16.82	-11 37 02.45	-12.8 ± 2.0	-20.2 ± 1.7	-16.3 ± 1.6	-3.4 ± 1.4	10.8	-4.37	-0.24	0.150	5945	10.7	10.4	10.9
72203	14 46 03.06	-68 45 45.89	7.8 ± 1.6	-41.6 ± 3.7	-51.5 ± 3.7	9.2 ± 0.8	1.4	-4.95	-0.23	—	5608	15.1	15.1	15.1
72456	14 48 59.14	-29 33 32.18	-2.2 ± 1.7	-14.8 ± 1.8	-9.4 ± 1.2	12.0 ± 1.5	2.3	-4.99	-0.23	—	5900	9.6	9.2	11.1
72562	14 50 13.22	-21 31 35.69	-23.8 ± 1.7	-16.2 ± 1.3	-38.1 ± 4.7	-43.7 ± 3.2	2.9	-5.05	0.26	—	5640	8.9	8.0	9.0
73061	14 55 50.63	-18 22 02.47	17.8 ± 1.7	31.7 ± 2.2	-1.1 ± 0.7	-11.6 ± 2.4	3.9	-4.98	-0.07	0.044	5258	6.2	4.6	7.6
73132	14 56 45.38	-09 53 09.89	38.3 ± 2.6	11.9 ± 2.5	-4.0 ± 0.6	43.2 ± 2.5	18.2	-4.49	-0.63	—	5712	14.8	14.7	16.1
74267	15 10 41.30	-07 32 40.95	-44.1 ± 1.7	-49.9 ± 2.0	-8.8 ± 1.2	-12.1 ± 2.0	5.3	-5.01	0.09	0.043	5913	5.2	3.7	5.3
74464	15 13 00.26	-03 41 33.90	-26.0 ± 1.7	-30.9 ± 1.7	-38.3 ± 3.8	-7.8 ± 1.5	3.4	-5.18	0.08	—	5542	5.6	4.7	7.0
74544	15 13 54.97	-36 52 46.59	-20.2 ± 1.7	-28.5 ± 1.8	-19.8 ± 3.0	-16.5 ± 1.2	3.5	-4.92	0.03	0.063	5975	0.4	0.4	0.5
74568	15 14 09.52	-17 30 51.95	-30.6 ± 1.7	-50.6 ± 2.5	1.6 ± 0.6	19.0 ± 3.0	2.6	-4.98	-0.51	—	5749	16.1	13.8	16.1
74904	15 18 27.59	-00 47 10.37	27.0 ± 1.6	36.0 ± 1.9	-21.9 ± 2.0	2.4 ± 1.9	2.9	-5.16	-0.25	—	5118	6.2	4.6	6.3
74975	15 19 18.79	+01 45 55.46	53.8 ± 1.7	90.2 ± 1.6	-13.4 ± 0.3	-10.4 ± 1.6	1.7	—	0.31	—	6573	2.5	2.2	2.5
74989	15 19 25.31	-03 49 03.33	18.6 ± 1.6	9.7 ± 1.3	-53.0 ± 3.8	14.6 ± 1.1	2.4	-4.92	-0.02	—	5542	11.1	10.7	11.6
78312	15 59 24.61	-61 06 19.81	-23.0 ± 1.7	-20.2 ± 1.4	16.2 ± 1.1	-26.0 ± 3.4	3.2	-5.08	0.18	0.062	5857	5.2	6.3	7.7
78408	16 00 23.00	-45 27 09.88	-24.4 ± 1.7	-49.1 ± 2.2	-44.9 ± 3.4	0.3 ± 0.3	3.4	-5.20	0.23	0.078	5576	5.4	4.6	6.0
78521	16 01 50.34	-44 26 04.33	-0.7 ± 1.6	-24.4 ± 2.3	-49.5 ± 3.8	3.7 ± 0.4	0.9	-5.11	0.27	—	5505	1.1	1.0	2.3
78998	16 07 34.40	-31 33 08.79	27.2 ± 1.7	25.1 ± 1.6	-20.8 ± 1.7	-5.9 ± 1.6	3.5	-5.09	0.15	0.069	5652	7.9	6.7	8.6
79149	16 09 17.03	-35 29 55.23	-52.5 ± 1.6	-60.3 ± 2.1	-26.8 ± 5.5	-21.3 ± 1.5	2.5	-5.11	0.13	—	5777	6.7	6.7	8.0
79240	16 10 17.45	-47 54 51.44	-1.7 ± 1.6	-30.2 ± 3.8	-57.2 ± 7.2	0.5 ± 0.5	2.6	-5.10	0.25	0.107	5833	6.5	5.2	6.4
79296	16 10 58.69	-14 23 02.44	-58.2 ± 1.6	-42.6 ± 1.6	-0.1 ± 0.3	-45.2 ± 1.7	1.7	—	0.3	—	5554	10.3	8.8	10.4
79672	16 15 37.27	-08 22 09.99	11.4 ± 1.6	27.0 ± 1.4	-14.5 ± 0.2	-22.6 ± 0.8	-	-4.90	0.22	—	6090	2.1	1.6	3.3
79749	16 16 36.19	-10 11 22.77	-36.1 ± 1.7	-29.4 ± 1.5	-22.7 ± 2.3	-19.4 ± 0.9	3.9	-5.00	0.05	—	5592	7.4	5.8	8.6
80064	16 20 30.97	-46 15 46.32	8.3 ± 1.6	-8.3 ± 2.6	-40.0 ± 5.0	-5.3 ± 0.9	1.6	-4.61	-0.01	—	5237	13.3	13.3	14.6
80081	16 20 38.83	-56 02 28.83	-7.3 ± 1.7	-43.8 ± 4.8	-50.9 ± 6.7	-57.0 ± 7.0	2.7	-5.00	-1.04	—	5714	13.5	13.5	15.1
80120	16 21 16.12	-01 52 11.83	23.7 ± 1.7	32.0 ± 2.5	-24.5 ± 4.8	2.5 ± 1.9	2.6	-5.01	-0.79	—	5744	13.9	13.8	15.6
80129	16 21 20.82	-13 06 20.69	-64.3 ± 1.7	-73.2 ± 2.2	4.1 ± 0.7	4.4 ± 3.5	3.2	-5.00	-0.01	0.045	5407	4.6	3.6	6.0
80171	16 21 55.43	-24 59 28.69	-20.2 ± 1.7	-35.7 ± 2.1	-68.5 ± 6.1	14.6 ± 1.8	2.3	-5.04	0.21	—	5764	6.0	5.2	6.1
80217	16 22 31.87	-12 25 43.06	-23.9 ± 1.7	-23.5 ± 1.6	-42.6 ± 6.7	-2.6 ± 1.5	4.7	-5.18	0.19	0.092	5857	10.1	8.6	10.2
80486	16 25 45.15	-33 34 01.63	22.8 ± 1.9	18.7 ± 1.9	-18.2 ± 1.7	3.2 ± 0.6	9.3	-5.26	-0.13	—	5972	4.3	3.6	5.4
80608	16 27 30.85	-10 08 34.38	-18.1 ± 1.7	-17.9 ± 1.5	-18.8 ± 1.4	-1.2 ± 0.9	4.4	-4.52	0.11	0.097	5767	1.0	1.0	1.2
80655	16 28 00.40	-17 50 40.95	-3.8 ± 1.7	-14.2 ± 1.7	-9.8 ± 0.7	25.9 ± 1.9	2.6	-5.13	0.19	—	5689	9.7	8.4	9.7
80680	16 28 17.28	-46 19 03.44	-2.1 ± 1.8	3.1 ± 1.6	12.8 ± 0.9	-2.8 ± 0.3	5.4	-4.98	0.13	0.086	6108	2.6	2.4	3.4
80759	16 29 20.61	-42 02 00.17	-36.3 ± 2.1	-41.4 ± 2.2	-8.4 ± 2.7	-3.7 ± 0.5	11.5	-4.55	-0.18	0.089	6066	0.3	0.3	1.8
80784	16 29 43.24	-18 40 50.84	62.4 ± 1.6	76.3 ± 1.9	-36.2 ± 2.2	-30.1 ± 3.3	2.5	-5.06	-0.32	—	5687	14.8	13.1	15.7
80982	16 32 15.52	-43 49 19.90	-1.1 ± 1.7	-10.2 ± 1.8	-23.3 ± 2.2	3.8 ± 0.5	2.8	-5.04	-0.45	—	5642	13.6	13.5	15.1
81129	16 34 07.27	-10 40 40.46	-62.4 ± 1.6	-75.4 ± 2.2	-54.5 ± 4.4	26.8 ± 4.7	2.7	-5.17	-0.35	—	4970	11.9	10.6	13.6
81179	16 34 52.27	-18 18 14.23	-39.2 ± 1.7	-35.7 ± 1.6	-23.8 ± 2.4	-17.5 ± 0.8	3.8	—	-0.61	0.053	5592	16.1	15.3	16.1
81229	16 35 25.33	-48 41 53.95	-17.8 ± 1.6	-33.3 ± 2.7	-30.3 ± 5.0	-24.3 ± 3.2	3.0	-5.16	0.12	0.069	5771	7.3	5.6	7.3
81240	16 35 32.20	-53 03 55.77	6.8 ± 1.7	13.0 ± 1.7	11.8 ± 1.9	-9.9 ± 1.1	3.0	-5.08	-0.14	0.045	5766	9.8	8.6	11.0
81274	16 35 57.49	-00 24 41.44	-21.1 ± 1.7	-26.9 ± 1.5	0.2 ± 0.6	2.8 ± 1.2	3.0	-4.96	-0.1	0.071	5947	5.3	4.5	5.5
81347	16 36 48.55	-06 17 39.49	-33.8 ± 1.6	-31.2 ± 1.5	-9.2 ± 0.5	-10.9 ± 0.8	2.7	-5.06	0.32	0.051	5632	9.6	8.5	9.9
81369	16 37 04.05	-62 14 25.05	11.7 ± 2.1	-2.2 ± 2.2	-26.3 ± 2.6	5.0 ± 1.0	11.8	-4.93	-0.19	—	6000	7.2	6.0	8.2
81478	16 38 31.09	-57 28 11.31	-29.0 ± 1.9	-18.4 ± 1.7	28.8 ± 1.4	-9.8 ± 0.9	9.8	-4.07	-0.7	—	5126	13.6	12.1	15.1
81533	16 39 12.46	-47 18 36.77	-27.2 ± 1.6	-34.9 ± 1.9	-12.8 ± 2.7	-28.2 ± 3.2	2.7	-4.83	0.07	—	5554	12.0	10.6	12.1
81592	16 39 46.95	-51 59 39.16	-1.6 ± 1.7	0.2 ± 1.5	6.6 ± 0.9	-16.7 ± 1.2	4.5	—	-0.67	0.068	5661	15.7	15.4	16.0
81767	16 42 07.30	-29 07 29.98	13.7 ± 1.7	16.0 ± 1.6	-16.2 ± 1.0	-21.2 ± 1.6	3.4	-5.11	-0.04	0.048	5764	10.7	10.0	10.8
81845	16 43 01.59	-39 30 33.14	12.8 ± 1.6	6.0 ± 1.7	-18.1 ± 1.6	26.8 ± 2.7	2.5	-5.19	-0.36	—	4965	12.0	12.0	13.6
81952	16 44 26.67	-05 41 14.21	-35.4 ± 1.7	-31.1 ± 1.5	-19.2 ± 1.4	-9.9 ± 0.9	3.6	-4.93	-0.09	—	5542	12.9	11.6	14.5
82613	16 53 19.40	-44 18 03.89	-16.1 ± 1.7	-18.8 ± 1.6	-5.3 ± 1.2	11.1 ± 1.1	2.6	-4.76	-0.08	0.062	5929	1.8	0.9	3.0
82632	16 53 29.73	-46 19 58.64	-21.6 ± 1.6	-39.6 ± 2.8	-46.2 ± 6.5	10.2 ± 1.3	2.1	-4.98	0.08	—	5726	12.3	10.6	12.4
83001	16 57 40.18	-45 20 48.71	10.1 ± 1.7	7.9 ± 1.6	-10.5 ± 0.9	30.5 ± 3.0	2.8	-4.91	-0.38	0.039	5698	12.8	12.5	13.2
83177	16 59 59.72	-31 35 36.33	-28.4 ± 1.7	-31.8 ± 1.7	-15.9 ± 2.0	7.0 ± 1.2	2.5	-4.98	0.08	—	5857	4.4	2.4	4.9
83217	17 00 24.75	-87 12 11.19	59.6 ± 1.6	-6.6 ± 2.1	-81.1 ± 2.2	-8.6 ± 1.1	1.7	-5.00	-0.18	—	5254	6.6	5.2	7.6
83373	17 02 22.82	-11 53 36.41	-38.3 ± 1.6	-41.0 ± 1.6	-14.5 ± 0.5	7.7 ± 1.2	2.3	-4.48	-0.18	—	4989	13.5	12.5	14.3
83578	17 04 52.71	-27 22 59.50	-102.6 ± 1.7	-104.6 ± 1.7	-19.0 ± 2.6	-3.3 ± 1.3	2.4	-4.80	-0.2	—	5857	9.2	8.9	9.4
83707	17 06 28.92	-47 50 45.06	49.7 ± 1.6	41.8 ± 1.6	-26.4 ± 1.0	-21.2 ± 1.5	2.2	-4.89	0.11	—	5797	4.4	2.6	4.5
83983	17 10 04.91	-56 26 57.36	-4.3 ± 1.6	-20.0 ± 1.9	-18.7 ± 1.7	-29.1 ± 2.2	3.0	-5.10	0.18	—	5655	8.7	8.6	10.1
85285	17 25 36.62	-21 37 54.45	47.2 ± 1.6	47.9 ± 1.6	-4.2 ± 0.4	1.4 ± 0.4	1.8	-4.94	-0.42	—	5671	12.6	12.0	13.4

Continued on next page

Table A.1 – continued from previous page

HIP	α	δ	V_r	U	V	W	$V \sin i$	$\log R'_{HK}$	$[Fe/H]$	EW	T_{eff}	Age	σ_{age}^{low}	σ_{age}^{high}
85454	17 27 46.43	-46 57 03.74	23.8 ± 1.7	5.8 ± 2.5	-53.3 ± 5.2	-23.4 ± 2.4	3.2	-5.09	-0.12	0.138	5664	5.3	4.1	7.0
85747	17 31 19.75	-39 09 55.10	38.7 ± 1.7	38.7 ± 1.7	-6.9 ± 0.4	12.3 ± 1.1	3.9	-5.03	-0.03	0.058	6105	5.5	4.1	6.3
87083	17 47 39.67	-55 47 26.20	-27.8 ± 1.6	-41.7 ± 1.8	-19.5 ± 2.0	-7.9 ± 1.0	1.3	—	-0.09	—	5263	14.5	13.9	15.2
87664	17 54 24.08	-33 37 07.47	-19.0 ± 1.6	-21.4 ± 1.6	-55.0 ± 4.5	8.2 ± 0.7	2.6	-5.04	-0.09	—	5512	9.8	9.3	10.1
88631	18 05 46.73	-23 31 03.82	54.7 ± 1.6	60.9 ± 1.8	-55.1 ± 7.3	-46.5 ± 5.4	2.9	-5.10	0.28	—	5557	10.5	10.3	10.8
88650	18 05 57.34	-29 55 02.11	15.1 ± 1.6	13.3 ± 1.6	9.8 ± 1.1	-20.5 ± 2.3	2.3	-5.18	0.06	—	5426	13.3	12.9	14.6
88942	18 09 17.67	-22 54 30.38	60.3 ± 1.6	66.6 ± 1.6	-49.2 ± 2.0	-40.9 ± 1.4	1.6	-5.07	0.17	—	5307	13.3	12.3	14.4
88963	18 09 33.29	-10 49 20.47	-37.9 ± 1.7	-33.7 ± 1.6	-18.1 ± 0.6	-5.0 ± 0.3	4.1	-4.46	-0.33	0.112	5315	13.9	13.2	14.5
89321	18 13 33.22	-33 29 56.61	-6.9 ± 1.6	-7.6 ± 1.6	-66.8 ± 5.0	4.0 ± 0.4	2.0	-5.09	0.21	—	5553	9.9	9.4	10.6
90212	18 24 26.56	-29 31 54.77	-46.5 ± 1.7	-46.1 ± 1.7	-41.7 ± 2.1	-12.8 ± 1.1	2.8	—	0.0	0.061	5913	1.6	1.5	2.9
90896	18 32 27.19	-37 05 18.27	12.1 ± 1.6	8.0 ± 1.8	-12.3 ± 2.5	-17.4 ± 3.2	2.3	-5.10	0.04	—	5698	12.0	10.6	13.6
92250	18 48 01.48	-10 08 46.71	56.3 ± 1.6	59.9 ± 1.5	-0.3 ± 1.3	-24.8 ± 1.1	1.7	-4.98	-0.57	—	4817	13.4	12.5	14.2
92304	18 48 47.45	-30 05 48.79	-38.3 ± 2.1	-34.1 ± 2.0	-68.6 ± 8.7	-4.8 ± 1.9	11.5	-4.44	-0.18	—	5571	16.0	13.1	16.0
92639	18 52 32.61	-36 35 03.03	-65.4 ± 1.6	-66.9 ± 1.6	-32.9 ± 3.8	4.6 ± 1.7	2.2	-5.05	-0.33	—	5625	12.9	11.6	13.3
92915	18 55 51.69	-42 07 35.63	-7.3 ± 1.7	-7.1 ± 1.6	4.7 ± 0.3	0.7 ± 0.6	4.8	-4.44	-0.28	0.105	5716	10.1	9.5	10.6
93195	18 58 56.49	-00 30 14.35	29.5 ± 1.6	37.1 ± 1.4	-2.2 ± 1.1	5.2 ± 0.2	0.8	-4.84	-0.1	—	5160	7.7	6.3	8.9
93281	19 00 00.83	-69 56 39.27	4.3 ± 1.7	-33.8 ± 2.6	-50.8 ± 3.1	-7.5 ± 0.8	2.6	-4.42	1.5	0.402	5493	16.1	16.1	16.1
93584	19 03 33.56	-72 23 30.91	$- \pm -$	$- \pm -$	$- \pm -$	$- \pm -$	-	-4.80	1.5	0.608	6050	12.8	12.1	14.1
94061	19 08 56.91	-17 32 08.90	-49.2 ± 1.6	-42.6 ± 1.5	-39.2 ± 1.2	-13.5 ± 1.2	1.8	-5.09	0.19	—	5538	9.9	8.9	11.2
94244	19 11 01.96	-25 48 50.13	-53.8 ± 1.6	-46.3 ± 1.6	-46.7 ± 2.5	4.4 ± 0.8	1.3	-4.74	0.15	—	5216	10.5	9.9	11.0
96635	19 38 51.52	-25 52 19.57	-29.6 ± 1.7	-32.0 ± 1.6	-39.3 ± 1.6	-22.2 ± 1.7	5.3	-4.17	0.28	—	5015	0.1	0.1	0.4
96881	19 41 36.13	-35 43 33.33	-11.0 ± 1.6	-26.5 ± 2.1	-73.8 ± 6.6	-41.5 ± 4.3	1.8	-4.98	0.12	—	5681	9.7	9.5	9.9
97125	19 44 23.73	-26 56 57.18	14.0 ± 1.6	9.8 ± 1.5	-46.2 ± 6.1	-38.4 ± 4.2	2.4	-5.13	0.35	—	5562	10.9	10.2	11.4
97213	19 45 26.56	-50 52 04.81	-30.7 ± 1.6	-40.2 ± 2.0	-82.5 ± 9.2	24.7 ± 1.3	1.8	-5.08	0.18	—	5668	8.6	8.0	8.7
97676	19 51 01.53	-02 51 39.51	-6.6 ± 1.6	-14.1 ± 1.4	-12.5 ± 1.1	-45.8 ± 3.3	2.2	-5.03	-0.12	—	5455	12.9	12.1	13.5
97704	19 51 22.29	-01 32 04.40	-27.7 ± 1.6	-36.4 ± 3.0	11.1 ± 5.0	28.2 ± 3.9	0.8	-5.02	-0.56	—	5358	2.7	0.4	2.7
98049	19 55 29.78	-29 05 49.18	33.4 ± 1.7	38.3 ± 1.6	-1.7 ± 0.6	0.0 ± 1.2	2.8	-4.67	0.05	—	5760	5.7	5.5	7.2
98274	19 58 04.32	-48 08 01.07	-21.2 ± 1.7	-22.7 ± 1.5	8.6 ± 0.5	1.5 ± 1.1	4.2	-4.46	-0.33	0.073	5626	11.5	11.2	11.9
98373	19 59 09.92	-41 49 58.42	-10.3 ± 1.6	-22.2 ± 2.9	-60.5 ± 11.5	-14.6 ± 3.9	-	—	-0.75	—	5964	2.4	1.7	3.5
98599	20 01 38.18	-22 06 39.12	-15.3 ± 1.9	-9.0 ± 1.6	-18.8 ± 1.1	4.3 ± 0.8	8.0	-5.09	0.12	0.113	6210	2.8	2.1	3.2
99034	20 06 23.89	-14 54 43.68	-15.9 ± 1.6	1.7 ± 1.6	-37.7 ± 2.0	3.3 ± 0.7	1.5	-5.04	-0.01	—	5763	8.7	7.6	8.7
99115	20 07 19.66	-35 32 19.07	-40.7 ± 1.6	-32.7 ± 1.4	-56.8 ± 3.1	15.3 ± 0.9	2.4	-5.15	0.31	—	5626	8.6	7.7	9.8
99174	20 08 03.19	-67 44 49.37	18.8 ± 1.6	11.2 ± 1.2	-10.6 ± 0.8	-11.1 ± 0.9	3.0	-4.69	-0.05	—	5644	12.3	10.6	13.6
99661	20 13 26.74	-46 12 03.70	-30.4 ± 1.6	-29.1 ± 1.4	-21.9 ± 2.1	15.0 ± 1.0	2.9	-5.12	0.19	0.069	5816	6.3	5.5	6.7
99971	20 16 55.65	-10 58 56.39	59.8 ± 1.6	85.2 ± 2.5	-31.1 ± 3.4	-23.4 ± 0.7	0.8	-4.98	-0.22	—	5494	13.7	12.9	14.6
100359	20 21 13.23	-81 36 57.32	12.5 ± 1.6	-48.1 ± 3.3	-46.8 ± 2.4	-20.4 ± 1.1	1.1	-5.13	0.09	—	5851	5.8	5.8	6.3
100474	20 22 31.34	-26 09 35.60	-1.6 ± 1.6	-9.4 ± 1.5	-8.4 ± 0.9	-16.1 ± 1.8	2.3	-4.86	0.13	—	5558	9.9	9.9	10.0
100492	20 22 41.87	-10 18 06.70	-49.7 ± 1.6	-54.3 ± 1.5	-29.7 ± 0.8	-14.5 ± 2.1	2.0	-4.79	-0.31	—	5002	13.5	12.6	14.2
100649	20 24 30.53	-34 42 58.70	10.3 ± 1.6	19.1 ± 1.8	-66.8 ± 7.1	-3.1 ± 1.0	2.8	-5.10	0.19	—	5661	6.9	5.7	8.1
100942	20 27 59.75	-51 39 51.96	-10.4 ± 1.7	24.0 ± 3.8	-6.4 ± 1.0	52.5 ± 5.2	2.5	-5.01	-0.04	—	5854	9.8	8.1	9.8
101399	20 33 00.34	-62 29 46.90	-13.2 ± 1.6	-27.6 ± 2.0	-43.2 ± 4.4	14.9 ± 1.2	1.9	-5.02	0.17	—	5668	8.5	7.1	8.7
102418	20 45 14.01	-30 57 20.32	10.7 ± 1.7	-6.0 ± 1.9	-16.0 ± 1.7	-30.7 ± 2.6	2.6	-4.97	0.11	0.070	6102	0.4	0.4	1.0
103883	21 02 58.28	-32 35 16.95	-25.6 ± 1.7	-32.9 ± 2.1	-10.5 ± 0.9	-0.6 ± 2.4	3.9	—	-0.8	0.087	6185	8.6	7.1	10.1
103898	21 03 06.63	-52 46 05.56	48.9 ± 1.6	57.0 ± 2.4	-35.3 ± 2.5	-0.6 ± 3.3	2.7	-5.23	-0.15	—	5001	5.3	5.3	6.6
103917	21 03 18.14	-69 10 16.46	-10.7 ± 1.7	-26.2 ± 1.9	-14.6 ± 1.7	0.4 ± 1.1	4.9	-5.04	-0.21	—	6085	6.5	5.6	6.6
103941	21 03 36.57	-39 41 16.52	-21.4 ± 1.6	-34.1 ± 2.4	-38.6 ± 4.4	-8.0 ± 2.8	-	—	-0.74	—	5707	13.2	13.2	14.6
103962	21 03 51.65	-73 45 10.31	-63.8 ± 1.7	-105.3 ± 6.1	-11.7 ± 4.3	7.7 ± 2.8	2.6	-5.03	-0.04	—	5711	10.2	9.7	10.2
103978	21 04 02.92	-70 25 43.04	55.7 ± 1.7	43.6 ± 1.2	-37.2 ± 1.1	-16.3 ± 1.6	3.0	-4.99	-0.25	0.044	6009	3.1	3.0	4.5
103986	21 04 07.11	-42 58 02.13	7.2 ± 1.7	19.7 ± 2.2	-13.4 ± 1.7	11.5 ± 2.4	3.7	-4.98	-0.37	0.053	6158	6.5	6.4	7.6
104024	21 04 31.23	-44 27 42.45	-7.9 ± 1.7	-22.4 ± 2.5	-17.9 ± 2.3	-11.8 ± 2.5	3.3	-4.59	-0.29	—	5498	14.3	14.3	15.5
104065	21 05 00.33	-66 15 14.05	60.3 ± 1.7	53.3 ± 1.7	-30.3 ± 0.9	-19.5 ± 2.1	2.6	-5.02	0.09	—	5878	4.5	2.4	5.0
104083	21 05 13.30	-66 57 28.31	11.3 ± 1.7	-19.4 ± 3.4	-34.3 ± 3.6	-15.6 ± 1.5	2.8	-5.22	0.29	0.090	6074	2.5	1.2	2.5
104199	21 06 39.12	-46 16 40.94	-77.3 ± 1.7	-66.5 ± 1.6	-84.1 ± 9.5	52.2 ± 1.1	2.5	-5.00	-0.42	—	5766	13.1	12.7	14.6
104200	21 06 39.82	-26 54 25.67	-32.1 ± 1.6	-60.4 ± 5.0	11.0 ± 2.5	-12.9 ± 4.5	1.5	-4.94	0.12	—	5872	4.4	1.7	4.4
104226	21 06 57.17	-28 26 55.55	18.5 ± 1.6	-13.1 ± 3.2	7.8 ± 0.6	-40.1 ± 3.3	2.2	-5.09	0.16	—	5401	12.9	12.8	14.6
104246	21 07 14.11	-38 54 14.67	-21.2 ± 1.7	-9.7 ± 1.4	0.8 ± 0.3	20.9 ± 1.4	3.7	-5.07	-0.15	0.051	5989	6.1	5.5	7.1
104435	21 09 19.18	-03 53 32.79	7.1 ± 1.7	6.4 ± 4.7	11.7 ± 5.0	7.0 ± 4.4	4.3	-4.50	-0.69	—	5858	11.3	10.0	12.6
104445	21 09 27.25	-60 31 29.14	-12.2 ± 1.7	-28.3 ± 2.5	-10.1 ± 1.6	-6.3 ± 1.9	3.2	-4.93	0.07	0.050	5913	7.8	6.2	7.8
104470	21 09 45.25	-53 02 06.49	2.2 ± 1.6	2.7 ± 1.3	-46.1 ± 6.7	13.1 ± 2.5	2.2	-4.98	0.24	—	5750	3.3	1.0	3.3
104768	21 13 27.69	-49 47 40.58	17.9 ± 1.6	23.6 ± 1.6	6.6 ± 0.9	-2.7 ± 1.4	2.9	-5.10	-0.06	—	5597	8.2	6.6	9.6
104946	21 15 30.42	-05 27 53.11	-28.8 ± 1.7	-38.3 ± 2.1	-21.8 ± 1.1	-10.9 ± 2.5	2.8	-5.05	0.05	0.057	6003	7.5	7.2	7.8
105007	21 16 03.67	-58 30 31.51	38.2 ± 1.6	40.2 ± 2.0	-45.0 ± 3.9	3.8 ± 3.5	2.6	-5.14	0.08	—	5509	12.7	11.8	13.2
105066	21 17 02.13	-01 04 38.73	-23.0 ± 1.6	-32.7 ± 1.4	-19.1 ± 1.1	-13.1 ± 1.7	2.6	-4.51	0.23	—	5585	6.9	5.1	7.4
105109	21 17 28.67	-47 01 59.80	-6.4 ± 1.8	-9.1 ± 1.4	-44.8 ± 4.9	5.9 ± 1.3	5.9	-5.00	-0.21	—	6133	6.3	6.0	6.5
105177	21 18 24.20	-72 08 45.80	-11.9 ± 1.7	-25.3 ± 1.7	-3.4 ± 1.1	-3.4 ± 1.3	3.0	-4.95	-0.39	0.055	6017	6.2	5.1	7.5
105198	21 18 34.05	-39 15 15.35	-28.7 ± 1.7	-31.2 ± 1.5	-49.8 ± 4.1	6.3 ± 1.7	2.1	-4.96	-0.24	—	6081	6.0	4.6	6.3
105408	21 21 02.31	-46 51 09.50	-16.8 ± 1.7	-29.9 ± 2.0	-12.7 ± 1.3	-4.5 ± 1.9	4.4	-4.66	0.01	0.071	5959	1.7	0.6	2.0
105483	21 21 53.68	-04 10 27.46	-24.2 ± 1.6	-32.2 ± 1.2	-34.6 ± 1.3	-25.2 ± 1.9	2.6	-5.01	0.16	—	5514	11.3	9.9	11.3
105742	21 25 02.56	-67 37 24.23	14.4 ± 1.7	12.2 ± 1.1	-19.9 ± 1.5	3.2 ± 1.6	2.3	-4.99	0.11	0.051	6018	4.1	3.7	4.6
105789	21 25 28.67	-23 34 53.56	41.7 ± 1.7	76.3 ± 4.4	-44.0 ± 5.0	-7.9 ± 2.2	3.7	-5.00	-1.11	0.042	6057	16.1	15.4	16.1
105845	21 26 17.25	-27 10 11.57	-46.0 ± 1.7	-22.6 ± 1.5	-43.4 ± 3.5	28.6 ± 1.3	2.5	-5.04	-0.02	0.038	5901	2.3	0.7	3.0
105899	21 26 51.69	-02 44 10.84	-10.6 ± 1.7	-42.0 ± 4.4	-21.4 ± 2.0	-42.6 ± 5.8	2.4	-4.95	-0.23	—	5886	6.4	5.1	6.4
106100	21 29 31.88	-49 30 27.37	32.5 ± 1.6	25.0 ± 1.2	-29.5 ± 2.5	-15.8 ± 1.4	0.9	-4.75	-0.02	—	5555	4.3	2.0	4.3
106102	21 29 33.07	-27 08 02.19	6.7 ± 1.6	-24.3 ± 2.3	42.8 ± 3.0	-16.9 ± 1.4	0.7	-4.86	-0.53	—	5605	11.3	11.0	11.6
106288	21 31 39.78	-45 54 03.00	8.8 ± 1.6	-69.4 ± 6.4	-0.4 ± 0.2	-77.4 ± 6.1	1.8	-4.97	-0.27	—	5625	11.7	11.7	11.8

Continued on next page

Table A.1 – continued from previous page

HIP	α	δ	V_r	U	V	W	$V \sin i$	$\log R'_{HK}$	$[Fe/H]$	EW	T_{eff}	Age	σ_{age}^{low}	σ_{age}^{high}
106336	21 32 11.50	-40 11 53.30	11.6 ± 1.6	15.1 ± 5.9	-54.4 ± 3.8	-3.5 ± 6.4	2.4	—	-0.94	—	5671	15.9	15.8	16.1
106353	21 32 23.51	-20 57 26.71	32.1 ± 1.6	50.4 ± 1.4	-1.5 ± 0.7	-1.8 ± 1.3	2.2	-4.93	-0.18	—	5070	9.1	7.8	10.6
106369	21 32 37.84	-34 20 37.59	-25.9 ± 1.7	-50.1 ± 2.7	-17.7 ± 1.1	-13.3 ± 2.7	4.0	-4.97	0.07	0.060	5958	3.5	2.4	3.5
106577	21 35 05.93	-54 35 03.69	-20.4 ± 1.7	-33.2 ± 2.1	-9.0 ± 1.3	0.4 ± 1.8	2.9	-4.75	-0.04	0.049	5836	7.6	7.5	7.8
106700	21 36 44.23	-54 14 09.19	-44.7 ± 1.6	-55.1 ± 2.4	-31.5 ± 3.5	21.0 ± 1.5	1.5	-5.00	-0.01	—	5670	6.6	5.5	6.8
106825	21 38 08.42	-02 18 11.34	6.8 ± 1.6	86.2 ± 3.8	-27.4 ± 1.7	28.4 ± 1.7	1.0	-5.00	-0.01	—	5160	12.9	11.6	14.1
106868	21 38 40.70	-18 41 31.50	7.0 ± 1.6	29.3 ± 1.8	-52.1 ± 3.3	-13.9 ± 1.3	0.9	-4.96	-0.66	—	5633	13.9	13.3	14.5
106997	21 40 10.65	-24 41 34.17	8.4 ± 1.7	11.2 ± 1.2	15.7 ± 1.4	4.0 ± 1.6	3.0	-5.00	0.01	0.055	5962	7.6	6.1	7.6
107001	21 40 11.84	-09 47 40.95	-6.9 ± 1.7	0.1 ± 0.9	-40.9 ± 2.4	-21.5 ± 1.9	3.4	-5.09	0.18	0.064	6066	3.3	3.0	3.7
107020	21 40 27.75	-02 01 03.28	-38.8 ± 1.6	-40.0 ± 1.3	-44.6 ± 1.4	-13.4 ± 2.0	0.3	-4.87	-0.18	—	5618	3.6	2.5	3.6
107239	21 43 14.94	-84 08 36.92	-0.0 ± 1.6	-9.0 ± 1.0	-24.2 ± 1.7	22.6 ± 1.5	2.5	-4.91	-0.14	—	5705	8.6	7.8	9.4
107350	21 44 31.32	+14 46 18.98	-17.1 ± 2.2	-14.6 ± 0.7	-21.5 ± 1.8	-10.8 ± 1.1	13.0	-4.42	-0.27	0.107	5938	9.9	9.5	10.3
107370	21 44 50.08	-32 41 39.92	-29.9 ± 1.6	-36.1 ± 1.8	-19.8 ± 1.3	5.4 ± 1.9	2.2	-4.94	0.24	—	5788	4.5	3.8	6.5
107397	21 45 11.96	-50 26 47.66	28.0 ± 1.7	27.7 ± 1.3	-26.4 ± 1.6	-7.7 ± 1.5	2.7	-5.04	0.26	0.048	5909	5.0	4.5	5.0
107453	21 45 50.00	-41 13 47.25	-10.8 ± 1.6	-30.4 ± 7.3	-31.8 ± 9.8	-11.7 ± 6.3	2.7	-5.17	0.07	0.070	5616	2.0	1.2	3.4
107817	21 50 32.95	-27 20 12.43	46.3 ± 1.7	80.1 ± 4.7	-15.6 ± 2.3	-2.9 ± 3.1	2.3	-4.99	-0.23	0.048	6014	6.6	6.5	6.6
107922	21 51 53.74	-65 03 28.90	31.9 ± 1.7	30.9 ± 1.6	-2.6 ± 1.3	-17.5 ± 1.3	4.3	-5.07	0.03	0.056	6125	4.6	3.4	5.7
107975	21 52 29.91	+28 47 36.73	18.4 ± 1.8	13.5 ± 0.3	15.3 ± 1.7	-7.1 ± 0.6	5.6	-5.03	-0.82	—	6286	6.8	6.6	7.0
107985	21 52 36.28	-26 01 35.61	-17.0 ± 1.6	-27.0 ± 1.5	-44.3 ± 2.6	-13.4 ± 2.1	2.4	-4.75	0.11	—	5689	0.1	0.1	1.2
108256	21 55 53.78	-70 32 12.39	-35.3 ± 1.7	-42.8 ± 1.6	8.5 ± 0.9	9.1 ± 1.3	3.1	-4.75	-0.61	0.036	5587	13.1	13.1	14.6
108290	21 56 21.08	-36 48 49.88	20.8 ± 1.8	21.5 ± 1.3	-22.8 ± 1.6	-11.9 ± 1.5	6.4	-5.04	-0.01	0.045	6133	4.3	3.9	4.6
108438	21 58 01.09	-05 12 15.06	-18.4 ± 1.6	-19.7 ± 1.0	-39.5 ± 2.0	-19.2 ± 2.2	2.6	-4.68	0.07	0.074	5851	6.7	5.4	7.3
108708	22 01 14.71	-19 18 45.82	-21.4 ± 1.7	-35.4 ± 2.1	-16.9 ± 0.9	-4.2 ± 2.1	3.2	-4.44	0.38	0.065	5790	1.8	1.1	1.8
108754	22 01 49.17	-03 35 51.63	-38.7 ± 1.9	-45.8 ± 3.7	-16.8 ± 1.4	14.0 ± 2.0	8.8	-5.10	-0.4	—	6068	7.8	7.7	9.2
108985	22 04 44.28	-25 07 13.29	23.5 ± 1.7	36.5 ± 2.4	-20.7 ± 2.5	-11.6 ± 1.5	2.7	-5.03	-0.05	0.043	5945	4.9	4.8	6.4
108996	22 04 49.72	-23 43 46.41	11.8 ± 1.7	15.0 ± 1.1	7.1 ± 0.6	-2.1 ± 1.5	3.7	-4.54	0.02	0.045	5760	2.0	1.9	2.9
109058	22 05 35.17	-09 53 50.31	0.8 ± 1.6	-13.5 ± 1.1	-7.2 ± 0.9	-14.3 ± 1.5	1.3	-4.57	0.01	—	5376	2.9	2.7	5.4
109133	22 06 22.43	-23 06 02.00	-53.7 ± 1.6	-83.4 ± 6.2	-18.7 ± 0.6	5.1 ± 4.4	1.6	-5.08	0.16	—	5794	5.6	4.5	6.4
109491	22 10 51.32	-63 05 57.95	39.4 ± 1.7	-15.8 ± 2.9	-26.2 ± 1.0	-54.4 ± 2.2	3.4	-5.11	-0.14	—	5726	4.1	3.7	4.9
109782	22 14 12.34	-44 42 49.65	29.0 ± 1.7	19.6 ± 1.0	-31.0 ± 2.1	-19.0 ± 1.4	2.6	-4.92	0.05	—	5701	3.1	2.0	4.4
110248	22 19 54.40	-76 29 41.66	2.7 ± 1.7	-30.5 ± 1.9	-17.6 ± 1.3	-15.2 ± 1.3	5.3	-4.64	0.05	0.057	6007	4.3	3.7	5.0
110262	22 20 04.17	-33 41 15.96	9.4 ± 2.2	4.3 ± 1.2	-1.4 ± 0.4	-8.6 ± 1.9	13.0	-4.66	-0.29	—	6274	6.0	5.2	7.4
110663	22 25 04.26	-13 59 53.91	-7.5 ± 1.7	-27.3 ± 1.3	-17.3 ± 0.9	-13.8 ± 1.6	4.4	-4.43	0.01	—	5377	5.9	3.4	5.9
110785	22 26 37.38	+04 23 37.55	-13.9 ± 1.9	-52.7 ± 3.2	-14.0 ± 1.3	-13.6 ± 2.0	8.4	-5.14	-0.14	—	6148	3.7	3.4	3.9
110939	22 28 40.31	-64 35 13.07	12.3 ± 1.7	28.6 ± 2.1	-19.5 ± 1.4	16.0 ± 2.4	2.9	-4.96	-0.32	0.045	5910	8.8	8.6	9.0
111151	22 31 08.05	-71 14 20.59	19.3 ± 1.8	-19.8 ± 2.4	-37.9 ± 2.2	-16.5 ± 1.2	7.3	-4.94	-0.49	0.040	5967	9.1	9.1	10.5
111286	22 32 40.56	-65 26 09.40	96.0 ± 1.6	83.0 ± 3.0	-119.9 ± 7.8	0.4 ± 6.9	2.2	-5.07	0.21	—	5760	7.1	5.6	7.1
111697	22 37 36.08	-21 47 50.61	-20.4 ± 1.7	-36.8 ± 3.3	-19.8 ± 1.6	-0.9 ± 2.5	3.4	-4.98	-0.05	0.058	5990	5.2	4.4	5.5
112100	22 42 21.96	-06 52 16.06	20.6 ± 1.7	0.2 ± 0.9	14.2 ± 1.0	-16.4 ± 1.4	3.6	-4.75	0.12	—	5952	4.0	2.4	5.0
112199	22 43 26.18	-08 25 07.03	9.0 ± 1.8	26.5 ± 2.3	3.3 ± 0.9	0.8 ± 1.7	6.0	-5.02	-0.13	0.069	6258	3.6	3.3	4.8
112688	22 49 12.13	-32 45 02.29	17.1 ± 1.7	-11.9 ± 2.2	11.3 ± 1.0	-23.7 ± 1.7	3.3	-4.98	-0.22	0.051	5964	4.7	4.7	6.0
112826	22 50 54.52	-62 48 52.85	4.4 ± 1.7	8.8 ± 1.0	-0.1 ± 0.7	0.3 ± 1.3	4.2	-5.05	0.12	—	5583	3.7	3.1	4.0
112935	22 52 24.07	+09 50 08.39	11.4 ± 1.7	-58.1 ± 1.2	-6.9 ± 1.3	-33.8 ± 1.3	3.9	-5.06	-0.24	—	6200	4.6	3.2	4.6
113010	22 53 11.77	-37 50 21.01	5.2 ± 1.6	-16.4 ± 2.0	-21.7 ± 2.2	-14.7 ± 1.7	-	-4.98	-0.51	—	4847	14.5	14.3	16.1
113142	22 54 42.29	-46 24 48.25	10.1 ± 1.7	3.3 ± 0.9	7.5 ± 0.9	-10.9 ± 1.5	2.2	-4.95	0.1	—	5927	3.2	2.3	5.0
113231	22 55 49.97	-07 49 21.39	-28.0 ± 1.6	-81.3 ± 3.4	-47.1 ± 1.7	-18.7 ± 2.3	1.2	-4.93	-0.38	—	5576	12.8	11.8	14.1
113670	23 01 21.33	-35 05 45.25	30.7 ± 1.6	-33.5 ± 4.2	-79.2 ± 7.2	-53.9 ± 2.7	1.2	-4.97	-0.43	—	5488	12.7	12.3	13.1
113807	23 02 48.44	-82 42 29.17	-22.5 ± 1.6	-100.2 ± 3.5	-38.8 ± 2.3	-3.2 ± 1.1	2.5	-5.27	-0.15	—	5012	10.5	10.5	12.1
114016	23 05 24.31	-15 25 52.63	-3.2 ± 1.6	24.8 ± 3.2	-14.4 ± 1.8	5.4 ± 1.5	2.7	-5.19	0.01	0.057	5093	7.4	6.1	9.1
114032	23 05 33.24	-54 17 08.44	41.8 ± 1.6	36.8 ± 2.0	-74.4 ± 7.0	-5.2 ± 3.5	1.8	-5.05	-0.16	—	5803	9.9	8.6	10.9
114098	23 06 32.45	-00 11 46.10	-32.2 ± 1.6	32.3 ± 1.8	-9.6 ± 1.0	39.3 ± 1.4	1.5	-4.93	-0.38	—	4962	12.5	11.4	13.5
114188	23 07 27.54	-55 56 52.78	7.6 ± 1.7	-3.1 ± 2.5	-1.0 ± 1.5	-10.7 ± 4.2	3.6	-4.46	1.5	—	6366	13.3	13.1	13.3
114226	23 07 56.23	-70 02 23.15	16.7 ± 1.7	38.2 ± 2.6	-7.7 ± 0.9	9.0 ± 2.1	3.5	-5.08	-0.02	0.045	5832	6.6	6.0	6.8
114244	23 08 15.89	-17 03 33.75	27.0 ± 1.7	44.6 ± 5.7	-23.7 ± 5.1	-25.1 ± 1.5	3.1	-5.09	0.25	—	5660	7.8	6.5	7.8
114328	23 09 16.62	-40 59 28.32	-19.5 ± 1.6	-40.4 ± 2.4	-11.1 ± 0.9	3.3 ± 1.8	1.8	-5.01	0.04	—	5784	9.9	9.3	10.6
114402	23 10 08.00	-74 36 26.97	44.0 ± 1.6	-0.6 ± 2.2	-21.2 ± 1.0	-49.4 ± 2.2	2.0	-4.99	-0.46	—	5689	15.1	14.9	15.6
114422	23 10 22.80	-42 21 54.25	-18.8 ± 1.6	-39.9 ± 3.4	-29.3 ± 3.2	4.5 ± 2.0	2.1	-4.66	0.15	0.045	5822	1.2	1.2	1.9
114477	23 11 01.52	-50 58 06.39	16.2 ± 1.6	24.7 ± 1.6	-74.2 ± 5.7	13.0 ± 2.6	1.5	-5.01	0.04	—	5094	12.8	12.7	13.1
114590	23 12 51.35	-51 41 09.58	4.5 ± 1.7	10.4 ± 1.4	-33.6 ± 4.5	9.2 ± 2.3	3.2	-5.07	0.05	—	5732	9.9	8.6	9.9
114638	23 13 22.33	-60 26 44.45	17.5 ± 1.6	19.7 ± 1.3	-14.0 ± 0.9	-3.6 ± 1.6	1.9	-5.08	0.11	—	5642	12.0	10.6	12.4
114967	23 17 08.14	-45 40 39.21	7.6 ± 1.6	-9.4 ± 1.2	-67.5 ± 5.3	-2.6 ± 1.5	2.2	-5.10	0.08	—	5485	11.0	10.7	11.4
114982	23 17 17.81	-54 56 05.09	21.2 ± 1.9	0.3 ± 1.3	-36.8 ± 3.3	-12.6 ± 1.7	7.5	-4.67	-0.06	0.060	6203	5.0	4.5	5.0
115074	23 18 27.70	-01 53 55.38	-12.8 ± 1.7	-17.2 ± 1.5	-48.6 ± 4.0	-18.6 ± 3.1	4.1	-5.04	0.06	0.056	6154	6.1	4.8	6.1
115151	23 19 29.20	-70 19 23.44	6.3 ± 1.6	-32.8 ± 2.3	-28.4 ± 1.7	-11.0 ± 1.2	1.6	-4.86	-0.1	0.058	5953	8.0	7.1	8.7
115337	23 21 40.88	-41 08 36.46	1.8 ± 1.7	-28.6 ± 2.5	-11.1 ± 0.9	-13.2 ± 1.8	4.2	-5.08	0.17	0.080	5993	4.1	3.5	4.1
115342	23 21 44.44	-10 51 42.84	24.9 ± 1.6	-20.0 ± 3.2	-22.0 ± 4.3	-42.0 ± 3.0	0.9	—	-1.13	—	5711	16.1	15.4	16.1
115381	23 22 23.78	-00 24 53.53	-4.0 ± 1.6	-11.7 ± 0.6	-48.8 ± 2.5	-29.2 ± 2.1	1.3	-5.02	-0.23	—	5118	13.1	13.1	14.6
115386	23 22 25.72	-46 35 33.86	7.0 ± 1.6	-18.1 ± 1.8	-37.8 ± 2.8	-9.5 ± 1.5	1.4	-5.05	0.06	—	5512	3.2	2.3	3.2
115418	23 22 48.50	-53 03 16.88	23.3 ± 1.8	-6.2 ± 2.3	-37.3 ± 4.0	-18.9 ± 1.5	6.0	-4.99	0.01	0.054	6156	4.6	3.5	5.7
115468	23 23 26.85	-08 52 56.71	-38.7 ± 1.7	-81.8 ± 7.5	-44.4 ± 2.8	7.2 ± 3.1	2.6	-4.92	-0.01	0.049	5967	0.4	0.4	1.0
115572	23 24 38.95	-01 44 29.01	-48.4 ± 1.6	-53.7 ± 3.9	-62.0 ± 3.0	12.2 ± 2.6	2.9	-5.12	-0.29	—	5147	4.2	3.8	5.6
115582	23 24 45.21	-40 25 08.77	0.5 ± 1.7	-8.0 ± 1.1	-96.7 ± 10.0	2.4 ± 1.6	2.0	-4.99	-0.21	—	5906	9.0	8.8	9.2
115659	23 25 49.16	-32 15 05.69	-10.1 ± 1.6	-50.2 ± 5.9	2.8 ± 0.6	-6.1 ± 2.5	2.4	—	-0.94	—	5733	15.0	15.0	16.1
115673	23 26 07.62	-15 13 37.11	-23.3 ± 1.6	-23.0 ± 2.0	-57.9 ± 5.4	-0.9 ± 2.8	1.7	-5.05	0.02	—	5559	10.0	9.8	10.2
115861	23 28 26.86	-37 45 25.79	33.7 ± 1.6	-11.5 ± 1.6	-21.5 ± 1.4	-39.7 ± 1.6	1.8	-5.07	0.17	—	5567	8.1	6.6	8.8

Continued on next page

Table A.1 – continued from previous page

HIP	α	δ	V_r	U	V	W	$V \sin i$	$\log R'_{HK}$	$[Fe/H]$	EW	T_{eff}	Age	σ_{age}^{low}	σ_{age}^{high}
115929	23 29 16.38	-51 35 16.83	11.3 ± 1.6	3.2 ± 0.7	8.3 ± 1.0	-13.7 ± 1.5	2.0	-4.91	-0.33	0.036	5563	14.1	14.1	14.2
116122	23 31 44.26	-53 46 11.81	19.9 ± 1.6	-11.2 ± 1.3	-26.8 ± 1.2	-19.9 ± 1.4	2.2	-4.66	0.07	0.042	5740	5.6	5.3	7.1
116258	23 33 23.82	-12 39 52.61	6.1 ± 1.6	-27.4 ± 1.3	-5.9 ± 0.7	-13.5 ± 1.6	3.5	-4.44	-0	—	5037	9.5	8.5	10.8
116298	23 33 50.31	-45 38 56.78	25.6 ± 1.7	-5.9 ± 1.7	-17.8 ± 1.4	-27.5 ± 1.6	3.3	-5.05	0.04	0.052	5846	7.6	6.1	7.7
116376	23 34 54.65	-26 55 18.70	-3.8 ± 1.6	-41.9 ± 3.9	-46.3 ± 4.3	-14.1 ± 2.3	2.4	-4.56	-0.01	—	5545	9.1	9.1	9.2
116517	23 36 44.57	-42 21 44.29	37.7 ± 1.6	10.0 ± 0.8	-27.8 ± 2.8	-33.6 ± 1.5	2.9	-5.10	0.23	—	5602	7.2	5.8	8.6
116519	23 36 45.78	-17 14 12.49	-26.3 ± 1.6	-94.9 ± 6.7	-47.0 ± 2.9	-4.2 ± 2.6	1.9	—	0.24	—	5178	6.6	5.5	8.0
116554	23 37 15.39	-45 28 32.53	-14.3 ± 1.6	-11.1 ± 0.8	-57.3 ± 4.9	21.0 ± 1.6	1.1	-5.01	0.03	—	5296	12.9	12.6	13.1
116559	23 37 17.40	-01 31 11.56	-22.3 ± 1.6	-13.5 ± 1.0	-25.5 ± 1.4	9.9 ± 1.6	1.8	-5.11	0.24	—	5585	12.4	11.8	12.5
116635	23 38 09.95	-25 13 16.10	-2.4 ± 1.8	-46.3 ± 5.9	-36.9 ± 4.7	-15.0 ± 2.8	6.0	-4.51	-0.08	0.076	5948	4.3	3.0	4.8
116691	23 38 50.61	-28 16 04.29	-6.3 ± 2.1	-29.1 ± 3.2	-16.5 ± 1.8	-3.0 ± 2.3	12.0	-4.77	-0.04	—	6279	4.6	4.6	5.8
116756	23 39 44.86	-00 44 26.20	-3.4 ± 1.7	-9.1 ± 1.1	-8.7 ± 1.2	-1.6 ± 1.5	3.5	-4.84	-0.1	0.056	5683	11.3	10.4	11.7
116821	23 40 38.45	-31 54 50.13	-14.2 ± 1.8	-43.0 ± 4.0	-22.6 ± 2.2	1.3 ± 2.1	5.2	-4.99	-0.16	0.049	6198	3.6	2.8	4.9
116951	23 42 22.25	-08 49 43.62	-6.8 ± 1.6	59.8 ± 7.3	-9.6 ± 1.2	8.8 ± 1.5	1.5	-5.03	-0.56	—	5730	8.6	7.1	10.1
117043	23 43 36.24	-03 18 47.16	-1.3 ± 1.7	-14.0 ± 1.5	-18.8 ± 2.0	-9.3 ± 1.8	2.9	-4.71	-0.03	0.054	5981	4.4	4.4	6.5
117144	23 44 54.20	-47 20 41.01	17.6 ± 1.6	46.6 ± 6.5	-24.7 ± 3.4	4.2 ± 3.6	2.5	-5.15	0.09	—	5480	6.8	5.1	7.4
117247	23 46 26.71	-23 01 40.36	9.3 ± 1.6	27.3 ± 1.3	6.2 ± 0.4	-3.2 ± 1.6	1.6	-4.89	-0.24	—	4973	12.2	11.3	13.4
117427	23 48 36.92	-15 12 38.27	-0.2 ± 1.6	-35.2 ± 2.4	-43.9 ± 3.0	-18.0 ± 2.0	2.5	-4.78	0.23	—	5601	4.2	2.9	4.4
117499	23 49 38.30	-67 56 39.05	-0.6 ± 1.6	-67.1 ± 4.2	-54.0 ± 3.4	-2.8 ± 1.2	1.2	-4.94	-0.29	—	5691	12.2	11.4	13.2
117696	23 52 10.24	-11 43 14.52	-13.4 ± 1.9	-15.8 ± 1.7	-27.2 ± 3.6	3.0 ± 7.7	8.2	-4.36	-1.13	0.078	5781	16.1	15.8	16.1
117702	23 52 14.42	-61 25 30.54	-28.1 ± 1.6	-0.0 ± 0.9	-156.1 ± 9.7	113.9 ± 5.4	0.7	-5.06	-0.71	—	5081	13.0	12.5	13.4
117708	23 52 19.98	-18 01 33.39	-17.6 ± 1.7	-22.4 ± 1.7	-21.9 ± 1.5	9.6 ± 1.7	3.1	-5.01	0.08	0.081	6279	2.0	0.6	2.1
117713	23 52 24.37	-09 33 15.46	29.9 ± 1.7	-42.8 ± 4.7	-39.3 ± 5.4	-51.0 ± 2.9	3.9	—	-0.71	—	5698	15.2	13.1	16.1
117905	23 54 54.46	-19 07 49.76	-10.3 ± 1.6	-3.5 ± 0.4	-0.2 ± 0.5	10.1 ± 1.6	2.2	-4.84	-0.29	—	5424	10.0	9.9	10.1
118143	23 57 50.13	-30 26 52.58	8.7 ± 1.6	46.2 ± 3.0	-36.9 ± 2.5	-1.2 ± 1.7	2.1	-4.96	0.12	—	5530	9.0	8.4	9.6
118228	23 58 51.76	-61 35 12.37	-11.3 ± 1.7	-29.1 ± 1.7	-15.0 ± 1.4	7.2 ± 1.4	4.4	-4.98	0.2	0.084	6097	3.2	3.2	3.4

Bibliography

C. Allen and A. Santillan. An improved model of the galactic mass distribution for orbit computations. *Revista Mexicana de Astronomia y Astrofisica*, 22:255–263, October 1991.

T. Antoja, F. Figueras, D. Fernández, and J. Torra. Origin and evolution of moving groups. I. Characterization in the observational kinematic-age-metallicity space. *A&A*, 490:135–150, October 2008. doi: 10.1051/0004-6361:200809519.

R. Asiain, F. Figueras, J. Torra, and B. Chen. Detection of moving groups among early type stars. *A&A*, 341:427–436, January 1999.

W. Benz and M. Mayor. Photoelectric rotational velocities of late-type dwarfs. *A&A*, 138:183–188, September 1984.

J. Binney and M. Merrifield. *Galactic astronomy*. 1998.

D. E. Blackwell and M. J. Shallis. Stellar angular diameters from infrared photometry - Application to Arcturus and other stars; with effective temperatures. *MNRAS*, 180:177–191, July 1977.

A. M. Boesgaard and E. D. Friel. Chemical composition of open clusters. I - Fe/H from high-resolution spectroscopy. *ApJ*, 351:467–479, March 1990. doi: 10.1086/168484.

A. M. Boesgaard and G. Steigman. Big bang nucleosynthesis - Theories and observations. *ARA&A*, 23: 319–378, 1985. doi: 10.1146/annurev.aa.23.090185.001535.

J. Bovy, D. W. Hogg, and S. T. Roweis. The Velocity Distribution of Nearby Stars from Hipparcos Data. I. The Significance of the Moving Groups. *ApJ*, 700:1794–1819, August 2009. doi: 10.1088/0004-637X/700/2/1794.

L. Casagrande, L. Portinari, and C. Flynn. Accurate fundamental parameters for lower main-sequence stars. *MNRAS*, 373:13–44, November 2006. doi: 10.1111/j.1365-2966.2006.10999.x.

P. Cassen, T. Guillot, and A. Quirrenbach, editors. *Extrasolar Planets*, 2006. doi: 10.1007/978-3-540-31470-7.

A. N. Cox. *Allen's astrophysical quantities*. 2000.

G. M. De Silva, C. Sneden, D. B. Paulson, M. Asplund, J. Bland-Hawthorn, M. S. Bessell, and K. C. Freeman. Chemical Homogeneity in the Hyades. *AJ*, 131:455–460, January 2006. doi: 10.1086/497968.

G. M. De Silva, K. C. Freeman, J. Bland-Hawthorn, M. Asplund, and M. S. Bessell. Chemically Tagging the HR 1614 Moving Group. *AJ*, 133:694–704, February 2007. doi: 10.1086/510131.

R. De Simone, X. Wu, and S. Tremaine. The stellar velocity distribution in the solar neighbourhood. *MNRAS*, 350:627–643, May 2004. doi: 10.1111/j.1365-2966.2004.07675.x.

W. Dehnen. The Distribution of Nearby Stars in Velocity Space Inferred from HIPPARCOS Data. *AJ*, 115: 2384–2396, June 1998. doi: 10.1086/300364.

W. Dehnen. The Effect of the Outer Lindblad Resonance of the Galactic Bar on the Local Stellar Velocity Distribution. *AJ*, 119:800–812, February 2000. doi: 10.1086/301226.

W. Dehnen and J. J. Binney. Local stellar kinematics from HIPPARCOS data. *MNRAS*, 298:387–394, August 1998. doi: 10.1046/j.1365-8711.1998.01600.x.

P. Demarque, J.-H. Woo, Y.-C. Kim, and S. K. Yi. Y^2 Isochrones with an Improved Core Overshoot Treatment. *ApJS*, 155:667–674, December 2004. doi: 10.1086/424966.

D. K. Duncan, A. H. Vaughan, O. C. Wilson, G. W. Preston, J. Frazer, H. Lanning, A. Misch, J. Mueller, D. Soyumer, L. Woodard, S. L. Baliunas, R. W. Noyes, L. W. Hartmann, A. Porter, C. Zwaan, F. Middelkoop, R. G. M. Rutten, and D. Mihalas. CA II H and K measurements made at Mount Wilson Observatory, 1966-1983. *ApJS*, 76:383–430, May 1991. doi: 10.1086/191572.

B. Edvardsson, J. Andersen, B. Gustafsson, D. L. Lambert, P. E. Nissen, and J. Tomkin. The Chemical Evolution of the Galactic Disk - Part One - Analysis and Results. *A&A*, 275:101–+, August 1993.

O. J. Eggen. Stellar Groups in the Old Disk Population. *PASP*, 81:553–+, October 1969. doi: 10.1086/128823.

O. J. Eggen. Stellar groups. I. The Hyades and Sirius groups. *MNRAS*, 118:65–+, 1958.

D. A. Fischer and J. Valenti. The Planet-Metallicity Correlation. *ApJ*, 622:1102–1117, April 2005. doi: 10.1086/428383.

G. Gonzalez. The stellar metallicity-giant planet connection. *MNRAS*, 285:403–412, February 1997.

J. I. González Hernández and P. Bonifacio. A new implementation of the infrared flux method using the 2MASS catalogue. *A&A*, 497:497–509, April 2009. doi: 10.1051/0004-6361/200810904.

D. F. Gray. *The Observation and Analysis of Stellar Photospheres*. 2008.

R. O. Gray, C. J. Corbally, R. F. Garrison, M. T. McFadden, E. J. Bubar, C. E. McGahee, A. A. O'Donoghue, and E. R. Knox. Contributions to the Nearby Stars (NStars) Project: Spectroscopy of Stars Earlier than M0 within 40 pc-The Southern Sample. *AJ*, 132:161–170, July 2006a. doi: 10.1086/504637.

R. O. Gray, C. J. Corbally, R. F. Garrison, M. T. McFadden, E. J. Bubar, C. E. McGahee, A. A. O'Donoghue, and E. R. Knox. Contributions to the Nearby Stars (NStars) Project: Spectroscopy of Stars Earlier than M0 within 40 pc-The Southern Sample. *AJ*, 132:161–170, July 2006b. doi: 10.1086/504637.

T. J. Henry, D. R. Soderblom, R. A. Donahue, and S. L. Baliunas. A Survey of Ca II H and K Chromospheric Emission in Southern Solar-Type Stars. *AJ*, 111:439–+, January 1996. doi: 10.1086/117796.

G. Hinshaw, J. L. Weiland, R. S. Hill, N. Odegard, D. Larson, C. L. Bennett, J. Dunkley, B. Gold, M. R. Greason, N. Jarosik, E. Komatsu, M. R. Nolta, L. Page, D. N. Spergel, E. Wollack, M. Halpern, A. Kogut, M. Limon, S. S. Meyer, G. S. Tucker, and E. L. Wright. Five-Year Wilkinson Microwave Anisotropy Probe Observations: Data Processing, Sky Maps, and Basic Results. *ApJS*, 180:225–245, February 2009. doi: 10.1088/0067-0049/180/2/225.

J. Holmberg, B. Nordström, and J. Andersen. The Geneva-Copenhagen survey of the Solar neighbourhood II. New uvby calibrations and rediscussion of stellar ages, the G dwarf problem, age-metallicity diagram, and heating mechanisms of the disk. *A&A*, 475:519–537, November 2007. doi: 10.1051/0004-6361:20077221.

J. Holmberg, B. Nordström, and J. Andersen. The Geneva-Copenhagen survey of the solar neighbourhood. III. Improved distances, ages, and kinematics. *A&A*, 501:941–947, July 2009. doi: 10.1051/0004-6361/200811191.

J. S. Jenkins, H. R. A. Jones, Y. Pavlenko, D. J. Pinfield, J. R. Barnes, and Y. Lyubchik. Metallicities and activities of southern stars. *A&A*, 485:571–584, July 2008. doi: 10.1051/0004-6361:20078611.

D. R. H. Johnson and D. R. Soderblom. Calculating galactic space velocities and their uncertainties, with an application to the Ursa Major group. *AJ*, 93:864–867, April 1987. doi: 10.1086/114370.

P. Kalas, J. R. Graham, E. Chiang, M. P. Fitzgerald, M. Clampin, E. S. Kite, K. Stapelfeldt, C. Marois, and J. Krist. Optical Images of an Exosolar Planet 25 Light-Years from Earth. *Science*, 322:1345–, November 2008. doi: 10.1126/science.1166609.

A. Kaufer, O. Stahl, S. Tubbesing, P. Nørregaard, G. Avila, P. Francois, L. Pasquini, and A. Pizzella. Commissioning FEROS, the new high-resolution spectrograph at La-Silla. *The Messenger*, 95:8–12, 1999.

D. Lafrenière, R. Jayawardhana, and M. H. van Kerkwijk. Direct Imaging and Spectroscopy of a Planetary-Mass Candidate Companion to a Young Solar Analog. *ApJ*, 689:L153–L156, December 2008. doi: 10.1086/595870.

C. Marois, B. Macintosh, T. Barman, B. Zuckerman, I. Song, J. Patience, D. Lafrenière, and R. Doyon. Direct Imaging of Multiple Planets Orbiting the Star HR 8799. *Science*, 322:1348–, November 2008. doi: 10.1126/science.1166585.

M. Mayor and D. Queloz. A Jupiter-mass companion to a solar-type star. *Nature*, 378:355–359, November 1995. doi: 10.1038/378355a0.

M. Mayor, S. Udry, C. Lovis, F. Pepe, D. Queloz, W. Benz, J.-L. Bertaux, F. Bouchy, C. Mordasini, and D. Segransan. The HARPS search for southern extra-solar planets. XIII. A planetary system with 3 super-Earths (4.2, 6.9, and 9.2 M_{Earth}). *A&A*, 493:639–644, January 2009. doi: 10.1051/0004-6361:200810451.

D. Mihalas and P. M. Routly. *Galactic astronomy*. 1968.

D. Montes, J. López-Santiago, M. C. Gálvez, M. J. Fernández-Figueroa, E. De Castro, and M. Cornide. Late-type members of young stellar kinematic groups - I. Single stars. *MNRAS*, 328:45–63, November 2001. doi: 10.1046/j.1365-8711.2001.04781.x.

B. Nordström, M. Mayor, J. Andersen, J. Holmberg, F. Pont, B. R. Jørgensen, E. H. Olsen, S. Udry, and N. Mowlavi. The Geneva-Copenhagen survey of the Solar neighbourhood. Ages, metallicities, and kinematic properties of ∼14 000 F and G dwarfs. *A&A*, 418:989–1019, May 2004. doi: 10.1051/0004-6361:20035959.

R. W. Noyes, L. W. Hartmann, S. L. Baliunas, D. K. Duncan, and A. H. Vaughan. Rotation, convection, and magnetic activity in lower main-sequence stars. *ApJ*, 279:763–777, April 1984. doi: 10.1086/161945.

D. B. Paulson and S. Yelda. Differential Radial Velocities and Stellar Parameters of Nearby Young Stars. *PASP*, 118:706–715, May 2006. doi: 10.1086/504115.

D. B. Paulson, C. Sneden, and W. D. Cochran. Searching for Planets in the Hyades. IV. Differential Abundance Analysis of Hyades Dwarfs. *AJ*, 125:3185–3195, June 2003. doi: 10.1086/375209.

Y. V. Pavlenko. Lithium Lines in the Spectra of M Dwarfs: UX Tau C. *Astronomy Reports*, 44:219–226, April 2000. doi: 10.1134/1.163844.

M. A. C. Perryman, L. Lindegren, J. Kovalevsky, E. Hoeg, U. Bastian, P. L. Bernacca, M. Crézé, F. Donati, M. Grenon, F. van Leeuwen, H. van der Marel, F. Mignard, C. A. Murray, R. S. Le Poole, H. Schrijver, C. Turon, F. Arenou, M. Froeschlé, and C. S. Petersen. The HIPPARCOS Catalogue. *A&A*, 323:L49–L52, July 1997.

D. Pourbaix, A. A. Tokovinin, A. H. Batten, F. C. Fekel, W. I. Hartkopf, H. Levato, N. I. Morrell, G. Torres, and S. Udry. S_b^9: The ninth catalogue of spectroscopic binary orbits. *A&A*, 424:727–732, September 2004. doi: 10.1051/0004-6361:20041213.

D. Queloz, S. Allain, J.-C. Mermilliod, J. Bouvier, and M. Mayor. The rotational velocity of low-mass stars in the Pleiades cluster. *A&A*, 335:183–198, July 1998.

S. Randich, R. Pallavicini, G. Meola, J. R. Stauffer, and S. C. Balachandran. Membership, lithium, and metallicity in the young open clusters IC 2602 and IC 2391: Enlarging the sample. *A&A*, 372:862–878, June 2001. doi: 10.1051/0004-6361:20010339.

N. Reid. Proper motions from Schmidt plates. II - The Hyades. *MNRAS*, 257:257–302, July 1992.

N. C. Santos, M. Mayor, D. Naef, F. Pepe, D. Queloz, S. Udry, M. Burnet, J. V. Clausen, B. E. Helt, E. H. Olsen, and J. D. Pritchard. The CORALIE survey for southern extra-solar planets. IX. A 1.3-day period brown dwarf disguised as a planet. *A&A*, 392:215–229, September 2002. doi: 10.1051/0004-6361:20020876.

R.-D. Scholz, M. Odenkirchen, S. Hirte, M. J. Irwin, F. Borngen, and R. Ziener. Absolute proper motions and Galactic orbits of M5, M12 and M15 from Schmidt plates. *MNRAS*, 278:251–264, January 1996.

B. W. Silverman. *Density estimation for statistics and data analysis*. 1986.

J. Skuljan, J. B. Hearnshaw, and P. L. Cottrell. Velocity distribution of stars in the solar neighbourhood. *MNRAS*, 308:731–740, September 1999. doi: 10.1046/j.1365-8711.1999.02736.x.

M. A. Smith and D. F. Gray. Fourier analysis of spectral line profiles - A new tool for an old art. *PASP*, 88: 809–823, December 1976. doi: 10.1086/130029.

M. C. Smith, G. R. Ruchti, A. Helmi, R. F. G. Wyse, J. P. Fulbright, K. C. Freeman, J. F. Navarro, G. M. Seabroke, M. Steinmetz, M. Williams, O. Bienaymé, J. Binney, J. Bland-Hawthorn, W. Dehnen, B. K. Gibson, G. Gilmore, E. K. Grebel, U. Munari, Q. A. Parker, R.-D. Scholz, A. Siebert, F. G. Watson, and T. Zwitter. The RAVE survey: constraining the local Galactic escape speed. *MNRAS*, 379:755–772, August 2007. doi: 10.1111/j.1365-2966.2007.11964.x.

J. Tonry and M. Davis. A survey of galaxy redshifts. I - Data reduction techniques. *AJ*, 84:1511–1525, October 1979. doi: 10.1086/112569.

S. Udry and N. C. Santos. Statistical Properties of Exoplanets. *ARA&A*, 45:397–439, September 2007. doi: 10.1146/annurev.astro.45.051806.110529.

J. A. Valenti and D. A. Fischer. Spectroscopic Properties of Cool Stars (SPOCS). I. 1040 F, G, and K Dwarfs from Keck, Lick, and AAT Planet Search Programs. *ApJS*, 159:141–166, July 2005. doi: 10.1086/430500.

F. van Leeuwen. Validation of the new Hipparcos reduction. *A&A*, 474:653–664, November 2007. doi: 10.1051/0004-6361:20078357.

A. Wolszczan and D. A. Frail. A planetary system around the millisecond pulsar PSR1257 + 12. *Nature*, 355:145–147, January 1992. doi: 10.1038/355145a0.

J. T. Wright. Do We Know of Any Maunder Minimum Stars? *AJ*, 128:1273–1278, September 2004. doi: 10.1086/423221.

S. Yi, P. Demarque, Y.-C. Kim, Y.-W. Lee, C. H. Ree, T. Lejeune, and S. Barnes. Toward Better Age Estimates for Stellar Populations: The Y^2 Isochrones for Solar Mixture. *ApJS*, 136:417–437, October 2001. doi: 10.1086/321795.